

**The influence of coagulation factor XIII-A V34L mutation on  
clot formation and stability**

Adomas Baranauskas

Submitted in accordance with the requirements for the degree of  
Doctor of Philosophy

The University of Leeds  
Faculty of Medicine and Health

October, 2019



The candidate confirms that the work submitted is his own and that appropriate credit has been given where reference has been made to the work of others.

This copy has been supplied on the understanding that it is copyright material and that no quotation from the thesis may be published without proper acknowledgement.

The right of Adomas Baranauskas to be identified as Author of this work has been asserted by him in accordance with the Copyright, Designs and Patents Act 1988.

## Acknowledgements

This research has been carried out by myself (Adomas Baranauskas) with the support of Dr Cédric Duval, Professor Robert Ariëns, Dr Richard Cubbon and Miss Helen McPherson. Dr Cédric Duval has contributed in training, advice and support in almost every matter throughout the PhD project, with significant contributions when using recombinant protein purification equipment as well as performing blood vessel isolation and FeCl<sub>3</sub> injury during *in vivo* experiments. Professor Robert Ariëns has contributed to the work by advising and structuring the workflow of the project while providing feedback on data interpretations and thesis writing. Dr Richard Cubbon has contributed by familiarising me with light sheet microscope and image acquisition. Miss Helen McPherson has contributed by teaching me clot contraction experiments as well as overall good laboratory practice.

In addition, I would love to take the opportunity to acknowledge people more personally and express my gratitude as follows:

First and foremost, it would be an understatement saying that I had great supervision during my PhD here in LICAMM, University of Leeds. My supervisors Professor Robert Ariëns and Dr Cédric Duval were nothing but excellent, showing perfect balance between guiding me and trusting me with a freedom to act, which made feel like I was always able to use any given opportunity without worrying about failure. I was constantly surprised and humbled by the fact how frequently they made time for me to ask for advice or help, which I realise, has been an unbelievably fortunate situation for a PhD student and ensured that I have made the most out of my diverse research project. I am extremely grateful to both of my lovely supervisors for allowing me on-board and being remarkably inspiring, caring and thoughtful leaders.

So many people have made my PhD experience enjoyable, that it would be difficult to name them all! Every single person from the Ariëns and Philippou group people made me feel like a part of a close, friendly and supportive community. I am grateful to all, who helped me along the way, cheered me up and facilitated my PhD work in the process.

Huge thanks to all of the core team and, especially Mrs Julie Mawson, who made sure that I always had clean equipment to work with even if it meant bothering her at unusual hours.

I'd like to thank Miss Helen McPherson for being so caring and thinking about the wellbeing of the whole group. Helen seemed to always know where things are put, how to run any experiment, and most importantly, proactively helped everyone at any moment.

I am very grateful to Dr Richard Cubbon and Dr Ruth Hughes for familiarising me with light sheet imaging as well as Dr Nadira Yusupovna Yuldasheva and Dr Mike Drozd for expanding my knowledge about *in vivo* work.

Big thanks to Dr Nathan Asquith for being a great friend, both encouraging and uplifting at moments of stress.

I am also grateful to Dr Stephen Baker, who seemed to always have interesting matters to discuss, a joke to crack and made the office hours sociable.

I would love to thank Dr Kingsley Simpson as well, for being a massive fun in the lab.

And last, but not least, I am forever grateful to my supportive family and my love Ieva, who has always been by my side, keeping me motivated to work hard and inspiring me with her unbelievable work ethic.

## Abstract

**Background:** Coagulation factor XIII (FXIII) is a key enzyme in stabilising blood clots by cross-linking fibrin molecules together, amongst other effects on fibrinolysis and matrix protein stabilisation. The human FXIII-A V34L sequence variant leads to increased activation rates, forming clots with thinner fibrin fibres and smaller pores, and has been reported to show protective effects against thrombotic diseases like venous thromboembolism. However, the complete mechanism(s) underpinning this effect has hitherto remained elusive.

**Aim:** To establish a murine FXIII-A L34V model and study the role of this sequence variant, as well as that of FXIII itself, in thromboembolic disease.

**Methods:** FXIII-A Knock-Out (FXIII<sup>-/-</sup>, already available in the laboratory), FXIII-A 34Val (generated by MRC Harwell for Leeds) and FXIII-A 34Leu (common variant, wild-type) mice were compared in their growth, plasma FXIII activation rates (biotin incorporation assay), turbidity for clot structure, fibrinogen concentrations (ELISA assay) and FXIII-A antigen levels (western-blotting). Whole blood clotting and lysis was measured by rotational thromboelastometry (ROTEM). Whole blood clot contraction, erythrocyte extrusion (haemoglobin) and two-hour clot weights were quantified. For pulmonary and cerebral embolism models, FeCl<sub>3</sub> vascular injury was performed on inferior vena cava and carotid artery, respectively. Lungs or brains were optically cleared and imaged with a light sheet microscope. Pulmonary emboli volume and count were quantified using software, while cerebral emboli were quantified manually.

**Results:** No significant differences between 34Leu and 34Val mice growth, whole blood contraction, serum haemoglobin, clot weight, ROTEM, plasma FXIII-A and fibrinogen levels were observed. FXIII<sup>-/-</sup> mice plasma contained no FXIII-A antigen, showed negligible fibrin cross-linking activity and had similar levels of fibrinogen as FXIII sufficient mice. FXIII<sup>-/-</sup> clots were less firm, easier to lyse, slower to form, retained fewer red blood cells, were lighter and formed thicker fibres than FXIII sufficient clots. 34Leu mice plasma showed increased FXIII-A activation rates over 34Val mice plasma. Increasing FXIII activation rates (34Leu > 34Val > FXIII<sup>-/-</sup>) increased both pulmonary emboli count and volume, while the trend in cerebral embolism differences was inconclusive.

**Conclusion:** The murine FXIII-A 34Leu variant showed increased activation rates over the 34Val variant and altered thromboembolisation, particularly in the venous circulation. Potentially, increased FXIII activation may enhance venous thromboembolism by protecting emboli against fibrinolysis during their transit to the lungs. In the high shear stress arterial environment, effects of mechanical stabilisation by FXIII may counterbalance any effects on fibrinolysis. These studies show a potentially important role for FXIII-mediated clot stabilisation and protection against fibrinolysis that impact on thromboembolic diseases. Pulmonary embolism dependence on FXIII could be clinically relevant, where FXIII inhibition would act as prophylaxis for patients with a high risk of pulmonary embolism.

## Table of contents

<b>Acknowledgements</b> .....	<b>ii</b>
<b>Abstract</b> .....	<b>iv</b>
<b>Table of contents</b> .....	<b>vi</b>
<b>List of tables</b> .....	<b>xi</b>
<b>List of figures</b> .....	<b>xii</b>
<b>List of equations</b> .....	<b>xiv</b>
<b>List of abbreviations</b> .....	<b>xv</b>
<b>Chapter 1 Introduction</b> .....	<b>1</b>
1.1 Cardiovascular diseases and thrombosis .....	2
1.2 Venous thromboembolism .....	4
1.3 Atherothrombosis.....	5
1.4 Immune system in coagulation .....	8
1.5 Coagulation cascade .....	9
1.6 Fibrinogen.....	12
1.7 Fibrinolysis.....	14
1.8 Role of FXIII.....	16
1.9 FXIII deficiency .....	20
1.10 FXIII Structure.....	21
1.11 FXIII A and B subunits .....	23
1.12 FXIII activation .....	26
1.13 FXIII cross-linking effects.....	29
1.14 FXIII-A V34L .....	30
1.15 FXIII-A V34L sequence variant in arterial and venous thromboembolism .....	31
1.16 Models of thrombosis.....	33
1.17 Study rationale and hypotheses.....	39
1.18 Aims.....	40
1.19 Objectives .....	40
<b>Chapter 2 Methods</b> .....	<b>42</b>
2.1 mFXIII-A gene PCR amplification .....	43
2.2 Agarose gel electrophoresis .....	44
2.3 DNA recovery from agarose gel.....	44
2.4 TA cloning.....	45

2.5	<i>E. coli</i> Transformation, Growth and Glycerol Stock .....	47
2.5.1	Transformation .....	47
2.5.2	Transformation quality assurance .....	48
2.6	Bacterial growth.....	48
2.7	DNA extraction .....	49
2.8	Restriction digestion .....	49
2.9	Gene – vector ligation.....	50
2.10	Site-directed mutagenesis .....	50
2.11	DNA sequencing .....	51
2.12	Expression and purification of recombinant GST-mFXIII-A protein from <i>E. coli</i> .....	52
2.12.1	Expression .....	52
2.12.2	Purification .....	53
2.13	SDS-PAGE gels .....	54
2.14	BCA assay.....	55
2.15	Recombinant mFXIII-A activation rate assay.....	56
2.16	Mice variants and animal husbandry .....	58
2.17	Murine blood collection and plasma preparation .....	58
2.18	Growth curve .....	59
2.19	Blood clot contraction, serum haemoglobin and clot weight.....	59
2.19.1	Clot contraction .....	59
2.19.2	Clot supernatant haemoglobin .....	60
2.19.3	Clot weight .....	61
2.20	Thromboelastometry.....	62
2.21	Mice plasma experiments.....	63
2.22	Plasma FXIII antigen levels .....	63
2.23	Plasma fibrinogen levels.....	64
2.24	Plasma FXIII biotin incorporation assay .....	65
2.25	Plasma turbidity.....	67
2.26	<i>In Vivo</i> thromboembolism model .....	68
2.26.1	Vascular injury, organ harvest and optical clearing .....	68
2.26.2	Light sheet fluorescence microscopy .....	69
2.26.3	Imaris image reconstruction and analysis .....	70
2.26.4	Manual emboli counting .....	72
2.27	Statistical analysis and outliers.....	73

<b>Chapter 3 <i>In vitro</i> recombinant mFXIII-A work .....</b>	<b>75</b>
3.1 Introduction.....	76
3.2 Aims.....	83
3.3 Methods.....	83
3.3.1 mFXIII-A gene PCR amplification .....	83
3.3.2 TA cloning .....	84
3.3.3 Restriction digestion and gene – vector ligation .....	85
3.3.4 <i>E. coli</i> Transformation, Growth and Glycerol stock.....	85
3.3.5 Site-directed mutagenesis .....	86
3.3.6 DNA sequencing.....	87
3.3.7 mFXIII-A Expression and Purification .....	88
3.3.8 Recombinant mFXIII-A activation rate assay.....	90
3.4 Results.....	91
3.4.1 WT mFXIII-A cDNA amplification from pCMV-SPORT6 vector.....	91
3.4.2 WT mFXIII-A DNA ligation into pLIVE vector.....	92
3.4.3 mFXIII-A L34V mutagenesis.....	94
3.4.4 Amplification of mFXIII-A WT and L34V DNA sequences from pLIVE vector and ligation with pCR 2.1 vector .....	94
3.4.5 Restriction digestion of mFXIII-A WT and L34V in pCR 2.1 vector and ligation with pGEX-6P-1 vector .....	95
3.4.6 Protein expression and purification.....	97
3.4.7 Recombinant mFXIII-A activation rate assay.....	101
3.5 Discussion .....	103
<b>Chapter 4 L34V mouse characterisation and <i>ex vivo</i> work .....</b>	<b>106</b>
4.1 Introduction.....	107
4.2 Aims.....	108
4.3 Methods.....	109
4.3.1 Murine blood collection and plasma preparation .....	109
4.3.2 Growth curve .....	109
4.3.3 Plasma FXIII antigen and fibrinogen levels .....	109
4.3.4 Plasma FXIII biotin incorporation assay .....	109
4.3.5 Clot contraction, serum haemoglobin and clot weight .....	109
4.3.6 Thromboelastometry.....	110
4.3.7 Plasma turbidity.....	110
4.4 Results.....	111

4.4.1	Growth curve.....	111
4.4.2	Plasma FXIII antigen and fibrinogen levels .....	112
4.4.3	Plasma FXIII biotin incorporation assay .....	114
4.4.4	Clot contraction, clot supernatant haemoglobin and clot weight.....	115
4.4.5	Thromboelastometry .....	118
4.4.6	Plasma turbidity.....	121
4.5	Discussion .....	123
<b>Chapter 5 <i>In vivo</i> murine FeCl<sub>3</sub> induced pulmonary and cerebral thromboembolism models.....</b>		<b>128</b>
5.1	Introduction.....	129
5.2	Aims .....	134
5.3	Methods.....	134
5.3.1	Pulmonary embolism.....	134
5.3.2	Cerebral embolism .....	136
5.4	Results .....	139
5.4.1	Pulmonary embolism.....	139
5.4.2	Cerebral embolism .....	144
5.4.3	Brain clearing optimisation .....	146
5.5	Discussion .....	146
<b>Chapter 6 Discussion .....</b>		<b>153</b>
6.1	Summary of data .....	154
6.2	Overall discussion .....	157
6.3	Limitations and improvements .....	169
6.3.1	mFXIII-A purification.....	169
6.3.2	Rotational thromboelastometry and flow .....	169
6.3.3	FeCl <sub>3</sub> vascular injury model.....	170
6.3.4	Brain image software analysis.....	170
6.4	Future work .....	171
6.4.1	Thrombin concentrations.....	171
6.4.2	Confocal lysis .....	171
6.4.3	Magnetic tweezers .....	171
6.4.4	Atomic force microscopy single fibrin fibre measurements .	172
6.4.5	Scanning electron microscopy .....	172
6.4.6	Alternative fibrin cross-linking proteins.....	172

6.4.7	Non-thrombin FXIII activators.....	173
6.4.8	IVC stenosis model.....	173
6.4.9	Inflammation.....	173
6.4.10	Pulmonary burden .....	174
6.4.11	Stroke severity.....	174
<b>Chapter 7 References .....</b>		<b>175</b>
<b>Chapter 8 Appendices .....</b>		<b>196</b>
8.1	Appendix 1.....	197
8.2	Appendix 2.....	199
8.3	Appendix 3.....	201
8.4	Appendix 4.....	204

## List of tables

<b>Table 2.1 ROTEM<sup>®</sup> conditions and reagent volumes used</b> .....	<b>62</b>
<b>Table 3.1 PCR amplification primers and their sequences.</b> .....	<b>84</b>
<b>Table 3.2 mFXIII-A PCR amplification cycling parameters.</b> .....	<b>84</b>
<b>Table 3.3 PCR thermal cycling parameters used in transformation quality assurance runs.</b> .....	<b>86</b>
<b>Table 3.4 PCR primers used in site-directed L34V mutagenesis of mFXIII-A.</b> .....	<b>86</b>
<b>Table 3.5 PCR thermal cycling parameters used in L34V site-directed mutagenesis.</b> .....	<b>87</b>
<b>Table 3.6 Primers (and sequenced vectors) used in mFXIII-A sequencing.</b> .....	<b>88</b>
<b>Table 3.7 Buffers used in ÄKTAprime during mFXIII-A chromatography run.</b> .....	<b>89</b>
<b>Table 3.8 Steps of mFXIII-A loading into GStrap FF column using ÄKTAprime.</b> .....	<b>89</b>
<b>Table 3.9 Steps of mFXIII-A and GST elution from GStrap FF column using ÄKTAprime.</b> .....	<b>90</b>
<b>Table 3.10 Clustal Omega web tool alignment of a portion CMV-SPORT6 vector containing WT mFXIII-A sequence with a PCR amplification product. Full sequence available in Appendix 1. ....</b>	<b>92</b>
<b>Table 3.11 Clustal Omega web tool alignment of WT mFXIII-A insert in pLIVE vector with a pLIVE+mFXIII-A DNA template. Full sequence available in Appendix 2.</b> .....	<b>93</b>
<b>Table 3.12 Clustal Omega alignment of a portion of pLIVE vector containing WT (34Leu) and 34Val mFXIII-A sequences.</b> .....	<b>94</b>
<b>Table 3.13 Clustal Omega web tool alignment of inserted WT and L34V mFXIII-A sequences into pGEX-6P-1 vector.</b> .....	<b>97</b>

## List of figures

<b>Figure 1.1 Virchow's triad of thrombosis.....</b>	<b>3</b>
<b>Figure 1.2 Coagulation cascade schematic.....</b>	<b>12</b>
<b>Figure 1.3 Schematic of transglutaminase reaction of FXIII.....</b>	<b>17</b>
<b>Figure 1.4 Schematic of the conversion of fibrinogen into fibrin, and fibrin fibre formation.....</b>	<b>19</b>
<b>Figure 1.5 Structural model of the FXIII A<sub>2</sub>B<sub>2</sub> tetramer.....</b>	<b>23</b>
<b>Figure 1.6 Schematic representation of FXIII activation.....</b>	<b>27</b>
<b>Figure 1.7 SEM pictures of inferior vena cava thrombus generated with FeCl<sub>3</sub> injury.....</b>	<b>36</b>
<b>Figure 1.8 Illustration of FeCl<sub>3</sub> vascular injury.....</b>	<b>38</b>
<b>Figure 2.1 Explanatory schematic of a TA cloning technique.....</b>	<b>46</b>
<b>Figure 2.2 Fibrin polymerisation curve example schematic.....</b>	<b>67</b>
<b>Figure 2.3 Imaris software marking the surfaces of emboli post light sheet microscope imaging.....</b>	<b>72</b>
<b>Figure 3.1 In vitro recombinant mFXIII-A workflow schematic.....</b>	<b>78</b>
<b>Figure 3.2 pLIVE and pGEX-6P-1 vector schematics.....</b>	<b>82</b>
<b>Figure 3.3 Gel electrophoresis of PCR amplified mFXIII-A gene fragment.....</b>	<b>91</b>
<b>Figure 3.4 Agarose gel electrophoresis of pCR 2.1 vector (+mFXIII-A) and pLIVE vector restriction digest samples.....</b>	<b>93</b>
<b>Figure 3.5 Gel electrophoresis of PCR amplified mFXIII-A WT and L34V gene fragments.....</b>	<b>95</b>
<b>Figure 3.6 Agarose gel electrophoresis of pCR 2.1 vector (+mFXIII-A WT and L34V) and pGEX-6P-1 vector restriction digest samples.....</b>	<b>96</b>
<b>Figure 3.7 WT mFXIII-A elution from GSTrap FF column graph.....</b>	<b>98</b>
<b>Figure 3.8 SDS page gel of mFXIII-A Wild-Type, L34V and cleaved GST tag.....</b>	<b>99</b>
<b>Figure 3.9 SDS-PAGE gels of mFXIII-A WT and L34V activation rate assay.....</b>	<b>101</b>
<b>Figure 3.10 Example logarithmic curve fit to the recombinant mFXIII- A activation rate assay SDS-PAGE band intensity data.....</b>	<b>102</b>
<b>Figure 3.11 Activation rate comparison between 34Leu and 34Val mFXIII-A.....</b>	<b>103</b>
<b>Figure 4.1 Growth curve of 34Leu and 34Val mice.....</b>	<b>111</b>
<b>Figure 4.2 Western blotting SDS-PAGE gels showing FXIII<sup>-/-</sup>, 34Val and 34Leu mice plasma FXIII-A antigen and IgG levels.....</b>	<b>112</b>

<b>Figure 4.3 FXIII plasma antigen levels. ....</b>	<b>113</b>
<b>Figure 4.4. Plasma fibrinogen levels of 34Leu, 34Val and FXIII-/- mice. ....</b>	<b>114</b>
<b>Figure 4.5 34Val, 34Leu and FXIII-/- mice plasma mFXIII-A biotin incorporation rates. ....</b>	<b>115</b>
<b>Figure 4.6 34Leu, 34Val and FXIII-/- mice whole blood clot volume after 60, 90 and 120 min of clotting. ....</b>	<b>116</b>
<b>Figure 4.7 Supernatant haemoglobin amount (% initial) after 60, 90 and 120 min of clotting. ....</b>	<b>117</b>
<b>Figure 4.8 Two-hour clot weights from 34Leu, 34Val and FXIII-/- murine blood. ....</b>	<b>118</b>
<b>Figure 4.9 ROTEM clot CT, MCF and LT with and without platelet activity in FXIII-/-, 34Val and 34Leu blood. ....</b>	<b>120</b>
<b>Figure 4.10 34Val, 34Leu and FXIII-/- mice plasma coagulation turbidity analysis. ....</b>	<b>122</b>
<b>Figure 5.1 Schematic depicting a light sheet microscopy principle. ..</b>	<b>133</b>
<b>Figure 5.2 FeCl<sub>3</sub> inferior vena cava injury model surgery photographs. ....</b>	<b>135</b>
<b>Figure 5.3 FeCl<sub>3</sub> carotid artery injury model surgery photographs. ....</b>	<b>136</b>
<b>Figure 5.4 AlexaFluor<sup>647</sup> fluorescence channel light sheet microscope image reconstruction of the brain. ....</b>	<b>138</b>
<b>Figure 5.5 Top-down snapshots of left and right lung 3D reconstruction post IVC FeCl<sub>3</sub> injury and light sheet microscopy imaging. ....</b>	<b>139</b>
<b>Figure 5.6 FXIII-/-, 34Val and 34Leu mice total pulmonary emboli count following IVC FeCl<sub>3</sub> injury. ....</b>	<b>140</b>
<b>Figure 5.7 FXIII-/-, 34Val and 34Leu mice total pulmonary emboli volume following IVC FeCl<sub>3</sub> injury. ....</b>	<b>141</b>
<b>Figure 5.8 FXIII-/-, 34Val and 34Leu mice large (&gt;7000 μm<sup>3</sup>) and small (&lt;200 μm<sup>3</sup>) pulmonary emboli count following IVC FeCl<sub>3</sub> injury. ....</b>	<b>143</b>
<b>Figure 5.9 Top-down snapshot of mouse brain 3D reconstruction post carotid artery FeCl<sub>3</sub> injury and light sheet microscopy imaging. ....</b>	<b>144</b>
<b>Figure 5.10 FXIII-/-, 34Val and 34Leu mice total cerebral emboli count following carotid artery FeCl<sub>3</sub> injury. ....</b>	<b>145</b>
<b>Figure 6.1 Depiction of GST-FXIII-A fusion protein. ....</b>	<b>158</b>
<b>Figure 6.2 Vascular injury data interpretation schematic. ....</b>	<b>167</b>

## List of equations

<i>Equation 2.1 Gene insert amount calculation for insert vector ligation.</i> .....	47
<i>Equation 2.2 Equation for clot volume calculation from images.</i> .....	60
<i>Equation 2.3 Cylinder volume equation.</i> .....	60
<i>Equation 2.4 Equation for clot supernatant haemoglobin calculations.</i> .....	61

## List of abbreviations

Abbreviation	Description
34Leu	FXIII-A 34Leu variant
34Val	FXIII-A 34Val variant
3DISCO	Three-Dimensional Imaging of Solvent-Cleared Organs
A	adenosine
A <sub>2</sub> B <sub>2</sub>	FXIII heterotetramer
AFP	alpha-fetoprotein
AIS	atherothrombotic ischemic stroke
AP	activation peptide
AU	absorbance unit
BCA	bicinchonic acid
bp	base pair
BSA	bovine serum albumin
CAD	coronary artery disease
CT	clotting time
CV	column volume
CVD	cardiovascular disease
d	diameter
DBE	di-benzyl ether
DCM	dichlormethane
DVT	deep vein thrombosis
F	coagulation Factor
Fbg	fibrinogen
FpA	fibrinopeptide A
FpB	fibrinopeptide B
FXIIIa	activated coagulation factor XIII
FXIII-A	coagulation factor XIII A subunit
FXIII-B	coagulation factor XIII B subunit
GST	glutathione S-transferase
GST-AP	glutathione S-transferase-activation peptide
h	height
HMW	high molecular weight
iDISCO	immuno Three-Dimensional Imaging of Solvent-Cleared Organs
Ig	imunoglobulin
IPTG	isopropyl β-D-1-thiogalactopyranoside
IS	ischaemic Stroke
IVC	inferior vena cava
KO	FXIII-A knock-out variant
LB	lysogeny broth
LDL	low density lipoprotein
LgT	lag time
LPS	lipopolysaccharide
LT	lysis time

Max	maximum
MCF	mean clot firmness
MeOH	methanol
mFXIII-A	murine FXIII A subunit
MI	myocardial infarction
Min	minimum
OD	optical density
OR	odds ratio
oxLDL	oxidised low density lipoprotein
PAGE	polyacrylamide gel electrophoresis
PAI	plasminogen activator inhibitor
PBS	phosphate-buffered saline
PCR	polymerase chain reaction
PE	pulmonary embolism
PFA	paraformaldehyde
RBC	red blood cell
rhFXIII-A	recombinant human FXIII A subunit
ROTEM	rotational thromboelastometry
SDS	sodium dodecyl sulfate
SEM	scanning electron microscopy
serpin	serine protease inhibitor
T	thymine
TAFI	thrombin activatable fibrinolysis inhibitor
TBS	tris-buffered saline
TF	tissue factor
TFPI	tissue factor pathway inhibitor
t-PA	tissue-type plasminogen activator
u-PA	urokinase-type Plasminogen Activator
VCAM-1	vascular cell adhesion molecule-1
Vmax	maximum velocity
VTE	venous thromboembolism
vWF	von Willebrand factor
WHO	World Health Organisation
WT	wild-type
$\alpha$ 2-AP	alpha2-antiplasmin

# **Chapter 1 Introduction**

## **1.1 Cardiovascular diseases and thrombosis**

Cardiovascular disease (CVD) is the number one cause of death globally, accounting for 31% of global deaths, reaching 17.9 million cardiovascular related deaths worldwide in 2016 (WHO, 2017). The major contributor to cardiovascular disease is thrombosis: 85% CVD associated deaths are due to heart attack and stroke, while venous thromboembolism is responsible for over 500,000 deaths per year in Europe alone (Thrombosis UK, 2017) (Rosendaal, 2016). Thrombotic disease is not only a major killer, but also a critical financial burden, since 60% of patients with thrombosis get hospitalised and here in UK, venous thromboembolism (VTE) alone costs the NHS £198,000,000 (Thrombosis UK, 2017).

Thrombosis is the pathological consequences of the formation of an abnormal blood clot in the blood vessel lumen, which starts to obstruct the blood flow and causes damage to the surrounding vessel and downstream tissues (Stone et al., 2017). These thrombi can also break off, travel downstream and block the blood flow of smaller vessels elsewhere in a process called embolisation (Johannessen et al., 1988). Restricted blood flow or disrupted endothelial integrity causes a shortage of oxygen supply to the surrounding tissues making it unable to carry out basic cellular metabolism leading to cell death and tissue ischaemia (Ferris and Friesen, 1979). Examples of ischaemic diseases are thrombi in the brain (stroke) (Musuka et al., 2015), heart (myocardial infarction) (Saleh and Ambrose, 2018) and lung (pulmonary embolism) (Lavorini et al., 2013). Arterial and venous thrombosis are quite distinct from each other, developing in different

conditions, forming different types of clots and having unique risk factors (Previtali et al., 2011).

Knowledge about key pathophysiological determinants of thrombosis dates back to as far as the 19<sup>th</sup> century, when the German physician Rudolf Virchow (1821-1902) characterised thrombosis as a result of three key mechanistic elements: endothelial injury, stasis of blood flow and hypercoagulability – the so called Virchow’s triad shown in *Figure 1.1* (Kumar et al., 2010).

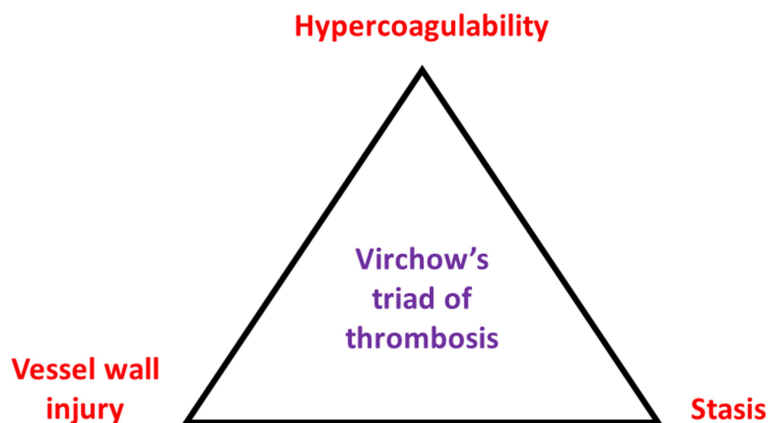


***Figure 1.1 Virchow's triad of thrombosis.***

*The triad proposing three major elements of thrombosis: blood stasis, hypercoagulability and vessel wall injury.*

It is commonly accepted that in VTE, hypercoagulability and stasis are more influential components of Virchow's triad that cause venous thrombosis than endothelial damage (Previtali et al., 2011). Venous thrombi are rich in red blood cells (RBC's) and fibrin, and less rich in platelets. Atherothrombosis, or arterial thrombosis associated with atherosclerosis, however, usually pivots around endothelial damage. Platelets, which patrol the intact endothelium

and are immediately activated by endothelial damage, aggregate on the damaged endothelium forming the initial thrombus, thereby playing a greater role in arterial thrombus formation (Harker, 1998). Atherosclerosis and ensuing arterial thrombosis is strongly promoted by inflammation and hyperlipidaemia, in contrast to venous thrombosis, which is largely promoted by stasis and hypercoagulability (Previtali et al., 2011).

## **1.2 Venous thromboembolism**

Venous thromboembolism (VTE) is the third most common thrombotic disease following myocardial infarction and stroke (Thrombosis UK, 2018). VTE includes two main clinical manifestations: deep vein thrombosis (DVT) and pulmonary embolism (PE), with PE following DVT in disease progression (Previtali et al., 2011). Venous thrombi form in low shear stress environments, where a reduction of laminar blood flow, stasis, is prominent (Kumar et al., 2010). Stasis usually occurs in patients with reduced mobility, since venous blood flow (especially in lower limbs) is facilitated by large surrounding muscle contraction which “squeeze” the blood up against the gravity (Verma et al., 2017). Blood vessel valves, present only in veins and heart, also ensure forward (and gravity defying upward) movement of blood (Ortega et al., 2019). In valve sinus pockets between the valve and the vessel wall, blood flow is the most static and oxygen supply to the endothelium can be insufficient due to vein endothelium being reliant on luminal oxygen supply. These ischaemic conditions promote endothelial activation and dysfunction (Esmon, 2009). Activated endothelium then secretes prothrombotic agents, such as von Willebrand factor (VWF), plasminogen activator inhibitor-1 (PAI-1), reactive oxygen species (ROS) and

vasoconstrictor endothelin-1 (Bovill and van der Vliet, 2011) as well as expresses surface adhesion molecules for white blood cell and platelet recruitment (Budnik and Brill, 2018). At the same time, distressed and dysfunctional endothelial cells produce lower amounts of thromboresistance mediators, such as antithrombin, Tissue factor pathway inhibitor (TFPI) and vasodilator nitrous oxide (NO) (Aird, 2005) further leading towards hypercoagulability. This hypercoagulable state may exist due to many different inherited and acquired factors usually causing an imbalance between procoagulant and anticoagulant mechanisms (Thomas, 2001). Common risk factors for hypercoagulability include surgery (Ulrych et al., 2016), cancer (Heit, 2007), oestrogen elevation (Tchaikovski and Rosing, 2010), anticoagulant deficiencies (Esmon, 2009), obesity (Stein and Goldman, 2009) and pregnancy (Simcox et al., 2015). Early detection of venous thrombosis development is essential, since lifestyle changes (Rosendaal, 2005) combined with anticoagulation are very effective at preventing further thrombotic episodes (Ageno and Huisman, 2000). It has recently been suggested that targeting local inflammation in venous flow could be a safer DVT prevention strategy than targeting coagulation mechanisms themselves, which imposes a high risk of bleeding (Budnik and Brill, 2018).

### **1.3 Atherothrombosis**

Atherothrombosis is a diffuse process starting in early childhood, progressing through the adult life and finally manifesting as stroke, coronary artery disease (CAD) or peripheral arterial disease (Viles-Gonzalez et al., 2004). Morbidity and mortality of atherothrombosis is unpredictable and its

prevalence is high, even with the efficient antithrombotic therapies available (Leys, 2001). Effectiveness of directly inhibiting coagulation factors, such as factor Xa and thrombin has been well established for thrombosis prevention, however being such a multifactorial, lifelong disease, atherothrombosis is still extremely widespread and difficult to treat. (Viles-Gonzalez et al., 2004)

Arterial thrombosis develops in an environment where blood flow rates and shear stress are high (Sakariassen et al., 2015). Arterial thrombosis is initiated due to atherosclerotic plaque growth and rupture, which exposes collagen fibres from the deeper layers of the vessel wall and promotes platelet aggregation/activation and fibrin clot formation (Otsuka et al., 2016). Platelets bind to the exposed collagen fibres via glycoprotein von Willebrand factor (vWF), using GPIb receptor (Kroll et al., 1991), and directly to collagen via platelet surface receptors GPVI (Nieswandt and Watson, 2003) and  $\alpha_2\beta_1$  (Wang et al., 2003). Upon binding, platelets get activated and spread through the injury area in order to cover it (Aslan et al., 2012). Activated platelets also release ADP, fibrinogen, calcium, factor V and vWF stored in the dense and alpha granules, therefore facilitating further platelet aggregation and coagulation (Coppinger et al., 2004, Heijnen et al., 1998). Platelet surface integrin  $\alpha_{IIb}\beta_3$  binds fibrinogen, which links platelets together and further aids platelet activation (Vickers, 1999). Finally, fibrinogen is converted to fibrin by thrombin and the fibrin mesh stabilises the initial platelet plug into a blood clot (van Kempen et al., 2014).

Atherosclerotic plaque formation is initiated by high levels of lipids in circulation, mostly low density lipoproteins (LDL) (FERENCE et al., 2017). Due to hypertension (PuDDu et al., 2000, Brandes, 2014), high blood glucose

(Esper et al., 2008), hyperlipidaemia (Humphries, 1993) and smoking (Michael Pittilo, 2000, Messner and Bernhard, 2014), the arterial endothelium gets damaged and becomes easily permeable to lipids (Mundi et al., 2018). LDL molecules are then able to invade the vessel wall and deposit in the intima layer underneath the endothelium (Mundi et al., 2018). Damaged endothelium also attracts monocytes via vascular cell adhesion molecule 1 (VCAM-1) (Ley and Huo, 2001), which then migrate through the endothelium in order to reach the lipid depositions (Gerhardt and Ley, 2015). Activated monocytes oxidise the LDL by secreting free radicals (Xing et al., 1998), differentiate into macrophages and ingest the oxidised LDL (oxLDL) (Bobryshev et al., 2016). Macrophages eventually fill up with oxLDL and become large foam cells, which are no longer able to carry out phagocytosis and therefore commit apoptosis (Tabas, 2010). Dying macrophage contents lead to further deposition of cell debris and oxLDL within the vessel wall (Tabas, 2010). Smooth muscle cells from the nearby tunica media also respond to the local cytokines, produced by endothelial cells, smooth muscle cells and fibroblasts (Wang et al., 2017), by migrating to the intima layer, proliferating over the growing fatty streak and forming the fibrous cap around it (Rudijanto, 2007). Growing atherosclerotic plaques eventually result in stenosis, a significantly obstructed blood flow, and may rupture therefore exposing plaque contents to the bloodstream, including tissue factor (Annex et al., 1995, Moreno et al., 1996), which is expressed by the foam cells. Tissue factor in turn initiates the extrinsic pathway of the coagulation cascade (Drake et al., 1989, Ardissino et al., 1997). Thrombin, ADP and collagen fibres present in the plaque activate platelets, initiate their

aggregation and thrombus formation (Badimon and Vilahur, 2014). The resulting thrombus occludes the blood flow even further, or completely, and may embolise downstream occluding smaller arteries (Badimon and Vilahur, 2014). Most known and lethal forms of arterial embolism are cerebral embolism (stroke) and myocardial infarction (Lyaker et al., 2013).

#### **1.4 Immune system in coagulation**

In recent decades, the traditional understanding of haemostasis being regulated only by the coagulation cascade and platelet activation has been increasingly challenged. New evidence keeps surfacing that activation of the immune system has a strong influence on blood coagulation and thrombotic pathology. Leukocytes can be a strong factor in inducing coagulation via the expression of tissue factor (Shantsila and Lip, 2009) secretion of procoagulant cytokines (Pham, 2006, Meier et al., 1985) and release of nuclear damage-associated molecular patterns from activated apoptotic leukocytes (Maugeri et al., 2014, Chow et al., 2010). What is more, the leukocyte cell surface provides a site for assembly and activation of coagulation factors (Tracy et al., 1985). The integral part of immunothrombosis, however, is attributed to neutrophil extracellular trap (NETs) formation. NETs occur upon neutrophil activation and recruitment to the vessel wall, when neutrophil nuclear contents are secreted in a form of a web-like structures comprised out of DNA, histones and intracellular granular components (Brinkmann et al., 2004). NETs have been shown to be abundant in DVT thrombi and to be important in DVT development, since NET disruption (Brill et al., 2012) and neutrophil (von Bruhl et al., 2012) depletion experiments have shown to inhibit venous thrombus formation.

NETs have also been shown to provide a scaffold of FXIII activation (von Bruhl et al., 2012), promote platelet adhesion as well as induce endothelial cell activation (Xu et al., 2009) and thrombomodulin-dependent protein C activation (Ammollo et al., 2011) due to histone toxicity. Additionally, neutrophil elastase has been shown to degrade anticoagulants, such as tissue-factor pathway inhibitor (TFPI) (Massberg et al., 2010). These processes initiate thrombus formation, platelet activation and promote further leucocyte recruitment into the clot via interactions with platelets and adhesion molecules on endothelial cells (Swystun and Liaw, 2016).

On the other hand, phagocytic leukocytes promote fibrinolysis (Simon et al., 1993) and thrombus resolution via clearance of coagulation factors (Swystun and Liaw, 2016) and activated platelets (Hoffmeister, 2011). Through these combined mechanisms, deregulated activation of leukocytes is a major player in thrombosis and vascular pathology. Recently, modulation of leukocyte interactions with other cell types and leukocyte-derived procoagulant secretion has been an attractive target for developing novel antithrombotic treatments (Swystun and Liaw, 2016).

## **1.5 Coagulation cascade**

The coagulation cascade is an enzymatic chain reaction involved in blood clotting and is traditionally divided into a coagulation-initiating tissue factor (extrinsic) pathway (Mackman et al., 2007), and a coagulation-amplifying contact surface (intrinsic) pathway (Wu, 2015). The tissue factor (TF) pathway begins with TF being expressed by a variety of intravascular cells, such as endothelial cells, monocytes as well as extravascular cells, such as fibroblasts, pericytes and smooth muscle cells (Drake et al., 1989). Under

normal, healthy circumstances, intravascular TF expression can be counteracted by TFPI present on the endothelium (Callander et al., 1992). However, during inflammation or endothelial damage, TF expression on intravascular cells can increase and TF may also become available to the blood on now exposed extravascular cells, which evokes a procoagulant stimulus (Butenas et al., 2009). When exposed to the circulating blood, TF will bind and activate serine protease factor VII (Rao and Rapaport, 1988). The contact pathway, on the other hand, is initiated by negatively charged surfaces and platelet secreted polyphosphates following endothelial damage and platelet activation. Coagulation factor XII is activated upon binding to the exposed negatively charged collagen (van der Meijden et al., 2009, Naudin et al., 2017) as well as misfolded protein aggregates, nucleic acids and platelet secreted polyphosphates (Naudin et al., 2017). Subsequently, FXIIa activates FXI, which, in turn activates FIX (Gailani and Renne, 2007). FIXa then couples with its cofactor FVIIIa and forms a tenase complex with FX (Autin et al., 2005). Tenase complex assembly results in efficient FX activation, which is also enhanced by the presence of negatively-charged phosphatidylserine derived from platelet membranes (Lentz, 2003). FX activation is also carried out by TF:FVIIa complex (Chaudhry and Babiker, 2019), therefore making FX activation a step where two pathways merge into a “common” coagulation pathway (*Figure 1.2*). Coagulation factor Xa is a prothrombin activating factor, which upon coupling with its cofactor FVa and forming a prothrombinase complex, converts inactive prothrombin into the active thrombin enzyme (Allen et al., 2000). Once thrombin is activated, it activates FXI, FVIII and FV, creating a positive feedback loop and amplifying

the coagulation even further (Jesty and Beltrami, 2005). Most importantly, activated thrombin catalytically converts fibrinogen into fibrin, and activates FXIII (Narayanan, 1999). Fibrin then polymerises and self-assembles into a fibrin mesh, whereas FXIIIa covalently cross-links the fibrin mesh, making it structurally robust and much more resistant to fibrinolysis. A summarising simple schematic can be seen below (*Figure 1.2*). FX (Owens and Mackman, 2010), prothrombin (Heldebrant and Mann, 1973) and FXIII (Muszbek et al., 1999) activation requires  $\text{Ca}^{2+}$  ions being present.

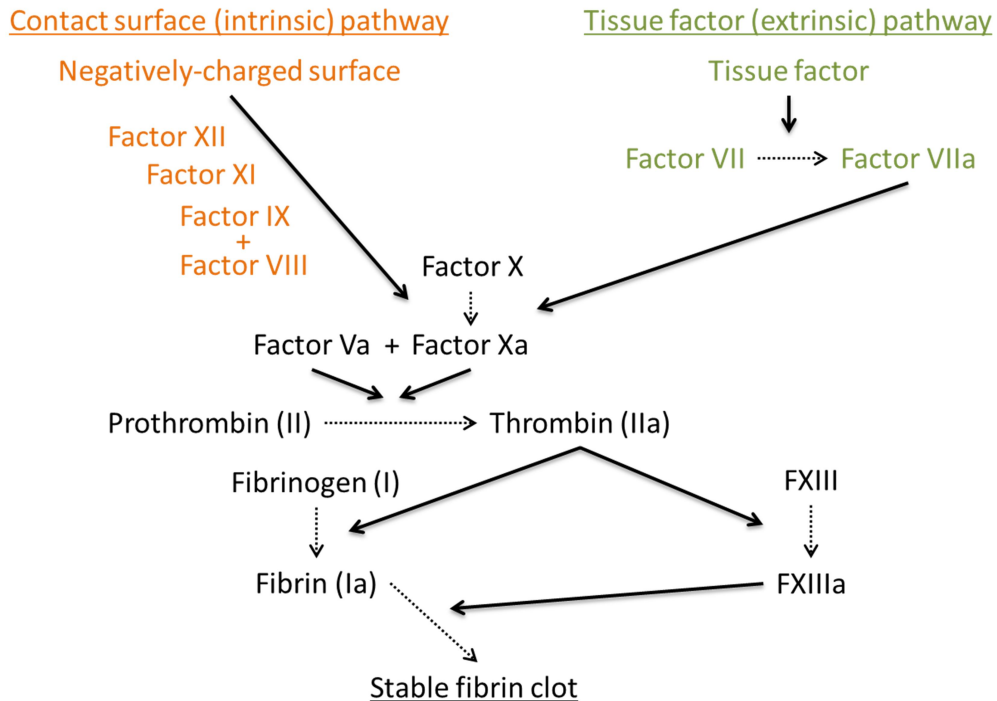


**Figure 1.2 Coagulation cascade schematic.**

Orange coloured coagulation factors constitute the contact surface pathway, which is initiated by blood being exposed to a negatively-charged surface like collagen or activated platelet membrane. Green coloured factors constitute the tissue factor pathway, which starts with exposure to tissue factor-bearing cells and activity. Both pathways then converge into a common pathway, which ultimately results in a stable fibrin clot. Dotted arrows denote coagulation factor conversion, while thick arrows illustrate the activity of coagulation factors.

## 1.6 Fibrinogen

Fibrinogen (initially named Factor I), is a structural protein, which upon conversion to fibrin polymerises and comprises the grid of the clot. Fibrinogen circulates at a concentration of 1.5-4.0 mg/mL and has a half-life of 4 days (Asselta et al., 2006). The fibrinogen (Fbg) molecule is comprised of three different polypeptide chains ( $A\alpha$ ,  $B\beta$ , and  $\gamma$ ) organized as dimers (6

chains in total) around a central N-terminal E-region and has two outer D C-terminal regions (*Figure 1.4, A*) (Mosesson, 2005). Thrombin cleaves fibrinopeptides A and B located in the E-region and so converts fibrinogen into fibrin (Scheraga, 1983). Cleavage of fibrinopeptide A (FpA) on the  $\alpha$ -chain, which happens first, exposes the A “knob” on the E-region, which is able to non-covalently bind the A hole in the D-region of another fibrin molecule (Weisel and Litvinov, 2013). This spontaneous process is called half-staggered fibrin polymerisation and results in protofibril formation (*Figure 1.4, B*) (Fowler et al., 1981). Next, thrombin cleaves fibrinopeptide B (FpB) on the  $\beta$ -chain, which releases the  $\alpha$ C-region of the  $\alpha$ -chain and opens the  $\alpha$ C-chains up (*Figure 1.4, C*) (Weisel and Litvinov, 2013). The now exposed B “knobs” are able to bind the B holes on the D-region as well (Litvinov et al., 2007), further reinforcing the D-E-D interactions that underpin fibrin polymerisation. The released and exposed  $\alpha$ C-chains are able to spontaneously bind  $\alpha$ C-chains of other fibrinogen molecules incorporated in nearby protofibrils. This results in a lateral aggregation of protofibrils and assists fibrin fibre formation (*Figure 1.4, D*) (Weisel and Litvinov, 2013). Fibrin protofibrils aggregate into ~130 nm wide fibrin fibres (Li et al., 2016b), which are extremely tensile and can sustain a 2.8-fold extension without being permanently lengthened and a 4.3-fold extension before rupturing (Liu et al., 2006). These numbers make fibrin one of the most extensible proteins observed, and one of the most elastic biological polymers known in nature, with almost comparable characteristics to spider silk.

## 1.7 Fibrinolysis

The fibrinolytic system is centred around the proteolytic activity of plasmin. Plasmin enzymatically degrades fibrin into multiple soluble degradation products. The inactive proenzyme plasminogen is converted into active plasmin by activator enzymes, a key step in fibrinolysis regulation and modulation (Rijken and Lijnen, 2009). Two main physiological plasminogen activators are tissue-type and urokinase-type plasminogen activators (t-PA and u-PA respectively) (Chapin and Hajjar, 2015). The main plasminogen activator out of both serine proteases is t-PA, however u-PA exerts complementary actions as well (Gurewich, 2016). t-PA is a fibrin specific plasminogen activator, which needs fibrin to be present in order to form a ternary complex with plasminogen and activate it efficiently (Kim et al., 2012). t-PA inhibition is key in reducing plasmin generation. This function is carried out by serine protease inhibitors (serpins) plasminogen activator inhibitor 1 and 2 (PAI-1 and PAI-2 respectively), which block the plasminogen activator active site (Carter and Church, 2009). Fibrin degradation is also inhibited by thrombin-activatable fibrinolysis inhibitor (TAFI) (Plug and Meijers, 2016). Plasmin and, more efficiently, thrombin (in presence of its cofactor thrombomodulin) converts circulating inactive TAFI precursor into its active form (Miljic et al., 2010). Activated TAFI reduces fibrinolysis by removing the C-terminal lysine residues of fibrin (Marx et al., 2004), that are involved in binding the lysine-binding sites on plasminogen and t-PA (Zhao et al., 1998, Boffa et al., 1999). Finally, studies on complement C3 have suggested that it also prolongs fibrinolysis and is cross-linked to fibrin by FXIII (Richardson et al., 2013). However, the

mechanism by which the inhibition of fibrinolysis takes place has not yet been fully elucidated.

$\alpha$ 2-AP also plays a very important role in the regulation of fibrinolysis (Rijken and Uitte de Willige, 2017). The antifibrinolytic effect of  $\alpha$ 2-AP comes from blocking the active site of the plasmin molecule (Abdul et al., 2016, Wiman et al., 1979).  $\alpha$ 2-AP circulates at 70  $\mu$ g/mL and is predominantly synthesized and secreted by the liver (Moroi and Aoki, 1976, Wiman and Collen, 1977). However, it has been shown that the kidney (Menoud et al., 1996) and the brain (Kawashita et al., 2013) could also be sites of  $\alpha$ 2-AP production.  $\alpha$ 2-AP is cross-linked via Gln2 and Gln14 residues in  $\alpha$ 2-AP and Lys303 residue in the  $\alpha$ -chain of fibrin (Kimura and Aoki, 1986, Tamaki and Aoki, 1982, Ichinose et al., 1983). Other less commonly cross-linked sites in  $\alpha$ 2-AP are the Gln34, Gln431 and Gln459 residues (Lee et al., 2000). The process of  $\alpha$ 2-AP and fibrin cross-linking occurs quickly:  $\alpha$ 2-AP cross-linking is nearly maximal when  $\alpha$ -chain polymerization begins to occur (Tamaki and Aoki, 1981). Interestingly, the same study has shown that the cross-linking of  $\alpha$ 2-AP ceases at about 30% of incorporation, corresponding to approximately one  $\alpha$ 2-AP molecule per 25 molecules of fibrin. The cross-linking rate has been shown to rise with increasing FXIIIa concentrations, but the maximal incorporation rate does not change (Tamaki and Aoki, 1981). Remarkably, a common FXIII-A sequence variant, V34L, which is more rapidly activated by thrombin and calcium than the more frequent FXIII-A (34Val) variant, shows higher  $\alpha$ 2-AP incorporation rates when compared to 34Val variant. This has been shown in both plasma samples of healthy human subjects (Schroder

and Kohler, 2000) as well as in purified recombinant protein systems (Duval et al., 2016).

## **1.8 Role of FXIII**

Clots that are self-assembled from fibrin as described earlier are initially mechanically weak and highly susceptible to fibrinolysis. Coagulation factor XIII (FXIII) plays an essential part in blood clot formation, by making the clot much more resistant to fibrinolysis and enhancing its structural stability (Ariens et al., 2000). The structural stability of the haemostatic clot is greatly increased by FXIII forming isopeptide bonds (*Figure 1.4, D*) between two  $\gamma$ -chains ( $\gamma$ - $\gamma$ ) (Chen and Doolittle, 1971), two  $\alpha$ -chains ( $\alpha$ - $\alpha$ ) (Cottrell et al., 1979) or far less regularly, two  $\alpha$ - and  $\gamma$ -chains of fibrin (Standeven et al., 2007) (Siebenlist and Mosesson, 1996). FXIII cross-linking transglutaminase reaction always occurs between glutamine and lysine residues (Chen and Doolittle, 1971, Matsuka et al., 1996, Sobel and Gawinowicz, 1996). FXIII catalytically active Cys314 residue, located in a catalytic core of FXIII-A, is carrying the cross-linking reaction out by replacing the ammonia of a glutamine residue on one protein (e.g. fibrin) molecule with an amino group on a lysine residue on another protein molecule, and subsequently creating a covalent isopeptide bond between these two residues (*Figure 1.3*).

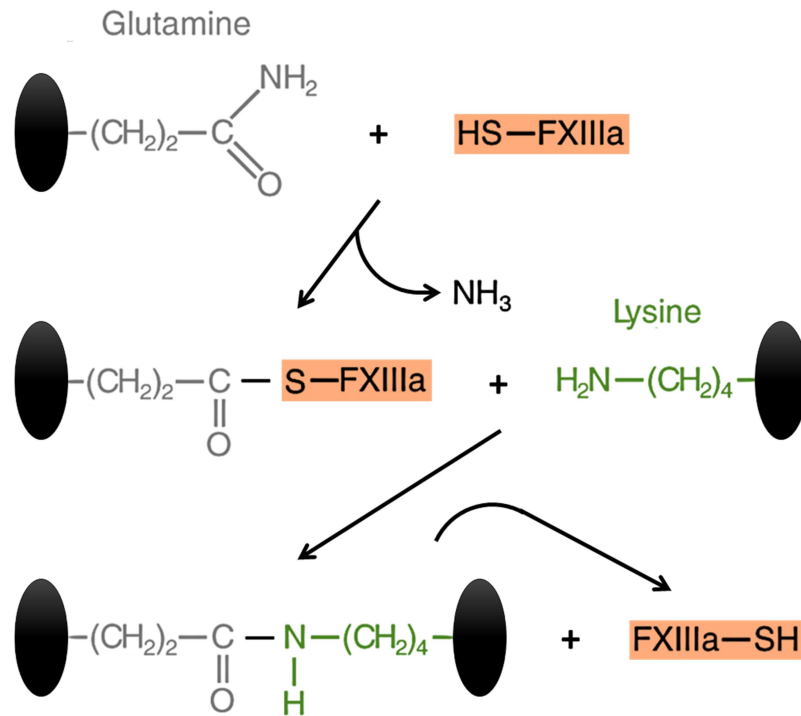


**Figure 1.3 Schematic of transglutaminase reaction of FXIII.**

*Cys314 residue of FXIIIa reacts with glutamine on one protein molecule (black oval), binding it and releasing ammonia ( $\text{NH}_3$ ) in the process. Then amino group of lysine residue on adjacent protein molecule is covalently bound to the glutamine residue, forming a  $\epsilon$ -( $\gamma$ -glutamyl)lysyl bond between and FXIIIa is released.*

Modification of fibrin by FXIII occurs in an orderly sequence; FXIII cross-linking favours  $\gamma$ -chains and occurs 10-fold faster than that of  $\alpha$ -chains (Lorand et al., 1998). This is extremely important for the protofibril longitudinal strength in the developing clot (Lorand, 2005) and is achieved through the tight end-to-end alignment of fibrin molecules (Lorand et al., 1998). FXIII also covalently cross-links fibrinolysis inhibitors such as  $\alpha_2$ -antiplasmin ( $\alpha_2$ -AP) (Sakata and Aoki, 1980), thrombin activatable fibrinolysis inhibitor (TAFI) (Valnickova and Enghild, 1998) and plasminogen activator

inhibitor (PAI) (Ritchie et al., 2000) to the  $\alpha$ -chain, which greatly increases fibrin resistance to lysis. The strongest antifibrinolytic effect comes from  $\alpha_2$ -AP cross-linking and a particular study has even suggested that all of the FXIII antifibrinolytic effect comes solely from  $\alpha_2$ -AP cross-linking (Fraser et al., 2011). Consequently, plasmin (main fibrinolytic enzyme) is inactivated by now local, cross-linked  $\alpha_2$ -AP and clot lysis is impaired. Cross-linking of  $\alpha_2$ -AP also increases its retention in the clot over time, especially during the platelet-induced clot retraction stage (Rijken et al., 2016).

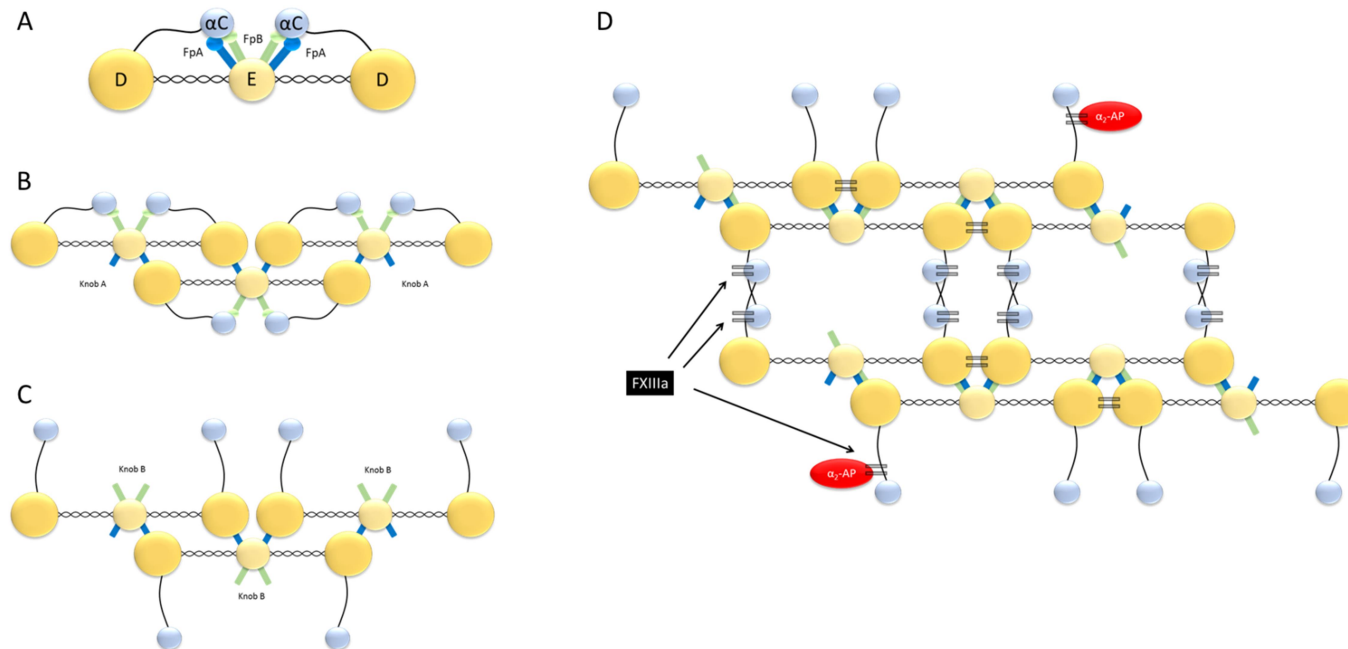


**Figure 1.4 Schematic of the conversion of fibrinogen into fibrin, and fibrin fibre formation.**

*Fibrinogen molecule contains a central E-, two distal D-regions and two  $\alpha$ C-domains (A). FpA is cleaved by thrombin and the exposed A knobs bind A holes on adjacent fibrinogen molecule D-regions, forming protofibrils (B). Next, FpB is cleaved, releasing the  $\alpha$ C-domains, and allowing  $\alpha$ -chains to open up (C). These then bind  $\alpha$ -chains of the other fibrin molecules in other protofibrils, laterally aggregating and forming fibrin fibres (D). Finally, activated FXIII covalently cross-links (denoted in “=” sign) two  $\gamma$ -chains, two  $\alpha$ -chains together, as well as fibrinolysis inhibitors to the  $\alpha$ -chain of fibrin, thus increasing the strength of the fibrin mesh.*

## **1.9 FXIII deficiency**

The importance of FXIII can be observed in patients with FXIII deficiencies and developing numerous bleeding disorders. FXIII deficiencies can be two-fold: a lack of B-subunit (and in turn A-subunit) and a lack of FXIII-A alone (Duval, 2012). Severe FXIII deficiency leads to impaired fibrin cross-linking, less resistance to fibrinolysis and mechanical instability of clots, resulting in various clinical bleeding symptoms, such as umbilical cord bleeding and intracranial bleeding (Biswas et al., 2014), impaired wound healing (Lauer et al., 2002) and miscarriage in pregnancy (Inbal and Muszbek, 2003). Protein (including FXIII) deficiencies can be classed as congenital or acquired, as well as protein deficiency due to indirect mutations affecting expression or function of FXIII.

Congenital FXIII deficiencies are usually inherited as autosomal recessive disorder and are mostly encountered in areas of high consanguinity, such as rural Middle Eastern regions (Dorgalaleh et al., 2017). The most common signs of FXIII deficiency are mucosal bleeding, pre- and post-medical intervention bleeding and predisposition to haemorrhage. More severe cases include intracranial bleeding and haemarthrosis (Hayward, 2018, Pitkanen et al., 2017). Brain haemorrhage is a leading cause of mortality in FXIII deficiency, followed by neonatal umbilical cord bleeding (Malkhassian and Sharma, 2019). Currently the prevalence of congenital FXIII deficiency in the general population is 1 per 2 million. An early detection of the disorder in heterozygous patients is very important, since the bleeding risk can be effectively managed and morbidity prevented (Biswas et al., 2014). Prophylaxis in maintaining FXIII levels above 3-5% by administering patients

10-20 U/kg FXIII every 4 to 6 weeks is preventing life-threatening spontaneous bleeding (Lorand et al., 1993).

Acquired FXIII deficiencies are mostly caused by heightened FXIII consumption and immune-mediated inhibition. Increased consumption and decreased synthesis have been identified as two possible mechanisms to reduce FXIII levels by 20% to 70% (Jain and Acharya, 2018). Certain autoantibodies have been shown to inhibit the cross-linking sites on fibrin monomers (Komaromi et al., 2011). Due to acquired FXIII deficiencies being rare, research published on the matter is not extensive, but published reports show data on acquired FXIII deficiency in haemorrhagic stroke, liver cirrhosis and inflammatory bowel disease (Malkhassian and Sharma, 2019).

### **1.10 FXIII Structure**

Plasma FXIII is a 325-kDa non-covalent heterotetrameric ( $A_2B_2$ ) protransglutaminase comprising of two catalytic FXIII-A (83.3 kDa) and two carrier FXIII-B (76.5 kDa) subunits (Ashcroft et al., 2000). Plasma concentration of the  $A_2B_2$  is approximately 22  $\mu\text{g/mL}$  and its half-life is around 9-14 days (Karimi et al., 2009, Fickenscher et al., 1991). Cellular FXIII consist only of the A-subunit dimer, however in plasma, two B-subunits act as hydrophilic shells providing stability for hydrophobic A subunits in the aqueous environment of the blood (Duval, 2012). The A-subunit molecular structure has been identified by X-ray crystallography (Yee et al., 1994), but B-subunit tertiary structure is still largely unknown. Therefore, the perceived structure of the complete heterodimeric  $A_2B_2$  FXIII molecule is only hypothetical and has largely been based on EM studies (Carrell et al., 1989) and, more recently, by elegant AFM studies (Protopopova et al., 2019). Each

FXIII-B plasma carrier peptide consists of ten repetitive “sushi” domains that are held together by double internal disulphide bonds (Carrell et al., 1989). In the circulation, the B-subunit binds to fibrinogen, helping FXIII to get close to fibrinogen and exert its effects on clot stabilisation (Souri et al., 2015). The tetramer structural model of FXIII based on crystallography (Yee et al., 1994), AFM (Protopopova et al., 2019) and EM studies (Carrell et al., 1989) consists of globular A- and strand-like B-subunits oriented symmetrically to a central axis (Figure 1). The first 37 amino acid residues at the N-terminus of an A subunit comprise a 4 kDa activation peptide (AP), which, upon Arg37-Gly38 cleavage by thrombin, is released alongside the FXIII-B subunit and converts inactive FXIII to its active (FXIII-A<sub>2</sub>, FXIIIa) form (Gupta et al., 2016). FXIII activation by thrombin also requires Ca<sup>2+</sup> to be present as a cofactor (Lorand, 1986). In circulation FXIII-B exists in approximately equal amount as a bound A<sub>2</sub>B<sub>2</sub> constituent as it is in freely circulating form (Ichinose et al., 1986). Around 99% of FXIII-A, however, exists in A<sub>2</sub>B<sub>2</sub> complex (Katona et al., 2014).

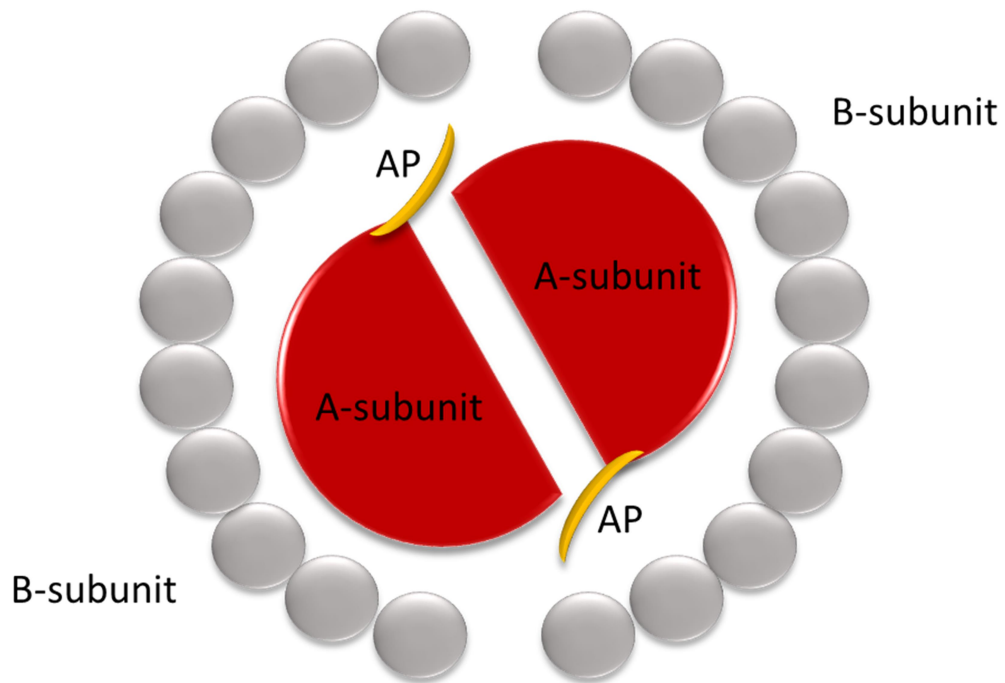


**Figure 1.5 Structural model of the FXIII A<sub>2</sub>B<sub>2</sub> tetramer.**

*FXIII-A subunit, B-subunit and activation peptide (AP) duos are arranged around a central axis of symmetry. Hydrophobic A-subunits (red) including AP's (yellow) are enclosed by flexible, hydrophilic B-subunits (grey).*

### **1.11 FXIII A and B subunits**

FXIII-A is expressed in megakaryocytes, monocytes and macrophages (Adany et al., 1987, Weisberg et al., 1987, Muszbek et al., 1988), primarily in the bone marrow (Wolpl et al., 1987). A classical secretion pathway signal sequence has not been detected in the FXIII-A gene and the extracellular secretion mechanism is presently unknown (Thomas et al., 2016, Cordell et al., 2010). FXIII-A is also stored in platelet cytoplasm as a homodimer (FXIII-A<sub>2</sub>) and gets externalised upon platelet activation by thrombin and collagen (Kattula et al., 2018, Bagoly et al., 2012, Mitchell et al., 2014). FXIII-A<sub>2</sub> dimer is also stored in a variety of different cells ranging from monocytes,

monocyte-derived macrophages to dendritic cells, chondrocytes, osteoblasts, and osteocytes (Nurminskaya and Kaartinen, 2006, Muszbek et al., 2011). The full protein sequence of FXIII-A comprises 731 amino acids, with the first 37 forming the activation peptide. FXIII-A molecule can be divided into five structural regions, with starting from N-terminus an activation peptide (amino acids 1-37),  $\beta$ -sandwich (38-184), catalytic core (185-515),  $\beta$ -barrel 1 (516-628) and  $\beta$ -barrel 2 (629-727) (Yee et al., 1994). The catalytic core is the functional domain, which carries out the transamination function of FXIII. The three most important amino acids involved in catalytic activity are called the “catalytic triad” and comprise of Cys314, His373 and Asp394 (Yee et al., 1994). Cys314 is normally hidden by the activation peptide and by Tyr560 of the  $\beta$ -barrel 1 domain, but gets exposed during activation (Komaromi et al., 2011).

FXIII-B is a glycoprotein consisting of 10 tandem sushi domains, each comprising of approximately 60 amino acids and each containing a pair of disulphide bonds (Carrell et al., 1989). Singh *et al.* performed individual cysteine mutations and demonstrated that all of the 20 disulphide bonds are important for FXIII-B secretion, function and structural stability (Singh et al., 2019). The first two N-terminal sushi domains are associated with FXIII-A<sub>2</sub>, while domains 4 and 9 are involved with the antiparallel interaction of two FXIII-B subunits (Souri et al., 2008a, Katona et al., 2014). Individual FXIII-B molecules associate together to form dimers, as shown in AFM (Protopopova et al., 2019), however it is not yet understood how and when they dissociate in order to bind to the FXIII-A molecules to form A<sub>2</sub>B<sub>2</sub>. Locating the FXIII-B finding site on the FXIII-A molecule could elucidate the association

mechanism and could potentially be useful in formulating a more efficient FXIII-A delivery to FXIII-B molecules in FXIII-A deficient patient's blood and prolong supplemented FXIII-A half-life (Bagoly and Muszbek, 2019). Interestingly, FXIII-B subunits that are unable to dimerise but possess functional sushi domains 1 and 2 can still form A<sub>2</sub>B<sub>2</sub> heterotetramers (Souri et al., 2008a, Katona et al., 2014). FXIII-B is synthesised in and secreted by hepatocytes (Nagy et al., 1988, Wolpl et al., 1987, Muszbek et al., 1988) and contains a 20 amino acid leader sequence, which indicates a classical secretion pathway (Ichinose, McMullen et al. 1986) (Webb, Coggan et al. 1989). FXIII-B circulates in excess and presumably assembles into the A<sub>2</sub>B<sub>2</sub> complex at the site of A-subunit release, however the mechanism by which this occurs has not yet been elucidated in detail. FXIII-B has been shown to accelerate fibrin cross-linking by binding to the  $\gamma$ -chain of the fibrinogen molecule and by facilitating the formation of a complex between fibrinogen, FXIII and thrombin (Souri et al., 2015). In circulation, plasma FXIII binding to fibrinogen is primarily mediated by the interaction between fibrinogen  $\gamma$ -chain C-terminal region and FXIII-B subunit (Siebenlist, Meh et al. 1996). FXIII-B is crucial for the stability of FXIII-A in circulation and it has been shown that the half-life of plasma FXIII-A is exceptionally low (~3 days) in a patient with FXIII-B deficiency (Saito et al., 1990). Recombinant FXIII-B injection in FXIII-B<sup>-/-</sup> mice increased plasma FXIII-A levels (Souri et al., 2008b), clearly indicating a role for FXIII-B in stabilising the FXIII-A subunit in circulation. However, FXIII-B deficiency still results in normal FXIII-A levels inside cells, such as monocytes, macrophages and platelets (Souri et al., 2015).

## **1.12 FXIII activation**

FXIII A<sub>2</sub>B<sub>2</sub> heterotetramer activation is a two-step process (*Figure 1.6*). The first step involves thrombin cleaving the peptide bond between residues Arg37 and Gly38 releasing the activation peptide from the N-terminus of FXIII-A (Lorand and Konishi, 1964). The second step is FXIII-B dissociation, which is dependent on Ca<sup>2+</sup> ions being present (Turner et al., 2004)

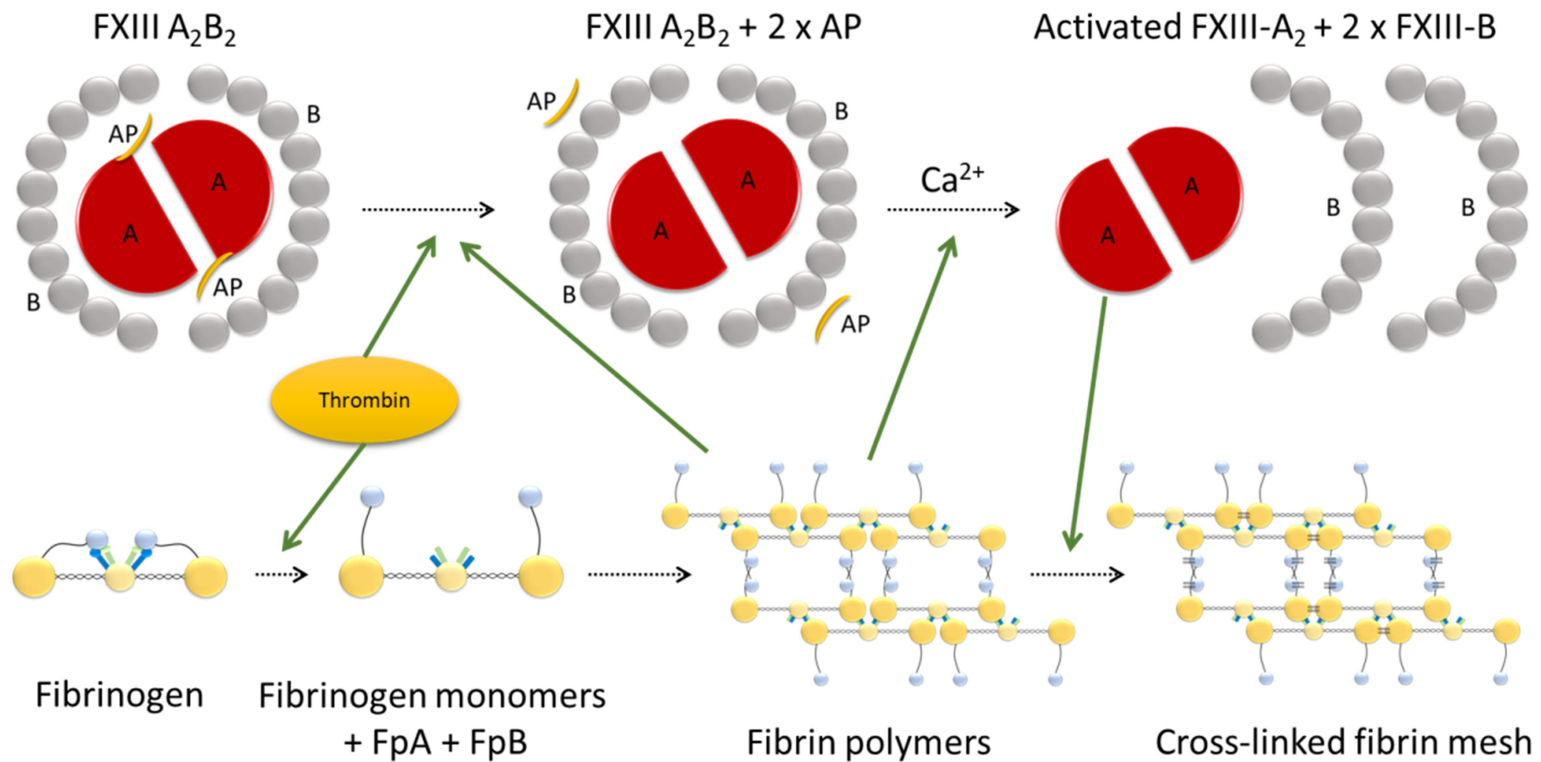


**Figure 1.6 Schematic representation of FXIII activation.**

*FXIII is activated in two steps: activation peptide (AP) cleavage by thrombin, and B-subunit dissociation from the FXIII-A dimer in the presence of calcium. Both steps are enhanced by the presence of polymerising fibrin, ensuring that FXIII activation occurs at the time of fibrin polymerisation. Activated FXIII-A dimer then covalently cross-links fibrin polymers and strengthens the mesh.*

Polymerising fibrin has been shown to reduce the concentration of thrombin needed to activate plasma FXIII by ~100 fold (Greenberg et al., 1987). Platelet FXIII-A<sub>2</sub> activation required 50% of the thrombin concentration required to activate plasma FXIII A<sub>2</sub>B<sub>2</sub>, however activation was not enhanced by the presence of fibrin (Greenberg et al., 1987). This suggests that B-subunit inhibits A-subunit cleavage in the absence of fibrin. Interestingly, only non-cross-linked fibrin polymers induce this enhancing effect and could serve to ensure that FXIIIa generation subsides after FXIII activity is not required anymore (Lewis et al., 1985). The fact that fibrin polymers and not monomers increase FXIII activation serves the purpose of minimising FXIII activation prior to the formation of FXIII substrate: polymerising fibrin (Lewis et al., 1985). Because thrombin-mediated AP cleavage timely coincides with fibrinopeptide A cleavage and fibrin polymerisation, cleaved fibrin could be a true promoter of FXIII-A AP cleavage (Janus et al., 1983). Later, it was shown that polymerising fibrin enhances activation of FXIII-A by forming a complex with FXIII-A, which is processed by thrombin much more efficiently than the uncomplexed plasma FXIII (Naski et al., 1991). The increase comes from a greatly increased thrombin affinity to FXIII, with a 30-fold decrease in Michaelis constant (Naski et al., 1991). Interestingly, the complex of thrombin, fibrin and FXIII does not only enhance FXIII activation, but also fibrin fibrinopeptide B cleavage, which progresses to fibrin  $\alpha$ -chain release and fibrin fibre formation (Naski et al., 1991). What is more, FXIII-B subunit has been shown to facilitate FXIII binding to fibrinogen (Siebenlist et al., 1996). In light of these findings it is clear, that colocalization of fibrin, thrombin and FXIII is extremely important and follows a timely manner of

activation and inhibition in order to ensure the stepwise process of the formation of the final blood clot.

FXIII-B dissociation from FXIII-A dimer is dependent on  $\text{Ca}^{2+}$  ions being present (Turner et al., 2004). Intracellular FXIII-A<sub>2</sub> is activated with thrombin and  $\text{Ca}^{2+}$  just as the plasma FXIII-A<sub>2</sub>B<sub>2</sub> (Muszbek et al., 1993), however it can also be slowly activated by  $\text{Ca}^{2+}$  alone without thrombin induced proteolysis (Polgar et al., 1990). Upon activation with thrombin and calcium, plasma FXIII-A<sub>2</sub>B<sub>2</sub> and FXIII-A<sub>2</sub> dissociate into active monomers (Anokhin et al., 2017), while B subunits form a dimeric FXIII-B<sub>2</sub> (Protopopova et al., 2019). These novel findings are in line with the crystal structure of activated cellular FXIIIa (Stieler et al., 2013) and with molecular dynamics simulations, suggesting that after the activation of plasma FXIII, the A<sub>2</sub> inter-subunit interface is weakened (Gupta et al., 2016, Dodt et al., 2016). In equilibrium ~25% of A- and B-subunits dissociate while ~75% remain as a complex (Protopopova et al., 2019, Katona et al., 2014).

### **1.13 FXIII cross-linking effects**

Both  $\gamma$ -chain and  $\alpha$ -chain cross-linking reactions have distinct effects on fibrin polymerisation, fibre formation and mechanical properties of fibre network. Complete cross-linking of fibrin fibres greatly increases their stiffness and elasticity (Helms et al., 2012). The  $\gamma$ -chain cross-linking greatly enhances the structural robustness of the clots (Standeven et al., 2007). Moreover,  $\gamma$ -chain cross-linking enhances fibrin fibre elasticity via altered force-extension relationship of the protofibrils, and slightly reduces fibre extensibility as well (Houser et al., 2010). The mechanical robustness following FXIIIa cross-linking also becomes apparent at the fibre and whole clot level, however this

appears more dependent on  $\alpha$ -chain cross-linking (Collet et al., 2005). It has been shown that in experimental conditions where  $\gamma$ -chain cross-linking is abolished, clot fibres affected by  $\alpha$ -chain cross-linking are thicker and take less time to thicken (Duval et al., 2014). Also,  $\alpha$ -chain cross-linking couples constituent protofibrils in a more compact manner and therefore stiffens the fibrin fibre (Piechocka et al., 2017, Kurniawan et al., 2014). In addition,  $\alpha$ -chain cross-linking is responsible for fibre straightening and increased fibre resistance to fibrinolysis in the absence of  $\alpha_2$ -antiplasmin (Duval et al., 2014). Clots which undergo  $\alpha$ -chain cross-linking also retain a significantly larger proportion of red blood cells when the clots contracts (Byrnes et al., 2015, Aleman et al., 2014). Interestingly, this effect is only mediated by plasma FXIIIa and not platelet FXIIIa (Kattula et al., 2018). FXIIIa cross-linking activity also affects the process of clot contraction itself. It has been shown that inhibiting FXIIIa activity reduces both the extent and velocity of clot contraction (Tutwiler et al., 2016). Cross-linking of TAFI and PAI to fibrin  $\alpha$ -chain greatly increases fibrin resistance to lysis (Sakata and Aoki, 1980). Consequently, plasmin (main fibrinolytic enzyme) is inactivated by now local, cross-linked  $\alpha_2$ -AP and clot lysis is impaired. Cross-linking of  $\alpha_2$ -AP also increases its retention in the clot over time, especially during the platelet-induced clot retraction stage (Rijken et al., 2016).

### **1.14 FXIII-A V34L**

A common human FXIII-A sequence variant (valine mutated to leucine at residue 34, V34L) has been shown to demonstrate increased FXIII activation rates through increased proteolysis of FXIII-A by thrombin and earlier release of the activation peptide (Ariens et al., 2000). These events result in

increased cross-linking activity during the first 30 min after FXIII activation by thrombin, however full pre-activation of both 34Val and 34Leu variants equalised their cross-linking activity output, showing that cross-linking activity increase for 34Leu variant only comes from increased activation rate and the mutation does not increase the enzymatic activity of FXIII-A itself (Wartiovaara et al., 2000). FXIII-A V34L has also been shown to lead to the formation of clots with denser, thinner fibrin fibres, smaller pore sizes (Ariens et al., 2000) and higher resistance to lysis (Collet et al., 2000), which is deemed prothrombotic. Clinical studies of FXIII-A V34L have indicated, however, that the 34Leu variant associates with a protective effect in most thrombotic diseases such as coronary artery disease (Voko et al., 2007), myocardial infarction (Shafey et al., 2007) and deep vein thrombosis (Wells et al., 2006), while it has been associated with an increased risk of thrombotic microangiopathies (Sucker et al., 2009), aneurysmal subarachnoid haemorrhage (Ladenvall et al., 2009) and Alzheimer's disease (Gerardino et al., 2006).

### **1.15 FXIII-A V34L sequence variant in arterial and venous thromboembolism**

In the last two decades, multiple studies have shown that the FXIII-A V34L variant is protective against deep vein thrombosis (DVT) (Wells et al., 2006, Pourgheysari et al., 2014), stroke (Elbaz et al., 2000), coronary artery disease (CAD) (Voko et al., 2007) and myocardial infarction (Shafey et al., 2007).

The first large meta-analysis including 12 studies provided evidence that FXIII-A V34L variant has a significant protective effect in VTE with an odds-

ratio (OR) of 0.63 for homozygote patients (Wells et al., 2006). Later, a study from Iran with 267 subjects also found a protective V34L effect (OR: 0.107). Additionally, a recent study has shown that FXIII supplementation stabilized venous thrombi in DVT and led to fewer PE episodes in mice, suggesting that FXIII cross-linking activity indeed protects by stabilising otherwise weaker clots, which become less prone to embolisation (Shaya et al., 2019). Furthermore, a 120 patient study in PE has shown that reduced FXIII-A levels are more prominent in PE patients, lower FXIII-A levels increase occlusion rates and PE patients have weaker clots (Kucher et al., 2003). This in a sense suggests that FXIII-A activity could be protective against PE, making a faster activated 34Leu FXIII-A variant potentially protective.

A large meta-analysis of 16 studies involving 12,399 subjects has shown that the FXIII-A V34L variant is protective against CAD with a homozygous OR of 0.89 (Voko et al., 2007). The same year, another research team published a meta-analysis of 12 studies with 8743 patients on FXIII-A V34L in acute myocardial infarction. This meta-analysis showed an OR of 0.79 for heterozygous Val/Leu patients, and a not statistically significant OR of 0.83 for homozygous patients. This non-significant result may be due to a relatively low frequency of the homozygous genotype.

The association of FXIII-A V34L with atherothrombotic ischemic stroke (AIS), however, remains controversial. In 2000, a French study on 456 patients concluded a protective effect (homozygous 34Leu OR: 0.57) of the 34Leu variant in ischaemic stroke (Elbaz et al., 2000). Later, a study in Italy showed an opposite (increase) in stroke risk (homozygous 34Leu OR: 1.25) with the 34Leu variant (Rubattu et al., 2005). There are several other studies showing

an inconclusive or absent association with ischaemic stroke, such as a 664 patient study in Austria (Endler et al., 2003) showing homozygous 34Leu OR: 1.02. Also a large meta-analysis, consisting of 8,800 patients from 16 studies found a lack of association between the 34Leu sequence variant and acute ischaemic stroke, with Leu/Leu vs. Val/Val OR: 0.90, 95% CI=0.73-1.11 (Li et al., 2012). However, a subsequent study has shown that despite 34Leu sequence variant not increasing the occurrence of ischaemic stroke, it increased the severity of the outcome, making a fatality from acute ischaemic stroke three times more likely than compared with 34Val patients (Shemirani et al., 2014). The latter study suggested that a lack of association with occurrence does not paint the full picture of FXIII effects on ischaemic stroke, and that it still remains an area for further investigation.

### **1.16 Models of thrombosis**

Different to humans, murine FXIII-A 34Leu allele represents the most common (wild-type) sequence variant in mice and the only existing variant in laboratory mice. There is 86.9% homology between the murine and human FXIII-A subunits and 77.5% between B subunits allowing comparisons between murine 34Val and 34Leu variants to be relevant for human physiology and pathology. Therefore, in order to compare 34Leu and 34Val FXIII-A variants in mice, I will utilise novel L34V mFXIII-A genetically modified mice and a recombinant version of this murine sequence variant for my PhD studies.

For *in vivo* investigations, there are various murine models for thrombosis, which utilise different modalities to initiate thrombosis in mice. Some employ optical and chemical means or their combinations, such as laser induced

(Hechler et al., 2005) or photochemical vascular injuries (Eitzman et al., 2000), while others utilise procoagulant injections, such as collagen-epinephrine (Maurice et al., 2006). A commonly used stenosis model is also used for inducing venous thrombosis (Payne and Brill, 2017), while a FeCl<sub>3</sub> vascular injury model is a commonly utilised model for arterial thrombosis (Neeves, 2015).

The stenosis model, in which a suture is ligated around the inferior vena cava, obstructing the flow by ~90% (Brill et al., 2011), is particularly suited to reproduce natural mechanisms involved in venous thrombotic pathology, where blood flow is restricted, becomes static and hypercoagulable. However, the downside of this model is the time and skill required in order to properly control the experiment, since achieved thrombus sizes as well as total occlusion rates are variable (Diaz et al., 2012). It has also been reported that side branches of occluded vessel also influence the reproducibility of the model (Brandt et al., 2014).

A complete occlusion (stasis) model is also utilised in thrombus generation, where suture is ligated completely around the inferior vena cava and reliably generates a venous thrombus (Diaz et al., 2012). However, even though stasis model results in good reproducibility and mimic human DVT formation, stasis model was not used due to formed thrombus occluding the vessel fully and not producing emboli during the formation of the thrombus. Equally, if the sutures were later opened in order to let the thrombus travel downstream, embolisation would not be studied since the emboli would not be created from blood shear stress evoked on the forming thrombus, but

rather letting the formed thrombus itself travel downstream, yielding little information on thrombus stability and dislodging dynamics.

The FeCl<sub>3</sub> injury model is a simpler, more accessible method, however, the mechanism(s) by which this agent induces thrombosis are far less understood and less likely to reflect human pathophysiology (section 5.1). However, as a highly reproducible model for intravascular clot formation, the model remains valuable depending on the aim of the study.

As primary responders to endothelial damage and exposed subendothelial constituents, platelets are a rich component of arterial (“white”) thrombi, while venous thrombi are far less populated by platelets, but rather rich in red blood cells and are named “red” thrombi (Lippi and Favalaro, 2018). For studies focussed on clot stability, the FeCl<sub>3</sub> vessel injury model remains highly suitable as the resulting clot structure is largely representative of thrombi in either the arterial or venous circulation. FeCl<sub>3</sub> generated clots are suitable in studying fibrin polymerisation effects since they contain numerous fibrin fibres, as observed with scanning electron microscope (SEM) both by our research team (*Figure 1.7*) and others (Eckly et al., 2011).

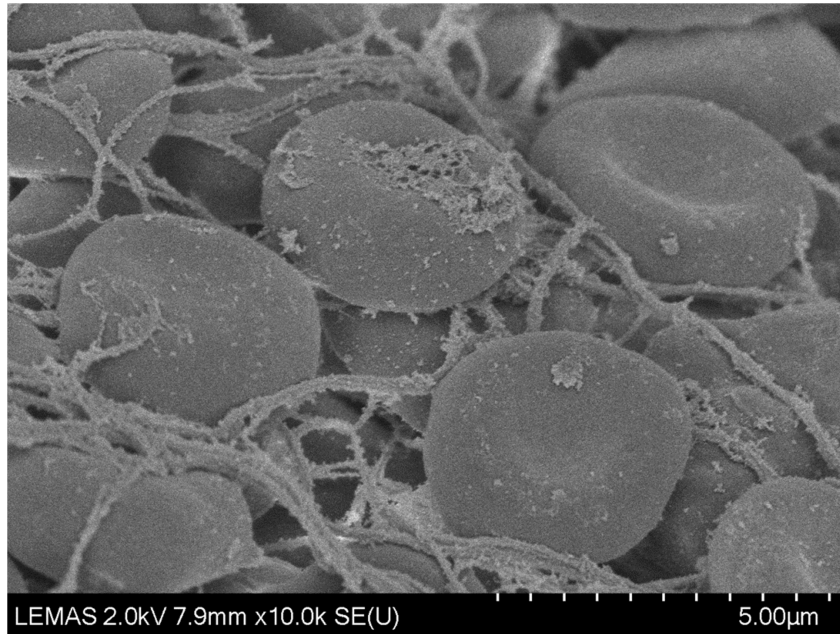


**Figure 1.7 SEM pictures of inferior vena cava thrombus generated with  $\text{FeCl}_3$  injury.**

*Fibrin fibres are covering red blood cells. Credit: surgical procedure by Dr Cédric Duval, imaging by Dr Fraser Macrae.*

However, for studies focussed on how thrombosis is triggered, the  $\text{FeCl}_3$  model may be less suitable. In the  $\text{FeCl}_3$  vascular injury model,  $\text{FeCl}_3$  is carefully applied by gently touching the vessel wall with a  $\text{FeCl}_3$  pre-soaked piece of filter paper. As firstly described by Kurz et al. (1990),  $\text{FeCl}_3$  causes redox-induced injury to the endothelial cells lining the vessel wall, leading to exposure of tissue factor on the luminal side of vessel (Li et al., 2013) and the consequent initiation of the extrinsic pathway of the coagulation cascade (Li et al., 2016a). The intra-vessel thrombus that is produced by this injury is also expected to embolise, thereby contributing to occlusion of downstream vessels and causing thromboembolic disease (Schoenwaelder and Jackson, 2015). *Figure 1.8* illustrates the principle of  $\text{FeCl}_3$  injury model. Emboli

coming from the inferior vena cava travel to lungs and result in pulmonary embolism, while emboli originating from the carotid artery result in ischaemic stroke. The  $\text{FeCl}_3$  injury model is the most widely used and most reproducible thrombosis model developed to date (Neeves, 2015).

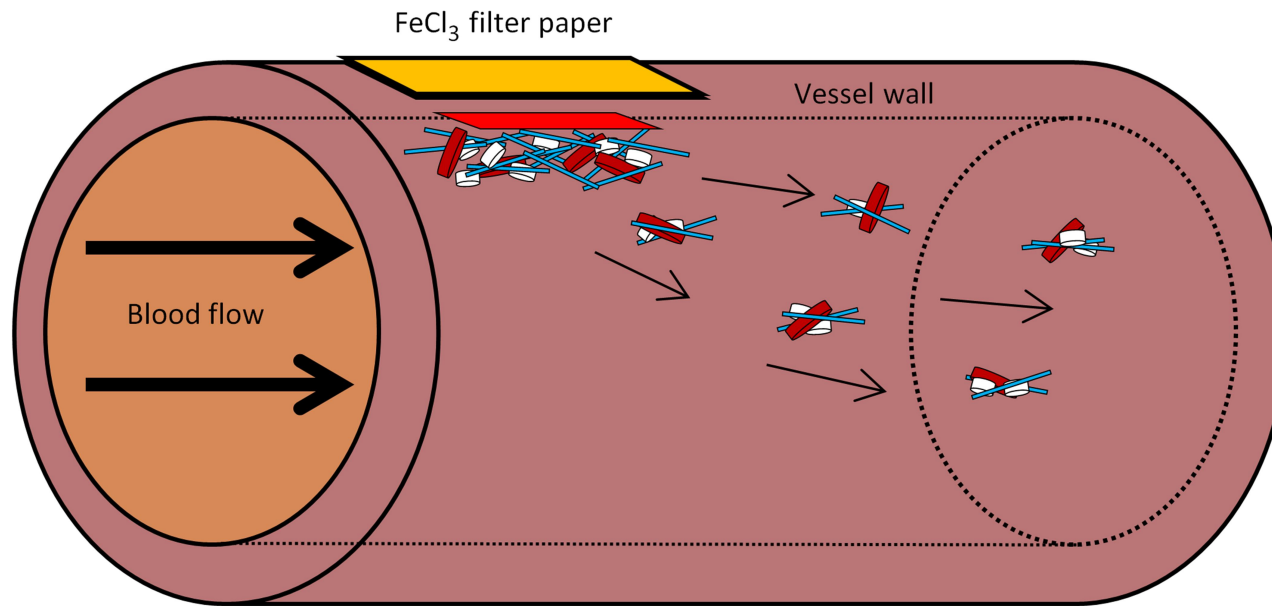


**Figure 1.8 Illustration of FeCl<sub>3</sub> vascular injury.**

*FeCl<sub>3</sub> soaked filter paper is placed onto the vessel wall (orange rectangular), FeCl<sub>3</sub> diffuses through the wall to damage the endothelium (red rectangle), which denudes to expose subendothelial layers. The blood is exposed to tissue factor expressed by subendothelial cells such as fibroblasts and smooth muscle cells, which initiates coagulation leading to fibrin formation. Endothelial damage also exposes negatively charged collagen fibres, which facilitates platelet (white disks) recruitment and initiates the contact pathway of coagulation leading to further generation of a fibrin (blue sticks) mesh and incorporation of red blood cells (red disks) into the thrombus. Parts of the local thrombus then dislodge and embolise further downstream.*

## 1.17 Study rationale and hypotheses

In light of the published literature on the V34L FXIII-A variant, with its reported protective capabilities against thrombosis, and effects on clot structure and coagulation/fibrinolysis dynamics, it was decided that a closer look at this FXIII-A variant needs to be taken using an *in vivo* model of thrombosis. The mechanisms of action of V34L in thrombotic disease has not yet been fully elucidated, and there are no other reports yet utilising a transgenic L34V animal model to study thrombosis. The first aim in my PhD studies was to confirm that known activation rate differences between human FXIII-A 34Val and 34Leu variants are reflected in analogous murine FXIII variants. Following activation rate comparison, my next aim was to study the effects on clotting, in order to investigate whether FXIII activation rate changes result in expected coagulation alterations as described in previous human FXIII studies. Finally, the main question to address in my PhD studies was whether murine thromboembolic diseases manifest differently with 34Leu and 34Val variants. In order to do so, both arterial and venous murine thromboembolism models were established and used to investigate the effects these FXIII-A variants have in thromboembolic pathology.

The main hypotheses of the PhD studies were:

- 1) Murine FXIII-A 34Leu variant is activated faster than the 34Val variant and result in more fibrin cross-linking activity.
- 2) Clots affected by mFXIII-A 34Leu variant will have thinner fibres, be more resistant to fibrinolysis, firmer, retain more red blood cells and take less time to clot than the 34Val variant affected clots.

- 3) Established differences in clot firmness, stability and resistance to lysis between murine 34Leu and 34Val variants will manifest in different dislodging, embolisation dynamics and will reflect in occurrence rates and severities of thromboembolism, presumably 34Leu variant protecting against venous thromboembolism, as reported in human clinical studies.

### **1.18 Aims**

To establish a murine FXIII-A V34L model and study its role in thromboembolic disease.

### **1.19 Objectives**

My specific project objectives were:

- 1) To generate a murine FXIII-A L34V cDNA construct using site-directed mutagenesis and express it in *E. coli* alongside the Wild-Type (34Leu) variant.
- 2) To compare activation rates of murine 34Leu and 34Val variants *in vitro* utilising a biotin incorporation assay.
- 3) To characterise the newly generated L34V genotype mice (MRC Harwell) and establish its phenotype for comparison to Wild-Type (34Leu) mouse.
- 4) To utilise mFXIII-A 34Leu, 34Val and Knock-Out (FXIII-A -/-) mice in studying their whole blood and plasma coagulation parameters, such as plasma FXIII-A antigen and fibrinogen levels, clot contraction dynamics, RBC retention, clot firmness and lysis parameters.

- 5) To establish murine  $\text{FeCl}_3$  vascular injury models for studying both arterial and venous thromboembolism.
- 6) To optimise organ optical clearing and optical sectioning methodologies using organic solvents and light sheet microscopy.
- 7) To establish an efficient and reliable emboli quantification method using Imaris image analysis software and use it to compare both venous and arterial thromboembolism dynamics between the mice variants.

## **Chapter 2 Methods**

## 2.1 mFXIII-A gene PCR amplification

Primers used in mFXIII-A gene PCR amplification were designed using a primer design program on Thermo-Fisher Scientific website <https://www.thermofisher.com/order/custom-oligo/enterSequences>.

Full designed primer sequences can be found in section 3.3.1. PCR primers were then ordered from Thermo-Fisher Scientific and resuspended in ddH<sub>2</sub>O at 100 µM.

### A) from a DNA vector:

A mix of 20 ng pCMV-SPORT6 vector (Source Bioscience, Nottingham, UK) containing a WT mFXIII-A gene, 1 µL of 10 mM dNTP mix (Thermofisher), 125 ng of both forward and reverse primers, 5 µL of 10X reaction buffer and 2.5 U Platinum<sup>®</sup> Taq DNA Polymerase High Fidelity (Invitrogen) was prepared, and 50 µL of the mix added into the thermal cycler (MJ Research; Waltham, MA, USA). PCR cycling parameters were followed according to Platinum<sup>®</sup> kit manufacturer's instructions which can be found in section 3.3.1. Successful amplification was checked and DNA fragment extraction was performed using agarose gel electrophoresis (section 2.2).

### B) from a bacterial colony:

PCR mix for one reaction included 1 µL of 20 µM primer mix, 25 µL of MyTaq<sup>™</sup> Red Mix (Bioline, London, UK), 24 µL of ddH<sub>2</sub>O and a pen point sized smear of *E. coli* from an agar plate. PCR mixes were then added into the thermal cycler (MJ Research) and run according to MyTaq<sup>™</sup> Red Mix manufacturer's guidelines. Cycling parameters used can be found in section 3.3.1. 5 µL PCR reactions were then run

in the agarose gel (section 2.2) in order to confirm successful DNA transformation into *E. coli*.

## **2.2 Agarose gel electrophoresis**

Agarose gel runs utilise an electric field to separate negatively charged DNA molecules inside an agarose gel mesh based on their size.

2 g of agarose (Bioline, London, UK) was added into 200 mL TAE buffer (40mM Tris, 20mM acetic acid and 1mM EDTA) and the mix was microwaved until boiling point, mixed and boiled again. 10 µL of 10 mg/mL ethidium bromide (Sigma-Aldrich, Dorset, UK) was added to the mixture, mixed and poured into the gel making frame. The frame was then left to cool at 4°C until agarose mixture solidified into gel. The gel was transferred into a gel tank and 5 µL of DNA samples, premixed with 6X gel loading dye (appendix 3), as well as 10 µL HyperLadder™ 1kb molecular weight standard (Bioline, London, UK), were loaded into the gel. For DNA band extraction up to 45 µL of the samples were used. A 100 V current was applied for 1 h. Gels were imaged using G:Box XR5 imager (Syngene, Cambridge, UK) and Genesys (California, US) software.

## **2.3 DNA recovery from agarose gel**

DNA recovery is based on the ability of DNA to bind to silica membranes in the presence of chaotropic salts and to be eluted with water.

Agarose gel parts containing the DNA band of interest were identified under UV light and cut out using a scalpel. Wizard SV® Gel and PCR Clean-Up System kit (Promega; Wisconsin, USA) was then used to extract the DNA

from agarose gel, following kit manufacturer's instructions for using vacuum pump.

## **2.4 TA cloning**

TA cloning technique (also known as "T" or "rapid" cloning) utilises DNA topoisomerase I to insert a DNA sequence ending in adenine (A) nucleotide on the 3' end into a recipient vector having complementary thymine nucleotide (T) tail (*Figure 2.1*). The technique utilises the Taq DNA polymerase, which unlike most DNA polymerases does not carry out 3' to 5' proofreading activity. During PCR, the lack of proofreading activity results in Taq DNA polymerase adding a single A on the 3' end of the gene insert, which is ready to bind the T on the recipient vector. Post TA cloning, the resulting double stranded circular DNA allows for increased efficiency in DNA restriction by restriction enzymes.

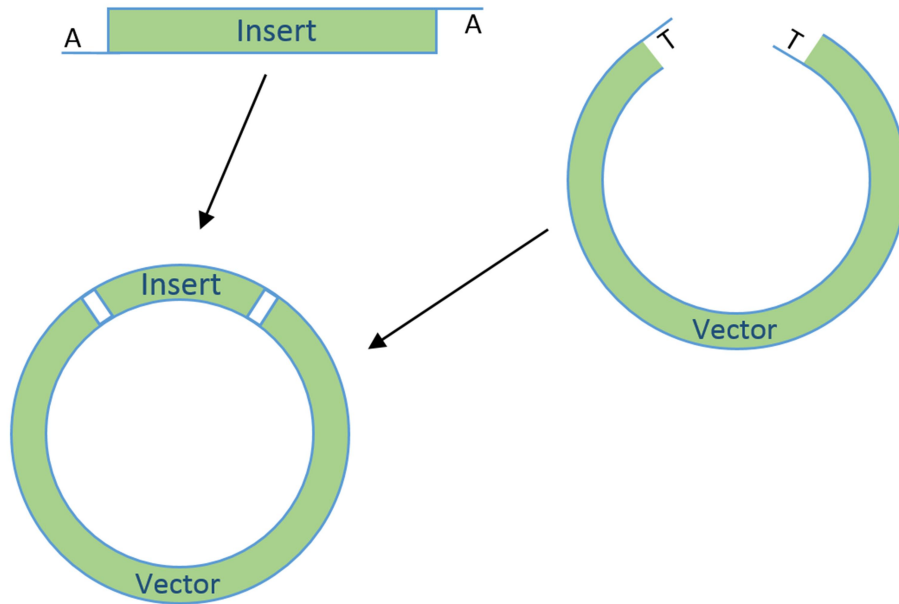


**Figure 2.1 Explanatory schematic of a TA cloning technique.**

*Gene insert sequence ends in adenine (A) nucleotide on the 3' end, while recipient vector contains thymine (T) nucleotide on the recipient 3' end. Complementary sequence match allows gene fragment to be inserted into the vector by DNA topoisomerase I.*

TOPO TA cloning kit (Thermo-Fisher Scientific) was used to perform TA cloning. 1  $\mu\text{L}$  of 10 ng/ $\mu\text{L}$  pCR2.1-TOPO (further: pCR 2.1) vector, ddH<sub>2</sub>O, salt solution (inside the kit) and 0.5-4.0  $\mu\text{L}$  PCR product were mixed in a final volume of 6  $\mu\text{L}$  and incubated at 4°C for at least 30 min. Ratios of 3:1, 1:1 and 1:3 of gene insert (PCR product) to pCR 2.1 vector were used in order to increase bacterial transformation success rate. **Equation 2.1** was used to calculate the amount of insert DNA in ng needed for a 1:1 insert:vector ratio in the ligation reaction:

$$\text{Gene insert amount needed} = \frac{10 \text{ ng of vector} * \text{Insert length in base pairs}}{\text{Vector length in base pairs}}$$

***Equation 2.1 Gene insert amount calculation for insert vector ligation.***

## **2.5 *E. coli* Transformation, Growth and Glycerol Stock**

### **2.5.1 Transformation**

Lysogeny Broth (LB) Agar (LabM; Bury, UK) (5 g/L Yeast extract, 5 g/L NaCl, 12 g/L Agar, 10 g/L Tryptone, topped up with ddH<sub>2</sub>O) was autoclaved at 121°C for 15 min, cooled down to 50°C and 100 µg/mL ampicillin (Sigma-Aldrich), or 50 µg/mL kanamycin (Sigma-Aldrich) was added. 20 mL of LB agar was then poured into 10 cm sterile petri plates (Corning, High Wycombe, UK) and left to solidify for 30 minutes. SOC medium (Thermofisher) was then defrosted and heated to 42°C in a thermal bath. Competent bacteria cells were thawed on ice for 30 minutes. 50 µL of bacterial cells were then added to 50 mL falcon tubes (Greiner bio-one, Stonehouse, UK) together with up to 20 µL of DNA. The reaction tube was gently swirled and incubated on ice for 30 min. Bacteria there then “shocked” by incubating the transformation tubes at 42°C for 45 seconds and placing on ice for 2 minutes. 500 µL of warm SOC media (Thermofisher) was then added to the tubes and incubated at 37°C, shaking at 220 rpm for 1 hour. Three different volumes of transformed bacteria (50 µL, 150 µL and 300 µL) were spread on each agar plate surface until dry. Plates were wrapped in

paraffin film and incubated overnight at 37°C. In the morning, grown colonies were observed and plates were stored at 4°C.

### **2.5.2 Transformation quality assurance**

Post agar plate culturing (section 2.5.1), half of each selected bacterial colony was taken to perform a PCR reaction (section 2.1 B), and run through the agarose gel (section 2.2) in order to confirm that 2196 base pair mFXIII-A DNA insert was successfully inserted in the vector and transformed.

## **2.6 Bacterial growth**

LB (LabM; Bury, UK) (5 g/L Yeast extract, 5 g/L NaCl, 10 g/L Tryptone, topped up with ddH<sub>2</sub>O) for bacterial growth was first made and 100 µg/mL of ampicillin, or 50 µg/mL kanamycin, was added to 5 mL of LB broth in 50 mL falcon tubes. Multiple individual colonies from the transformation (section 1.9.1) step, which have been confirmed to contain an insert (section 2.5.2), were added into separate 50 mL tubes and incubated for 4 hours at 37°C, 220 rpm. 1.6 ml of each culture growth was then distributed equally into three 50 mL tubes containing 5 mL LB broth + antibiotic and incubated at 37°C, 220 rpm for 16 hours. In cases of bulk growth for higher DNA extraction yields, each 5 mL culture growth was added into their own 250 mL LB broth + antibiotic mixes instead. At each 37°C, 220 rpm step, tubes or flasks used were not sealed shut in order to allow airflow.

1 mL of grown bacteria culture was added into a 2 mL tube and mixed with 1 mL of Glycerol (Fisher Scientific, Loughborough, UK). Glycerol stock tubes were stored at -80°C for later use.

## **2.7 DNA extraction**

The overnight bacterial growth cultures were spun down using a Rotanta 460 Lab Benchtop centrifuge (Hettich, Massachusetts, USA) at RT, 4650 g for 3 min and product pellet was processed using the QIAprep® Spin Miniprep Kit (Qiagen, Manchester, UK), according to the manufacturer's instructions. The extraction was carried out using centrifugation steps and Nuclease-free water for DNA elution. The concentrations of DNA acquired were determined using a Nanodrop ND 1000 spectrophotometer (Fisher Scientific) at A280nm. Purified DNA was stored at -20°C for future restriction digestion and vector ligation. Some of the plasmid DNA was sent for sequencing (section 2.11) in order to assess the integrity of the gene sequence. In cases of bulk DNA extraction from 250 mL bacterial growth media, PureYield™ Plasmid Maxiprep System (Promega) was used instead, following manufacturer's instructions for vacuum use. The kit allows endotoxin clearance from the cell lysate and purifies DNA based on binding to a silica membrane, washing through with ethanol and eluting the DNA product in water.

## **2.8 Restriction digestion**

Restriction enzymes cleave double stranded DNA at specific restriction sites, thereby allowing both a gene insert and a recipient vector to be primed for ligation.

10µL restriction reaction mixes consisted of 1 µg vector DNA, 20 U restriction enzyme and 1X CutSmart Buffer (New England Biolabs). Restriction reaction was carried out in a thermal cycler (MJ Research) at 37°C for 1 hour then

stored at 4°C until further use. Experiment specific restriction digest details can be found in section 3.3.3.

## **2.9 Gene – vector ligation**

Gene insert and vector post restriction digestion were run onto and extracted from an agarose gel and were ligated together in quantity ratios of 5:1, 3:1, 1:1, 1:3 and 1:5. Ligation reaction consisted of: 100 ng of vector, X ng of insert according to the insert:vector ratio, 1.0 U T4 ligase and 1X T4 buffer (Promega) to reach a total volume of 20 µL. *Equation 2.1* (section 2.4) was used to calculate the amount of insert DNA in ng needed for a 1:1 insert:vector ratio in the ligation reaction. The ligation mix was stored overnight at 4°C. Experimental specific ligation details can be found in section 3.3.3.

## **2.10 Site-directed mutagenesis**

Site-directed mutagenesis utilises designed PCR primers, which contain a desired nucleotide swap. The resulting PCR product sequence thereafter contains the introduced mutation.

Primers used in site-directed mutagenesis were designed using a primer design program on the Agilent website ([www.agilent.com/store/primerDesignProgram.jsp](http://www.agilent.com/store/primerDesignProgram.jsp)). Primer sequences can be found in section 3.3.5. SDS-PAGE purified primers were then ordered from Thermo-Fisher Scientific and resuspended in ddH<sub>2</sub>O at 100 µM. QuikChange II Site-Directed Mutagenesis Kit (Agilent Technologies, Stockport, UK) was used to perform mutagenesis on mFXIII-A gene in pLIVE expression vector (section 3.3.5). A mix of 20 ng pLIVE vector (containing mFXIII-A gene), 1 µl of 10 mM dNTP

mix, 1X reaction buffer, 125 ng of both forward and reverse primers and 2.5 U *PfuUltra* High-Fidelity DNA Polymerase (Agilent) was prepared and 50  $\mu$ L of the mix added into the thermal cycler (MJ Research; Waltham, MA, USA). PCR cycling parameters were followed according to the QuikChange<sup>®</sup> kit manufacturer's instructions and can be found in section 3.3.5. Following the PCR reaction, 1  $\mu$ L of 10 U/ $\mu$ L Dpn I restriction enzyme was added to the PCR mix for 1 hour at 37°C in order to digest the parental DNA in the mix.

## **2.11 DNA sequencing**

DNA sequencing was performed after most PCR amplification, site-directed mutagenesis and ligation product transfection experiments. Sequencing confirmed, that each step of the recombinant mFXIII-A construct formation was performed using a correct mFXIII-A gene sequence without any newly introduced, unwanted mutations in the gene.

Sequencing was carried out by DNA Sequencing and Services, Dundee University, UK (<https://www.dnaseq.co.uk/>). 30  $\mu$ L of 80-200 ng DNA and 3.2 pmole of each primer were sent per reaction. Sequences of primers used can be found in section 3.3.6. Sequence checking was performed using Clustal Omega DNA sequence alignment tool:

(<http://www.ebi.ac.uk/Tools/msa/clustalo/>).

## **2.12 Expression and purification of recombinant GST-mFXIII-A protein from *E. coli***

### **2.12.1 Expression**

10  $\mu$ L of BL21-GOLD (DE3) *E. coli* cells transformed with pGEX-6P-1 34Leu or 34Val GST-mFXIII were grown from glycerol stock overnight at 37°C, 225 rpm in starter cultures, comprising of 180 mL autoclaved Terrific Broth (12 g/L Tryptone, 24 g/L Yeast Extract, 8 mL/L Glycerol), 20 mL autoclaved phosphate buffer (23.2 g/L  $\text{KH}_2\text{PO}_4$ , 164 g/L  $\text{K}_2\text{HPO}_4 \cdot 3\text{H}_2\text{O}$ ), 200  $\mu$ L of 100 mg/mL ampicillin.

The following day, 200 mL starter cultures were transferred into 1800 mL of autoclaved Terrific Broth, 200 mL phosphate buffer, and 2 mL of 100 mg/mL ampicillin mix and left incubating at 37°C, 180 rpm. When the resulting 2.2L culture reached the absorbance of 1.0 OD at A620 (measured with PowerWave HT spectrophotometer, Biotek; Swindon, UK), 2.2mL of 1M Isopropyl  $\beta$ -D-1-thiogalactopyranoside (IPTG; Sigma-Aldrich) was added, temperature was reduced to 30°C and the culture was left to shake overnight at 180 rpm. Adding IPTG allowed the release of a gene repressor from the lac operon and initiated mFXIII-A gene transcription.

Following overnight culturing, bacteria were centrifuged at 4,500 g, 4°C, for 10 min using an Avanti J-26XP Series High-Speed Centrifuge (Beckman Coulter; High Wycombe, UK). Culture supernatants were then discarded and pellets resuspended in 180 mL ice cold PBS (Sigma-Aldrich; 140 mM NaCl, 10 mM phosphate buffer, 3 mM KCl, pH 7.4). The samples were centrifuged at 4,500 rpm, 4°C for 30 min and pellets were dry-frozen at -20°C until purification.

### **2.12.2 Purification**

Purification of Glutathione S-transferase (GST) tagged mFXIII-A protein was performed using GSTrap FF Glutathione Sepharose column (GE Healthcare and Life Sciences, Little Chalfont, UK) and the process was carried out as follows:

Frozen culture pellets from the expression stage were resuspended in 176 mL ice cold PBS for 120 min at RT, stirring at 200 rpm using a magnetic stirrer. 1.76 mL of 100 mg/mL Lysozyme (Sigma-Aldrich) as well as 177.6  $\mu$ L of 1 M Dithiothreitol (Thermofisher) were added into the resuspension solution and left to stir for another 30 min at RT, 200 rpm in order for cell lysis to take place. Next, 177.8  $\mu$ L of 2 mg/mL Aprotinin, 177.8  $\mu$ L of 1 mM Pepstatin A (Sigma-Aldrich), 444  $\mu$ L of 4 mM Leupeptin (Sigma-Aldrich) and 0.138 g of Benzamidinium hydrochloride (Sigma-Aldrich) were added and the lysate was stirred gently for another 30 min at 4°C, 200 rpm while the protease inhibitors helped to stop endogenous proteases cleaving mFXIII-A. Protease inhibition proceeded by adding 444  $\mu$ L of 100 mM PMSF (Thermofisher), 898  $\mu$ L of 10% Sodium Deoxycholate (Sigma-Aldrich) and stir-incubating the lysate for another 30 min at RT, 200 rpm. Solubilisation of GST-mFXIII-A was then aided by forcibly adding 9 mL of 20% Triton X-100 (Sigma-Aldrich) and stirring the solution at 4°C, 200 rpm. 94.5  $\mu$ L of 10 mg/mL DNaseI (New England Biolabs) and 945  $\mu$ L of 1 M MgCl<sub>2</sub> (Sigma-Aldrich) were added and the solution was stirred at 4°C for 10 min. DNA degradation was stopped by adding 2.29 mL of 0.5 M EDTA (Sigma-Aldrich). Samples were centrifuged at 22,000 g at 4°C for 20 min using Avanti J-26XP Series High-Speed Centrifuge (Beckman Coulter), 2 g of Streptomycin

Sulphate (Sigma-Aldrich) was mixed into the supernatant and the solution was centrifuged on the same settings once more. The final supernatant was topped up to 300 mL with PBS, filtered through 0.22 µm Express™PLUS filter (Merck Millipore; Watford, UK), degased and loaded onto GSTrap FF Glutathione Sepharose column overnight using ÄKTAprime (GE Healthcare and Life Sciences) system (section 3.3.7). The lysate bottle was covered with ice blocks over the duration of loading. The following morning the GSTrap FF column was stored horizontally at 4°C until late afternoon, then 16 mL GST Equilibration buffer (buffer list can be found in section 3.3.7) containing a vial of 500 units PreScission™ Protease (Fisher Scientific) mix was slowly injected into the column and left incubating overnight at 4°C in a horizontal position. The PreScission™ step was skipped when the desired purification product was GST-bound mFXIII-A fusion protein. The following day, the column was connected to ÄKTAprime for elution (section 3.3.7). mFXIII-A (as well as GST) fractions were collected, pooled, concentrated using 30,000 MWCO Vivaspin 20 Columns (Sigma-Aldrich) at 4°C, 4,500 g in a Rotanta 460 Lab Benchtop centrifuge (Hettich, Massachusetts, USA). The final protein concentration was measured using BCA assay (section 2.14). Aliquots of desirable volumes of both mFXIII-A-34Val and mFXIII-A-34Leu were stored at -80°C until further use.

## **2.13 SDS-PAGE gels**

The SDS-PAGE gel technique uses an electric field to separate proteins in a Bis-Tris gel mesh. Proteins are not innately equally charged, therefore negatively charged sodium dodecyl sulfate (SDS) molecule is first mixed with the proteins, so they move towards the positive electrode in a size-

dependent manner regardless of their charged amino acid count. SDS binds to the proteins in proportion to their relative molecular mass making separation by size accurate.

5 µg protein samples containing 1X NuPAGE™ Sample Reducing Agent and 1X NuPAGE™ LDS Sample Buffer (ThermoFisher; Loughborough, UK) were first heated denatured at 70°C for 10 min, incubated on ice for 2 minutes and centrifuged briefly at 14,500 g in an Eppendorf MiniSpin Plus (Hamburg, Germany) microcentrifuge. 500 mL of 1X NuPAGE™ MES (ThermoFisher) buffer was prepared and poured into the gel tank. 20 µL of denatured protein samples alongside 10 µL of Precision Plus Protein™ Dual Color Standards (Bio-Rad Laboratories; California, USA) were run in NuPAGE™ 4-12% Bis-Tris Gel (Invitrogen; California, USA) for 1 hour at 200V. Post run, gels were washed with double distilled water (ddH<sub>2</sub>O) and stained with GelCode Blue Stain (ThermoFisher) for 1 hour at room temperature. The gel was then left washing in a shaking ddH<sub>2</sub>O filled box for an hour, with ddH<sub>2</sub>O being changed every 15 minutes. The final wash step was left overnight at 4°C and the gel was imaged the following day using G:Box XR5 imager (Syngene) and Genesys (California, US) software.

## **2.14 BCA assay**

The bicinchonic acid assay (BCA or Smith assay) allows quantification of the total protein amount in the sample. During the BCA assay, Cu<sup>2+</sup> is added to the sample, which is reduced to Cu<sup>+</sup> ions by peptide bonds in protein. Cu<sup>+</sup> is then chelated by added bicinchonic acid and the resulting product complex is purple (562 nm). Since both copper related reactions are dependent on the

amount of protein present in the sample, total protein concentration can be determined by comparing sample colour intensity to a protein standard.

The samples were diluted 1:10 in ddH<sub>2</sub>O in a 96 well plate (Greiner Bio One Ltd; Stonehouse, UK) and standards were prepared in serial dilutions of 1000 µg/mL bovine serum albumin (BSA) protein (1000, 800, 600, 400 and 200 µg/mL) (Sigma-Aldrich). 25 µL of each standard and samples were dispensed to the plate wells and ddH<sub>2</sub>O was used as a blank. All samples and standards were loaded in duplicate. 200 µL of 50:1 ratio of bicinoninic acid:copper II sulphate solution (Bicinoninic Acid Kit for Protein Determination; Sigma-Aldrich) was added to plate wells and incubated at 37°C for 30 minutes. The plate was read on a Bio-Tek Powerwave plate reader at 562 nm and the standard curve was determined by plotting the concentration of the standards against the absorbance minus the blank absorbance value. mFXIII-A elution sample total protein concentration was derived by relating sample absorbance to the standard curve.

### **2.15 Recombinant mFXIII-A activation rate assay**

The FXIII-A activation rate assay is based on the quantification of the amount of GST-activation peptide (GST-AP) cleaved by thrombin from the GST-mFXIII-A fusion protein at different time-points. Fusion protein is expressed with a GST bound to the N-terminus of FXIII-A, therefore, when thrombin cleaves off the 37 residue activation peptide, the 26 kDa GST is removed as well. This GST-AP loss over time is observed on the SDS-PAGE gel.

0.5 mL Eppendorf tubes were labelled for 0, 1, 2, 5, 10, 20, 40, 60 and 120 minute time-points and 10 µg (15 µL) of recombinant GST-mFXIII-A diluted in Tris-Buffered Saline (TBS; 50 mM Tris-Cl, 150 mM NaCl, pH 7.4) was added into the tubes. 5 µL of activation mix consisting of 100 mM CaCl<sub>2</sub> and 2.5 U/mL murine thrombin was then added to all time-point tubes as quickly as possible, tubes were vortexed and put onto 37°C heat block. At each time-point, 10.5 µL of stop solution (7.5 µL of 4x Loading Buffer + 3 µL of 10x Reducing Agent) was added into corresponding tubes, which were put onto a 90°C heat block for 10 minutes. Time-point “0” tubes contained stop solution prior to adding the activation mix to serve as negative control. After heating, the tubes were put on ice awaiting SDS-PAGE gel run. The SDS-PAGE run was carried out as described in Methods section 2.13 while loading all 30 µL of each sample.

Band intensities of the 83 kDa species (activated FXIII-A) were measured 3 times using GeneTools software (Syngene; Bangalore, India), and the averages were used as data. Band intensities were blanked by subtracting time-point 0 values from each time-point value. Band intensity values were also divided by the intensity of the ~65 kDa host cell protein band at respective time-points in order to normalise each time-point value, and adjust for differences in loading amounts. Adjusted intensity amounts were plotted against time and the natural logarithmic function ( $y = \ln(x^a) + c$ ) was fit to the chart using Excel (Microsoft; Redmond, WA, USA). The exponents (“a”) of both variants were treated as rate and 34Leu activation rate was expressed as % value of 34Val average rate. Paired two-tailed student’s T-test was

carried out using Prism 7 (GraphPad; San Diego, CA, USA). Experiments were carried out 3 times.

## **2.16 Mice variants and animal husbandry**

All procedures were approved by the University of Leeds Ethics Committee and performed under the Home Office Animals (Scientific Procedures) Act 1986. Mice were kept in individually ventilated cages, same gender per cage, no more than 5 mice per cage after weaning, on 12h light and dark cycles, at 20-22°C with 55-60% humidity.

C57BL/6 background FXIII-A Knock-Out (F13A1<sup>-/-</sup> or FXIII<sup>-/-</sup>) mice were obtained by backcrossing 10 generations of CBA/129 F13A1<sup>-/-</sup> (Lauer et al., 2002) and C57BL/6 WT mice.

C57BL/6 background FXIII-A L34V (34Val) mice were obtained from Genome Editing Mice for Medicine (GEMM; MRC Harwell Institute, Oxford, UK). These mice were generated using CRISPR/Cas9 gene editing method.

C57BL/6 background Wild-Type FXIII-A (34Leu) mice were obtained from MRC Harwell Institute (Oxford, UK).

Experiments on mice were performed at their age of 7 weeks ( $\pm$  3 days).

## **2.17 Murine blood collection and plasma preparation**

Mice, aged 7 weeks ( $\pm$  3 days), were first anaesthetised with 3% isoflurane and 2% oxygen gas mix. 450  $\mu$ L of blood was then drawn from the exposed inferior vena cava (IVC) into a 50  $\mu$ L 109 mM trisodium citrate (Sigma-Aldrich) solution. Immediately after blood taking, animals were sacrificed by cervical dislocation. Blood was then immediately used for whole blood

experiments, while plasma was collected by centrifuging whole blood (14,000 g, 10 min).

## **2.18 Growth curve**

Both Wild-Type mFXIII-A (34Leu) and mFXIII-A-L34V (34Val) variant mice were weighed weekly for 10 weeks, starting on day 21 since birth. There were 10 mice, 5 per gender in each group.

Mice were statistically compared using unpaired student's T-test (Prism 7 software).

## **2.19 Blood clot contraction, serum haemoglobin and clot weight**

At first, glass tubes (BIO/DATA corp.; Horsham, PA, USA) were siliconised for 10 minutes using Sigmacote<sup>®</sup> siliconising reagent (Sigma-Aldrich; St. Louis, MO, USA) and rinsed with ddH<sub>2</sub>O. Clotting of FXIII-/-, 34Val and 34Leu mice blood (n=10) was then initiated in the glass tube using: 460 µL whole blood diluted with saline 1/4 and 40 µL of the activation mix consisting 1 pM final tissue factor PPP-Reagent (Thrombinoscope B.V.; Maastricht, Netherlands) and 10 mM final CaCl<sub>2</sub> (Fisher Scientific; Hampton, NH, USA). Clot formation and contraction were left to occur at 37°C for 2 hours. The experiments were performed in duplicate assessing two glass tubes per mouse.

### **2.19.1 Clot contraction**

Photographs of clots were taken at time-points 0, 30, 60, 90, and 120 minutes. Images were analysed using ImageJ software (publicly available; creator: Wayne Rasband) and clot volumes derived using the **Equation 2.2**.

Total solution in the glass tube volume was known (500  $\mu\text{L}$ ) and digital clot/solution volumes were calculated from the images using diameter (d) and height (h) measures as well as a cylinder volume.

$$\text{Actual clot vol. } (\mu\text{L}) = \frac{\text{measured digital clot vol. (Pixels}^3) \times \text{total actual solution vol. (500 } \mu\text{L)}}{\text{measured total digital solution vol. (Pixels}^3)}$$

**Equation 2.2 Equation for clot volume calculation from images.**

$$\text{Digital vol. (Pixels}^3) = \pi \left(\frac{d}{2}\right)^2 h$$

**Equation 2.3 Cylinder volume equation.**

*Cylinder volume equation used to calculate digital volumes of clots and blood from images taken. Both the diameter (d) and height (h) was measured in pixels.*

Clot volumes from FXIII-/-, 34Val and 34Leu mice (n=10) were statistically compared using Two-Way ANOVA and Tukey's multiple comparisons tests (Prism 7 software).

### **2.19.2 Clot supernatant haemoglobin**

At time-points 0, 30, 60, 90, and 120 minutes, 20  $\mu\text{L}$  of gently resuspended supernatant was diluted with 30  $\mu\text{L}$  ddH<sub>2</sub>O, vortexed and kept at room temperature for 20 minutes. Water entering red blood cells via osmosis burst the cells open extruding haemoglobin into the solution. Resulting solutions were then transferred to Greiner 384 Well Plate (Sigma-Aldrich; St. Louis,

MO, USA) and read at wavelengths 380 nm, 415 nm and 450 nm. Supernatant haemoglobin amounts were then derived using the adapted Harboe method **Equation 2.4** (Malinauskas, 1997).

$$Hb (g/dL) = \frac{(1/d)(167.2A_{415} - 83.6A_{380} - 83.6A_{450})D}{1000}$$

$d = \text{pathlength in cm (0.2 cm)}$

$D = \text{serum dilution factor } \left(\frac{2}{5}\right)$

**Equation 2.4 Equation for clot supernatant haemoglobin calculations.**

Time-point 30, 60, 90 and 120 min values were divided by time-point 0 values and multiplied by a 100 in order to express haemoglobin values as % of initial value. Haemoglobin values were normalised in order to compensate for natural variation in red blood cell and haemoglobin levels in mice. Haemoglobin values between mice variants were compared using Two-Way ANOVA and Tukey's multiple comparisons tests (Prism 7 software). n=10.

### **2.19.3 Clot weight**

After 120 minutes of whole blood clotting, supernatant was removed and clots were dried and weighed. Clot weights between mice variants were compared using One-Way ANOVA and Tukey's multiple comparisons tests (Prism 7 software). n=10 (n=9 for FXIII<sup>-/-</sup>, because the clot of the first FXIII<sup>-/-</sup> mouse clot was lost and not weighed).

## 2.20 Thromboelastometry

Rotational thromboelastometry is performed by rotating a pin, which is submerged into the whole blood sample. As blood clots, it becomes more viscous and increasingly resists the rotating pin. Measurement of this resistance is used to derive coagulation metrics of the blood sample.

Thromboelastometry was performed using freshly collected FXIII<sup>-/-</sup>, 34Val and 34Leu (n=10) mouse blood (section 2.17), ROTEM<sup>®</sup> Pup & Pin mini cups (Tem Innovations GMBH; Munich, Germany), EXTEM<sup>®</sup> (tissue factor and heparin inhibitor), STARTEM<sup>®</sup> (CaCl<sub>2</sub>), FIBTEM<sup>®</sup> (platelet inhibitor cytochalasin D) kit solutions, 20 nM mouse tPA (2B Scientific; Heyford, UK) and ROTEM<sup>®</sup> *delta* thromboelastometer. Three different conditions were run for each blood sample: a normal clotting condition, a clotting / lysis condition and a clotting condition with platelet inhibition (Table 2.1).

**Table 2.1 ROTEM<sup>®</sup> conditions and reagent volumes used**

Condition	Reagent	Volume (μL)
Clotting	EXTEM	7.0
	STARTEM	7.0
	Blood	105.0
Clotting / Lysis	EXTEM	7.0
	STARTEM	7.0
	Blood	103.3
	Murine tPA	1.7
Platelet inhibition	EXTEM	7.0
	FIBTEM	7.0
	Blood	105.0

First all the reagents were added at the base of the cup and on the opposite sides so that reagents would not mix. Then, blood was added, pipetted up and down once and immediately slid into the ROTEM measurement

machine. ROTEM measurements were recorded for at least 2.5 hours. Clotting Time (CT), Mean Clot Firmness (MCF) and Lysis Time (LT) were derived from ROTEM charts.

Each of these parameters were analysed between mice variants using One-Way ANOVA and Tukey's multiple comparisons tests (Prism 7 software). n=10 (n=6 for FIBTEM FXIII<sup>-/-</sup>, because 4 clots have not formed).

## **2.21 Mice plasma experiments**

Plasma from 10 Wild-Type mFXIII-A (34Leu), 10 mFXIII-A-L34V (34Val) mice and 9 mFXIII-A FXIII<sup>-/-</sup> mice were analysed in multiple *in vitro* and *in vivo* assays. A single FXIII<sup>-/-</sup> male mouse was omitted from all analyses due to its mFXIII-A antigen levels being similar to 34Leu and 34Val mice, most likely due to a genotyping error.

## **2.22 Plasma FXIII antigen levels**

Plasma FXIII activity is dependent on the amount of FXIII present, therefore western blotting was used to determine mFXIII-A antigen levels in 34Leu, 34Val and FXIII<sup>-/-</sup> mice plasma. A high molecular weight (HMW) IgG band was used as a loading control. Samples constituting of 10 µL 1/200 plasma, 3.75 µL of NuPAGE™ LDS Sample Buffer and 1.5 µL of 10X NuPAGE™ Sample Reducing Agent (ThermoFisher; Loughborough, UK) were denatured at 70°C for 10 min, and run in NuPAGE™ 4-12% Bis-Tris Gels (Invitrogen, California, USA) as per section 2.13, alongside 10 µL of Precision Plus Protein™ Dual Color Standard (Bio-Rad Laboratories, California, USA). A 200 V current was applied for 90-120 min. Sample bands were then transferred onto Odyssey® (LI-COR Biosciences; Lincoln, NE, USA)

nitrocellulose membrane in a sandwich apparatus (Bio-Rad Laboratories) for 90 min stirring in ice cold Odyssey<sup>®</sup> Transfer Buffer (LI-COR Biosciences). Membranes were treated with Odyssey<sup>®</sup> Blocking Buffer for 1 hour at RT, then incubated with primary antibody mix of Rabbit anti-FXIIIa #17223-1-AP (Proteintech Group, Inc; Rosemont, IL, USA) diluted 1/500 in Odyssey<sup>®</sup> Blocking Buffer + 0.2% Tween20 and shaking overnight at 4°C, 100 rpm. Membrane washing was performed three times with TBS-T (0.1% v/v Tween20, Sigma-Aldrich) and once with TBS, then incubated in secondary antibodies mix of IRDye 680RD Goat anti-Rabbit IgG and IRDye<sup>®</sup> 800CW Donkey anti-Mouse IgG (LI-COR Biosciences; Lincoln, NE, USA) diluted 1/20,000 in Odyssey<sup>®</sup> Blocking Buffer + 0.2% Tween20, for 1 hour at RT in the dark, with shaking at 150 rpm. Another 3x TBS-T and 1x TBS washing step was carried out and membranes were imaged using LI-COR Odyssey<sup>®</sup> CLx Imaging System.

FXIII antigen levels from western blot images were expressed as FXIII antigen band fluorescence over HMW IgG band fluorescence. The corresponding ratios from each of the mouse variants were compared using One-Way ANOVA and Tukey's multiple comparisons statistical tests (Prism 7 software). n=10 (n=9 for FXIII<sup>-/-</sup>). The experiment was carried out once.

### **2.23 Plasma fibrinogen levels**

Coagulation and FXIII activity is heavily dependent on fibrinogen levels, therefore mouse plasma fibrinogen antigen levels were quantified using Mouse Fibrinogen Antigen ELISA Kit (MyBioSource; San Diego, CA, USA) and following manufacturer's instructions, using plasma dilution 1/100,000.

Fibrinogen levels between mouse variants were compared using One-Way ANOVA and Tukey's multiple comparisons statistical tests (Prism 7 software). n=10 (n=9 for FXIII<sup>-/-</sup>). The experiment was carried out once.

## **2.24 Plasma FXIII biotin incorporation assay**

Biotin incorporation assay is based on the principle that FXIII covalently cross-links amines and therefore incorporates 5-(biotinamido) pentylamine into fibrin. The amount of cross-linked biotin is detected by adding streptavidin-alkaline phosphatase conjugate, which binds the incorporated biotin and is able to carry out the sample colorimetric change in presence of phosphatase substrate. Finally, the amount of sample absorbance is measured, which directly correlates with FXIII activity.

Biotin incorporation assay was used to determine cross-linking activity of FXIII in 34Leu, 34Val and FXIII<sup>-/-</sup> plasma. The assay is based on FXIII-catalysed cross-linking of 5-(biotinamido) pentylamine to fibrinogen coated to a microtiter plate well, and by measuring the phosphatase activity after incubation with a streptavidin-alkaline phosphatase conjugate (Ariens et al., 2000).

96 Well MaxiSorp Nunc-Immuno™ microtiter plates (Thermo Fisher Scientific; Waltham, MA, USA) were coated with 100 µL of 40 µg/mL human fibrinogen (MilliporeSigma; Burlington, MA, USA) for 40 minutes at RT. Plates were then emptied, and non-specific binding was blocked by adding 300 µL of 1% Bovine Serum Albumin (Sigma-Aldrich; St. Louis, MO, USA) / TBS pH 8.3 (40 mM Tris, 140 mM NaCl), for 90 minutes at 37°C. Plates were then washed 4 times with 300 µL of TBS pH 8.3 and 10 µL mouse plasma

(diluted 1/50 in TBS pH 8.3) added to the plates. Cross-linking was initiated with 90  $\mu$ L master mix consisting of 0.1 mM DL-Dithiothreitol (Sigma-Aldrich; St. Louis, MO, USA), 270 nM EZ-Link™ pentylamine-biotin (Thermo Fisher Scientific; Waltham, MA, USA), 10 mM CaCl<sub>2</sub> (Fisher Scientific; Hampton, NH, USA) and 1 U/mL murine alpha-thrombin (Haematologic Technologies, Inc.; Essex, VT, USA). Reaction was stopped at time-points 0, 5, 10, 15, 20, 25, 30 minutes by adding 200  $\mu$ L 200 mM EDTA. After all reactions were completed, the plates were washed 4 times using 300  $\mu$ L TBS-T (0.1% Tween® 20, Sigma-Aldrich; St. Louis, MO, USA). Plate incubation with 100  $\mu$ L of 2 mM streptavidin alkaline phosphatase (Thermo Fisher Scientific; Waltham, MA, USA) in 1% BSA/TBS-T solution was then carried out for 1 hour at 37°C. Plates were washed 4 times with 300  $\mu$ L TBS-T, before adding 100  $\mu$ L of phosphatase substrate in a form of 1 mg/mL p-nitrophenyl phosphate (Thermo Fisher Scientific; Waltham, MA, USA) in 1M diethanolamine (Sigma-Aldrich; St. Louis, MO, USA) solution. Once absorbance (405 nm) of any plate wells reached an OD of ~0.7, the reaction was stopped using 100  $\mu$ L of 4M NaOH (Sigma-Aldrich; St. Louis, MO, USA). Absorbance values were blanked against T = 0 values and plotted against time (min). Linear regression trendlines intercepting 0 ( $y = kx$ ) were fitted to the mean absorbance values (0, 5, 10, 15 and 20 min) for each mFXIII-A variant and their gradients “k” were compared. All gradient values were calculated as % of mean 34Val values and expressed as % activation. Differences were compared using One-Way ANOVA and Tukey's multiple comparisons statistical tests (Prism 7 software). n=10 (n=9 for FXIII-/-).

## 2.25 Plasma turbidity

Turbidity assay is based on changes in light scattering of initially transparent soluble fibrinogen sample, which becomes increasingly translucent as fibrinogen, upon conversion to fibrin, polymerises into the insoluble fibrin matrix. Important metrics of fibrin polymerisation can be derived from the plasma turbidity curve. An example schematic of fibrin polymerisation curve and parameters associated can be seen below (*Figure 2.2*).

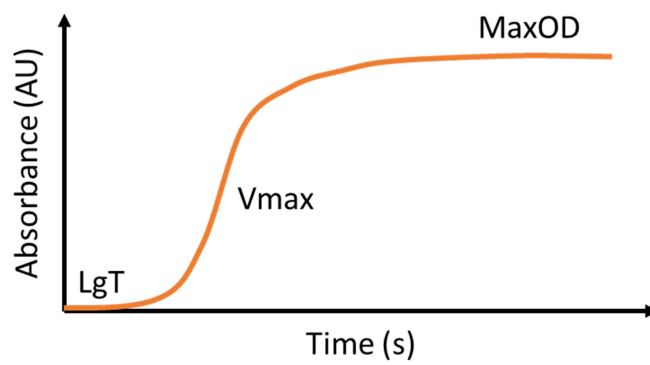


**Figure 2.2 Fibrin polymerisation curve example schematic.**

*Lag time (LgT) is the portion of the fibrin polymerisation curve, which denotes the time it takes for the absorbance to start increasing. Vmax is the maximal velocity of absorbance increase seen in the steepest, linear portion of the curve. MaxOD is the highest OD value the curve achieves.*

Murine plasma was first diluted 2:3 with of TBS (40 mM Tris, 140 mM NaCl, pH 7.4) and 40  $\mu$ L dispensed into Greiner 384 well plate. 10  $\mu$ L of activation mix (0.5 U/mL murine thrombin, 200 mM  $\text{CaCl}_2$  in TBS) was then added to the well in order to initiate clotting. Immediately after initiation of clotting,

plates were mixed for 3 seconds and read at 340 nm every 12 seconds for 220 minutes using a PowerWave HT Microplate Spectrophotometer.

Absorbance values were blanked against initial values and plotted against time (sec). Maximum absorbance (MaxOD) and maximum clotting velocity (Vmax) data were analysed using One-Way ANOVA and Tukey's multiple comparisons tests (Prism 7 software). Fibrin polymerisation lag time (LgT) data was analysed using non-parametric Kruskal-Wallis and Dunn's multiple comparisons tests. n=10 (n=9 for FXIII-/-).

## **2.26 *In Vivo* thromboembolism model**

### **2.26.1 Vascular injury, organ harvest and optical clearing**

Mice were weighed and anaesthetised by intraperitoneal injection (12.5  $\mu$ L x body weight in grams) of 100 mg/mL ketamine / 0.6 mg/mL atropine / 20 mg/mL xylazine. 200  $\mu$ L of fluorophore (100  $\mu$ g of AlexaFluor<sup>647</sup>-Fbg / 10 g of total mouse weight) was then injected via the tail vein. Carotid artery or *inferior vena cava* (IVC) were then isolated, and 10% or 2.5% FeCl<sub>3</sub> (respectively) soaked 1.5 mm x 4.5 mm filter paper (Whatman; Maidstone, UK) was applied for 3 minutes. The IVC was injured with a less concentrated FeCl<sub>3</sub> because higher concentration resulted in an excessive number of emboli in the lung. After 3 minutes, the filter paper was removed, the blood vessel was washed with saline and the mouse was kept in the dark for further 57 minutes. The mouse was then slowly perfused through the heart with 20 mL PBS (+ 50 U/mL heparin), 15 mL 4% (PFA) and 10 mL of FITC-Albumin gelatin (0.8 mg/mL FITC-Albumin in 2% w/v gelatin). Immediately after perfusion the mouse was placed under ice for at least 30 min for the

gelatin to solidify. All subsequent steps were performed in the dark. Lungs or brain were harvested and put in into 4% PFA overnight, at 4°C, shaking at 220 rpm. The next day, the organs were dehydrated in 20%, 40%, 60%, 80% and 100% methanol solution for an hour each, shaking at 200 rpm, at RT. Organs were left overnight in 100% methanol. The following day, right and left lungs were surgically separated while the brains were processed as whole organ. Optical clearing began with incubating organs in 66% Dichloromethane (DCM; Sigma-Aldrich, Dorset, UK) / 34% Methanol for 3 hour at RT, shaking at 220 rpm. Organs were then incubated in 100% DCM solution for 15 min twice at RT, shaking at 220 rpm. Finally, organs were transferred into Benzyl Ether (DBE 98%; Sigma-Aldrich, Dorset, UK) and incubated at least for 72 hours at RT until imaging.

### **2.26.2 Light sheet fluorescence microscopy**

Light sheet microscope is able to optically section the sample into sheets 5 µm thick by illuminating a single plane at the time. Perpendicular to excitation plane, the emitted light is collected at the objective and images are stored as a stack, capturing the whole sample, ready to be analysed as a full-sized reconstruction.

The light sheet OLYMPUS (Tokyo, Japan) MVX10 Research Macro Zoom Microscope hardware laser power was set to 25%, and the 0.63x OLYMPUS MVPLAPO 2 XC objective set to 3.5 scale with lens protector on. The sample pool was filled with ECI (Sigma-Aldrich), which has the same refractive index as DBE. The cleared sample was mounted onto the sample holder and immersed into the microscope sample pool. The microscope was set to work with 470 nm and 630 nm wavelengths, at 0.63x optical zoom, 50% sheet

width from both sides, 5  $\mu\text{m}$  sheet thickness and ECi medium. First, the sample was centred in the field of view, focused on the green channel and then on the red channel (by correcting the chromatic aberration). Once both colours were in focus, the software laser was adjusted to the lowest power (usually 30-70% green and 100% red laser power) which still covers the whole 0 – 65k signal intensity spectrum. Next, coordinates of the top and the bottom of the sample were selected. The software was instructed to separate stacks by colour channels (“splitting by filter”), so that the microscope first images the organ in one colour channel and then the other. The imaging resulted in two separate image stacks for green channel (vasculature) and red channel (emboli). Finally a top down cross section animation was created in the imaging software ImSpector 5.1.1 (LaVision BioTec GmbH, Bielefeld, Germany) (Schonle, 2006).

### **2.26.3 Imaris image reconstruction and analysis**

The image stack was loaded onto Imaris 9.2.1 software (Bitplane; Belfast, Northern Ireland) and an initial 3D image was generated. First, both colour channels were adjusted for min intensity of 0 and max intensity of 65535. Base colours of FITC-hydrogel and AlexaFluor<sup>647</sup>-fibrinogen were set to blue (Red: 1.0 / Green: 1.0 / Blue: 0.0) and yellow (Red: 0.0 / Green: 0.2 / Blue: 0.5) respectively. Next, gamma was set for both colours so the vasculature and emboli were visible, but the background and artefacts were not. Yellow gamma was defaulted to 0.1, while blue gamma defaulted to 1.0 before any adjustments. At this point both the image and the 3D rotating animation were exported.

Next, volumetric analysis of the emboli was performed using the “Volume” tool in the software. Imaris was instructed to locate yellow (emboli) surfaces above a certain, manually adjusted threshold, which was selected based on smallest clot visibility (threshold low enough, so the smallest visible clots were selected, but particles that were invisible by eye, were not being selected yet). It was possible to assess and clarify whether the software selection was satisfactory, because surface marking happened in real time, while adjusting the selected intensity threshold. By marking the emboli surfaces, the software was then able to calculate emboli count and volumes ( $\mu\text{m}^3$ ).  $50 \mu\text{m}^3$  was selected as a cut off size for emboli, because smallest capillaries in the brain and lung are  $\sim 4\text{-}5 \mu\text{m}$  in diameter, therefore a sphere able to occlude such capillary is  $\sim 50 \mu\text{m}^3$  in volume. The software then marked the surfaces in silver (Figure 2.3) based on selected intensity threshold.

Emboli counts and volumes from each mouse variant were compared using One-Way ANOVA and Tukey's multiple comparisons tests (Prism 7 software).  $n=10$ .

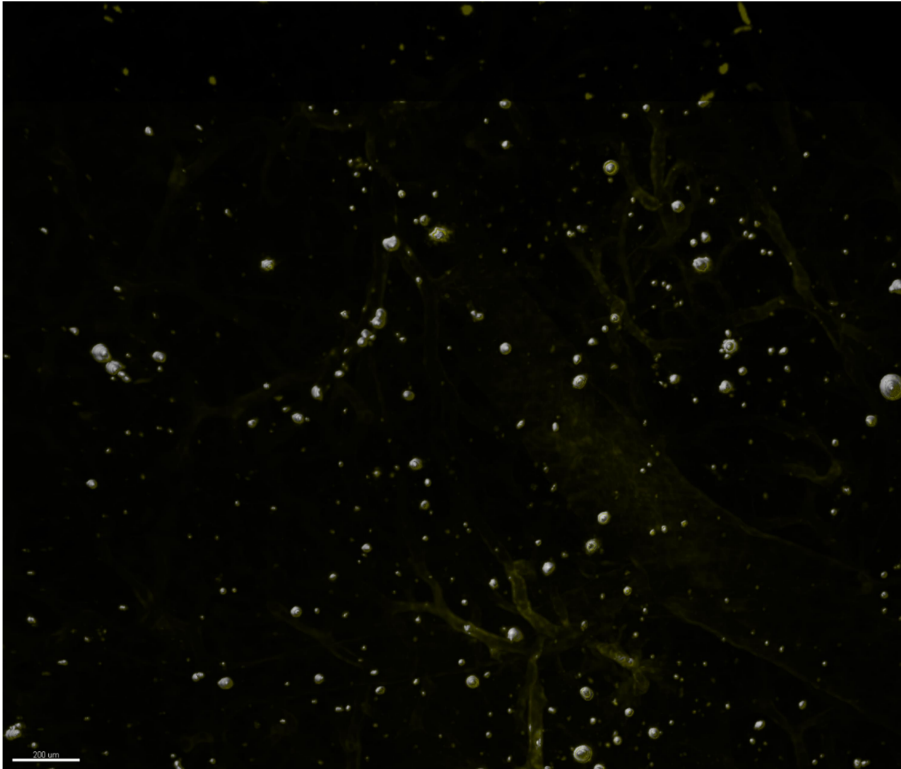


*Figure 2.3 Imaris software marking the surfaces of emboli post light sheet microscope imaging. Yellow AlexaFluor<sup>647</sup> channel indicates fibrinogen fluorescence. High intensity yellow emboli were marked by silver surface marking tool. Marked emboli were later analysed for their count and volume. Surrounding vessels were made brighter for presentation purposes.*

#### **2.26.4 Manual emboli counting**

Manual, as opposed to software, emboli counting was employed on brain sample 3D models recreated in Imaris software, because of numerous highly fluorescent artefacts present in brain images, which masked a great proportion of lower intensity emboli. Since the software could not distinguish the origins of fluorescent spots, visible emboli were counted by eye while ignoring the fluorescent smears originating from artefacts.

The AlexaFluor<sup>647</sup> channel was set for min intensity of 0 and max intensity of 65535. Gamma was set to 5, so everything was clearly visible (vasculature, artefacts and emboli). The organ was zoomed in to an extent so that it occupies the most space on the screen while being fully visible as a whole. “Grid” function was then set up in a way that an approximately 8x10 squares of the grid overlaid the organ image. Emboli in each square were counted using a handheld Tally Counter.

Emboli counts from each mouse variant were compared using One-Way ANOVA and Tukey's multiple comparisons tests (Prism 7 software).

## **2.27 Statistical analysis and outliers**

All data sets were first tested for normal Gaussian distribution using Shapiro-Wilk test for normality. If the data set passed the normality test ( $P > 0.05$ ), data was analysed using parametric tests. Otherwise, data was analysed using their non-parametric equivalents.

For a single comparison between two mice variants, student's T-test was used for parametric analysis and Mann-Whitney test for non-parametric measures.

For comparison of three mice variants of a single variable, One-Way ANOVA combined with Tukey's multiple comparisons tests were used for parametric analysis. Otherwise non-parametric tests used were Kruskal-Wallis and Dunn's multiple comparison tests.

For comparisons of three mice variants of multiple variables or time-points, a Two-Way ANOVA paired with Tukey's multiple comparisons tests were used for parametric analysis. All datasets of multiple group comparisons were of

sufficient sample size and passed the normality test, therefore the parametric analysis equivalent was used in all multiple group, multiple variable occasions.

If any experimental design variation or technical inconsistency provided enough confidence that a certain value could be an outlier, that value and all other values associated were excluded from all sets of data. Similarly, if a single value is abnormally high or low compared to the rest of the associated data set, it was considered a possible outlier. In order to assess whether it should be excluded, the 1.5 interquartile range Tukey's rule (Hoaglin et al., 1986) was used: any data point which was 1.5 times the interquartile ranges below the first quartile ( $< Q1 - 1.5 \times (Q3 - Q1)$ ) or above the third quartile ( $> Q3 + 1.5 \times (Q3 - Q1)$ ), was considered an outlier.

**Chapter 3 *In vitro* recombinant  
mFXIII-A work**

### 3.1 Introduction

This PhD project intended to start with *in vitro* recombinant FXIII-A (rFXIII-A) investigations. Previous studies (Ariens et al., 2000, Duval et al., 2016) had shown that human rhFXIII-A 34Leu is activated faster and produces clots with denser, thinner fibrin fibres that are more resistant to fibrinolysis than the more common form: FXIII-A 34Val. In these studies, the experiments determining these features were performed both *in vitro* with plasma human FXIII-A and *in vivo*, injecting the human rhFXIII-A into FXIII-A deficient mice. In this PhD project, before moving onto the main focus – *in vivo* murine FXIII-A investigations, we wanted to confirm that these V34L mutation effects can be replicated with murine recombinant FXIII-A (mFXIII-A). Therefore, a series of experiments were carried out to perform mutagenesis, insert murine FXIII-A DNA into the expression vector, express purified mFXIII-A protein and, finally, compare activation rates of expressed recombinant mFXIII-A 34Leu and 34Val *in vitro*.

The WT murine FXIII-A contains Leucine at residues 34, and a Valine variation at this residue does not naturally occur in mice. In order to investigate the differences between murine Wild-Type (34Leu) and mutant L34V (34Val) mFXIII-A, these proteins needed to be produced in bacteria using recombinant expression at sufficiently high levels. *E. coli* bacterial cell line was chosen, since FXIII-A does not normally undergo any post translational modifications (Hansson and Stenflo, 2005). Therefore a rapid, low cost and high efficiency bacterial expression system was used for protein expression. A series of experiments were carried out to reach the protein expression stage and a summary of a workflow can be found in the

schematic below (*Figure 3.1*), while in depth explanation behind these actions are described further.

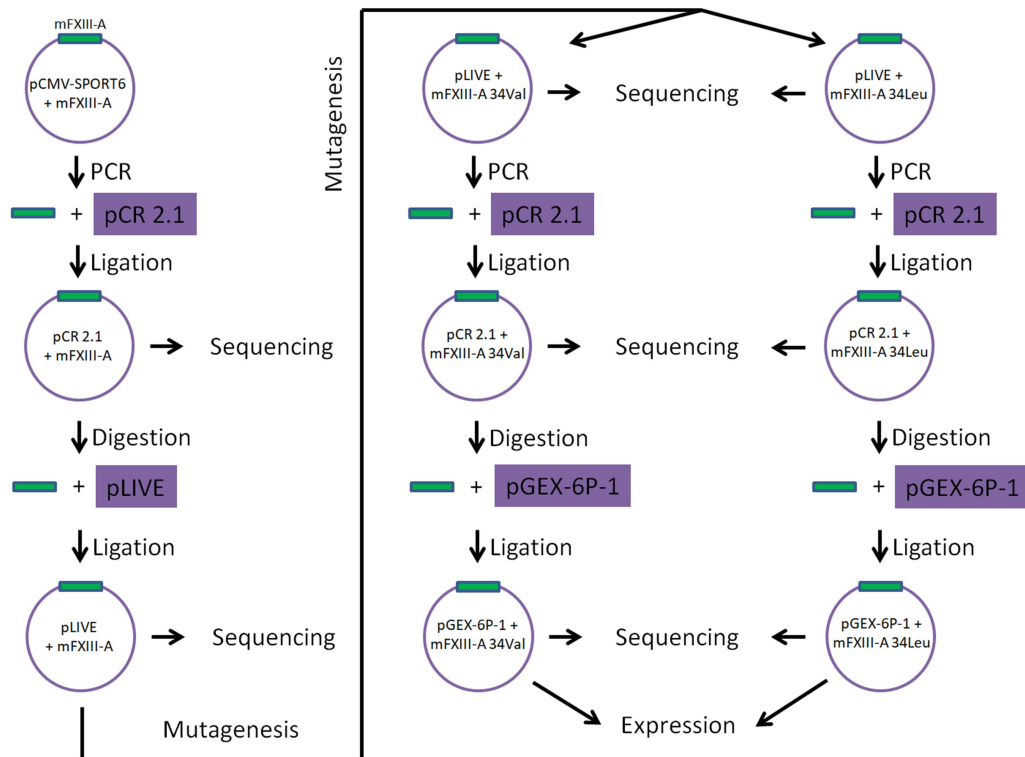


**Figure 3.1** *In vitro* recombinant mFXIII-A workflow schematic.

The WT mFXIII-A (34Leu) gene insert from pCMV-SPORT6 vector was amplified by PCR and ligated into pCR 2.1 vector via TA cloning. Then, the ligation product was restriction digested in order to cut the mFXIII-A DNA insert out and ligate it with pLIVE vector. Site-directed mutagenesis was then performed on mFXIII-A in pLIVE vector in order to generate mFXIII-A 34Val DNA construct. Both mFXIII-A 34Val and 34Leu mFXIII-A DNA inserts were taken through the steps of PCR amplification from pLIVE vector and inserted into pCR 2.1 vector again. This allowed the mFXIII-A inserts to be primed by restriction enzymes for ligation into pGEX-6P-1 expression vector. Once in the expression vector, both 34Val and 34Leu mFXIII-A were expressed and their activation rates compared. After each ligation step, *E. coli* were transformed with ligation product, cultured, lysed and their plasmid (containing mFXIII-A DNA) collected for sequencing, in order to confirm that PCR amplification has not introduced any unwanted mutations in mFXIII-A DNA construct. Green bar represents mFXIII-A DNA insert and purple colour represents recipient DNA vector.

Three bacterial vectors were utilised in this project:

1. pCR 2.1, in order to insert mFXIII-A DNA in a double stranded circular vector and introduce restriction sites for further restriction digestion.
2. pLIVE, a mammalian expression vector in order to transfect FXIII deficient mice and express mFXIII-A *in vivo*.
3. pGEX-6P-1, a bacterial expression vector in order to express recombinant mFXIII-A and compare 34Leu and 34Val variant activation rates *in vitro*.

Chronologically, insertions were performed in the order listed (pCR 2.1 → pLIVE → pGEX-6P-1), however, to show the reasoning behind inserting mFXIII-A into each vector, the explanation will start from bacterial expression.

In order for *E. coli* to express FXIII-A protein, the bacteria needed to be transfected with a vector containing the mFXIII-A gene. The 4984 bp pGEX-6P-1 bacterial expression vector (*Figure 3.2*) was used, which contained a glutathione S-transferases (GST) sequence before the FXIII-A gene sequence allowing bacteria to express the protein with a 26 kDa GST tag attached to it. Protein expressed in this fashion had increased solubility and could then be purified from the bacterial lysate using affinity chromatography. GST fusion protein was bound to the glutathione chromatography column, all the remaining lysate constituents washed through the column uncollected, and the protein of interest was then recovered by cleavage from the bound GST tag using PreScission (GE Healthcare; Chicago, IL, USA) protease.

FXIII cDNA used in the expression vector had to be inserted into a double stranded bacterial vector in a specific location within the vector. Therefore, in order for the cDNA fragment to bind the vector sequence, both have been prepared using restriction enzymes. A restriction enzyme is able to cleave DNA at a particular sequence (restriction site), and in this case it was used to both open up a recipient vector at particular restriction site and prepare the FXIII-A insert so its beginning and ending sequences match the prepared recipient vector pocket.

Restriction enzymes need a circular DNA to dock onto and initially generated PCR amplified mFXIII-A cDNA was only a double stranded fragment (2196 bp). pCR 2.1 was therefore used as an intermediary step between linear mFXIII-A cDNA fragment and a bacterial plasmid insert. PCR product was ligated with a pCR 2.1 vector via TA cloning method, resulting in a mFXIII-A cDNA being inside a double stranded vector and ready to be cut at the right restriction site. Correct areas of restriction were also contained within pCR 2.1 vector itself, allowing cut products to be inserted into many different bacterial and mammalian expression vectors. We have utilised two different sets of restriction enzymes in order to prime FXIII-A cDNA and recipient vectors to be inserted into both a bacterial expression vector pGEX-6P-1 and mammalian expression vector pLIVE.

pLIVE vector (*Figure 3.2*) contains a mammalian albumin promoter sequence before the gene insert sequence allowing the gene to be expressed in mammalian cells. In this project, the pLIVE vector containing mFXIII-A was intended to be used in transfecting live FXIII-A Knock-Out (F13A1<sup>-/-</sup> or KO)

mice hepatocytes (using hydrodynamic gene transfer technique) in an attempt to generate a L34V mutant mice. Our research group, however, acquired mFXIII-A L34V (34Val) genetically modified mice strain, and the manual transfection method with pLIVE vector was no longer required to be developed. The possibility of inducing FXIII-A expression and secretion remains unknown as the signalling peptide of the protein has not been identified, and the protein may be expressed through non-classical secretion pathways (Cordell et al., 2010).

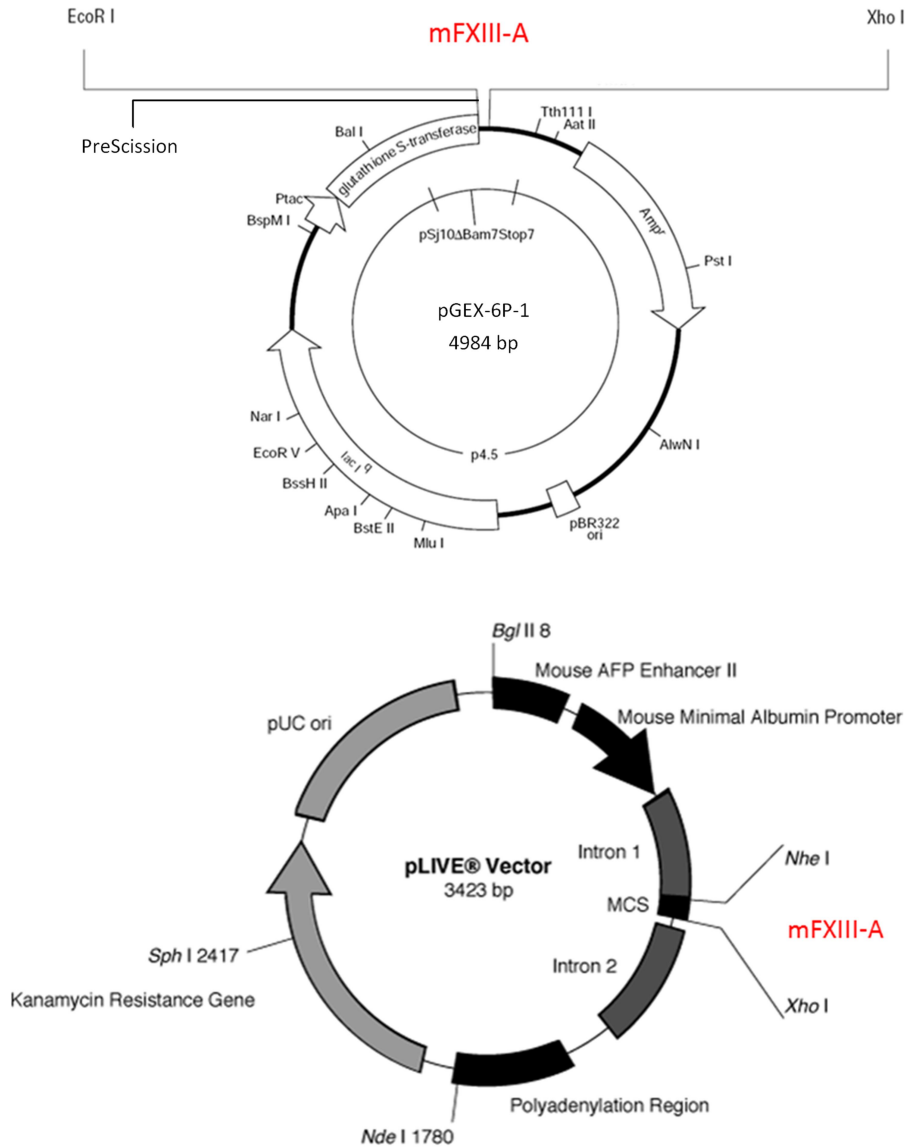


**Figure 3.2 pLIVE and pGEX-6P-1 vector schematics.**

Schematic of pLIVE (top) and pGEX-6P-1 (bottom) vectors indicating antibiotic resistance gene sites, vector sizes, mFXIII-A insertion sites (indicated by panning out bars) and corresponding restriction enzymes shown beside the bars. pBR322 ori and pUC ori are replicons for *E.coli*, AMP – ampicillin, lac – lac operon, Ptac – Tac promoter, alpha-fetoprotein enhancer (AFP) enhancer II region enhances albumin promoter, MCS – multiple cloning site. Other letter-number combinations denote restriction enzymes. Adapted from [www.mirusbio.com](http://www.mirusbio.com) and [www.lifescience-market.com](http://www.lifescience-market.com) product page.

Finally, in order to make the comparison between WT (34Leu) and 34Val variant proteins, mFXIII-A gene was mutated using site-directed mutagenesis. pLIVE vector containing mFXIII-A Wild-Type (34Leu) gene was cloned using a designed primer which contained a C to G nucleotide swap, resulting in DNA sequence coding for mFXIII-A 34<sup>th</sup> amino acid swap. Site-directed mutagenesis product DNA was then cloned into PCR 2.1 and, subsequently, into the pGEX-6P-1 vector for mFXIII-A expression in *E. coli*. Post expression, both WT and 34Val recombinant proteins were compared in their activation rates through activation peptide cleavage rate quantification by SDS-PAGE.

## **3.2 Aims**

To generate mFXIII-A Wild-Type (34Leu) and 34Val protein variants in order to assess the effects of this mutation on FXIII activation rate in murine FXIII.

## **3.3 Methods**

### **3.3.1 mFXIII-A gene PCR amplification**

A 2196 bp mFXIII-A cDNA sequence from pCMV-SPORT6 vector was amplified using PCR for insertion into pLIVE and following a method detailed in section 2.1. Primers used for PCR amplification of mFXIII-A cDNA as well as restriction sites contained within them are shown in *Table 3.1*. Primers pLIVE-F1/R1 were used to generate pLIVE inserts from pCMV-SPORT6 vector, while pGEX6P1\_F/R primers were used to clone cDNA from a pLIVE

vector into pGEX-6P-1 vector. The PCR cycling parameters are listed in *Table 3.2*.

**Table 3.1 PCR amplification primers and their sequences.** Restriction sites in the sequences are highlighted and their respective restriction enzymes are underlined.

Primer (Recipient vector)	Sequence
pGEX6P1_F (pGEX-6P-1)	5'TCCAGTAAAGGAATTCATGTCAGATA3' <u>EcoRI</u>
pGEX6P1_R (pGEX-6P-1)	5'TGATGTTACTCGAGCCTTCTGGG3' <u>XhoI</u>
pLIVE-F1 (pLIVE)	5' CTCAGGAGCGCTAGCAGGAT3' <u>NheI</u>
pLIVE-R1 (pLIVE)	5' CAGCCCACTCGAGCCTTC3' <u>XhoI</u>

**Table 3.2 mFXIII-A PCR amplification cycling parameters.**

Segment	Cycles	Temperature (°C)	Time (s)	Stage
1	1	94	180	Denaturation
2	35	94	45	Denaturation
		55	60	Annealing
		68	132	Extension
3	1	4	any	Storage

### 3.3.2 TA cloning

Amplified mFXIII-A cDNA fragments were run on agarose gel (section 2.2), recovered from the gel (section 2.3) and ligated with a pCR 2.1 vector as indicated in section 2.4.

### **3.3.3 Restriction digestion and gene – vector ligation**

mFXIII-A insert in pCR 2.1 as well as either pLIVE or pGEX-6P-1 vectors were primed for future ligation by using respective restriction enzymes.

DNA amplification using pLIVE-F1 and pLIVE-R1 primers allowed for subsequent restriction of the mFXIII-A insert out of pCR 2.1, using NheI and XhoI restriction enzymes. pLIVE vector was also digested using these enzymes.

DNA amplification using pGEX6P1\_F and pGEX6P1\_R primers allowed for subsequent restriction of the mFXIII-A insert out of pCR 2.1, using EcoRI and XhoI restriction enzymes. pGEX-6P-1 vector was also digested using these enzymes.

Restriction digestion was carried out as detailed in section 2.8, digestion product samples were run on agarose gel (section 2.2) and recovered from the gel (section 2.3). Cut mFXIII-A gene fragment and primed recipient expression vector were then ligated together as described in section 2.9.

### **3.3.4 *E. coli* Transformation, Growth and Glycerol stock**

mFXIII-A cDNA insert and vector (pCR 2.1, pLIVE or pGEX-6P-1) ligation products were used to transform competent XL1 Blue *E. coli* cells (Agilent Technologies, Stockport, UK) as described in section 2.5.1. Transformation success was investigated by running the PCR on bacterial plasmid, using cycling parameters listed in *Table 3.3* and inspecting reaction products on an agarose gel (detailed in section 2.2). Finally, successfully transformed bacterial colonies were cultured and grown for higher yields of DNA, as described in section 2.6. Parts of successful bacterial colonies were stored in

glycerol at -80°C as described in section 2.6, whilst the remainder of colonies were used for plasmid extraction, as detailed in section 2.7.

**Table 3.3 PCR thermal cycling parameters used in transformation quality assurance runs.**

Segment	Cycles	Temperature (°C)	Time (s)	Stage
1	1	95	600	Bacteria opening
2	35	95	45	Denaturation
		55	60	Annealing
		68	132	Extension
3	1	4	any	Storage

### 3.3.5 Site-directed mutagenesis

Site-directed mutagenesis was performed on WT (34Leu) mFXIII-A sequence contained in pLIVE plasmid, as detailed in section 2.10. Forward and reverse primers for site-directed mutagenesis PCR reaction were designed to contain a C to G and a G to C nucleotide swap at 34<sup>th</sup> amino acid sequence codon (*Table 3.4*) enabling the L34V mutagenesis. PCR reaction thermal cycling parameters were used as listed in *Table 3.5*.

**Table 3.4 PCR primers used in site-directed L34V mutagenesis of mFXIII-A.** Highlighted are the codons changed from the wild-type, while underlined are the base pair swaps designed from C to G in the forward primer and G to C in the reverse primer.

Primer	Sequence
mFXIIIIL34V-F	5'-GGAGCTACAAGGC <u>GTG</u> GTGCCAAGGGG-3'
mFXIIIIL34V-R	5'-CCCCTTGGCAC <u>CAC</u> GCCTTGTAGCTCC-3'

**Table 3.5 PCR thermal cycling parameters used in L34V site-directed mutagenesis.**

Segment	Cycles	Temperature (°C)	Time (s)	Stage
1	1	95	30	Denaturation
2	12	95	30	Denaturation
		55	60	Annealing
		68	132	Extension
3	1	4	120	Cooling down

### **3.3.6 DNA sequencing**

DNA sequencing (section 2.11) was performed after most PCR amplification, site-directed mutagenesis and ligation product transfection experiments. Primers below (Table 3.6) were used to sequence the mFXIII-A gene inside a pCR 2.1, pLIVE or pGEX-6-P1 vector. Sequencing confirmed that each step of the recombinant mFXIII-A construct formation was performed using a correct mFXIII-A gene sequence without introducing any unwanted mutations in the gene.

**Table 3.6 Primers (and sequenced vectors) used in mFXIII-A sequencing.**

Primer (vector)	Sequence
M13 F (pCR 2.1)	5'-GTAAAACGACGGCCAG-'3
M13 R (pCR 2.1)	5'-CAGGAAACAGCTATGAC-'3
pGEX6P1-F (pGEX-6P-1)	5'-GCAAGTATATAGCATGGCCTTTG-'3
pGEX6P1-R (pGEX-6P-1)	5'-TCTGACACATGCAGCTCCC-'3
pLIVE-F1 (pLIVE)	5'-GAGATGTAAAATTTTCATGATGTTTTTC-'3
pLIVE-R1 (pLIVE)	5'-ATATGGCTCTTGGAAATGGTCA-'3
mFXIII-A-F1	5'-AGAGTGGAATATGTCATTGGTTCG-'3
mFXIII-A-F2	5'-GCATCCTGGATACTTGCTTGT-'3
mFXIII-A-F3	5'-GGATTCCGGTGTGGAACCTACC-'3
mFXIII-A-F4	5'-TATGGAGCCAAGAAGACCCTC-'3
mFXIII-A-F5	5'-CCATCAAGGTCCGAGGTG-'3

### 3.3.7 mFXIII-A Expression and Purification

*E. coli* transformed with pGEX-6P-1/mFXIII-A 34Val or 34Leu plasmid were cultured and mFXIII-A expression was carried out as detailed in section 2.12.1. Following expression, mFXIII-A purification was carried out by lysing the bacteria and recovering expressed protein by affinity chromatography as detailed in section 2.12.2. ÄKTaprime chromatography was performed in two major steps: loading GST-mFXIII-A fusion protein onto GSTrap FF column

(Table 3.8) and elution mFXIII-A (Table 3.9). Listed steps were carried out using buffers listed below (Table 3.7).

**Table 3.7 Buffers used in ÄKTAprime during mFXIII-A chromatography run.**

Buffer	Constituents
GST Equilibration Buffer	1x PBS, 15% Glycerol, pH 7.4, 0.22 µm filtered, degased
GST Wash Buffer	1x PBS, 0.2% Triton X-100, 15% Glycerol, pH 7.4, 0.22 µm filtered, degased
GST Elution Buffer	H <sub>2</sub> O, 50 mM Tris-HCl, 20 mM Glutathione, pH 8.0, 0.22 µm filtered, degased
GST Column Regeneration Buffer	H <sub>2</sub> O, Urea 5 M, 0.22 µm filtered, degased

**Table 3.8 Steps of mFXIII-A loading into GSTrap FF column using ÄKTAprime.**

Step	Flow rate	Volume
1. Equilibration	15 mL/min	50 mL
2. Equilibration	15 mL/min	50 mL
3. Sample Loading	0.5 mL/min	250 mL
4. Wash 1	0.5 mL/min	60 mL
5. Wash 2	1.5 mL/min	170 mL
6. Equilibration	2.5 mL/min	250 mL

**Table 3.9 Steps of mFXIII-A and GST elution from GStrap FF column using ÄKTAprime.**

Step	Flow rate	Volume
1. FXIII-A Elution (Equil. Buffer)	1ml/min	35ml
2. GST Elution (Elution Buffer), Collected in 1 mL fractions	1ml/min	35ml
3. Equilibration	5ml/min	45ml
4. Urea column regeneration	5ml/min	45ml
5. Equilibration	5ml/min	45ml
6. 70% EtOH column regeneration, Collected in 2 mL fractions	5ml/min	45ml
7. Equilibration	5ml/min	100ml

Collected elution samples were pooled together, concentrated and concentrate was run in BCA assay (described in 2.14) in order to determine the protein content of the elution concentrate. SDS-PAGE runs were carried out after the mFXIII-A purification steps in order to check elution sample purity (section 2.13).

### **3.3.8 Recombinant mFXIII-A activation rate assay**

The difference between WT and L34V mFXIII-A activation rate was investigated using a GST-AP cleavage assay detailed in section 2.15.

## 3.4 Results

### 3.4.1 WT mFXIII-A cDNA amplification from pCMV-SPORT6 vector

In order to confirm a successful mFXIII-A gene fragment PCR amplification, agarose gel electrophoresis and DNA sequencing were performed.



***Figure 3.3 Gel electrophoresis of PCR amplified mFXIII-A gene fragment.***

PCR amplification of mFXIII-A WT cDNA from the pCMV-SPORT6 vector, containing NheI/XhoI restriction sites, was successful, as seen from a clear single 2196 base pair DNA band (*Figure 3.3*). Following amplification, the WT mFXIII-A cDNA insert was ligated with pCR 2.1 vector and sequenced. mFXIII-A cDNA fragment amplified from the pCMV-SPORT6 vector showed no mutations and was used in further experiments. Table 3.10 shows Clustal Omega web tool sequence alignment of PCR product sequencing and its template vector.

**Table 3.10 Clustal Omega web tool alignment of a portion CMV-SPORT6 vector containing WT mFXIII-A sequence with a PCR amplification product. Full sequence available in Appendix 1.**

CMV-SPORT6 pCR2.1 - WT	aagcaggatccagtaaagctgagaATGtcagatactccagcaagcaccttggggggagg -----ATGTCAGATACTCCAGCAAGCACCTTGGGGGGAGG *****
CMV-SPORT6 pCR2.1 - WT	CGAGCAGTCCCGCCAATAACTCCAATGCTGCAGAAGTGGACCTCCCAACTGAGGAGCTA CGAGCAGTCCCGCCAATAACTCCAATGCTGCAGAAGTGGACCTCCCAACTGAGGAGCTA *****
CMV-SPORT6 pCR2.1 - WT	CAAGGCCTGGTGCCAAGGGGTGTCAACCTGAAAGATTACCTGAATGTCACAGCTGTTTAC CAAGGCCTGGTGCCAAGGGGTGTCAACCTGAAAGATTACCTGAATGTCACAGCTGTTTAC *****
CMV-SPORT6 pCR2.1 - WT	CTGTTCAAGGAGAGATGGGACAGTAACAAGATTGATCACCACACAGACAAATATGACAAC CTGTTCAAGGAGAGATGGGACAGTAACAAGATTGATCACCACACAGACAAATATGACAAC *****

### 3.4.2 WT mFXIII-A DNA ligation into pLIVE vector

pCR 2.1 – mFXIII-A and pLIVE vector were restriction digested using Nhe I and Xho I. Following digestion, the products were checked with agarose gel run. *Figure 3.4* presents an agarose gel with bands of 2237 bp for the FXIII WT gene fragment cut out of the 3931 bp pCR 2.1 vector and a 3375 bp restriction cut pLIVE vector. Clear gel electrophoresis sample bands suggest that restriction digest was successful and no significant undesirable fragments were generated.

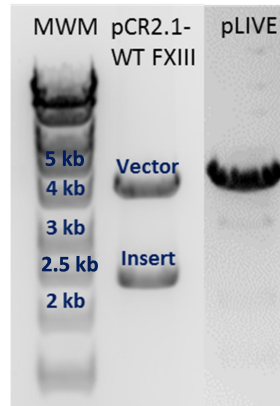


**Figure 3.4 Agarose gel electrophoresis of pCR 2.1 vector (+mFXIII-A) and pLIVE vector restriction digest samples.**

Following the confirmation of successful restriction digest, WT mFXIII-A insert cDNA was ligated with pLIVE vector. Ligation products were then sequenced and, as shown in *Table 3.11*, had no undesired mutations introduced.

**Table 3.11 Clustal Omega web tool alignment of WT mFXIII-A insert in pLIVE vector with a pLIVE+mFXIII-A DNA template. Full sequence available in Appendix 2.**

pLIVE+mFXIII-A	tttttctgctagcaggatccagtaaagctgagaATGTCAGATACTCCAGCAAGCACCTTT
mFXIII-A	-----ATGTCAGATACTCCAGCAAGCACCTTT *****
pLIVE+mFXIII-A	GGGGGAGGCGAGCAGTCCCGCCAATAACTCCAATGCTGCAGAAGTGGACCTCCCAACT
mFXIII-A	GGGGGAGGCGAGCAGTCCCGCCAATAACTCCAATGCTGCAGAAGTGGACCTCCCAACT *****
pLIVE+mFXIII-A	GAGGAGCTACAAGGCCTGGTGCCAAGGGGTGTCAACCTGAAAGATTACCTGAATGTCACA
mFXIII-A	GAGGAGCTACAAGGCCTGGTGCCAAGGGGTGTCAACCTGAAAGATTACCTGAATGTCACA *****
pLIVE+mFXIII-A	GCTGTTACCTGTTCAAGGAGAGATGGGACAGTAACAAGATTGATCACCACACAGACAAA
mFXIII-A	GCTGTTACCTGTTCAAGGAGAGATGGGACAGTAACAAGATTGATCACCACACAGACAAA *****

### 3.4.3 mFXIII-A L34V mutagenesis

A FXIII-A L34V construct was produced by site-directed mutagenesis of the mFXIII-A 34Leu cDNA contained in pLIVE vector using the primers listed in *Table 3.4*. The mutagenesis product was confirmed to be successful by DNA sequencing. DNA base pair substitution from C to G at position 103 resulted in L34V amino acid substitution and can be seen in Clustal Omega web tool alignment of mutant and WT mFXIII-A sequences (*Table 3.12*).

**Table 3.12 Clustal Omega alignment of a portion of pLIVE vector containing WT (34Leu) and 34Val mFXIII-A sequences. mFXIII-A L34V mutagenesis from WT FXIII-A in pLIVE vector with L34V point mutation highlighted. Underlined is the location of mFXIII-A amino acid codon number 34. Full sequence available in Appendix 3.**

pLIVE-WT	tttttctgctagcaggatccagtaaagctgagaATGTCAGATACTCCAGCAAGCACCTTT
pLIVE-L34V	-----ATGTCAGATACTCCAGCAAGCACCTTT *****
pLIVE-WT	GGGGGGAGGCGAGCAGTCCCGCCCAATAACTCCAATGCTGCAGAAGTGGACCTCCCAACT
pLIVE-L34V	GGGGGGAGGCGAGCAGTCCCGCCCAATAACTCCAATGCTGCAGAAGTGGACCTCCCAACT *****
pLIVE-WT	GAGGAGCTACAAGGCCTGGTGCCAAGGGGTGTCAACCTGAAAGATTACCTGAATGTCACA
pLIVE-L34V	GAGGAGCTACAAGGC <u>CT</u> GGTGCCAAGGGGTGTCAACCTGAAAGATTACCTGAATGTCACA *****
pLIVE-WT	GCTGTTCACCTGTTCAAGGAGAGATGGGACAGTAACAAGATTGATCACCACACAGACAAA
pLIVE-L34V	GCTGTTCACCTGTTCAAGGAGAGATGGGACAGTAACAAGATTGATCACCACACAGACAAA *****

### 3.4.4 Amplification of mFXIII-A WT and L34V DNA sequences from pLIVE vector and ligation with pCR 2.1 vector

WT and L34V mFXIII-A sequences were amplified from a pLIVE vector by PCR and inserted into pCR 2.1 vector for further restriction digestion. Agarose gel electrophoresis showed clear 2259 base pair bands of both WT and L34V mFXIII-A DNA fragments, which was indicative of successful DNA amplification (*Figure 3.5*). Sequencing was not performed at this stage due to it being a necessity in the next stage regardless.

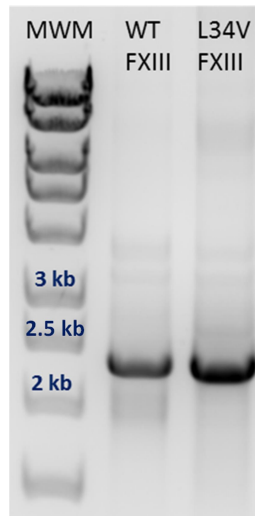


***Figure 3.5 Gel electrophoresis of PCR amplified mFXIII-A WT and L34V gene fragments.***

#### **3.4.5 Restriction digestion of mFXIII-A WT and L34V in pCR 2.1 vector and ligation with pGEX-6P-1 vector**

WT and L34V mFXIII-A gene sequences were cut out of pCR 2.1 vector using EcoRI/XhoI restriction enzymes and inserted into the cut pGEX-6P-1 vector. In order to confirm a successful restriction digest of gene insert out of pCR 2.1 vector as well as a successful pGEX-6P-1 vector digestion, agarose gel electrophoresis was run.

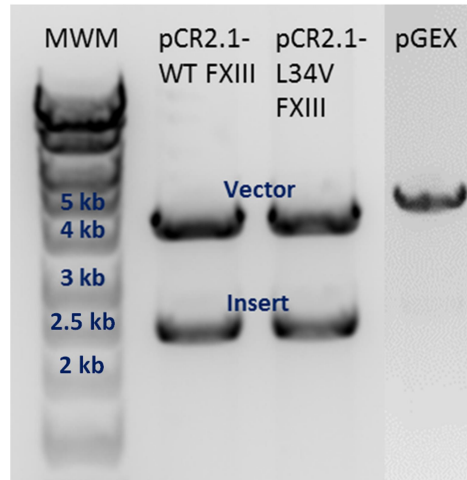


**Figure 3.6 Agarose gel electrophoresis of pCR 2.1 vector (+mFXIII-A WT and L34V) and pGEX-6P-1 vector restriction digest samples.**

Figure 3.6 presents an agarose gel electrophoresis bands of the 2259 bp WT and L34V gene fragments cut out of the 3931 bp pCR 2.1 vector and a 4969 bp restriction cut pGEX-6P-1 vector. Restriction was performed using EcoRI and XhoI restriction enzymes. Clear gel electrophoresis sample bands suggest that restriction digestion was successful and no significant undesirable fragments were generated.

Following ligation of WT and L34V inserts into pGEX-6P-1 vector, sequencing was performed. Table 3.13 shows pGEX-6P-1/WT aligned with a pGEX-6P-1/L34V. Results indicated that no undesired mutations were introduced during both DNA amplification and ligation steps.

**Table 3.13 Clustal Omega web tool alignment of inserted WT and L34V mFXIII-A sequences into pGEX-6P-1 vector.**

Included pGEX-6P-1 sequence alongside WT mFXIII-A sequence is shown for vector demonstration purposes. L34V point mutation is highlighted, while underlined is the location of mFXIII-A amino acid codon number 34. Full sequence available in Appendix 4.

pGEX6P1-WT	atcctccaaaatcgggatctggaagttctgttccagggggcccctgggatccccggaattcA
pGEX6P1-L34V	-----A *
pGEX6P1-WT	TGTCAGATACTCCAGCAAGCACCTTTGGGGGAGGCGAGCAGTCCCGCCAATAACTCCA
pGEX6P1-L34V	TGTCAGATACTCCAGCAAGCACCTTTGGGGGAGGCGAGCAGTCCCGCCAATAACTCCA *****
pGEX6P1-WT	ATGCTGCAGAAGTGGACCTCCCAACTGAGGAGCTACAAGGC <u>CTGGTGCCAAGGGGTGTCA</u>
pGEX6P1-L34V	ATGCTGCAGAAGTGGACCTCCCAACTGAGGAGCTACAAGGC <u>CTGGTGCCAAGGGGTGTCA</u> *****
pGEX6P1-WT	ACCTGAAAGATTACCTGAATGTCACAGCTGTTCACCTGTTC AAGGAGAGATGGGACAGTA
pGEX6P1-L34V	ACCTGAAAGATTACCTGAATGTCACAGCTGTTCACCTGTTC AAGGAGAGATGGGACAGTA *****

### 3.4.6 Protein expression and purification

Both WT and L34V mFXIII-A proteins were expressed in *E. coli* and purified using GSTrap FF chromatography. The L34V elution graph was identical to that of WT, therefore only WT graph is presented below (*Figure 3.7*). Once the desired protein had been eluted from the column, samples were concentrated into 200  $\mu$ L volume using 30,000 MWCO centrifuge membrane columns and protein concentrations were measured by BCA assay before samples were run onto SDS-PAGE gel electrophoresis.

The GSTrap FF column elution chart shows mFXIII-A and GST elution from GSTrap FF column (*Figure 3.7*). The spectroscopic peak of FXIII-A fraction had a left shoulder indicative that purity might be compromised.

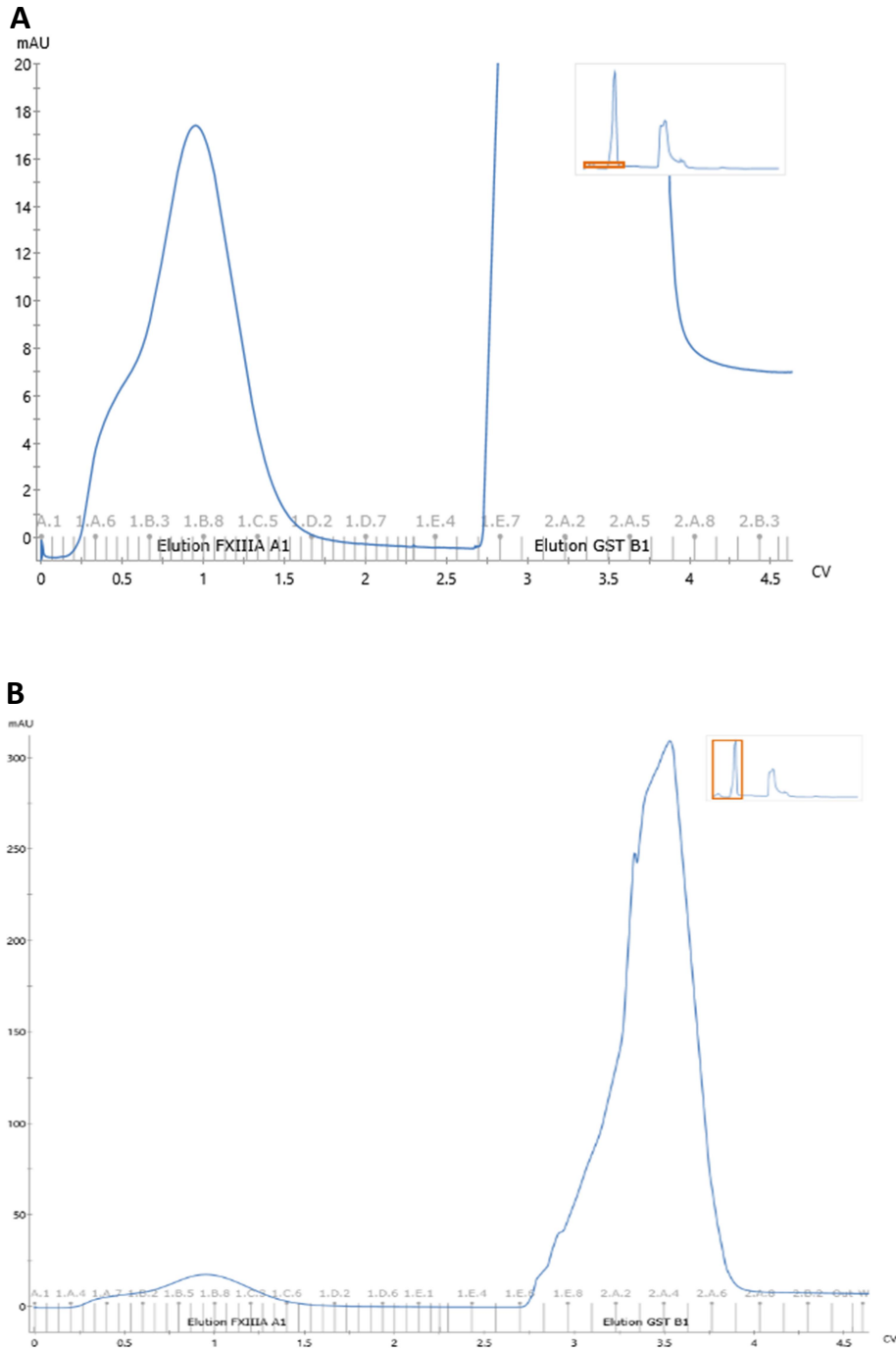


**Figure 3.7** WT mFXIII-A elution from GSTrap FF column graph. Blue line shows A280nm reading, while orange rectangle shows the magnified area of the full elution graph. Panel **A** zooms in on mFXIII-A elution curve, while panel **B** focuses on GST elution. AU – absorbance unit, CV – column volume.

SDS-PAGE of purified WT and L34V mFXIII-A, as well as their GST-bound versions revealed some issues with the purification step (Figure 3.8).

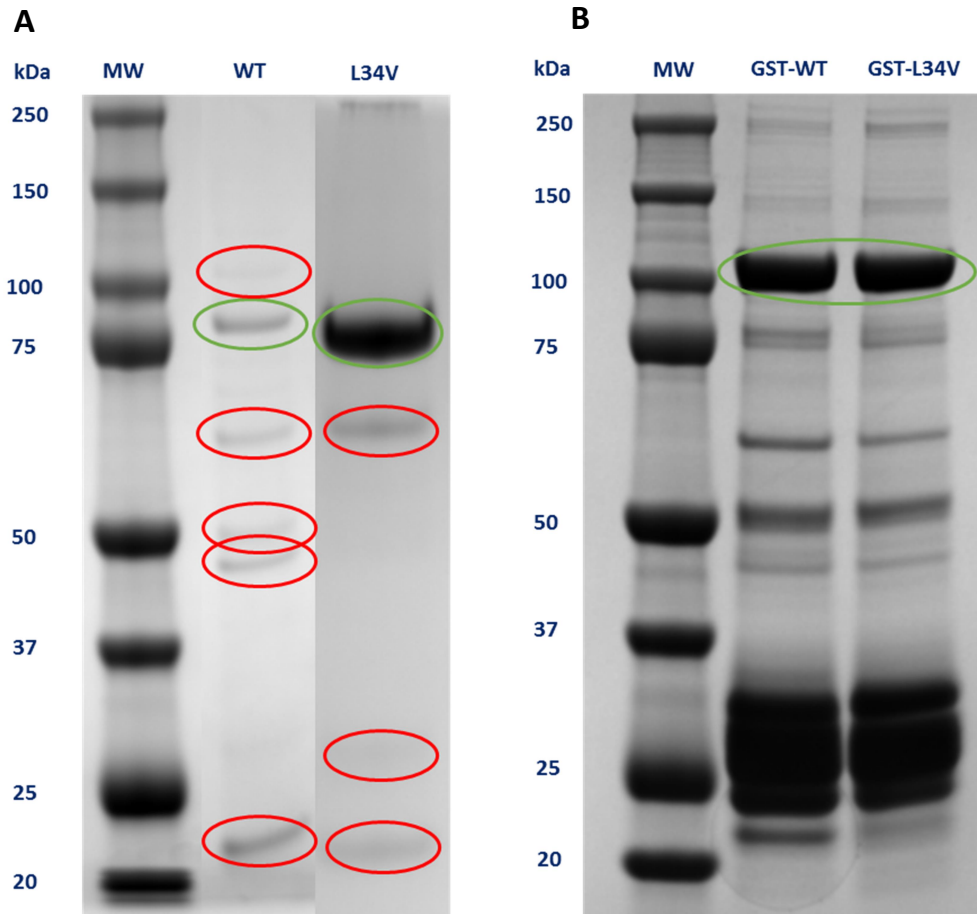


**Figure 3.8 SDS page gel of mFXIII-A Wild-Type, L34V and cleaved GST tag.**

*83 kDa WT and L34V mFXIII-A as well as WT and L34V GST-mFXIII-A bands are labelled green. Red ovals indicate host cell protein bands which were taken into the account while performing band intensity analysis for mFXIII-A concentration corrections. Theoretical GST size: 26 kDa. Reducing agent was used.*

Apart from 83 kDa mFXIII-A band (or ~110 kDa band for GST-bound variants) there were many other host cell protein bands present. The intensity of these bands (marked in red) were quantified alongside mFXIII-A band intensity and concentration of mFXIII-A was adjusted based on the mFXIII-A fraction in the sample. The concentrations obtained from the most successful purification run were as follows:

- (22% purity) WT mFXIII-A: 74.6 µg/mL
- (69% purity) L34V mFXIII-A: 1118.8 µg/mL

As for GST-bound variant gel (*Figure 3.8 B*) all band intensities were similar that we treated these samples as of similar purity, since not only the purity profiles were similar, but also total protein found was the same (~1.65 mg/mL). Interestingly, out of all purification runs, the L34V variant always purified significantly better. It can be seen in the most successful run results, which are 22% purity for WT sample and 69% purity for L34V.

### 3.4.7 Recombinant mFXIII-A activation rate assay

GST-AP cleavage assay revealed that the murine WT (34Leu) variant is activated significantly faster than the L34V variant. SDS-PAGE gels of both variants from the activation rate assay show the speed difference over two hour period of activation (*Figure 3.9*).

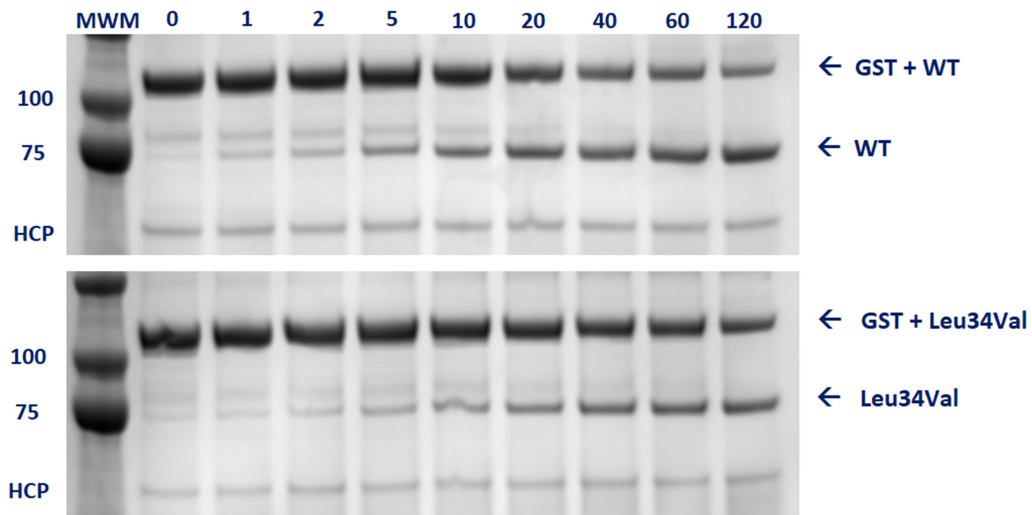


**Figure 3.9 SDS-PAGE gels of mFXIII-A WT and L34V activation rate assay.**

*Top numbers depict time-points in minutes, while left numbers show molecular weight marker band weight values in kDa. ~110 kDa GST-mFXIII-A fusion protein band is disappearing faster and 83 kDa activated mFXIII-A band is appearing faster in WT gel, showing that WT variants is being activated faster than the L34V variant of the protein. “HCP” denotes a ~65 kDa host cell protein (contaminant) band that was used as a loading control.*

Activation rates of both mFXIII-A variants were derived from SDS-PAGE band intensity changes and 34Leu values were expressed as % activation rate of 34Val. Figure 3.10 shows an example of one of the three repeat runs, where band intensity data was plotted, logarithmic curve fit and equation exponents extracted as described in section 2.15.

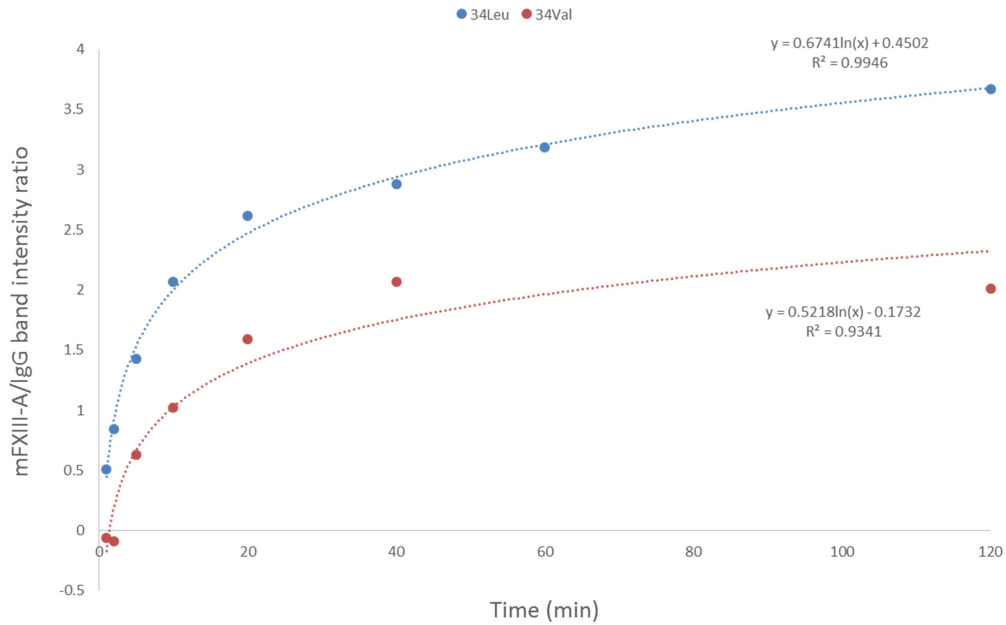


**Figure 3.10 Example logarithmic curve fit to the recombinant mFXIII-A activation rate assay SDS-PAGE band intensity data.**

Activation rate assay analysis showed that the 34Leu variant is activated at  $118\% \pm 29.4\%$  of the 34Val variant activation rate and is 18% faster than 34Val (Figure 3.11).

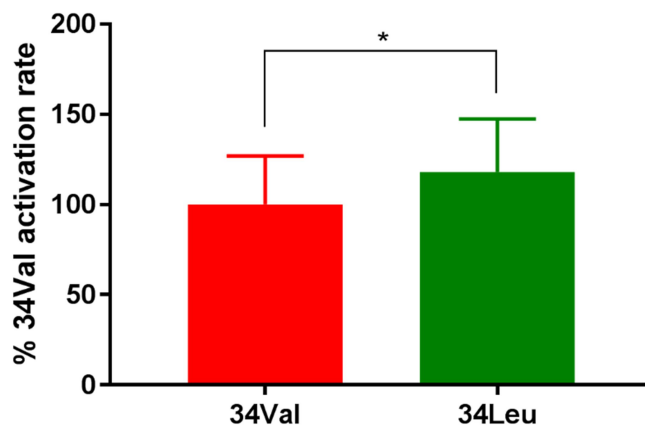


**Figure 3.11 Activation rate comparison between 34Leu and 34Val mFXIII-A.** 34Leu mFXIII-A variant shows increased activation rate when compared to 34Val variant, \*  $p < 0.05$ . 34Leu activation rate was expressed as % of 34Val activation rate. Data shown as mean  $\pm$  SEM. Statistical analysis: paired two-tailed student's T-test.  $n=3$ .

### 3.5 Discussion

Each step of the recombinant mFXIII-A cDNA L34V mutation and protein expression went smoothly and DNA products were both correct in sequence and high in yield. However, some difficulties appeared at the last stage of the *in vitro* mFXIII-A preparation - protein purification. Numerous purification re-runs were carried out to purify both WT and L34V mFXIII-A protein sufficiently, however attempts never reached the desired yield and purity. Judging from the SDS PAGE gel band intensity analysis, the purity of the protein was between 15% and 60% depending on the run. In order to accurately assess the amount of mFXIII-A present in the purification sample, the total amount of protein present (FXIII-A + host cell proteins) had to be determined by the bicinchoninic acid (BCA) assay. BCA assay consumed

close to a third of the protein yield and, therefore not enough protein would have been left for all planned *in vitro* investigations (clot formation, structure and mFXIIIa activity analyses). Also the final mFXIII-A concentrations were differing 20-fold between the variants, making accurate comparison between them experimentally difficult to make. The differences in purity profiles as well as yields simply came from runs not being done in parallel, but rather at different times during the PhD project. Considering low protein concentrations, strong difference in purity and the difficulty balancing out the amounts of protein to add to the assays, the comparison was considered unreliable. On the other hand, GST-mFXIII-A fusion purification resulted in 34Val and 34Leu variants showing identical purity profiles and came out in same concentrations while run parallel to each other at the same time. Therefore, FXIII activation rate comparison of these sets of proteins carried out with more confidence. The mFXIII-A 34Val and 34Leu variant activation rate comparison resulted to be in agreement with previously recombinant human FXIII-A (rhFXIII-A) published data. mFXIII-A 34Leu variant was shown to be activated around 18% faster than the 34Val variant, similarly to human data, where 34Leu variant has been reported to be faster activated than the 34Val variant, both plasma FXIII-A *in vitro* (Ariens et al., 2000) and recombinant FXIII-A *in vivo* (Duval et al., 2016), when injected to FXIII-A deficient mice. This gave confidence that when moving onto *ex vivo* mouse work we would see similar trend of 34Leu variant showing sped up activation and, in turn, increased cross-linking activity of FXIII compared to 34Val variant. Duval *et al.*, (2016) showed 43% activation rate increase with recombinant human FXIII-A *in vitro*, which is higher than 18% that we

observed with murine variant. The explanation could lie in low purity of our FXIII samples and host cell proteins interfering with thrombin activation of FXIII, or a possibly, that murine and human FXIII-A are distinct in their activation rates when comparing 34Leu and 34Val variants.

**Chapter 4 L34V mouse  
characterisation and *ex vivo* work**

## 4.1 Introduction

In this chapter the FXIII-A L34V (34Val) mouse model is phenotypically compared to FXIII-A Wild-Type (34Leu) and FXIII-A Knock-Out (FXIII<sup>-/-</sup>) mice variants. Characterising the newly acquired 34Val mouse variant was important in order to investigate possible phenotypical differences when compared to 34Leu and FXIII<sup>-/-</sup> mice in terms of FXIII activation and potential role in thrombosis. Coagulation is a multifactorial physiological function and singling out one coagulation factor comparison between mice variants means that any other variables have to be similar or at least accounted for. Therefore, we decided to first look into mice growth curve in order to investigate whether mice are going to have similar weight and metabolic rate at the same age. Then, plasma FXIII and fibrinogen levels were quantified. It was crucial that comparison of FXIII activity was performed in mice having similar levels of fibrinogen and FXIII itself. FXIII activation rate, as well as coagulation in general, is dependent on fibrinogen concentration. Assays, such as thromboelastometry and turbidity, measure mechanical properties and formation rates of clots, and therefore, the concentration of clot building block (fibrinogen) had to be similar. Blotting for FXIII antigen in murine plasma was also performed in order to confirm that FXIII<sup>-/-</sup> mice had no FXIII present and their molecular phenotype matched the expected genotype. Next, we performed plasma FXIII biotin incorporation assay in order to establish that increased 34Leu activation rate replicates human phenotype and is more readily activated *ex vivo* than the 34Val variant. Ariens *et al.* (2000) have shown this rate increase to be 2-fold with plasma human FXIII-A (phFXIII-A) *in vitro* and Duval *et al.* (2016) have shown that rhFXIII-A 34Leu

variant is 81% faster activated *in vivo* when injected in FXIII deficient mice. Both of the studies show FXIII activation rate effects manifest over the course of the first 15 minutes and up to 1 hour, suggesting that the effects persist even beyond first 60 minutes. This assay was also used to confirm that FXIII<sup>-/-</sup> murine plasma showed no FXIII activity. Next, in light of the published literature on clot contraction velocity (Tutwiler et al., 2016), RBC retention (Kattula et al., 2018) and thrombus weight (Byrnes et al., 2015) being heavily correlated with FXIII activity, we looked into these three parameters as well by forming murine whole blood clots *ex vivo*, measuring supernatant haemoglobin levels and weighing the clots. FXIII cross-linking is known to mechanically strengthen fibrin mesh and cross-link fibrinolysis inhibitors to fibrin, so we next performed whole blood thromboelastometry runs, which yielded clotting time, clot firmness and lysis time comparison data. Thromboelastometry was also performed both in presence and absence of platelet inhibitor in order to investigate influence of platelets on these parameters. And finally, murine plasma turbidity assay was performed and clotting velocity, fibre thickness and clotting lag time was derived. All these assays were crucial in establishing the effects of cross-linking by FXIII *ex vivo* before moving on to studying the systemic effects *in vivo*.

## **4.2 Aims**

To phenotypically compare the FXIII-A L34V (34Val) mouse model to FXIII-A Wild-Type (34Leu) and FXIII-A Knock-Out (FXIII<sup>-/-</sup>) mice variants.

## **4.3 Methods**

### **4.3.1 Murine blood collection and plasma preparation**

Each characterisation experiment used murine whole blood or plasma from FXIII-A Knock-Out (FXIII<sup>-/-</sup>), Wild-Type (34Leu) and F13AL34V (34Val) mice aged 7-14 weeks. The mice were kept as described in section 2.16 and bled as described in section 2.17.

### **4.3.2 Growth curve**

Both 34Val and 34Leu mice were weighed weekly for 10 weeks, starting on day 21 since birth (n=10).

### **4.3.3 Plasma FXIII antigen and fibrinogen levels**

Plasma from FXIII<sup>-/-</sup> (n=9), 34Val and 34Leu (n=10) mice was blotted for FXIII antigen quantification as described in section 2.22, while fibrinogen levels were measured using ELISA (section 2.23)

### **4.3.4 Plasma FXIII biotin incorporation assay**

FXIII<sup>-/-</sup> (n=9), 34Val and 34Leu (n=10) mice plasma was investigated for their plasma FXIII cross-linking activity, using a biotin incorporation assay (section 2.25).

### **4.3.5 Clot contraction, serum haemoglobin and clot weight**

Whole blood was taken from FXIII<sup>-/-</sup>, 34Val and 34Leu (n=10) and clotted in glass tubes as described in section 2.19 for 120 minutes. Every 30 minutes, glass tubes were photographed in order to investigate clot contraction (section 2.19.1), and 20  $\mu$ L of resuspended clot supernatant was taken in order to check for extruded number of red blood cells (quantified through

haemoglobin measurements) as detailed in section 2.19.2. Finally, after 2 hours, clots were dried and weighed as described in section 2.19.3.

#### **4.3.6 Thromboelastometry**

Whole blood from FXIII<sup>-/-</sup>, 34Val and 34Leu (n=10) mice was investigated for their clotting time, clot firmness and clot lysis time using a rotational thromboelastometry. Platelet inhibition by cytochalasin D was also performed in order to assess their role in clotting parameters mentioned. Section 2.20 describes thromboelastometry in detail.

#### **4.3.7 Plasma turbidity**

Turbidity assay was performed on FXIII<sup>-/-</sup> (n=9), 34Val and 34Leu (n=10) plasma by initiating coagulation and measuring sample opacity for 220 minutes as described in section 2.25.

## 4.4 Results

### 4.4.1 Growth curve

There was no difference between the weights of 34Leu and 34Val mice at any time point during 3-12 weeks (*Figure 4.1*). Both mice variants grew at the same rate and were not significantly different in weight over the 3-12 week time-course.

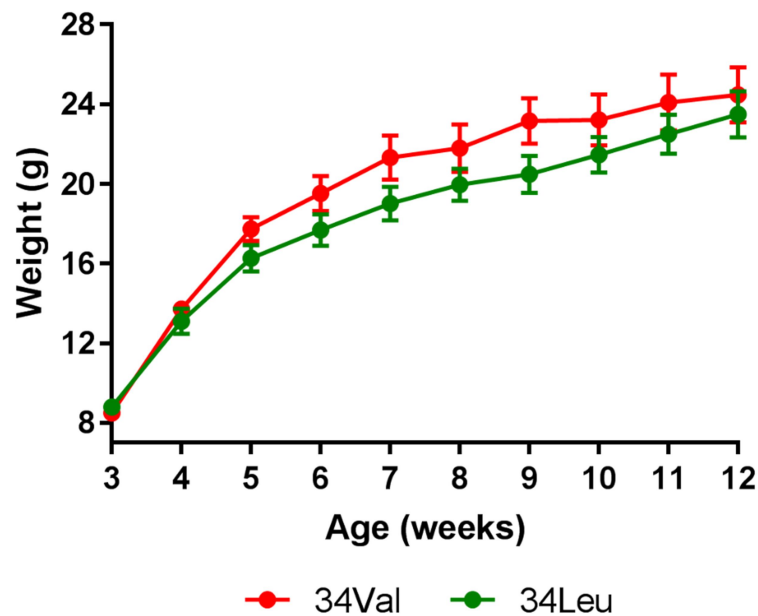


**Figure 4.1 Growth curve of 34Leu and 34Val mice.**

*No difference in mice weight was observed between the two mice mFXIII-A variant groups. Data shown as mean  $\pm$  SEM. Statistical analysis: unpaired two-tailed student's T-test. n=10.*

#### 4.4.2 Plasma FXIII antigen and fibrinogen levels

Western blotting revealed that there was no difference between 34Val and 34Leu mice mFXIII-A antigen levels ( $1.11 \pm 0.08$  FXIII / IgG ratio vs.  $1.06 \pm 0.24$  FXIII / IgG ratio respectively). As expected, FXIII<sup>-/-</sup> mice had no FXIII antigen present in their plasma (*Figure 4.3*). Due to a genotyping error, one male FXIII<sup>-/-</sup> mouse showed mFXIII-A antigen levels (*Figure 4.2*) similar to 34Leu and 34Val mice and therefore was excluded from further experiments that used plasma samples.

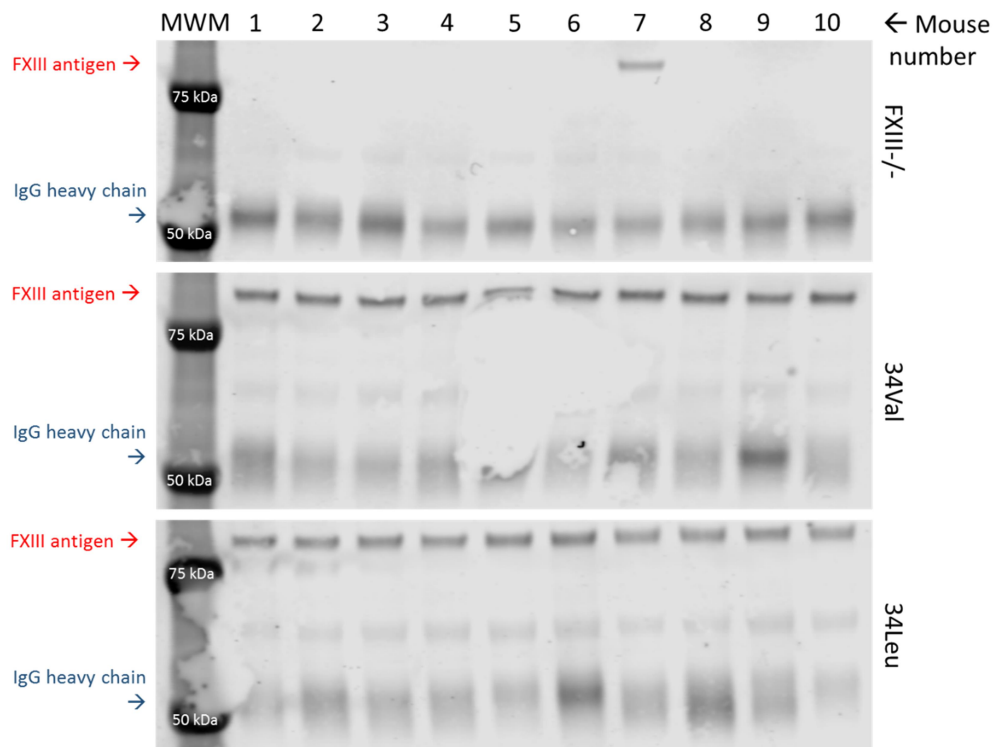


**Figure 4.2 Western blotting SDS-PAGE gels showing FXIII<sup>-/-</sup>, 34Val and 34Leu mice plasma FXIII-A antigen and IgG levels.**

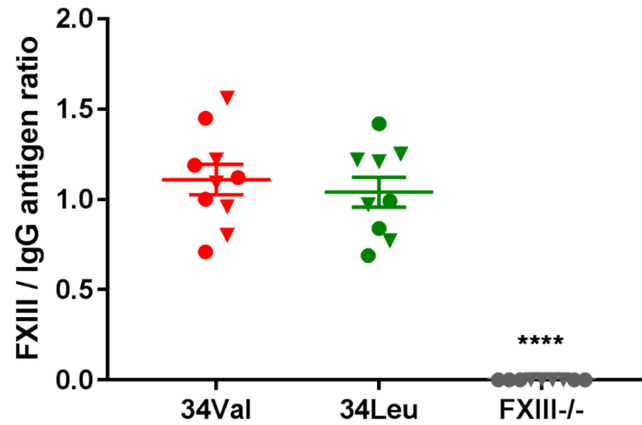


**Figure 4.3 FXIII plasma antigen levels.**

*FXIII antigen levels were expressed as FXIII / IgG antigen band intensity ratio. Data shown as mean  $\pm$  SEM. FXIII<sup>-/-</sup> mice plasma had shown to have no FXIII, \*\*\*\*  $p < 0.0001$  when compared to 34Leu and 34Val mice. Statistical analysis: One-Way ANOVA and Tukey's multiple comparisons statistical tests.  $n = 10$  ( $n = 9$  for FXIII<sup>-/-</sup>).*

There was no significant difference in plasma fibrinogen content between mice variants: 34Val:  $1.32 \pm 0.13$  mg/mL, 34Leu:  $1.42 \pm 0.06$  mg/mL and FXIII<sup>-/-</sup>:  $1.39 \pm 0.14$  mg/mL (Figure 4.4). Female FXIII<sup>-/-</sup> mice had 36.8% less median plasma fibrinogen ( $P < 0.01$ ) than the male mice ( $1.12 \pm 0.09$  mg/mL vs.  $1.77 \pm 0.58$  mg/mL respectively).

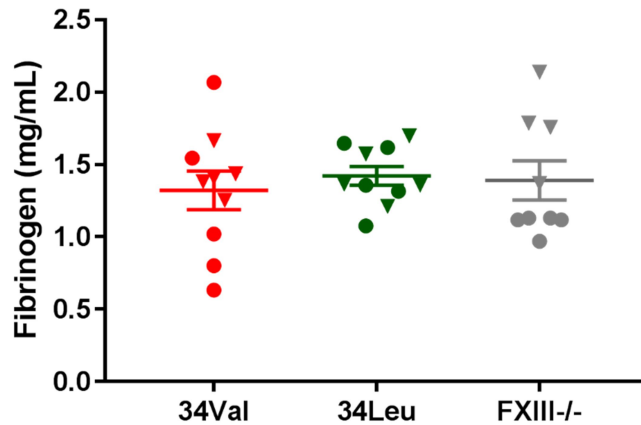


**Figure 4.4. Plasma fibrinogen levels of 34Leu, 34Val and FXIII<sup>-/-</sup> mice.**

Plasma from 34V, 34L and FXIII<sup>-/-</sup> mice showed no difference in fibrinogen content. Data shown as mean  $\pm$  SEM. Statistical analysis: One-Way ANOVA and Tukey's multiple comparisons tests.  $n=10$  ( $n=9$  for FXIII<sup>-/-</sup>).

#### 4.4.3 Plasma FXIII biotin incorporation assay

Plasma FXIII biotin incorporation assay (Figure 4.5) revealed that 34Leu mFXIII-A variant showed 39.5% higher cross-linking activity than 34Val variant ( $100.0 \pm 8.6\%$  for 34Val vs.  $139.5 \pm 12.5\%$  for 34Leu variant) despite both mouse strains having similar FXIII antigen levels (Figure 4.3), consistent with the increased activation rate (section 3.4.7) of murine FXIII 34Leu by thrombin. FXIII<sup>-/-</sup> mice have shown only  $2.3 \pm 0.5\%$  cross-linking activity of 34Val variant (even less compared to Wild-Type 34Leu mice), which confirms FXIII<sup>-/-</sup> phenotype.

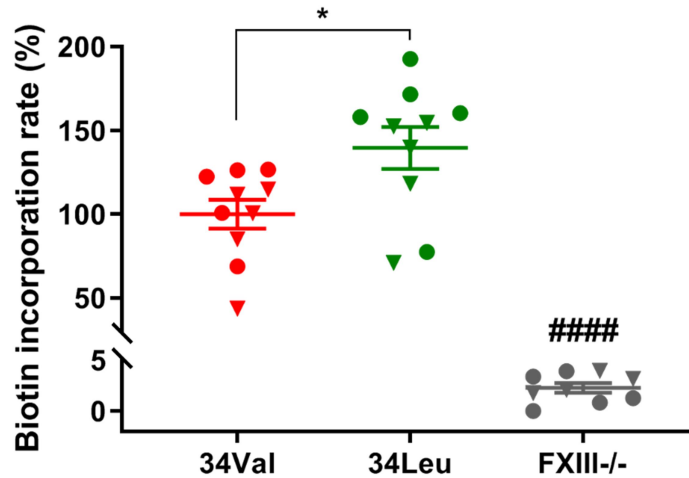


**Figure 4.5** 34Val, 34Leu and FXIII-/- mice plasma mFXIII-A biotin incorporation rates.

34Leu mFXIII-A variant shows significantly higher cross-linking activity than 34Val variant, \*  $p < 0.05$ . FXIII-/- variant shows negligible cross-linking activity when compared to 34Leu and 34Val mice, ####  $p < 0.0001$ . Data shown as mean  $\pm$  SEM. Statistical analysis: One-Way ANOVA and Tukey's multiple comparisons statistical tests.  $n = 10$  ( $n = 9$  for FXIII-/-).

#### 4.4.4 Clot contraction, clot supernatant haemoglobin and clot weight

Clot volumes between 34Val, 34Leu and FXIII-/- mice blood were not different at any of the time-points measured (Figure 4.6): at 60 min ( $78.0 \pm 12.1 \mu\text{L}$  vs.  $83.4 \pm 11.1 \mu\text{L}$  vs.  $91.5 \pm 16.3 \mu\text{L}$  respectively), 90 min ( $39.2 \pm 5.2 \mu\text{L}$  vs.  $41.4 \pm 3.1 \mu\text{L}$  vs.  $35.1 \pm 4.7 \mu\text{L}$  respectively) and 120 min ( $31.7 \pm 1.4 \mu\text{L}$  vs.  $39.5 \pm 2.7 \mu\text{L}$  vs.  $22.8 \pm 3.1 \mu\text{L}$  respectively). FXIII-/- mice appeared to show a steeper clot contraction curve which can be explained by their blood taking longer to start contracting (most samples did not form a clearly defined clot yet at 30 minute time-point, therefore the clot volume was more difficult to measure from the photographs taken).

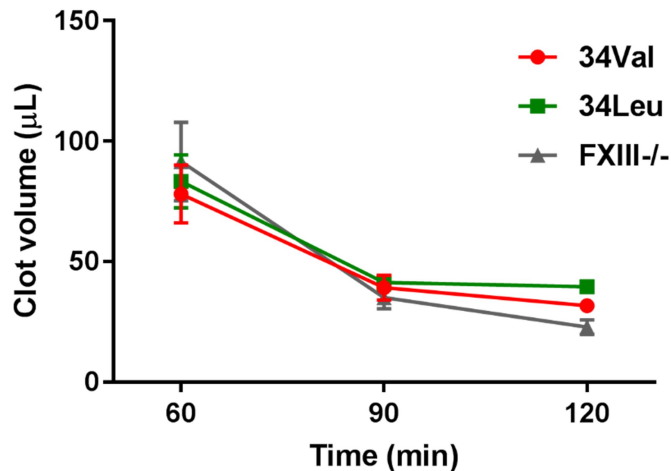


**Figure 4.6** 34Leu, 34Val and FXIII-/- mice whole blood clot volume after 60, 90 and 120 min of clotting.

34Val, 34Leu and FXIII-/- mice clot contraction showed no difference at any of the time-points. Data shown as mean  $\pm$  SEM. Statistical analysis: Two-Way ANOVA and Tukey's multiple comparisons tests.  $n=10$ .

Clot supernatant haemoglobin levels (% initial) were the same between 34Val and 34Leu mice at 60 min ( $26.4 \pm 2.6$  % vs.  $24.6 \pm 3.7$  % respectively), 90 min ( $33.6 \pm 3.8$  % vs.  $31.1 \pm 4.1$  % respectively) and 120 min ( $34.0 \pm 3.3$  % vs.  $34.4 \pm 4.6$  % respectively). However clot supernatant haemoglobin levels were significantly higher for FXIII-/- samples:  $48.7 \pm 7.0$  % (60 min),  $51.3 \pm 3.5$  % (90 min) and  $52.4 \pm 3.6$  % (120 min) (Figure 4.7).

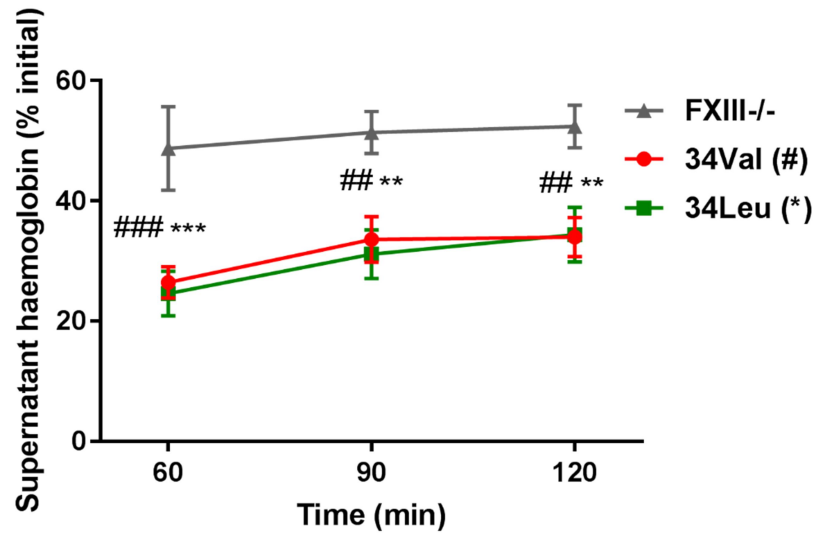


**Figure 4.7 Supernatant haemoglobin amount (% initial) after 60, 90 and 120 min of clotting.** 34Val and 34Leu supernatant haemoglobin values were not different at any time-point. FXIII-/- supernatant values were higher compared to both 34Val and 34Leu variants. \*\*  $p < 0.01$ , \*\*\*  $p < 0.001$  (FXIII-/- vs. 34Leu), ##  $p < 0.01$ , ###  $p < 0.001$  (FXIII-/- vs. 34Val). Data shown as mean  $\pm$  SEM. Statistical analysis: Two-Way ANOVA and Tukey's multiple comparisons tests.  $n = 10$ .

Clot weights were measured 2 hours after the initiation of clotting and subsequent clot contraction. There was no significant difference in clot weights between 34Val and 34Leu mice ( $31.3 \pm 1.3$  g and  $33.5 \pm 1.5$  g respectively), however FXIII-/- clots were significantly lighter ( $20.5 \pm 2.0$  g) than both 34Val ( $p < 0.001$ ) and 34Leu ( $p < 0.0001$ ) (Figure 4.8). A larger than 34% increase was observed when comparing mice that are mFXIII-A sufficient with mice that are FXIII-A deficient due to gene knock-out.

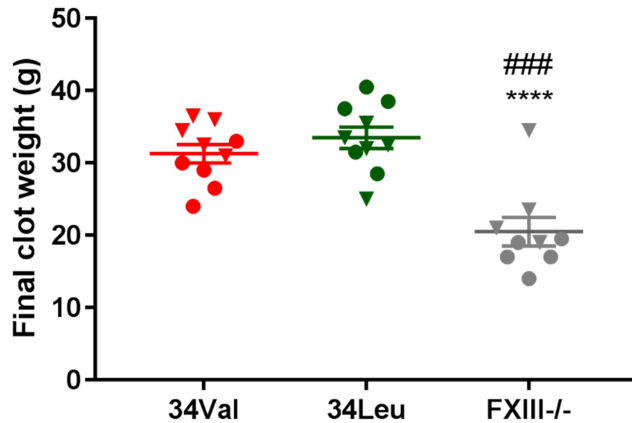


**Figure 4.8 Two-hour clot weights from 34Leu, 34Val and FXIII-/- murine blood.** Clots from 34Val and 34Leu showed no difference in final clot weight, but were both significantly heavier than that of FXIII-/- mice. \*\*\*\*  $p < 0.0001$  FXIII-/- vs. 34Leu, ###  $p < 0.001$  FXIII-/- vs. 34Val. Data bars shown as mean  $\pm$  SEM. Statistical analysis: One-Way ANOVA and Tukey's multiple comparisons tests.  $n = 10$  ( $n = 9$  for FXIII-/-).

#### 4.4.5 Thromboelastometry

As shown in Figure 4.9, under normal clotting conditions (EXTEM) no difference in Clotting Time (CT), Maximum Clot Firmness (MCF) and Lysis Time (LT) were observed between 34Val and 34Leu, however FXIII-/- clots were significantly slower to clot ( $42.6 \pm 3.4$  s and  $41.1 \pm 2.6$  s vs.  $64.0 \pm 4.6$  s respectively), far less stiff ( $56.9 \pm 1.4$  mm and  $58.5 \pm 1.0$  mm vs.  $17.4 \pm 1.3$  mm respectively) and quicker to lyse ( $4183.0 \pm 413.3$  s and  $3049.0 \pm 445.9$  s vs.  $1137.0 \pm 89.9$  s respectively). While platelets were inhibited, no difference in CT and MCF were observed between 34Val and 34Leu, however FXIII-/- clots were significantly slower to clot ( $42.4 \pm 3.2$  s and  $43.0 \pm 3.1$  s vs.  $76.7 \pm 8.0$  s respectively) and far less stiff ( $19.9 \pm 1.6$  mm and  $18.8 \pm 2.2$  mm vs.  $4.2 \pm 0.7$  mm respectively). In platelet inhibition FIBTEM

condition, MCF was strongly reduced (more than 65% reduction) when compared to EXTEM condition in both 34Leu and 34Val variants. Percentage reduction of clot firmness was even more pronounced in FXIII-/- whole blood (more than 75%).

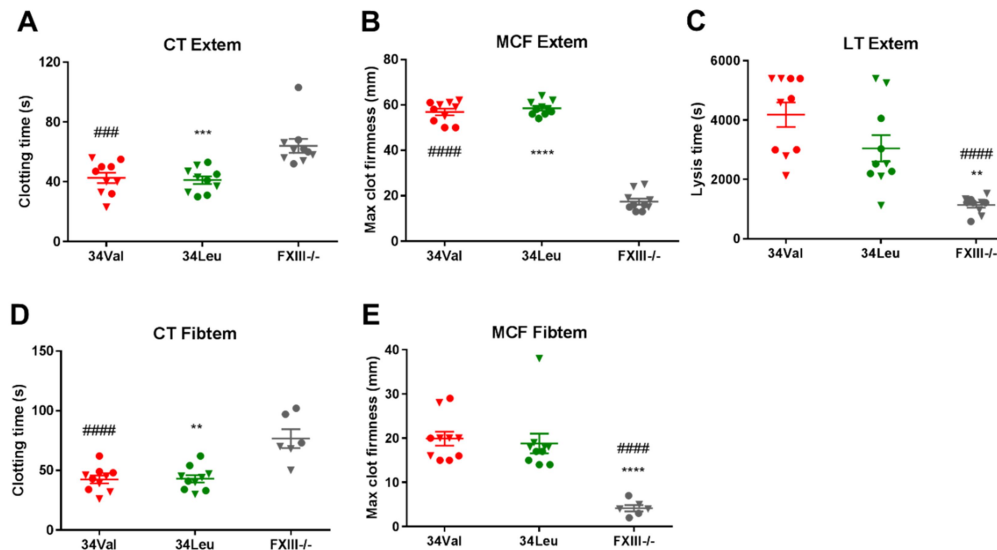


**Figure 4.9 ROTEM clot CT, MCF and LT with and without platelet activity in FXIII<sup>-/-</sup>, 34Val and 34Leu blood.** Blood from 34Val and 34Leu variants showed no difference in any of the parameters measured, however there were differences compared to FXIII<sup>-/-</sup> blood. In both EXTEM and FIBTEM (platelet inhibition), CT was significantly longer for FXIII<sup>-/-</sup> compared to both 34Val and 34Leu, \*\*  $p < 0.01$ , ### and \*\*\*  $p < 0.001$ , \*\*\*\*\*  $p < 0.0001$  (A and D). In both EXTEM and FIBTEM, MCF was significantly smaller for FXIII<sup>-/-</sup> compared to both 34Val and 34Leu, \*\*\*\*\* and \*\*\*\*  $p < 0.0001$  (B and E). LT was only performed in EXTEM condition only and it revealed a significant decrease for FXIII<sup>-/-</sup> compared with 34Val and 34Leu, \*\*\*\*\*  $p < 0.0001$ , \*\*  $p < 0.01$  (C). Data shown as mean  $\pm$  SEM. Statistical analysis: One-Way ANOVA and Tukey's multiple comparisons tests.  $n=10$  ( $n=6$  for FIBTEM FXIII<sup>-/-</sup>).

#### 4.4.6 Plasma turbidity

Mice plasma coagulation turbidity was measured in order to assess any differences in clotting lag time (LT), MaxOD (fibre thickness) and Vmax (clotting rate) between mice variants in an acellular system (*Figure 4.10*). Both the LT values ( $82.8 \pm 8.7$  s for 34Leu,  $118.8 \pm 24.0$  s for 34Val,  $81.3 \pm 9.1$  s for FXIII<sup>-/-</sup>) and Vmax values ( $0.020 \pm 0.003$  OD/s for 34Leu,  $0.016 \pm 0.002$  OD/s for 34Val,  $0.018 \pm 0.003$  OD/s for FXIII<sup>-/-</sup>) were not different between the mice variants. MaxOD values were not statistically different between the 34Leu ( $0.176 \pm 0.019$  AU) and the 34Val ( $0.145 \pm 0.014$  AU) or FXIII<sup>-/-</sup> variants ( $0.226 \pm 0.019$  AU). However, FXIII<sup>-/-</sup> MaxOD values were significantly higher than 34Val values ( $p < 0.05$ ), suggesting that plasma from FXIII<sup>-/-</sup> mice forms clots that have thicker fibrin fibres.

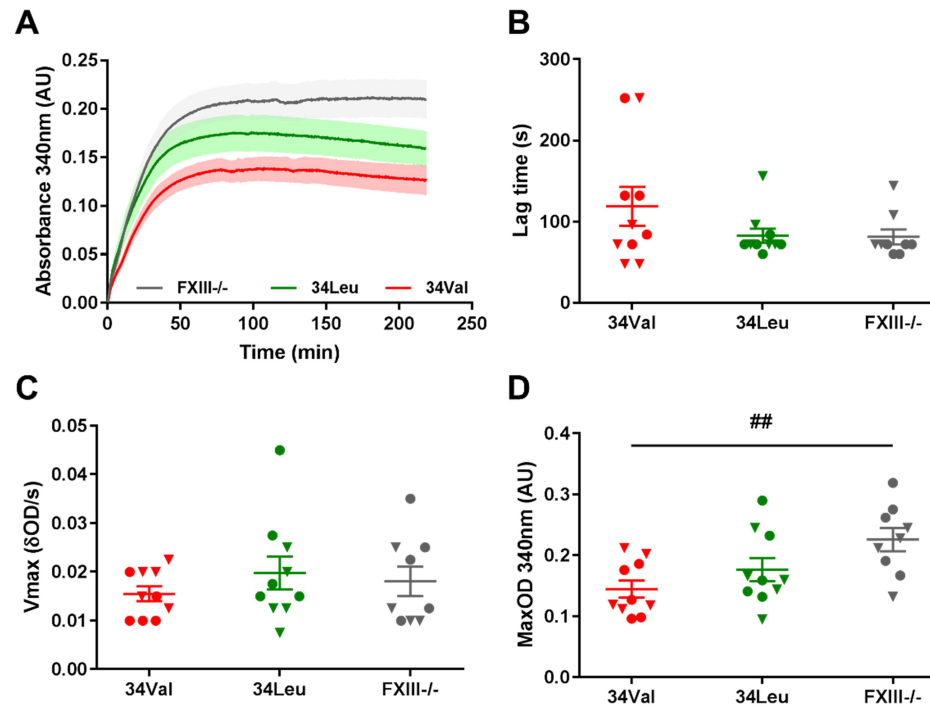


**Figure 4.10 34Val, 34Leu and FXIII-/- mice plasma coagulation turbidity analysis.**

Plasma coagulation turbidity was measured (A) and Lag time (B), Vmax (C), MaxOD (D) parameters quantified. Plasma from all mice variants showed no difference in Lag time and Vmax, however plasma from FXIII-/- mice showed a significantly larger MaxOD than 34Val, <sup>##</sup>  $p < 0.01$ . Statistical analysis: One-Way ANOVA and Tukey's multiple comparisons tests. Data shown as mean  $\pm$  SEM.  $n = 10$  ( $n = 9$  for FXIII-/-).

## 4.5 Discussion

By carrying out murine characterisation work described in this chapter, the phenotypes of FXIII<sup>-/-</sup>, 34Leu and 34Val mice were determined in detail. Phenotypical properties were chosen based on their known linkage to FXIII activity (e.g. clot contraction, RBC retention), being a standard mouse characteristic (growth curve) or being directly biochemically linked to the coagulation (e.g. plasma FXIII, fibrinogen levels). We could not find any differences in growth curve, plasma FXIII antigen and fibrinogen levels between 34Leu and 34Val mice. This meant that we were comparing mice of similar metabolism rate, clot building block (fibrinogen) concentrations and amount of plasma FXIII itself, at the age of 7-14 weeks. Plasma FXIII antigen assay also confirmed that our FXIII<sup>-/-</sup> mice did not possess any FXIII in their plasma (apart from one wrongly genotyped male mouse (*Figure 4.2*), which was excluded from all datasets). Similar fibrinogen levels between mice variants were very important, due to the fact that fibrinogen is known to increase FXIII activation rate, and therefore any functional FXIII comparison is influenced by this parameter.

Further *Ex vivo* investigations were carried out in order to assess functional differences between 34Leu and 34Val mFXIII-A, and to see how previously published recombinant human FXIII-A (rhFXIII-A) V34L data compares to the murine variant. Even though statistically there were no differences in turbidity, thromboelastometry and glass tube clotting experiments between 34Leu and 34Val variant, there were unexpected trends that are worth mentioning.

As previously established with plasma hFXIII-A *in vitro* by Ariens et al. (2000) and *in vivo* by Duval et al (2016), injecting rhFXIII-A in FXIII-A deficient mice, human FXIII-A V34L variant (rhFXIII-A 34Leu) is activated faster than the 34Val variant (2-fold and 1.8-fold respectively) and this translates into more fibrin cross-linking activity. This activation rate increase leading to more cross-linking activity using murine FXIII-A variant can also be seen in this project's work, described in sections 3.4.7 (1.2-fold *in vitro*) and 4.3.4 (1.4-fold *in vivo*).

Interestingly, FXIII-/- mice plasma has shown 2.3% of 34Val FXIII cross-linking activity as opposed to expected 0%, since FXIII-/- mice plasma contained no FXIII. However, this can be explained by either noise readings within the assay or the fact that fibrinogen is a target for the other transglutaminases, such as TG1 and TG2 (Murthy and Lorand, 1990, Murthy et al., 2000), which carry out FXIII-like cross-linking (Lorand, 2005).

Since FXIII-/- mice plasma has shown 2.3% and 34Leu - 139.5% of 34Val FXIII cross-linking activity, we can assume that any difference between these mice in coagulation, such as fibrin fibre thickness or lysis time, would be due to the difference in fibrin cross-linking activity. Interestingly, our findings did not necessarily follow a direct correlation where increasing fibrin cross-linking (FXIII-/- << 34Val < 34Leu) necessarily increased or decreased some coagulation parameters. For example, in published literature fibrin fibre thickness has been shown to decrease (Lim et al., 2003) and clot lysis time to increase (Stepien et al., 2009) with increasing FXIII activity (Duval et al., 2016), however, our mFXIII-A 34Leu data for clot lysis and fibre thickness were in between FXIII-/- and 34Val values: 34Leu fibres being 21.4% thicker

than 34Val (turbidity maxOD) and 34Leu clots taking 27.1% quicker to lyse (ROTEM Lysis Time). Although at odds with the published literature, the differences between 34Leu and 34Val in clot lysis time and fibre thickness were not statistically significant ( $P>0.05$ ).

FXIII-/- values were in agreement with previously published data, which shows that decreased FXIII cross-linking slows clot formation (Schroeder et al., 2001), decreases time to lyse (Lorand, 2000), fibrin fibres thickness (Lim et al., 2003), clot firmness (Jambor et al., 2009) and RBC's retention (more serum haemoglobin) during clot contraction (Aleman et al., 2014), which also resulted in lighter clot (Byrnes et al., 2015). In addition, during clot contraction studies, unlike 34Leu and 34Val, most FXIII-/- clots haven't yet fully formed or started retracting by 30 minute time-point, which is in agreement with previous literature on impaired retraction in FXIII-A deficient mice (Kasahara et al., 2010). In agreement with published literature (Kattula et al., 2018), between 30 and 60 minutes, the firmness of FXIII-/- fibrin mesh is increasing and reaching that of FXIII-sufficient clots, which enables platelets to then pull at an accelerated rate to reach similar clot volume at 60 minute timepoint. In their study, Kattula *et al.* showed that the velocity of FXIII-/- clot contraction was higher when compared to Wild-Type (34Leu) clots in the 30-60 min range (Kattula et al., 2018). Past the 60 min timepoint FXIII-/- and FXIII sufficient clots were contracting at a similar rate, in agreement with the study (Kattula et al., 2018).

Lack of differences between mFXIII-A 34Leu and 34Val variants in some cases could be due to less pronounced 34Leu cross-linking activity increase (39.5%) when compared to the human variant, that purified from plasma

showed a 2-fold activation rate increase *in vitro* (Ariens et al., 2000) and a 81% increase *in vivo*, when expressed in *E. coli* and injected into FXIII-deficient mice (Duval et al., 2016). This difference in activation rate increase could also originate from experimental differences. A previous study in FXIII-A V34L activation rates has shown that the FXIII activity difference between 34Leu and 34Val variants are also thrombin concentration dependent and increasing concentrations of thrombin mask this difference (Balogh et al., 2000). Also the difference could lay in the fact that recombinant human FXIII, having a 86.9 % homology with mice variant, could perform differently when injected in mice as opposed to the murine variant being expressed in plasma naturally.

Platelet supplementation therapy has been a common practice for increasing clot strength (Solomon et al., 2015) and it has been established that increased platelet reactivity enhances patient clot strength (Huang et al., 2015). Platelet inhibition during our rotational thromboelastometry experiments showed that platelets contribute substantially to clot firmness (186 % increase) and the effect is even more pronounced (314 % increase) when FXIII has not cross-linked fibrin fibres in FXIII<sup>-/-</sup> blood. These data suggest that the clot stiffening effect of platelets come from their own mechanical actions on fibrin fibres and not through secretion of FXIII, because the effect is present in FXIII knock-out mice, however the influence of other tissue transglutaminases (e.g. TG2) coming from activated platelets could be in play as well. Furthermore, these data suggest that platelet supplementation may rescue clot stiffening when FXIII activity is lacking.

Another point of consideration is an ability of granulocyte enzymes such as human neutrophil elastase (HNE) (Schmidt et al., 1975), cathepsin G and metalloproteinases to both proteolytically activate (Bagoly et al., 2012) and degrade FXIII (Klingemann et al., 1982). Since HNE cleavage site on FXIII-A subunit is the Val39-Gln40 peptide bond (Bagoly et al., 2008), it is close enough for Val34Leu mutation to possibly influence HNE dependent-FXIII-A activation rate as well. It could be worth exploring other (non-thrombin) FXIII activating enzymes in the future, especially since HNE activated FXIII-A activity has been shown to achieve fibrin cross-linking (Bagoly et al., 2008).

All considered, the data provided in this chapter show that FXIII-A 34Val mice are phenotypically similar to Wild-Type (FXIII-A 34Leu) mice and can be used for FXIII activity comparison. FXIII<sup>-/-</sup> mice were similar in terms of plasma fibrinogen levels, however every other (FXIII-A dependent) phenotypical trait was different. Comparatively, FXIII-A activation rates are also confirming the phenotype of all 3 murine variants used, with 34Leu mice showing faster FXIII activation than 34Val mice, and FXIII<sup>-/-</sup> mice showing no FXIII activation at all. Some clotting parameters, like lysis time and clot fibre thickness were different than expected based on the existing literature, however the differences were not statistically significant. It was unpredictable to not detect many of the expected differences between the 34Val and 34Leu variant in *ex vivo* studies and perhaps some of these differences were lost due to the sensitivity of the assays chosen. However, the main interest of the comparison lies in *in vivo* thrombosis models and that was investigated next.

**Chapter 5 *In vivo* murine FeCl<sub>3</sub>  
induced pulmonary and cerebral  
thromboembolism models**

## 5.1 Introduction

Studies showing that the FXIII-A V34L variant has effects on thrombotic disease have been appearing frequently in the last two decades, sparking an increased interest in FXIII. In particular, those studies that showed a protective effect of FXIII V34L in deep vein thrombosis (Wells et al., 2006, Pourgheysari et al., 2014), stroke (Elbaz et al., 2000), coronary artery disease (Voko et al., 2007) and myocardial infarction (Shafey et al., 2007) have raised a lot of interest. These clinical studies were largely observational, and the mechanism by which the 34Leu sequence variant exerts its protective effect(s) has not yet been elucidated. It was decided to investigate the differences in both venous and arterial thromboembolism dynamics between Wild-Type (34Leu), 34Val and FXIII<sup>-/-</sup> mice by establishing a murine thromboembolism model, to then elucidate the *in vivo* effects of different FXIII activity levels in stroke and pulmonary embolism.

In order to investigate the differences in clot embolisation dynamics between FXIII<sup>-/-</sup>, 34Leu and 34Val mice in both lungs and brains, we employed a FeCl<sub>3</sub> vascular injury technique. This method was first described by Kurz *et al.* (1990) and is now a widely used tool for thrombi generation (Neeves, 2015, Schoenwaelder and Jackson, 2015). Once filter paper soaked in FeCl<sub>3</sub> is applied onto the exterior of the blood vessel, FeCl<sub>3</sub> diffuses through the cell wall and damages the endothelium (Li et al., 2013). The nature of FeCl<sub>3</sub> effects, however, remains poorly understood. Initially, it was thought that iron from FeCl<sub>3</sub> accumulates inside the endothelium cells, promotes reactive oxygen species generation, raises cytotoxicity, causes endothelium denudation, which in turn exposes subendothelial elements and promotes

thrombus generation via extrinsic pathway of the coagulation cascade (Kurz et al., 1990). Later, numerous studies have shown that endothelial denudation is actually minimal and could not be the main reason for thrombus generation (Eckly et al., 2011, Barr et al., 2013, Woollard et al., 2009). It was also shown that presence of RBC's is crucial, because RBC haemolysis and subsequent haemoglobin oxidation promoted vascular injury and thrombosis (Woollard et al., 2009, Barr et al., 2013). Eckly and colleagues have revealed that ferric ion-rich spherical bodies form on the endothelium and promote tissue factor expression (Eckly et al., 2011). Subsequent studies have suggested that blood cell adhesion to the endothelium provides the reactive surface for platelet aggregation and coagulation, necessary for stable thrombus formation locally (Ciciliano et al., 2015). In this case, vascular injury is suggested to be a secondary propagator of coagulation and not the initiator. This, however, still remains to be confirmed and further looked into, in order to further define the FeCl<sub>3</sub> mechanism of action more precisely (Schoenwaelder and Jackson, 2015). Regardless, FeCl<sub>3</sub> remains the most widely used model for inducing thrombosis (Neeves, 2015), providing a strong and reproducible thrombotic response, mostly used for arterial thrombosis (Whinna, 2008, Ghosh et al., 2008, Owens et al., 2011, Tseng et al., 2006, Zhang et al., 2017), and less commonly for venous thrombosis (Wang et al., 2006, Marsh Lyle et al., 1998, Martinod et al., 2013, Aghourian et al., 2012).

By gently applying FeCl<sub>3</sub> soaked filter paper to the murine *inferior vena cava* (IVC) we generated clots that embolised and occluded blood vessels inside the lung, thus causing pulmonary embolism. To model embolism in the

cerebral circulation (stroke), we applied  $\text{FeCl}_3$  onto the murine carotid artery to generate clots, which embolised to the brain and occluded the cerebral vasculature. Before the procedure, mice were injected with fluorescent fibrinogen (tagged with AlexaFluor<sup>647</sup>), which allowed visualisation of the emboli. Mice vasculature was also made fluorescent by perfusing them with a gelatine mix containing FITC-conjugated albumin. Post-procedure brains or lungs were harvested, fixed, dehydrated in alcohol solution and optically cleared with ether based organic solvent. The resulting organs were transparent and ready to be imaged using a light sheet microscope.

This optical clearing method was first described by Erturk et al (Erturk et al., 2012) and was named Three-Dimensional Imaging of Solvent-Cleared Organs (3DISCO). Initially, the dehydration chemical used was tetrahydrofuran (THF) and its use resulted in tissue distortion. Later, another team figured out that THF can be substituted by methanol and dichloromethane (DCM), which not only eliminates the distortive tissue shrinkage problem, but also reduces natural tissue autofluorescence for reduced background noise (Renier et al., 2014, Renier et al., 2016). The team termed the method immuno-DISCO-plus (iDISCO+), which we adapted for our experimental protocol. Our method involved using increasing methanol concentrations for dehydration; DCM for further dehydration, background fluorescence reduction and tissue preparation for correct refractive index; and, finally, dibenzyl ether for optical tissue clearing by delipidation.

The principal of light sheet microscope is that a focused light sheet excites a single 5  $\mu\text{m}$  thick plane of sample, and light is emitted from the sample

perpendicularly where it gets collected in the objective. With the help of lenses, laser light coming from the source is focused into a flat 5  $\mu\text{m}$  thick light sheet, and therefore, at one time illuminates only a small amount of the organ keeping photodamage and fluorophore bleaching to a minimum. During imaging, both the sample and the objective lens are submerged in the pool of organic solvent which has the same refractive index as the cleared sample. Two sided excitation of the sample improves signal strength and detail, since light only needs to travel through half of the organ at most and is able to preserve the excitation strength and not get absorbed / scattered as much. Double sided imaging is repeated every time the control stage moves the sample up by 5  $\mu\text{m}$ . Image stacks are then combined together to recreate a three-dimensional image of the organ. Multiple channel capture allows the final organ model to contain differently coloured structures, which can be distinguished or colocalised in both two and three dimensions.

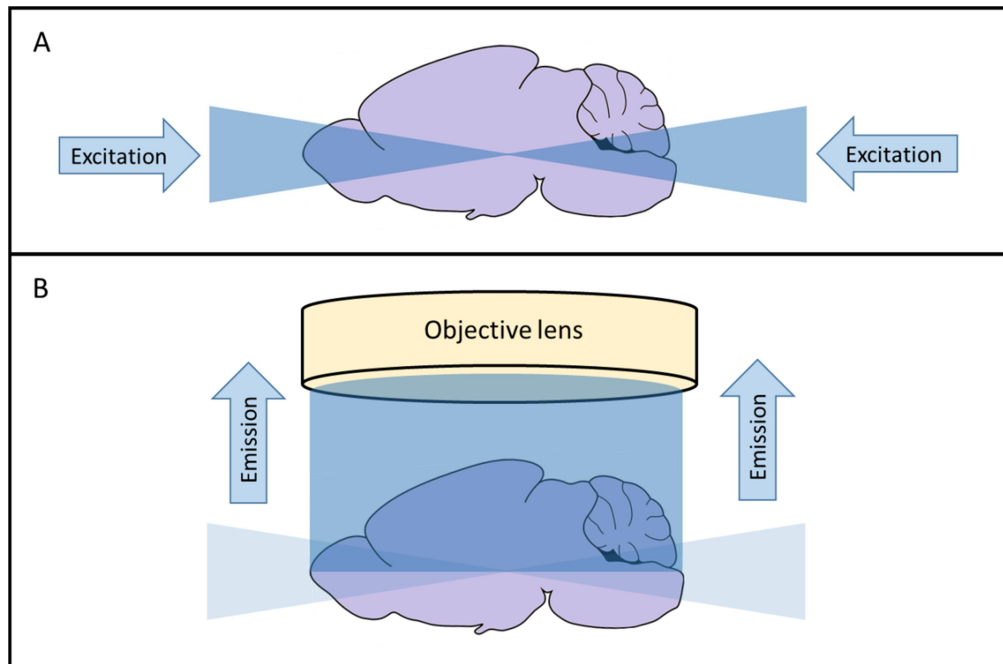


**Figure 5.1 Schematic depicting a light sheet microscopy principle.**

*The cartoon depicts a mouse brain sample getting first excited with a light sheet from both sides (A). Then, excited sample emits fluorescence perpendicular to the excitation direction, which is collected in the objective lens (B).*

Since the light sheet microscope is able to image the organ in 5  $\mu\text{m}$  sheets, and do so at 5  $\mu\text{m}$  steps, it is effectively able to capture all the emboli within the organ. The ability of light sheet images to be then compiled into a stack reconstructing a three dimensional organ was a critical part of this project. Newly established organ clearing procedures and high resolution light sheet microscope allowed us not only to establish the methodology, but also to investigate multiple murine variants in both venous and arterial thromboembolism within the last year of the project. The acquired imaging data was then analysed using image analysis software, where the embolism

occurrence (number of emboli), and severity (emboli volume) were determined.

## **5.2 Aims**

To establish a murine thromboembolism model and elucidate the effects of different FXIII activity levels in stroke and pulmonary embolism *in vivo*.

## **5.3 Methods**

### **5.3.1 Pulmonary embolism**

10 mice (5 males, 5 females) per 34Leu, 34Val and FXIII<sup>-/-</sup> variant were anaesthetised, and FeCl<sub>3</sub> application to the *inferior vena cava* (IVC) was performed as detailed in section 2.26.1. Photographs depicting the application of FeCl<sub>3</sub> can be seen in *Figure 5.2*.

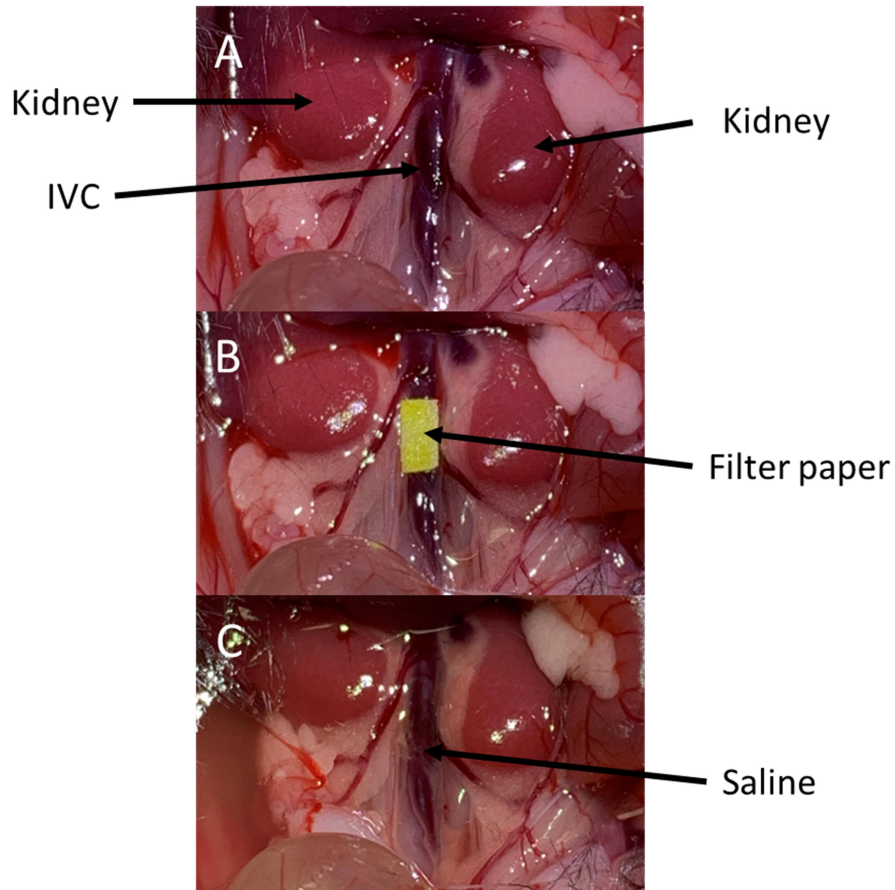


**Figure 5.2  $\text{FeCl}_3$  inferior vena cava injury model surgery photographs.**

*Panel A shows the IVC being exposed, prepared for injury. Panel B shows a 1.5mm X 4.5mm filter paper soaked in 2.5%  $\text{FeCl}_3$  placed on the exposed IVC. Panel C shows IVC after the filter paper is removed and the injury site is flooded by saline in order to wash excess  $\text{FeCl}_3$  away.*

Lungs were then harvested, dehydrated and optically cleared as described in section 2.26.1. After at least 72 hours post optical clearing, lungs were imaged by light sheet microscopy as detailed in section 2.26.2. After microscopy image acquisition, image stacks were loaded onto the Imaris image analysis software and organ 3D model reconstruction as well as embolism analysis was carried out as described in section 2.26.3.

### 5.3.2 Cerebral embolism

10 mice (5 males, 5 females) per 34Leu, 34Val and FXIII<sup>-/-</sup> variant were anaesthetised and FeCl<sub>3</sub> was applied to the carotid artery as detailed in section 2.26.1. Photographs depicting the FeCl<sub>3</sub> application can be seen in *Figure 5.3*.

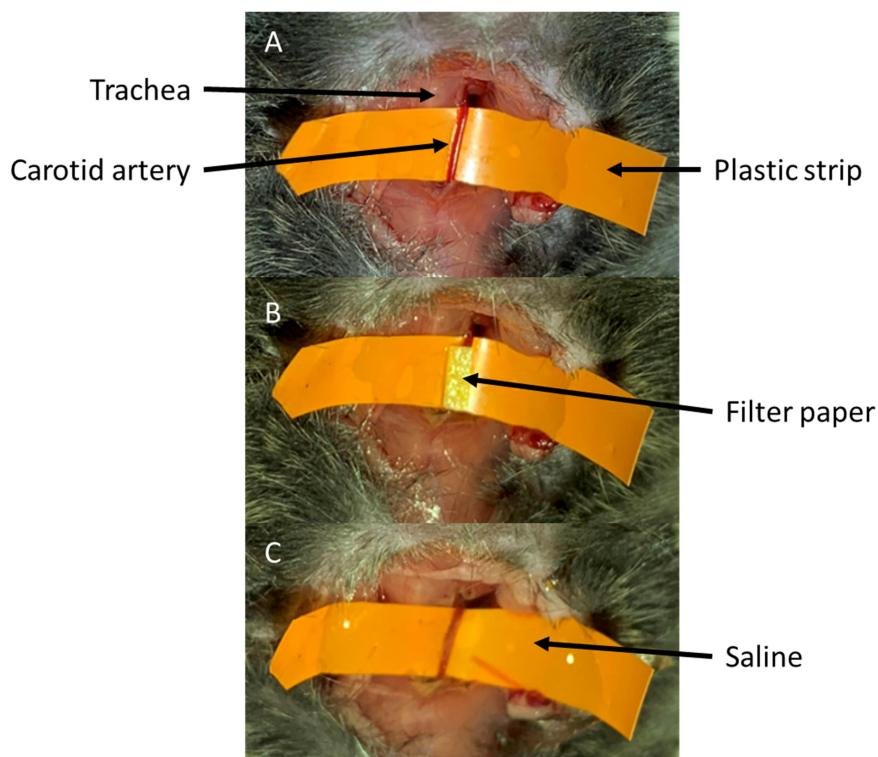


**Figure 5.3 FeCl<sub>3</sub> carotid artery injury model surgery photographs.**

*Panel A shows left carotid artery being isolated with a plastic strip, made ready for injury. Panel B shows a 1.5mm X 4.5mm filter paper soaked in 10% FeCl<sub>3</sub> and placed on the isolated carotid artery. Panel C shows carotid artery after the filter paper is removed and the injury site is flooded by saline in order to wash excess FeCl<sub>3</sub> away.*

After the injury, the brains were harvested, dehydrated and optically cleared as described in section 2.26.1. At least 72 hours after brain optical clearing, organs were imaged by light sheet microscopy as detailed in section 2.26.2. After microscopy acquisition, image stacks were loaded onto the Imaris image analysis software and organ 3D model reconstruction as well as embolism analysis was carried out as described in section 2.26.3.

For brain samples however, instead of software volumetric analysis, a manual emboli counting was carried out as described in section 2.26.4. The reason for manual counting was that the majority of brain samples contained high intensity large artefacts. Artefacts came from various origins, such as a stain of blood on the surface of the organ, surgical trauma, air bubbles inside the organ or strongly auto fluorescing overlapping tissue structures. The issue of selecting the full range of possible emboli in such samples proved to be problematic, because the intensity threshold adjustment was not able to eliminate the artefacts due to them being of a higher intensity than some of the smaller emboli. Under such circumstances, performing software calculation of emboli count always included fragments of artefacts and rendered the analysis flawed. Efforts were made to eliminate and compensate for the amount of artefact present, however the software analysis of brain embolism still contained some of the inaccuracies mentioned. It was then decided to do the manual counting of the emboli present in the brain. Manual counting meant that it was possible to distinguish artefacts from emboli, improving consistency with the sizes of emboli analysed (visibly by eye using the same sample magnification). *Figure 5.4* shows an example of such analysis, with black circles indicating

some of the emboli chosen and red oval indicating one of the larger artefacts.

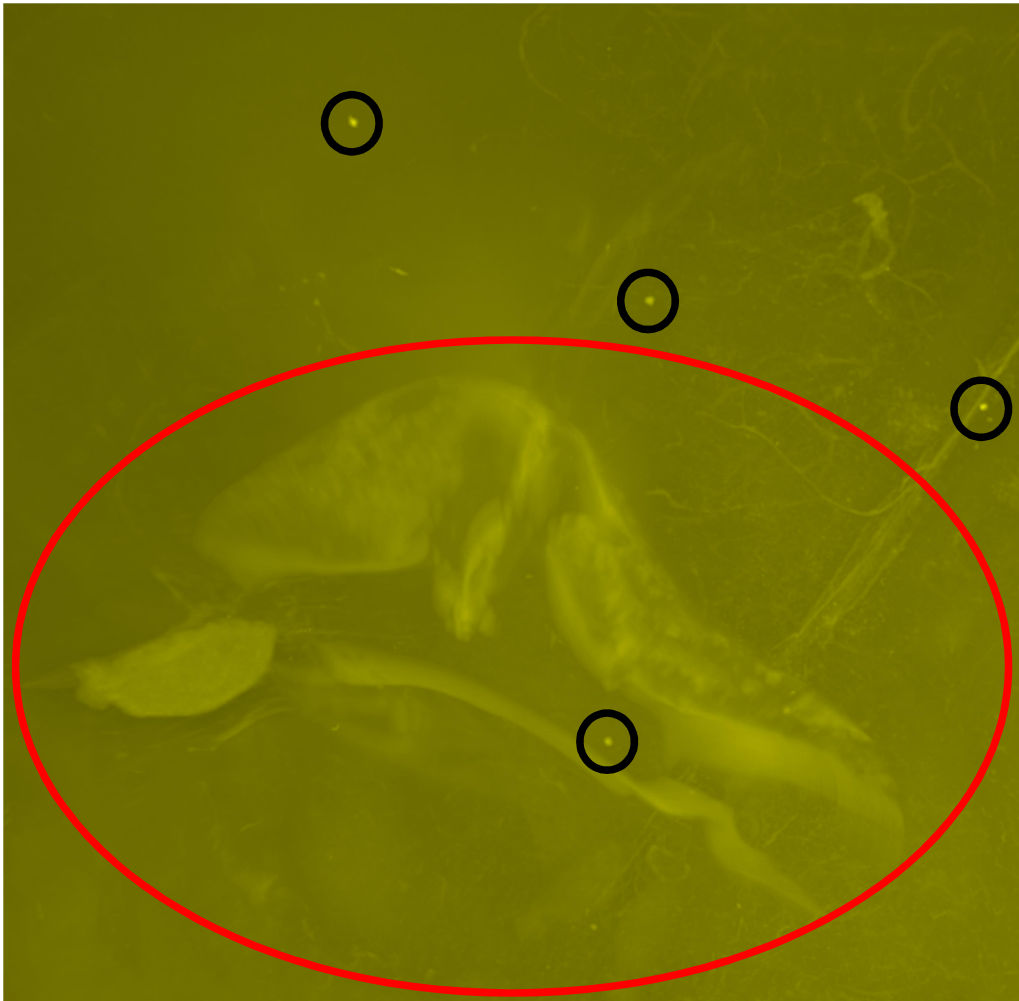


**Figure 5.4** *AlexaFluor<sup>647</sup> fluorescence channel light sheet microscope image reconstruction of the brain.*

*Black circles show examples of emboli that were counted manually. Red oval indicates one of the large artefacts that made accurate automatic software counting impossible.*

## 5.4 Results

### 5.4.1 Pulmonary embolism

Total clot volumes and emboli counts were derived for each mouse by adding clot volumes and counts from left and right lungs. Examples of both left and right lung 3D reconstructions can be seen in *Figure 5.5* as top-down snapshots.

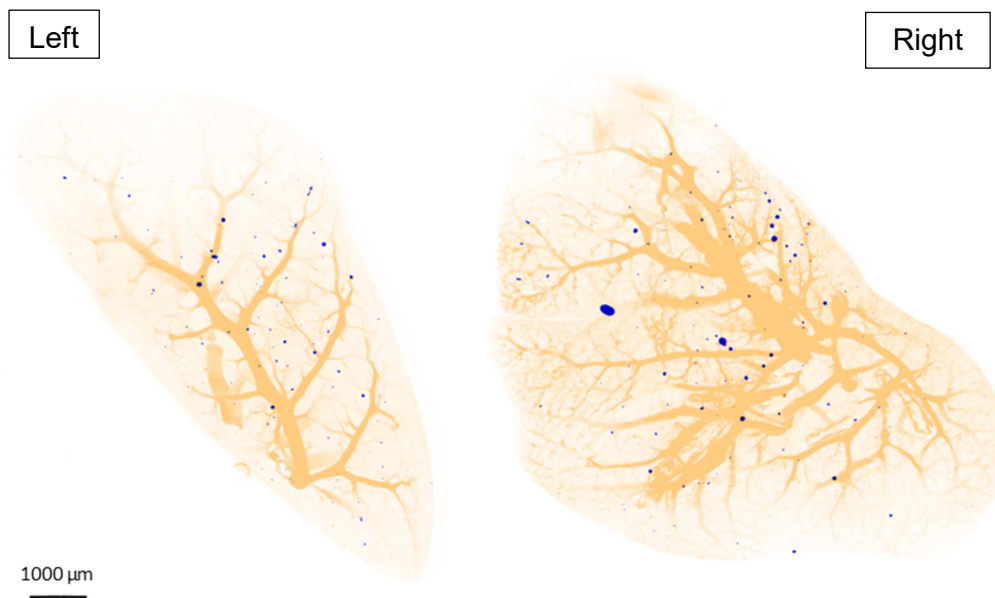


***Figure 5.5 Top-down snapshots of left and right lung 3D reconstruction post IVC FeCl<sub>3</sub> injury and light sheet microscopy imaging.***

*Yellow colour marks vasculature filled with FITC-albumin gelatin (emitting 488 nm), while blue represents emboli containing AlexaFluor<sup>647</sup> tagged fibrinogen (emitting 647 nm).*

Imaris software counting of emboli larger than  $50 \mu\text{m}^3$  revealed that increased FXIII cross-linking increased pulmonary emboli count ( $761.4 \pm 99.2$  average emboli for FXIII<sup>-/-</sup>,  $1106.0 \pm 131.2$  for 34Val, and  $1364.0 \pm 86.3$  for 34Leu mice) (*Figure 5.6*). The emboli count was significantly increased by 79.1% ( $p= 0.0019$ ) in 34Leu compared with FXIII<sup>-/-</sup> mice. While the other comparisons did not show statistical significance, there was a clear trend for increasing number of emboli with increased cross-linking, with 34Leu mice having 23.3% more total pulmonary emboli than 34Val mice, and 34Val mice showing 45.3% more emboli than FXIII<sup>-/-</sup> mice.

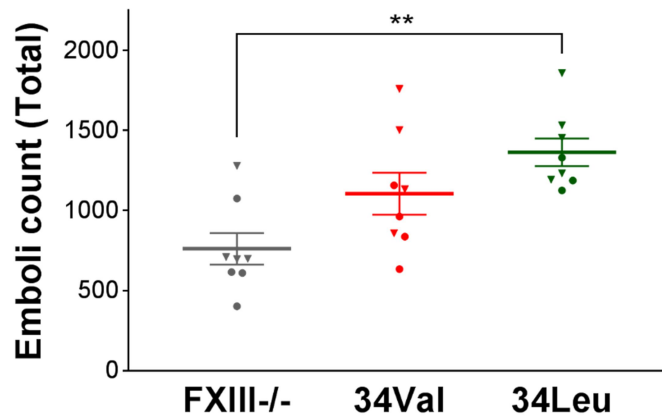


**Figure 5.6** FXIII<sup>-/-</sup>, 34Val and 34Leu mice total pulmonary emboli count following IVC FeCl<sub>3</sub> injury.

34Leu mice had significantly more pulmonary emboli than FXIII<sup>-/-</sup> mice (\*\*  $p<0.01$ ), whilst there were no significant differences between other mice variants (FXIII<sup>-/-</sup> vs. 34Val and 34Leu vs. 34Val). Statistical analysis: One-Way ANOVA and Tukey's multiple comparisons tests. Data shown as mean  $\pm$  SEM.  $n=8$ .

Imaris software volumetric analysis of emboli larger than  $50 \mu\text{m}^3$  revealed that increasing FXIII cross-linking increased total pulmonary emboli volume ( $1.05\text{e}7 \pm 1.3\text{e}6 \mu\text{m}^3$  for FXIII<sup>-/-</sup>,  $1.78\text{e}7 \pm 2.5\text{e}6 \mu\text{m}^3$  for 34Val and  $2.45\text{e}7 \pm 3.3\text{e}6 \mu\text{m}^3$  for 34Leu mice) (Figure 5.7). The total emboli volume was significantly increased by 133% ( $p=0.0021$ ) in 34Leu compared with FXIII<sup>-/-</sup> mice. While the other comparisons did not show statistical significance, there was a clear trend for increasing total volume of emboli with increased cross-linking, with 34Leu mice having 37.6% more total pulmonary emboli volume than 34Val mice, and 34Val mice showing 69.5% more total emboli volume than FXIII<sup>-/-</sup> mice.

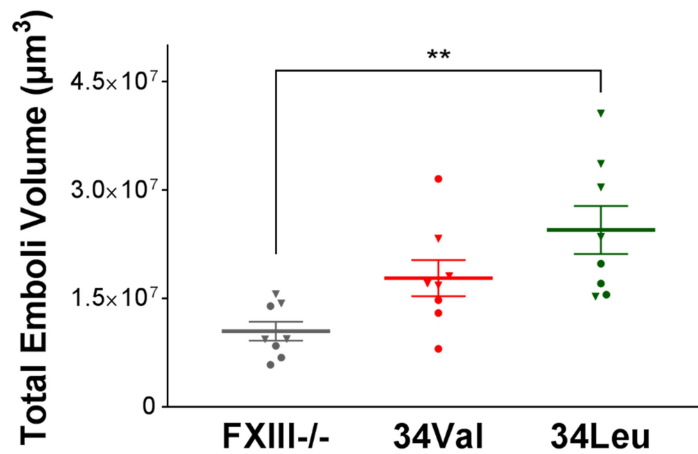


**Figure 5.7 FXIII<sup>-/-</sup>, 34Val and 34Leu mice total pulmonary emboli volume following IVC FeCl<sub>3</sub> injury.**

34Leu mice had significantly higher total pulmonary emboli volume than FXIII<sup>-/-</sup> mice (\*\*  $p < 0.01$ ), whilst there were no significant differences between other mice variants (FXIII<sup>-/-</sup> vs. 34Val and 34Leu vs. 34Val). Statistical analysis: One-Way ANOVA and Tukey's multiple comparisons tests. Data shown as mean  $\pm$  SEM.  $n=8$ .

Next, pulmonary embolism occurrence was also analysed by including only the data associated with emboli larger than  $7000 \mu\text{m}^3$ , which was on average the 25<sup>th</sup> percentile largest emboli based on volume. The same analysis was also performed using the 25<sup>th</sup> percentile smallest emboli data ( $<200 \mu\text{m}^3$ ). The large emboli data revealed that the trend of increasing emboli count with increasing cross-linking was still present with larger emboli, as seen in *Figure 5.8*. 34Leu mice ( $347.1 \pm 29.0$ ) had more large emboli than FXIII<sup>-/-</sup> ( $210.5 \pm 33.8$ ) and 34Val ( $234.1 \pm 29.5$ ) mice, which was nearly a 50% increase. 34Val and FXIII<sup>-/-</sup> mice, however, had nearly identical larger emboli counts. Emboli smaller than  $200 \mu\text{m}^3$  data show no statistical difference between FXIII<sup>-/-</sup> ( $229.8 \pm 50.0$  emboli), 34Val ( $309.4 \pm 47.9$  emboli) and 34Leu mice ( $337.0 \pm 21.8$  emboli). However a trend of small emboli generation increase was still evident with increasing FXIII cross-linking: moving from FXIII<sup>-/-</sup> to 34Val mice (34.6%), and 34Val to 34Leu mice (8.9%).

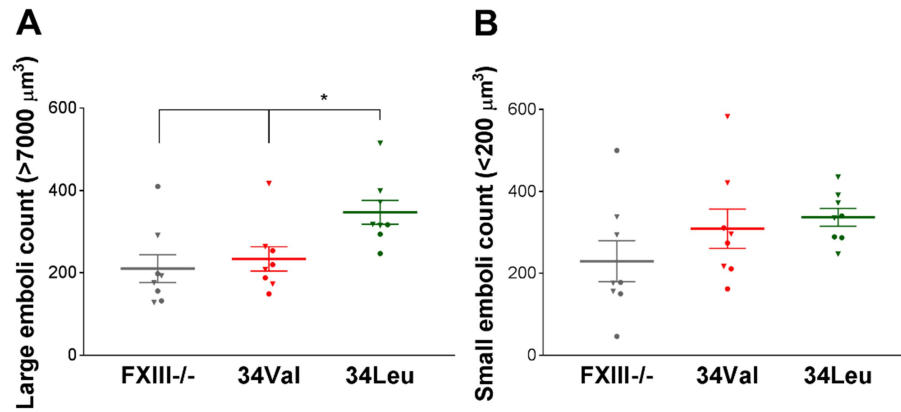


**Figure 5.8** *FXIII<sup>-/-</sup>, 34Val and 34Leu mice large (>7000 μm<sup>3</sup>) and small (<200 μm<sup>3</sup>) pulmonary emboli count following IVC FeCl<sub>3</sub> injury.*

**A:** *34Leu mice had significantly more pulmonary emboli than FXIII<sup>-/-</sup> and 34Val mice (\* p<0.05). There was no difference between FXIII<sup>-/-</sup> and 34Val mice large emboli count. Smallest large emboli size: 7000 μm<sup>3</sup>.* **B:** *There was no statistically significant difference between FXIII<sup>-/-</sup>, 34Val and 34Leu mice in small emboli count. Largest small emboli size: 200 μm<sup>3</sup>. Statistical analysis: One-Way ANOVA and Tukey's multiple comparisons tests. Data shown as mean ± SEM. n=8.*

### 5.4.2 Cerebral embolism

Emboli count was derived for each mouse by manually counting emboli in 3D brain reconstructions. Examples of such organ model can be seen in *Figure 5.9* as a top-down snapshot.

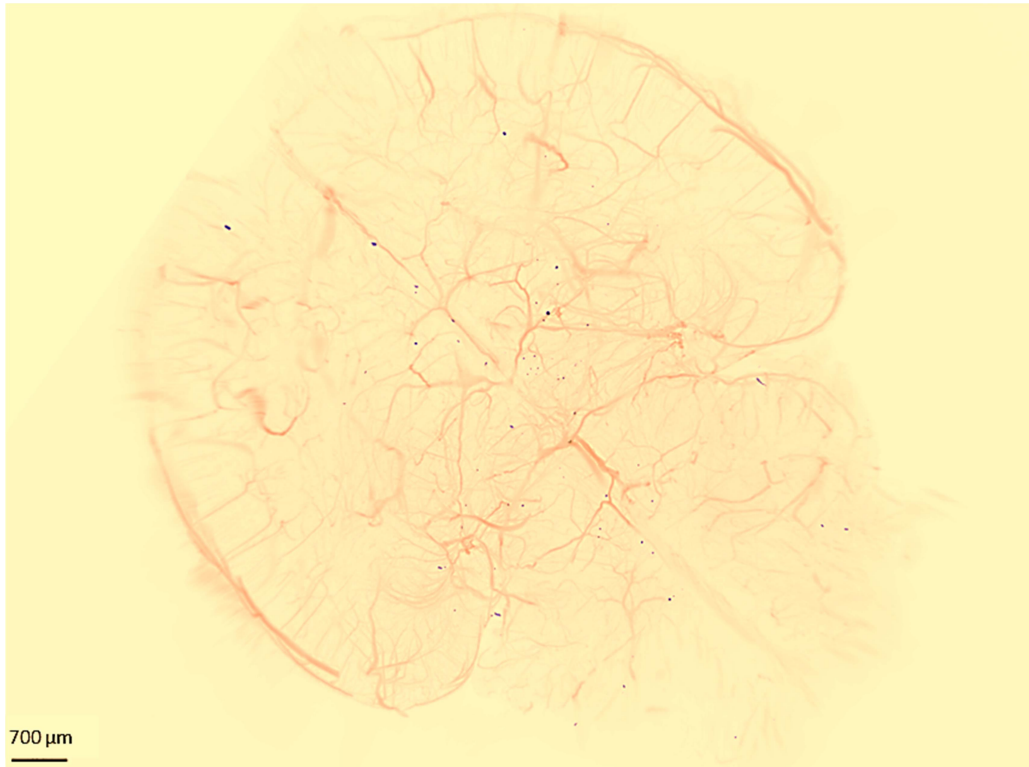


***Figure 5.9 Top-down snapshot of mouse brain 3D reconstruction post carotid artery FeCl<sub>3</sub> injury and light sheet microscopy imaging.***

*Red colour marks vasculature filled with FITC-albumin gelatin (emitting 488 nm), while dark blue are the emboli containing AlexaFluor<sup>647</sup> tagged fibrinogen (emitting 647 nm).*

Manual counting of murine brain emboli revealed that increased FXIII cross-linking inconsistently affected cerebral embolism occurrence ( $182.5 \pm 14.4$  cerebral emboli for FXIII<sup>-/-</sup>,  $136.8 \pm 20.0$  for 34Val, and  $166.0 \pm 10.7$  for 34Leu mice) (Figure 5.10). Although not statistically significant, 34Leu mice showed an increase of 21.3% in emboli count over 34Val mice and a 9% decrease when compared to FXIII<sup>-/-</sup> mice. 34Val mice showed a 25% emboli count reduction when compared to FXIII<sup>-/-</sup> mice. Also not statistically significant, however notable difference was that 34Val female mice had 60% more cerebral emboli than the 34Val male mice ( $168.4 \pm 34.3$  emboli vs.  $105.2 \pm 11.4$  emboli respectively).

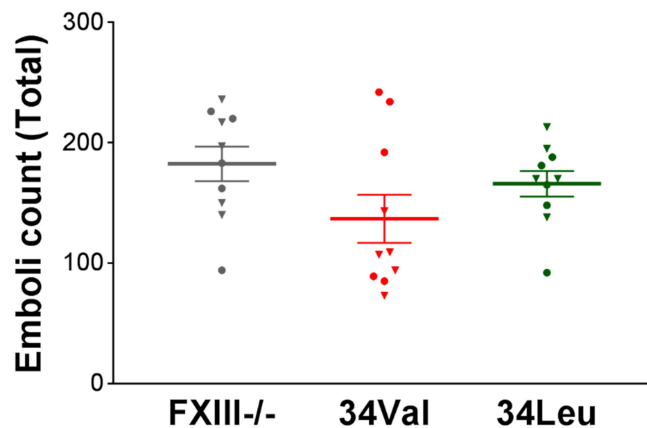


**Figure 5.10 FXIII<sup>-/-</sup>, 34Val and 34Leu mice total cerebral emboli count following carotid artery FeCl<sub>3</sub> injury.**

*There was no statistically significant difference between FXIII<sup>-/-</sup>, 34Val and 34Leu mice in cerebral emboli count. Statistical analysis: One-Way ANOVA and Tukey's multiple comparisons tests. Data shown as mean  $\pm$  SEM. n=10.*

### 5.4.3 Brain clearing optimisation

Attempts were made to enhance brain clearing in order to increase the emboli-to-background intensity ratio. However, neither the addition of 0.2% TWEEN20 (Sigma-Aldrich) to the dehydration solutions (to aid delipidation), nor the extension of the clearing time beyond a standard 72h period yielded any visible improvements in brain tissue clearing.

## 5.5 Discussion

The 2.5% FeCl<sub>3</sub> IVC injury pulmonary embolism model showed a clear trend, that increasing FXIII activity leads to an increased number of lung emboli occurring, along with the occurrence of larger clot emboli (increased total emboli volume in the lungs). A cut-off for emboli larger than 7000  $\mu\text{m}^3$  was used in order to see whether there is a difference in small or large emboli generation between the murine FXIII variants. This particular size cut-off was chosen, because it is, on average, a 25<sup>th</sup> percentile of largest emboli and 7000  $\mu\text{m}^3$  is the point at which emboli volume starts to increase exponentially. Smaller than 200  $\mu\text{m}^3$  emboli cut-off was also used for a small emboli subgroup, which represented the 25<sup>th</sup> percentile of lower overall clot volume. Interestingly, large emboli data show similar 34Val and FXIII-/- emboli counts, although in all emboli data, 34Val had 45% more emboli and 69% more total emboli volume. It is worth noting that the 7000  $\mu\text{m}^3$  cut-off emboli are categorised by fixed emboli volume alone, therefore having the same amount of larger emboli, but far more total (all sized) emboli volume means that 34Val mice generate smaller emboli than FXIII-/- mice. This is also indicated by FXIII-/- mice having noticeably less of the small (<200  $\mu\text{m}^3$ ) emboli (-25.7%) than the 34Val mice, however statistically not significant.

This could be an indication that the presence of cross-linking by FXIII increases the generation of smaller pulmonary emboli, but not larger emboli. Structural enhancement of the blood clot by FXIII cross-linking could help to keep a thrombus better anchored at the site of formation, preventing large emboli from occurring, but not preventing smaller emboli dislodging from the luminal side of the thrombus. At the same time, FXIII<sup>-/-</sup> thrombi could be more susceptible to losing larger chunks of the formed thrombus from the injury site due to a weaker fibrin mesh, therefore generating larger clots more often than the smaller ones. This trend and hypothesis of FXIII<sup>-/-</sup> generating larger emboli than the 34Val variant was not completely translatable to the comparison of the FXIII<sup>-/-</sup> and 34Leu mice. 34Leu mice generated considerably more large (+64.9%) and small (+46.6%) emboli when compared to the FXIII<sup>-/-</sup> mice. The marked emboli count increase was also consistent with total emboli count increase (+79.1%) and total emboli volume increase (+133.3%) when comparing 34Leu and FXIII<sup>-/-</sup> mice. Overall, increasing FXIII-A activity associated with increased all size venous emboli count and total emboli volume in the case of 34Leu mice, and the effect between 34Val and 34Leu mice was most noticeable in large venous emboli generation (48.3%) and least pronounced in small emboli generation (8.9% increase). A possible hypothesis to explain this apparent contradiction could be that the increased activation rate of 34Leu variant increases cross-linking of fibrinolysis inhibitors to fibrin, and therefore make the venous emboli that do occur, more resilient to fibrinolysis, and so increasing their number and volume over time.

The FeCl<sub>3</sub> carotid artery injury model for cerebral thromboembolism required optimisation in order to obtain a sufficient number of emboli occurring in the brain. The optimised 10% FeCl<sub>3</sub> injury for 3 minutes was close to the higher end of concentration used (4.0 - 12.5%) by other research teams (Chen et al., 2011, Bonnard and Hagemeyer, 2015, Chen et al., 2008, Robertson et al., 2009), as well as a study investigating FeCl<sub>3</sub> concentrations (2.5 – 12.5%) for carotid artery thrombosis (Li et al., 2013). However, the experimental conditions resulted in closely grouped data for all mice variants. Interestingly, cerebral embolism data did not establish a clear FXIII cross-linking-dependent trend, but rather showed an inconsistent relationship with cross-linking activity (FXIII<sup>-/-</sup> > 34Leu > 34Val). Similar to the pulmonary embolism data, FXIII 34Leu mice had 21% more cerebral emboli when compared to 34Val variant, however also showed 9% less emboli when compared to FXIII<sup>-/-</sup> variant. These data suggest that cross-linking by FXIII does not have a clear pro-thromboembolic effect as seen in the venous environment, since FXIII<sup>-/-</sup> mice produced the most cerebral emboli in the arterial model. A possible explanation for this apparent inconsistency could be that FXIII cross-linking stabilises the arterial clots at the vascular injury site, thereby reducing possible emboli from being formed. Mechanical strengthening of the clot through FXIII cross-linking could be stabilising the thrombi against a high shear, fast flowing arterial environment, where clots are affected by a strong force of flow. This clot stabilisation effect could, in turn, counteract any antifibrinolytic effects of cross-linking by FXIII by reducing the level at which emboli dislodge and embolise in the high shear arterial flow. Furthermore, due to the higher flow rates in the arterial

circulation, the time of transit of emboli from the site of vascular injury to the site of occlusion is less than in the venous circulation, reducing the time for fibrinolysis of emboli to occur prior to occlusion. Hence, it is possible that the mechanical clot stabilisation due to cross-linking in the high flow rate, high shear arterial circulation outweighs the antifibrinolytic effect of cross-linking, while the opposite occurs in the low flow rate, low shear venous environment.

One limitation of the carotid cerebral embolism model is the use of manual emboli counting. Manual counting made it impossible to measure emboli volume and detect small emboli that were invisible to the eye at the magnification and zoom displayed on the computer screen. This technical shortcoming made it impossible to tell whether the total emboli volume in the brain is changed with varying amounts of FXIII activity. Attempts were made to reduce the subjectivity when manually choosing and counting the emboli, by employing a consistency of selecting the emboli at a certain visual perception level (such as position of the screen, zoom level and colour intensity levels). In addition, blinding of the origin of the samples (FXIII-/-, 34Val or 34Leu) during analysis also contributed to the reliability of this data.

An additional limitation is that the FeCl<sub>3</sub> vascular injury model for thrombi generation represents a stimulus that is supra-physiological, and a poor reflection of the natural, slowly developing thrombosis pathophysiology in patients (Neeves, 2015). This is particularly relevant for deep vein thrombosis (Albadawi et al., 2017), where thrombi form due to blood stasis, pooling, hypercoagulability and endothelial dysfunction (Kumar et al., 2010). However, due to FeCl<sub>3</sub> being a highly reproducible and reliable thrombus

generation method, it is widely used in different studies of arterial and venous thrombosis (Schoenwaelder and Jackson, 2015, Neeves, 2015). Moreover, my studies were not focussed on factors that cause thrombosis, but rather the stability of the thrombi formed. Future studies would benefit by a further optimisation of *in vivo* thrombosis models and consider more disease-like environment reproducing models for venous thrombosis, such as a suture ligation stasis or stenosis models of the inferior vena cava (Albadawi et al., 2017, Diaz et al., 2012, Payne and Brill, 2017).

Notwithstanding the limitations mentioned above, the data collected from both arterial and venous models are tightly grouped and trend-setting. Concerning both cerebral and pulmonary embolism occurrence data between 34Leu and 34Val mice, the results are in agreement, 34Leu mice generating 23.3% more pulmonary emboli and 21.3% more cerebral emboli, when compared to 34Val mice. However, from a FXIII-A activation rate point of view, the cerebral embolism data does not follow a dependency trend of more FXIII activation (and activity) leading to more embolism. The observations of a pro-thromboembolic effect of increasing FXIII activity in arterial thromboembolism could indeed be counteracted by a stabilising effect of the cross-linking of thrombi at their arterial anchoring site. However, it is difficult to determine whether the combination of these effects actually translate into altered stroke severity without knowing the total emboli volume generated and emboli size (their occlusive capability). In the published clinical literature, the potential role of FXIII V34L in ischaemic stroke has also been controversial. In the year 2000, a French study on 456 patients concluded a protective effect of 34Leu variant in ischaemic stroke (Elbaz et

al., 2000). Later, a study in Italy showed an opposite effect of increased stroke risk associated with the 34Leu variant (Rubattu et al., 2005). Further studies have added to this controversy, showing an inconclusive relationship of FXIII 34Leu variant with stroke (Endler et al., 2003, Moskau et al., 2010). Two major meta-analysis studies have since concluded a lack of association between FXIII-A V34L and ischaemic stroke (Li et al., 2012, Wei et al., 2019). However, a particular study has suggested that, while the 34Leu sequence variant did not increase occurrence of ischaemic stroke, it did increase severity of the outcome, making fatality from ischaemic stroke three times more likely than compared to 34Val patients (Shemirani et al., 2014). Therefore, the study from Shemirani *et al.* findings suggest that stroke occurrence might not paint the full picture of the role of FXIII in ischaemic stroke, and that FXIII could potentially influence further development, and ultimately, the outcome of the disease, possibly by altering the fibrinolytic resistance of emboli.

In apparent contrast to the above, the venous pulmonary embolism data showed that both the emboli total volume and number of emboli produced were increased with increasing FXIII activity, indicating more severe venous thromboembolism. The data is again in apparent contradiction with a large meta-analysis study showing that FXIII-A 34Leu may be protective against venous thromboembolism (VTE) (Wells et al., 2006). However, when comparing naturally developed VTE, where clots formed in static, hypercoagulable environment, and not due to the acute endothelial damage caused by FeCl<sub>3</sub>, we are likely seeing different mechanisms of action getting influenced by FXIII activity. In a high shear stress arterial environment, FXIII

cross-linking activity could stabilise the thrombus at the site of injury and therefore be protective against embolism, while in lower shear stress environment in the venous circulation, clot stabilisation could not be as important. In the venous environment, the antifibrinolytic effect of FXIII could perhaps be more influential than mechanical clot stability, where protection from fibrinolysis is protecting and clot emboli that are generated, thereby providing a larger total volume of emboli generated. This very effect could be less noticeable in arterial environment since clots undergo higher shear stress and dislodge much earlier in their formation, therefore not being affected by the fibrinolytic system as much yet.

A recent study, using a 12 minute 4% FeCl<sub>3</sub> injury model on the femoral vein, suggested that FXIII activity may be protective against pulmonary embolism in mice by stabilising venous thrombi (Shaya et al., 2019). C57BL/6 background mice that received FXIII supplementation showed reduced number of embolic events captured by intravital microscopy and reduced emboli numbers in histologically sectioned lungs, when compared to control mice. However, in this study, the mice were FXIII sufficient, were injected with human FXIII, and also received a number of anticoagulants. Therefore, the comparison of these data with the data presented in this thesis has to be made very carefully as the two studies employed very different models to study pulmonary embolism. In order to investigate these apparent contradictions further, a comparison of data from an IVC ligation model, creating a reduced venous flow environment, would be very interesting and beneficial in understanding the role of FXIII in a venous thrombotic environment development.

## **Chapter 6 Discussion**

## 6.1 Summary of data

The work carried out in this PhD thesis was aimed at achieving the following main goals: 1) to develop and characterise a newly developed, world-first, murine FXIII-A V34L model; 2) to establish murine FeCl<sub>3</sub> vascular injury models for studying both arterial and venous thromboembolism; 3) to use these newly developed models alongside light sheet microscopy in order to observe systemic *in vivo* effects of FXIII-A V34L sequence variant on CVD. Various *in vitro* techniques were utilised to obtain murine FXIII-A 34Leu and 34Val recombinant proteins, *ex vivo* L34V mice characterisation assays were performed in order to determine the newly acquired mouse variant phenotype, and several new *in vivo* surgical and imaging techniques were developed and characterised to investigate effects of the FXIII-A V34L sequence variant on thrombosis.

My studies and experimental design started with the production of recombinant murine FXIII variants. The series of *E. coli* bacteria transformations, culturing and mFXIII-A DNA generation was successful at each step carried out, and the correct gene insert sequences were confirmed by sequencing along the way. Using site-directed mutagenesis the L34V variant DNA construct was successfully generated without introducing any unwanted mutations. Both the 34Val and 34Leu recombinant mFXIII-A DNA was inserted in the mammalian expression vector pLIVE and bacterial expression vector pGEX-6P-1. There was no longer a need to utilise pLIVE mFXIII-A for injection into FXIII-A Knock-Out (FXIII<sup>-/-</sup>) mice in order to generate L34V mice through hydrodynamic gene transfer, a method that usually leads to only transient and highly variable recombinant FXIII

expression at best. Instead, CRISPR generated L34V mice were obtained from the GEMM MRC Harwell Institute in Oxford during the second year of my PhD project, which replaced the need for hydrodynamic gene transfer with two robust and non-variable mouse strains of each genotype.

Both variants of recombinant mFXIII-A were expressed in *E. coli* and purified with GST tag either attached or removed from the protein. With the cleaved version, I originally planned to perform *in vitro* investigations comparing 34Val and 34Leu variants, however purification yields and protein purities were insufficient. Recombinant protein expression and purification for *in vitro* experimentation was chosen over FXIII-purification from mice plasma due to FXIII plasma purification resulting in low yields of FXIII and requiring thousands of mice to be bled in order to achieve required amounts as tested previously by my colleagues in the group. GST-bound mFXIII-A fusion protein was used to perform activation peptide cleavage assay, which revealed that 34Leu variant is activated 18% faster than the 34Val variant. The 18% increase is lower than the previously published 43% increase, using recombinant human FXIII-A injected in FXIII-A Knock-Out mice (Duval *et al.*, 2016), which could be due to high levels of impurities in my purified protein samples, or due to the fact that the GST tag was still present in the purified protein.

Since the CRISPR generated C57BL/6 background mFXIII-A L34V mice were received during the second year of my PhD project, I carried out their phenotypical characterisation. The FXIII-A 34Leu variant is the only existing variant in laboratory mice, therefore the newly generated 34Val mice enabled the comparison between Wild-Type 34Leu and generated 34Val mFXIII-A

variants. These newly acquired mice were compared not only to the C57BL/6 background Wild-Type 34Leu mice, but also to C57BL/6 background FXIII-A Knock-Out mice in order to have a negative control for FXIII activity. Furthermore, FXIII-/- mice data served as a useful addition in order to analyse the data sets from all three mice variants as a gradient of FXIII activation and activity: FXIII-/- << 34Val < 34Leu.

The 34Val and 34Leu mice were breeding, feeding and growing at a similar rate and their plasma fibrinogen levels, plasma FXIII-A antigen levels and plasma turbidity profiles were similar. Moreover, whole blood clot contraction, clot supernatant haemoglobin levels, clot weights and rotational thromboelastometry profiles were similar too. According to the expectation, plasma FXIII-A activation rates were different by 40%, 34Leu variant being faster activated, completely in agreement with a previous study using human recombinant FXII V34L variants injected in FXIII-/- mice (ref to Duval et al.). Although less pronounced, both these findings are in agreement with published human plasma FXIII-A activation rate difference between 34Val and 34Leu variants, showing a 2-fold rate difference (Ariens et al., 2000). These *ex vivo* results show that 34Val and 34Leu mice can be accurately compared, based on their difference solely on FXIII-A activation rate, using *in vivo* thrombosis model experiments.

The *ex vivo* data from the FXIII-/- mice showed as expected no plasma FXIII-A antigen levels present, negligible plasma cross-linking activity, clots taking longer to form, fibrin fibres being thicker, less stiff and easier to lyse than compared to the FXIII-A bearing mice data. Clots from FXIII-/- mice showed

less RBC incorporation and were therefore lighter than their WT counterparts.

The final year of my PhD project was dedicated primarily to the development of new *in vivo* thrombosis and thromboembolism models. Utilising the reliable and reproducible FeCl<sub>3</sub> vascular injury technique, I established both venous and arterial thromboembolism models; choosing the Inferior Vena Cava (IVC) for pulmonary emboli generation, and the carotid artery injury for cerebral emboli generation. In light of the published literature, it was originally hypothesised that the 34Leu mice would show reduced pulmonary emboli, while probably showing inconclusive effects in ischaemic stroke. However, increasing FXIII activation rate (FXIII<sup>-/-</sup> << 34Val < 34Leu), and therefore increasing early cross-linking activity, increased pulmonary emboli count and total emboli volume, while showing inconclusive effects on the counts and volumes of cerebral emboli.

## 6.2 Overall discussion

An 18% activation speed increase of 34Leu FXIII-A variant over the 34Val variant confirmed the expected and previously established difference (Ariens *et al.*, 2000), however the speed increase was lower than that showed by Duval *et al.* (2016) using human variant *in vitro* (81%) and in FXIII<sup>-/-</sup> mice (43%). The reason for a smaller difference in activation rates could lie in low purity of my murine FXIII samples and host cell proteins interfering with thrombin activation of FXIII. It could also be the case that the GST-tag, attached to the N-terminus of the activation peptide of FXIII-A is interfering with thrombin enzymatic activity being only 37 amino acids away from the thrombin cleavage site (*Figure 6.1*).

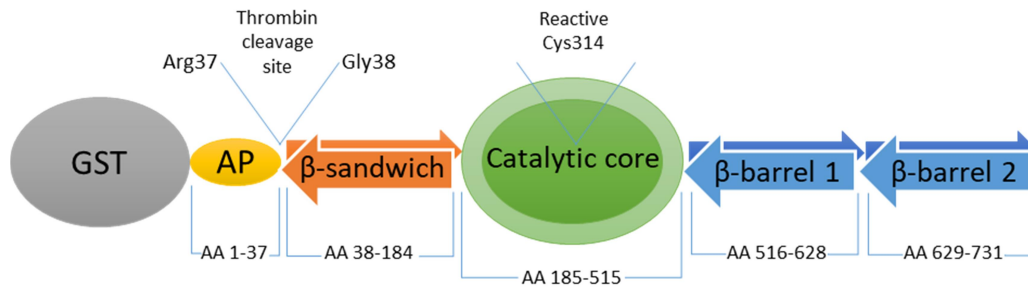


**Figure 6.1 Depiction of GST-FXIII-A fusion protein.**

*GST-FXIII-A fusion protein structure starting from N-terminus: GST tag, activation peptide (amino acids 1-37),  $\beta$ -sandwich (38-184), catalytic core (185-515),  $\beta$ -barrel 1 (516-628) and  $\beta$ -barrel 2 (629-727). Key sites, thrombin cleavage site and reactive catalytic cysteine314 residue, are marked with V insertion signs.*

Nevertheless, the findings confirmed that the murine FXIII-A variant behaves in the similar trend when compared to human FXIII-A variants, with the 34Leu variant showing enhanced activation rate over the 34Val variant.

The mouse characterisation results confirmed that the three mice variants investigated (FXIII<sup>-/-</sup>, 34Leu and 34Val) are phenotypically similar in general parameters, such as growth rate and weight, which may influence coagulation as shown in a study with 377 patients, where obese patients were more hypercoagulable after an injury (Kornblith et al., 2015) and a study with 100 obese patients showing that weight reduction modulates systemic inflammation and coagulation (Kobayashi et al., 2004). It was also shown that mice were growing at the similar rate and had similar levels of fibrinogen in their plasma, similar levels of FXIII-A antigen in their plasma (FXIII<sup>-/-</sup> mice have none) and once again confirmed that FXIII-A activation is increased for 34Leu variant, when compared to 34Val (and FXIII<sup>-/-</sup>) variant.

This time the activation rate difference was captured by measuring the kinetics of biotin incorporation into fibrin by FXIII, which is indicative of FXIII-A activation rate, while fully pre-activated 34Leu and 34Val mFXIII-A eventually show the same catalytic activity (Wartiovaara et al., 2000). Plasma FXIII-A from 34Leu mice showed 139.5% activity of the 34Val variant while FXIII-/- variant mice showed only 2.5% of the 34Val activity. Knowing that all three mice variants were phenotypically similar and the only difference between them was FXIII activation rate, we were confident moving forward, that experimental *ex vivo* and *in vivo* thrombosis model differences would be dependent solely on FXIII-A activation rate differences.

Interestingly, *ex vivo* results in plasma turbidity, whole blood thromboelastometry, clot contraction, clot supernatant haemoglobin levels and clot weight measurement experiments were similar between 34Val and 34Leu mice, and showed no statistical differences across the board. The turbidity assay was expected to show that murine 34Leu variant clots have a shorter lag time and form thinner fibrin fibres, as shown by Ariens *et al.*, 2000. Thromboelastometry was expected to show 34Leu clots to be firmer and to lyse slower, as shown in whole blood thromboelastometry studies inhibiting FXIII (Jambor et al., 2009) and 34Val vs. 34Leu turbidity lysis studies (Duval et al., 2016). 34Leu clot contraction was also expected to be enhanced, with increased red blood cell retention and higher clot weight. These expectations were based on the studies showing that FXIII activity is responsible for clot retraction in both mice (Kasahara et al., 2010) and humans (Tutwiler et al., 2016), RBC retention (Aleman et al., 2014, Byrnes et al., 2015) and clot weight (Kattula et al., 2018). Therefore, if FXIII activity is

responsible for these effects, FXIII activation rate resulting in more cross-linking activity was expected to have similar effects as well. The lack of differences between 34Leu and 34Val *ex vivo* results could stem from multiple reasons discussed below.

The 34Leu effects on coagulation could manifest only in a flowing circulatory environment, where both coagulation and fibrinolytic agents are being constantly refreshed to the site of clot formation. In a glass tube, turbidity plate well or ROTEM cup the blood is static and clotting factors are prone to depletion, therefore potentially masking FXIII activation rate effects otherwise present *in vivo*. Another reason could be that most of the expected differences arise from differences in fibrin  $\alpha$ -chain cross-linking carried out by the FXIII variants, which could be happening at different times when comparing human and murine clotting. Preliminary data collected by Dr Cedric Duval shows that  $\alpha$ -chain cross-linking in mice started and finished much earlier in time (and is complete within 10 min after initiation of clotting) when compared to the human variants (complete in 60-120 min). Any effects of differences in FXIII activation rates on clot structure could be overruled or cancelled by the much faster alpha-chain cross-linking rates in mice.

*Ex vivo* FXIII<sup>-/-</sup> values however were mostly different from both 34Val and 34Leu values, and agreed with published literature confirming the expected phenotype. In FXIII<sup>-/-</sup> data, clots took longer to form in ROTEM, as previously shown in published FXIII-poor human plasma thromboelastography studies (Schroeder et al., 2001). Additionally, ROTEM FXIII<sup>-/-</sup> data showed a decreased time to lysis, which agreed with published human whole blood experiments, showing that inhibiting cross-linking of

fibrin made clots more susceptible to lysis (Lorand et al., 1966). ROTEM clot firmness results also pointed to FXIII<sup>-/-</sup> clots being less firm, agreeing with an *in vitro* study inhibiting FXIII and showing that lack of FXIII activity makes whole blood clots less firm (Jambor et al., 2009). Moreover, turbidity data acquired showed that FXIII<sup>-/-</sup> plasma forms clots with increased fibrin fibres thickness when compared to FXIII sufficient mice, which agrees with scanning electron microscopy (SEM) study showing that increased FXIII activation (34Leu variant) forms thinner fibrin fibres (than 34Val variant) (Lim et al., 2003). FXIII<sup>-/-</sup> clots have also retained fewer red blood cells during clot contraction, which made the clots lighter. These findings are in agreement with previously published clot contraction studies using both mice (Aleman et al., 2014) and human (Byrnes et al., 2015) whole blood.

Even though *ex vivo* experiments did not show differences in clot structure, the activation rates were significantly different between 34Leu and 34Val variants and therefore could translate into different thromboembolism dynamics. Consequently, this provided sufficient rationale for the PhD project to next revolve around arterial and venous thrombosis model development and thromboembolism quantification.

During the final year of the PhD project both arterial and venous thromboembolism models were established, as well as light sheet microscopy image acquisition and emboli quantification methods were optimised. The choice of thrombus generation method, the FeCl<sub>3</sub> vascular injury technique, came from the particular focus of the project, clot embolisation. It could be argued that FeCl<sub>3</sub> vascular injury thrombi generation method represents a stimulus that is supra-physiological, and a

poor reflection of the natural, slowly developing thrombosis pathophysiology in patients (Neeves, 2015). This is particularly relevant for deep vein thrombosis (Albadawi et al., 2017), where thrombi form due to blood stasis, pooling, hypercoagulability and endothelial dysfunction (Kumar et al., 2010). Even though these concerns are valid while studying thrombosis itself and the origins of thrombus development, they are less of an issue when focusing on embolisation alone. This PhD project aimed to investigate the mechanisms by which FXIII-A 34Leu sequence variant affects embolisation dynamics, but not the thrombus development itself. It could be argued that the origins of the thrombus formation (endothelial damage, stasis or hypercoagulability) would influence the constitution of the clot itself, and therefore, affect embolisation as well, however as an initial murine 34Val vs. 34Leu embolisation investigation, constrained by project time limits, FeCl<sub>3</sub> vascular injury model was deemed to be the best fit for the purposes of the study. Subsequently, the *in vivo* thromboembolism data resulted in closely grouped datasets for all mice variants, proving the accuracy of the methodology developed. *In vivo* model findings also established a clear FXIII cross-linking-dependent pulmonary embolism trend, as well as interesting cerebral embolism observations.

The findings from both *in vivo* thromboembolism models showed that increasing activation rate of FXIII-A influenced arterial and venous thromboembolism differently. The differences observed could be primarily due to the shear stress differences between these two circulatory environments. In the venous circulation, more FXIII cross-linking activity increased pulmonary emboli generation in both total volume and count. It

could be argued that the antifibrinolytic effect of FXIII cross-linking activity was a major mechanism responsible for this. FXIII<sup>-/-</sup> mice generated clots that are likely more susceptible to fibrinolysis and could lose a considerable amount of thrombus volume before and during the embolisation, which reduced the emboli count. Even if a clot embolus is formed, faster lysis may completely dissolve the embolus during its transit from the vena cava to the pulmonary circulation, thereby reducing emboli counts. FXIII sufficient mice show increased resistance to fibrinolysis due to the cross-linking activity of FXIII, and therefore, preserved more thrombus volume available to embolise, and also preserved more clot emboli during their transit from the vena cava to the lungs, increasing pulmonary emboli counts. 34Leu mice, which had a faster activated FXIII, may show accelerated and enhanced antifibrinolytic activity of FXIII cross-linking, preserving even more thrombus volume able to progress into enhanced pulmonary embolism. This is in agreement with previous studies showing increased cross-linking of fibrinolysis inhibitors such as  $\alpha$ 2-antiplasmin into fibrin by FXIII 34Leu (Schroder and Kohler, 2000, Duval et al., 2016). Interestingly, thromboelastometry results gathered in this project did not show an increased resistance to lysis for 34Leu clots when compared to the 34Val variant, however FXIII<sup>-/-</sup> clots did lyse faster than FXIII sufficient clots. It may be that the thromboelastometry analysis is not sensitive enough to pick up subtle but significant differences between the two FXIII 34Leu and 34Val variants, or perhaps these differences only occur under flow conditions, where thrombotic and haemostatic agents are being refreshed at the thrombus formation site.

In the arterial environment, the high shear stress of blood flow invokes far more force on the forming thrombi than the low shear stress venous circulation environment. Fast flowing blood exerts pressure and shear stresses on the thrombus, making it potentially break and dislodging thrombus fragments to embolise downstream. Therefore, a mechanical strengthening of the fibrin clot by increased FXIII cross-linking activity could stabilise the arterial thrombus at the formation site, and reduce the amount of emboli generating and dislodging from the thrombus. This stabilisation effect could have potentially counteracted the antifibrinolytic effect of FXIII, where resistance to lysis could have promoted thrombus volume prevention, however at the same time could have enhanced thrombus stability and reduced chances of embolisation. Additionally, due to high shear of arterial circulation, thrombi could be spending less time at the formation site before traveling downstream than venous thrombi have, in addition to spending less time in transit from the thrombus site to the brain due to the high shear arterial circulation, and therefore, could have been influenced by thrombus-preserving antifibrinolytic effect of FXIII far less than those in the venous circulation. Consequently, fibrinolysis would have had less time to reduce the number and size of emboli reaching the brain.

The fact that 34Val mice generate less arterial emboli than FXIII<sup>-/-</sup> mice, may suggest that FXIII cross-linking greatly enhances the stability of arterial thrombi. However, 34Leu mice showed slightly increased emboli generation when compared to 34Val mice, suggesting that the faster activated 34Leu variant does not provide meaningful additional clot stability over 34Val variant, but perhaps rather provides additional fibrinolysis inhibition. The

reason that this counteracting effect was not observed in the venous circulation could be that a low shear stress of venous flow does not invoke enough force on the thrombus for the additional clot stability effect of 34Leu variant to be meaningful. Interestingly, thromboelastometry results have not shown 34Leu variant clots to be firmer than 34Val clots, however both FXIII sufficient variant clots were far firmer than the FXIII<sup>-/-</sup> clots. A published study with 313 post-surgery patients used ROTEM and shown that clot firmness was higher for the patients which had thromboembolic complications after the surgery (Hincker et al., 2014). Moreover, a French study (Collet et al., 2006) has shown that MI patient clots were more rigid as well. Therefore, it could be that the stabilisation effects of arterial thrombi are not related to the rigidity or firmness of the clot, but rather the elasticity of them. Further experiments investigating viscoelastic properties of arterial thrombi could elucidate these mechanical distinctions at play. Published literature conclusively point towards arterial thrombi being more resistant to lysis in pathology bearing patients. It has been reported (Undas and Ariens, 2011) that clots coming from advanced CAD (Fatah et al., 1992, Undas et al., 2007), acute MI (Undas et al., 2008), previous MI (Fatah et al., 1996, Collet et al., 2006, Meltzer et al., 2010, Guimaraes et al., 2009), acute stroke (Rooth et al., 2011, Undas et al., 2011) and previous stroke (Undas et al., 2009, Guimaraes et al., 2009) patients are taking longer to lyse, are less permeable and also take less time to initiate clotting. This suggests that, similarly to venous thrombosis, clots in arterial pathology are denser and more resistant to lysis (Undas, 2017), which are an established effects of FXIII activity (Hethershaw et al., 2014, Ariens et al., 2002). However, when

considering ischaemic stroke, meta-analysis studies point to inconclusive results of FXIII activity, concluding no direct correlation between the faster activated 34Leu variant and ischaemic stroke (Li et al., 2012, Wei et al., 2019), suggesting that in arterial thrombosis opposing mechanisms could be at play, balancing prothrombotic (enhanced clot density and resistance to lysis) effects of FXIII against the speculated anti-embolic effects of FXIII (clot stabilisation).

These dynamics between antifibrinolytic and stabilising effects of FXIII cross-linking could be the reason why FXIII activation rates affected venous thrombi generation in a clear FXIII-dependent manner, while arterial thrombi generation remained inconclusive (*Figure 6.2*).

The fact that pulmonary embolism shows a clear FXIII-dependent characteristic can potentially be therapeutically utilised. High PE risk patients, e.g. DVT or VTE patients, could be prophylactically given FXIII inhibitors (Lee and Ansell, 2011). Currently FXIII activation can be indirectly modulated by thrombin inhibitors, however if further research confirms a strong link between the severity of PE and FXIII activity, this research could lead into the new therapeutic development, whether a pharmacological one, such as FXIII inhibitory peptide, or perhaps gene therapy (possibly a L34V mutation) for the families with an established history of venous thrombosis.

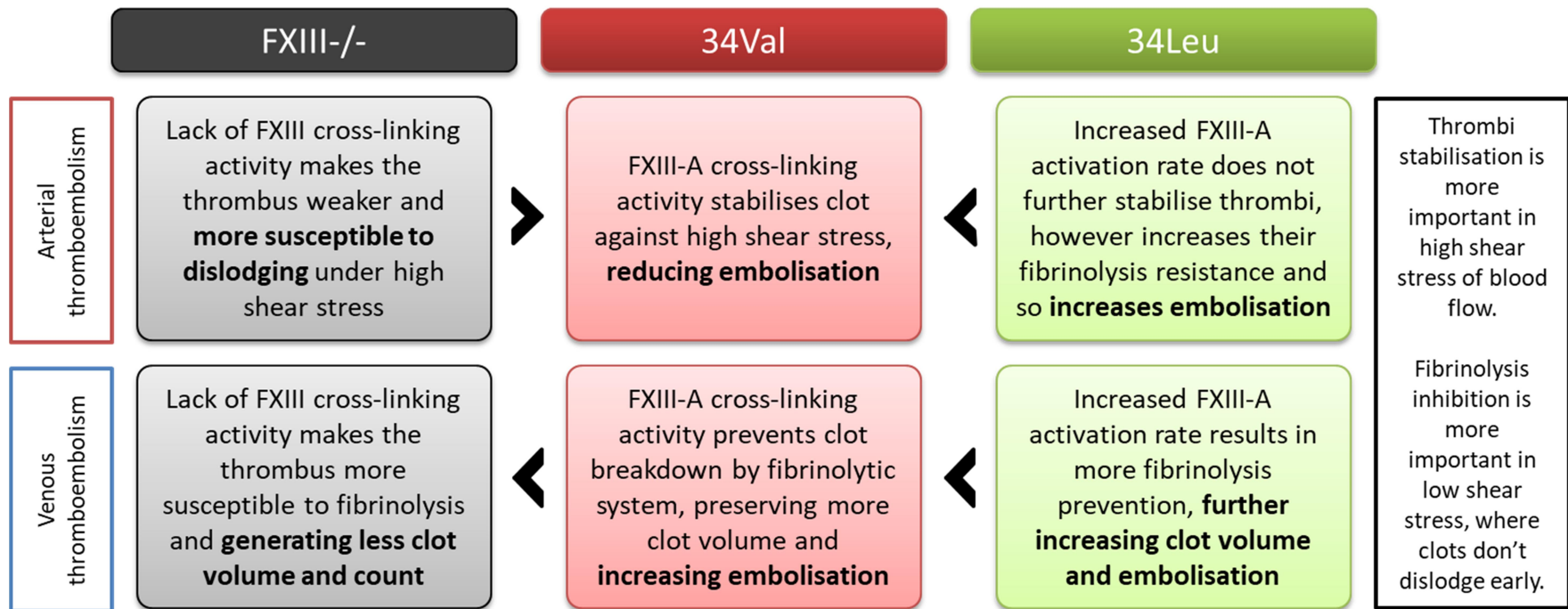


**Figure 6.2 Vascular injury data interpretation schematic.**

*Bold “<” and “>” signs show the direction of decreasing and increasing embolism amount when moving from FXIII-/-, to 34Val, to 34Leu mice data. Top three panels show the interpretation of arterial thromboembolism data, while the bottom three relate to venous thromboembolism. Black box on the right hand side discusses why cross-linking effects seen are specific to either arterial or venous environments.*

An interesting detail from the data collected during the PhD project comes from analysing gender differences. Almost in every occasion male and female mice had no significant difference in any of the parameters between gender groups, apart from one. Female FXIII<sup>-/-</sup> mice had 36.8% less median plasma fibrinogen ( $P < 0.01$ ) than the male mice. This could suggest a probable link between FXIII, sex hormones and fibrinogen. However, the consensus about fibrinogen levels being dependent on gender is not clear throughout the literature. A large meta-analytic study (Kamath and Lip, 2003) has concluded that most studies throughout Europe show that women have higher fibrinogen levels than men, even in adolescence (Prisco et al., 1996), while some studies failed to provide any significant differences (Tarallo et al., 1992). Furthermore, any other parameters were not indicative of any differences between FXIII<sup>-/-</sup> male and female mice.

Another gender difference, although not statistically significant, is clearly visible; 34Val female mice had 60% more cerebral emboli than the 34Val male mice. Interestingly, the difference between male and female 34Val mice in stroke occurrence is supported by multiple published studies; for example, a study with 1025 patients showing that the coagulation system (but not fibrinolytic system), signified by elevated prothrombin fragments, is accelerated with aging in female subjects (Inokuchi et al., 2017). Additionally, a study on rats following normothermic cardiopulmonary bypass has shown that female rats also have elevated prothrombin fragments 1+2 when compared to male rats (Kellermann et al., 2014). Another study with 546 Caucasian patients showed that in a group of subjects, which only had acute ischaemic stroke, but no atrial fibrillation, females had lower levels of

fibrinogen and elevated prothrombotic agents PAI-1, FVII and FVIII when compared to males (Kain et al., 2003). And finally, the CHADS score, designed to evaluate ischaemic stroke risk treats the female gender as a risk factor (Gage et al., 2001). Although the reported gender differences are few, in selected cases and weak, their potential links to coagulation should still be considered when investigating thrombosis further in the future endeavours beyond this PhD project.

### **6.3 Limitations and improvements**

#### **6.3.1 mFXIII-A purification**

The GST-FXIII-A fusion protein samples were equally impure between 34Val and 34Leu. Similar impurity profiles and similar protein concentrations made the activation rate comparison viable, however high impurity levels in the samples could have interfered with activation peptide cleavage by thrombin and, therefore, masked some of the activation rate difference (showing 18% as opposed to 43% in Duval et al. 2016 study). Acquiring a purer recombinant mFXIII-A samples could help elucidate whether *E. coli* impurities play a role in impairing/modulating or masking differences in FXIII-A activation.

#### **6.3.2 Rotational thromboelastometry and flow**

It is entirely possible, that differences between murine FXIII-A 34Leu and 34Val affected clots in terms of fibrinolysis and stiffening reveal themselves under flow conditions only. Inside a ROTEM cup, calcium, t-PA and tissue factor are spiked-in once at the beginning of the experiment, while in circulation, both coagulation and fibrinolytic agents are being constantly

refreshed. Therefore, if the effects of different FXIII variants are dependent on FXIII and other haemostatic factors being maintained and constantly delivered to the site of clot formation, only a flowing model of clotting and lysis would fully reveal that.

### **6.3.3 FeCl<sub>3</sub> vascular injury model**

FeCl<sub>3</sub> endothelial injury model on IVC does not mimic the natural VTE environment in human patients, where thrombi develop in a static, hypercoagulable environment as opposed to acute endothelial damage. More physiological IVC ligation and stenosis models could be employed to closer mimic naturally occurring pathology.

### **6.3.4 Brain image software analysis**

The Imaris image analysis software struggled to take relatively dim emboli into the account when larger artefacts were present. When compared with lung samples, even with 10% FeCl<sub>3</sub> (as opposed to 2.5% for lungs), the brain samples showed less emboli which were far dimmer and emitted lower fluorescence intensities. The brain is reported to be the most difficult to clear for light sheet microscopy, and all clearing protocols published for clearing the brain point towards the longest times for this process (Erturk et al., 2012, Renier et al., 2014). Therefore, the fact that emboli are not as clearly visible in cleared brain samples when compared to lungs is not surprising. Perhaps injecting a higher labelled fibrinogen concentration before the carotid artery injury, therefore producing emboli that contain a higher concentration of AlexaFluor<sup>647</sup> dye, could potentially increase the contrast of the emboli. Another possibility could be to divide the brain in half prior to clearing, so that the DBE encounters less thickness of the brain to perfuse through. However,

the core of the brain is very similarly cleared when compared to the edges of the brain, therefore this may not help to improve the clearing efficiency. Since brains are high in lipids, some clearing protocols (Richardson and Lichtman, 2015) suggest adding a detergent, such as 0.2% TWEEN20 (Sigma-Aldrich) to the dehydration methanol solutions in order to improve lipid clearing if extra clarity is needed. However, testing with addition of the detergent has not yielded any noticeable improvements. Finally, longer clearing times were suggested in the literature, however extending it over a standard 72 hours of DBE clearing did not yield visible clarity increase.

## **6.4 Future work**

### **6.4.1 Thrombin concentrations**

*Ex vivo* assays could be rerun using lower concentrations of thrombin, to see if the differences between FXIII-A 34Val and 34Leu mice would be more pronounced. This was realised after discovering a previously published study showing that with increasing concentrations of thrombin the activation rate difference between FXIII-A 34Leu and 34Val variants diminishes (Balogh et al. 2000).

### **6.4.2 Confocal lysis**

Clot lysis experiments using confocal microscopy would provide a more in-depth insight about the differences between mFXIII-A 34Leu and 34Val clots in resisting fibrinolysis.

### **6.4.3 Magnetic tweezers**

An in depth knowledge of how mFXIII-A 34Leu and 34Val affected clots differ in their viscoelastic properties could come from magnetic tweezers

experiments, where magnetic beads are trapped inside the clot and being pulled in different frequencies by utilising a magnetic field. Collected data would tell if 34Leu clots are more capable of storing the force applied to them (elasticity) by the high shear stress of arterial environment or are they more prone to permanent deformation (viscosity). A recent article published by my colleagues showed that recurrent VTE patients form clots that are less elastic and less viscous than clots from non-recurrent VTE patients (Baker et al., 2019), therefore showing that viscoelastic properties of clots are important in thromboembolism occurrence.

#### **6.4.4 Atomic force microscopy single fibrin fibre measurements**

By pulling onto a single fibrin fibre with an atomic force microscope cantilever, it is possible to measure the force required to break the fibre, as well as the force required to permanently deform it. This would allow investigating differences in fibrin fibre stiffness and extensibility between the mFXIII-A 34Leu and 34Val clots.

#### **6.4.5 Scanning electron microscopy**

Scanning electron microscopy could provide a close up look at the fibrin fibre thickness, density, clot mesh branching and porosity. mFXIII-A 34Leu and 34Val clot structural differences could potentially be revealed up close.

#### **6.4.6 Alternative fibrin cross-linking proteins**

A low fibrin cross-linking activity observed during FXIII-/- plasma biotin incorporation assay run was postulated to be either a background reading or perhaps TG1 or TG2 present in the plasma. This could be elucidated by repeating the assay on FXIII-/- plasma with TG inhibitors present.

#### **6.4.7 Non-thrombin FXIII activators**

34Leu and 34Val mFXIII-A activation and cross-linking activity could be looked into by using alternative FXIII activators, such as human neutrophil elastase (HNE). Since HNE proteolytic cleavage site on FXIII-A is different to that of thrombin, the activation rate difference between FXIII-A sequence variants could manifest differently and provide insight into characteristics of these FXIII-A variants.

#### **6.4.8 IVC stenosis model**

Future pulmonary embolism experiments and studies would benefit from using an inferior vena cava stenosis model. The stenosis model, in which a suture is ligated around the vein, obstructing the blood flow by ~90% (Brill et al., 2011), better mimics the natural venous thrombotic pathology in VTE patients' veins, where blood flow is restricted and becomes static. A closer reproduction to human thrombosis pathology could mean a more accurate simulation of thromboembolism as well.

#### **6.4.9 Inflammation**

Inflammation is a common contributing mechanism and cause of thrombosis in both arterial and venous environments. Embolism data in combination with inflammation present would be of interest from a human pathophysiology point of view. Therefore, a lipopolysaccharide (LPS)-induced systemic inflammation model, utilising an abdominal osmotic pump implant would be a plausible future investigation. Dr Cédric Duval is carrying out the investigation in IVC FeCl<sub>3</sub> injury leading to PE in presence of LPS-induced systemic inflammation at the present time.

#### **6.4.10 Pulmonary burden**

Mice breathing pattern investigation during the one hour inferior vena cava emboli generation could be investigated in order to study pulmonary burden and PE damage translation to the loss of pulmonary function.

#### **6.4.11 Stroke severity**

Mice brains affected by cerebral embolism could be investigated for their tissue oxygen deprivation and hypoxia damage, providing an insight into how differently 34Leu and 34Val FXIII-A variants affect the severity of stroke.

## **Chapter 7 References**

- ABDUL, S., LEEBEEK, F. W., RIJKEN, D. C. & UITTE DE WILLIGE, S. 2016. Natural heterogeneity of alpha2-antiplasmin: functional and clinical consequences. *Blood*, 127, 538-45.
- ADANY, R., NEMES, Z. & MUSZBEK, L. 1987. Characterization of factor XIII containing-macrophages in lymph nodes with Hodgkin's disease. *Br J Cancer*, 55, 421-6.
- AGENO, W. & HUISMAN, M. V. 2000. Low-molecular-weight heparins in the treatment of venous thromboembolism. *Curr Control Trials Cardiovasc Med*, 1, 102-105.
- AGHOURIAN, M. N., LEMARIE, C. A. & BLOSTEIN, M. D. 2012. In vivo monitoring of venous thrombosis in mice. *J Thromb Haemost*, 10, 447-52.
- ALBADAWI, H., WITTING, A. A., PERSHAD, Y., WALLACE, A., FLECK, A. R., HOANG, P., KHADEMHOSSEINI, A. & OKLU, R. 2017. Animal models of venous thrombosis. *Cardiovasc Diagn Ther*, 7, S197-S206.
- ALEMAN, M. M., BYRNES, J. R., WANG, J. G., TRAN, R., LAM, W. A., DI PAOLA, J., MACKMAN, N., DEGEN, J. L., FLICK, M. J. & WOLBERG, A. S. 2014. Factor XIII activity mediates red blood cell retention in venous thrombi. *J Clin Invest*, 124, 3590-600.
- ALLEN, G. A., MONROE, D. M., 3RD, ROBERTS, H. R. & HOFFMAN, M. 2000. The effect of factor X level on thrombin generation and the procoagulant effect of activated factor VII in a cell-based model of coagulation. *Blood Coagul Fibrinolysis*, 11 Suppl 1, S3-7.
- AMMOLLO, C. T., SEMERARO, F., XU, J., ESMON, N. L. & ESMON, C. T. 2011. Extracellular histones increase plasma thrombin generation by impairing thrombomodulin-dependent protein C activation. *J Thromb Haemost*, 9, 1795-803.
- ANNEX, B. H., DENNING, S. M., CHANNON, K. M., SKETCH, M. H., JR., STACK, R. S., MORRISSEY, J. H. & PETERS, K. G. 1995. Differential expression of tissue factor protein in directional atherectomy specimens from patients with stable and unstable coronary syndromes. *Circulation*, 91, 619-22.
- ANOKHIN, B. A., STRIBINSKIS, V., DEAN, W. L. & MAURER, M. C. 2017. Activation of factor XIII is accompanied by a change in oligomerization state. *FEBS J*, 284, 3849-3861.
- ARDISSINO, D., MERLINI, P. A., ARIENS, R., COPPOLA, R., BRAMUCCI, E. & MANNUCCI, P. M. 1997. Tissue-factor antigen and activity in human coronary atherosclerotic plaques. *Lancet*, 349, 769-71.
- ARIENS, R. A., LAI, T. S., WEISEL, J. W., GREENBERG, C. S. & GRANT, P. J. 2002. Role of factor XIII in fibrin clot formation and effects of genetic polymorphisms. *Blood*, 100, 743-54.
- ARIENS, R. A., PHILIPPOU, H., NAGASWAMI, C., WEISEL, J. W., LANE, D. A. & GRANT, P. J. 2000. The factor XIII V34L polymorphism accelerates thrombin activation of factor XIII and affects cross-linked fibrin structure. *Blood*, 96, 988-95.
- ASHCROFT, A. E., GRANT, P. J. & ARIENS, R. A. 2000. A study of human coagulation factor XIII A-subunit by electrospray ionisation mass spectrometry. *Rapid Commun Mass Spectrom*, 14, 1607-11.
- ASLAN, J. E., ITAKURA, A., GERTZ, J. M. & MCCARTY, O. J. 2012. Platelet shape change and spreading. *Methods Mol Biol*, 788, 91-100.

- AUTIN, L., MITEVA, M. A., LEE, W. H., MERTENS, K., RADTKE, K. P. & VILLOUTREIX, B. O. 2005. Molecular models of the procoagulant factor VIIIa-factor IXa complex. *J Thromb Haemost*, 3, 2044-56.
- BADIMON, L. & VILAHUR, G. 2014. Thrombosis formation on atherosclerotic lesions and plaque rupture. *J Intern Med*, 276, 618-32.
- BAGOLY, Z., FAZAKAS, F., KOMAROMI, I., HARAMURA, G., TOTH, E. & MUSZBEK, L. 2008. Cleavage of factor XIII by human neutrophil elastase results in a novel active truncated form of factor XIII A subunit. *Thromb Haemost*, 99, 668-74.
- BAGOLY, Z., KATONA, E. & MUSZBEK, L. 2012. Factor XIII and inflammatory cells. *Thromb Res*, 129 Suppl 2, S77-81.
- BAGOLY, Z. & MUSZBEK, L. 2019. Factor XIII: What does it look like? *J Thromb Haemost*, 17, 714-716.
- BAKER, S. R., ZABCZYK, M., MACRAE, F. L., DUVAL, C., UNDAS, A. & ARIENS, R. A. S. 2019. Recurrent venous thromboembolism patients form clots with lower elastic modulus than those formed by patients with non-recurrent disease. *J Thromb Haemost*, 17, 618-626.
- BALOGH, I., SZOKE, G., KARPATI, L., WARTIOVAARA, U., KATONA, E., KOMAROMI, I., HARAMURA, G., PFLIEGLER, G., MIKKOLA, H. & MUSZBEK, L. 2000. Val34Leu polymorphism of plasma factor XIII: biochemistry and epidemiology in familial thrombophilia. *Blood*, 96, 2479-86.
- BARR, J. D., CHAUHAN, A. K., SCHAEFFER, G. V., HANSEN, J. K. & MOTTO, D. G. 2013. Red blood cells mediate the onset of thrombosis in the ferric chloride murine model. *Blood*, 121, 3733-41.
- BISWAS, A., IVASKEVICIUS, V., THOMAS, A. & OLDENBURG, J. 2014. Coagulation factor XIII deficiency. Diagnosis, prevalence and management of inherited and acquired forms. *Hamostaseologie*, 34, 160-6.
- BOBRY SHEV, Y. V., IVANOVA, E. A., CHISTI AKOV, D. A., NIKIFOROV, N. G. & OREKHOV, A. N. 2016. Macrophages and Their Role in Atherosclerosis: Pathophysiology and Transcriptome Analysis. *Biomed Res Int*, 2016, 9582430.
- BOFFA, M. B., REID, T. S., JOO, E., NESHEIM, M. E. & KOSCHINSKY, M. L. 1999. Characterization of the gene encoding human TAFI (thrombin-activable fibrinolysis inhibitor; plasma procarboxypeptidase B). *Biochemistry*, 38, 6547-58.
- BONNARD, T. & HAGEMEYER, C. E. 2015. Ferric Chloride-induced Thrombosis Mouse Model on Carotid Artery and Mesentery Vessel. *J Vis Exp*, e52838.
- BRANDES, R. P. 2014. Endothelial dysfunction and hypertension. *Hypertension*, 64, 924-8.
- BRANDT, M., SCHONFELDER, T., SCHWENK, M., BECKER, C., JACKEL, S., REINHARDT, C., STARK, K., MASSBERG, S., MUNZEL, T., VON BRUHL, M. L. & WENZEL, P. 2014. Deep vein thrombus formation induced by flow reduction in mice is determined by venous side branches. *Clin Hemorheol Microcirc*, 56, 145-52.
- BRILL, A., FUCHS, T. A., CHAUHAN, A. K., YANG, J. J., DE MEYER, S. F., KOLLNBERGER, M., WAKEFIELD, T. W., LAMMLE, B., MASSBERG, S. & WAGNER, D. D. 2011. von Willebrand factor-mediated platelet

- adhesion is critical for deep vein thrombosis in mouse models. *Blood*, 117, 1400-7.
- BRILL, A., FUCHS, T. A., SAVCHENKO, A. S., THOMAS, G. M., MARTINOD, K., DE MEYER, S. F., BHANDARI, A. A. & WAGNER, D. D. 2012. Neutrophil extracellular traps promote deep vein thrombosis in mice. *J Thromb Haemost*, 10, 136-44.
- BRINKMANN, V., REICHARD, U., GOOSMANN, C., FAULER, B., UHLEMANN, Y., WEISS, D. S., WEINRAUCH, Y. & ZYCHLINSKY, A. 2004. Neutrophil extracellular traps kill bacteria. *Science*, 303, 1532-5.
- BUDNIK, I. & BRILL, A. 2018. Immune Factors in Deep Vein Thrombosis Initiation. *Trends Immunol*, 39, 610-623.
- BUTENAS, S., ORFEO, T. & MANN, K. G. 2009. Tissue factor in coagulation: Which? Where? When? *Arterioscler Thromb Vasc Biol*, 29, 1989-96.
- BYRNES, J. R., DUVAL, C., WANG, Y., HANSEN, C. E., AHN, B., MOOBERRY, M. J., CLARK, M. A., JOHNSEN, J. M., LORD, S. T., LAM, W. A., MEIJERS, J. C., NI, H., ARIENS, R. A. & WOLBERG, A. S. 2015. Factor XIIIa-dependent retention of red blood cells in clots is mediated by fibrin alpha-chain crosslinking. *Blood*, 126, 1940-8.
- CALLANDER, N. S., RAO, L. V., NORDFANG, O., SANDSET, P. M., WARN-CRAMER, B. & RAPAPORT, S. I. 1992. Mechanisms of binding of recombinant extrinsic pathway inhibitor (rEPI) to cultured cell surfaces. Evidence that rEPI can bind to and inhibit factor VIIIa-tissue factor complexes in the absence of factor Xa. *J Biol Chem*, 267, 876-82.
- CARRELL, N. A., ERICKSON, H. P. & MCDONAGH, J. 1989. Electron microscopy and hydrodynamic properties of factor XIII subunits. *J Biol Chem*, 264, 551-6.
- CARTER, J. C. & CHURCH, F. C. 2009. Obesity and breast cancer: the roles of peroxisome proliferator-activated receptor-gamma and plasminogen activator inhibitor-1. *PPAR Res*, 2009, 345320.
- CHAPIN, J. C. & HAJJAR, K. A. 2015. Fibrinolysis and the control of blood coagulation. *Blood Rev*, 29, 17-24.
- CHAUDHRY, R. & BABIKER, H. M. 2019. Physiology, Coagulation Pathways. *StatPearls*. Treasure Island (FL).
- CHEN, K., FEBBRAIO, M., LI, W. & SILVERSTEIN, R. L. 2008. A specific CD36-dependent signaling pathway is required for platelet activation by oxidized low-density lipoprotein. *Circ Res*, 102, 1512-9.
- CHEN, K., LI, W., MAJOR, J., RAHAMAN, S. O., FEBBRAIO, M. & SILVERSTEIN, R. L. 2011. Vav guanine nucleotide exchange factors link hyperlipidemia and a prothrombotic state. *Blood*, 117, 5744-50.
- CHEN, R. & DOOLITTLE, R. F. 1971. - cross-linking sites in human and bovine fibrin. *Biochemistry*, 10, 4487-91.
- CHOW, O. A., VON KOCKRITZ-BLICKWEDE, M., BRIGHT, A. T., HENSLER, M. E., ZINKERNAGEL, A. S., COGEN, A. L., GALLO, R. L., MONESTIER, M., WANG, Y., GLASS, C. K. & NIZET, V. 2010. Statins enhance formation of phagocyte extracellular traps. *Cell Host Microbe*, 8, 445-54.
- CICILIANO, J. C., SAKURAI, Y., MYERS, D. R., FAY, M. E., HECHLER, B., MEEKS, S., LI, R., DIXON, J. B., LYON, L. A., GACHET, C. & LAM,

- W. A. 2015. Resolving the multifaceted mechanisms of the ferric chloride thrombosis model using an interdisciplinary microfluidic approach. *Blood*, 126, 817-24.
- COLLET, J. P., ALLALI, Y., LESTY, C., TANGUY, M. L., SILVAIN, J., ANKRI, A., BLANCHET, B., DUMAINE, R., GIANETTI, J., PAYOT, L., WEISEL, J. W. & MONTALESCOT, G. 2006. Altered fibrin architecture is associated with hypofibrinolysis and premature coronary atherothrombosis. *Arterioscler Thromb Vasc Biol*, 26, 2567-73.
- COLLET, J. P., MOEN, J. L., VEKLIICH, Y. I., GORKUN, O. V., LORD, S. T., MONTALESCOT, G. & WEISEL, J. W. 2005. The alphaC domains of fibrinogen affect the structure of the fibrin clot, its physical properties, and its susceptibility to fibrinolysis. *Blood*, 106, 3824-30.
- COLLET, J. P., PARK, D., LESTY, C., SORIA, J., SORIA, C., MONTALESCOT, G. & WEISEL, J. W. 2000. Influence of fibrin network conformation and fibrin fiber diameter on fibrinolysis speed: dynamic and structural approaches by confocal microscopy. *Arterioscler Thromb Vasc Biol*, 20, 1354-61.
- COPPINGER, J. A., CAGNEY, G., TOOMEY, S., KISLINGER, T., BELTON, O., MCREDMOND, J. P., CAHILL, D. J., EMILI, A., FITZGERALD, D. J. & MAGUIRE, P. B. 2004. Characterization of the proteins released from activated platelets leads to localization of novel platelet proteins in human atherosclerotic lesions. *Blood*, 103, 2096-104.
- CORDELL, P. A., KILE, B. T., STANDEVEN, K. F., JOSEFSSON, E. C., PEASE, R. J. & GRANT, P. J. 2010. Association of coagulation factor XIII-A with Golgi proteins within monocyte-macrophages: implications for subcellular trafficking and secretion. *Blood*, 115, 2674-81.
- DIAZ, J. A., OBI, A. T., MYERS, D. D., JR., WROBLESKI, S. K., HENKE, P. K., MACKMAN, N. & WAKEFIELD, T. W. 2012. Critical review of mouse models of venous thrombosis. *Arterioscler Thromb Vasc Biol*, 32, 556-62.
- DODT, J., PASTERNAK, R., SEITZ, R. & VOLKERS, P. 2016. Free factor XIII activation peptide (fAP-FXIII) is a regulator of factor XIII activity via factor XIII-B. *Br J Haematol*, 172, 452-60.
- DORGALALEH, A., ALAVI, S. E., TABIBIAN, S., SOORI, S., MORADI, E., BAMEDI, T., ASADI, M., JALALVAND, M. & SHAMSIZADEH, M. 2017. Diagnosis, clinical manifestations and management of rare bleeding disorders in Iran. *Hematology*, 22, 224-230.
- DRAKE, T. A., MORRISSEY, J. H. & EDGINGTON, T. S. 1989. Selective cellular expression of tissue factor in human tissues. Implications for disorders of hemostasis and thrombosis. *Am J Pathol*, 134, 1087-97.
- DUVAL, C., ALI, M., CHAUDHRY, W. W., RIDGER, V. C., ARIENS, R. A. & PHILIPPOU, H. 2016. Factor XIII A-Subunit V34L Variant Affects Thrombus Cross-Linking in a Murine Model of Thrombosis. *Arterioscler Thromb Vasc Biol*, 36, 308-16.
- DUVAL, C., ALLAN, P., CONNELL, S. D., RIDGER, V. C., PHILIPPOU, H. & ARIENS, R. A. 2014. Roles of fibrin alpha- and gamma-chain specific cross-linking by FXIIIa in fibrin structure and function. *Thromb Haemost*, 111, 842-50.

- DUVAL, C., PHILIPPOU, H., ARIËNS, R.A.S. 2012. Factor XIII. *In: MARDER V.J., A. W. C., BENNETT J.S., SCHULMAN S., WHITE G.C. (ed.) Hemostasis and Thrombosis: Basic Principles and Clinical Practice.* Philadelphia: Lippincott Williams & Wilkins.
- ECKLY, A., HECHLER, B., FREUND, M., ZERR, M., CAZENAVE, J. P., LANZA, F., MANGIN, P. H. & GACHET, C. 2011. Mechanisms underlying FeCl<sub>3</sub>-induced arterial thrombosis. *J Thromb Haemost*, 9, 779-89.
- EITZMAN, D. T., WESTRICK, R. J., XU, Z., TYSON, J. & GINSBURG, D. 2000. Hyperlipidemia promotes thrombosis after injury to atherosclerotic vessels in apolipoprotein E-deficient mice. *Arterioscler Thromb Vasc Biol*, 20, 1831-4.
- ELBAZ, A., POIRIER, O., CANAPLE, S., CHEDRU, F., CAMBIEN, F. & AMARENCO, P. 2000. The association between the Val34Leu polymorphism in the factor XIII gene and brain infarction. *Blood*, 95, 586-91.
- ENDLER, G., FUNK, M., HAERING, D., LALOUSCHEK, W., LANG, W., MIRAFZAL, M., WAGNER, O. & MANNHALTER, C. 2003. Is the factor XIII 34Val/Leu polymorphism a protective factor for cerebrovascular disease? *Br J Haematol*, 120, 310-4.
- ERTURK, A., BECKER, K., JAHRLING, N., MAUCH, C. P., HOJER, C. D., EGEN, J. G., HELLAL, F., BRADKE, F., SHENG, M. & DODT, H. U. 2012. Three-dimensional imaging of solvent-cleared organs using 3DISCO. *Nat Protoc*, 7, 1983-95.
- ESMON, C. T. 2009. Basic mechanisms and pathogenesis of venous thrombosis. *Blood Rev*, 23, 225-9.
- ESPER, R. J., VILARINO, J. O., MACHADO, R. A. & PARAGANO, A. 2008. Endothelial dysfunction in normal and abnormal glucose metabolism. *Adv Cardiol*, 45, 17-43.
- FATAH, K., HAMSTEN, A., BLOMBACK, B. & BLOMBACK, M. 1992. Fibrin gel network characteristics and coronary heart disease: relations to plasma fibrinogen concentration, acute phase protein, serum lipoproteins and coronary atherosclerosis. *Thromb Haemost*, 68, 130-5.
- FATAH, K., SILVEIRA, A., TORNVALL, P., KARPE, F., BLOMBACK, M. & HAMSTEN, A. 1996. Proneness to formation of tight and rigid fibrin gel structures in men with myocardial infarction at a young age. *Thromb Haemost*, 76, 535-40.
- REFERENCE, B. A., GINSBERG, H. N., GRAHAM, I., RAY, K. K., PACKARD, C. J., BRUCKERT, E., HEGELE, R. A., KRAUSS, R. M., RAAL, F. J., SCHUNKERT, H., WATTS, G. F., BOREN, J., FAZIO, S., HORTON, J. D., MASANA, L., NICHOLLS, S. J., NORDESTGAARD, B. G., VAN DE SLUIS, B., TASKINEN, M. R., TOKGOZOGLU, L., LANDMESSER, U., LAUFS, U., WIKLUND, O., STOCK, J. K., CHAPMAN, M. J. & CATAPANO, A. L. 2017. Low-density lipoproteins cause atherosclerotic cardiovascular disease. 1. Evidence from genetic, epidemiologic, and clinical studies. A consensus statement from the European Atherosclerosis Society Consensus Panel. *Eur Heart J*, 38, 2459-2472.

- FERRIS, J. A. & FRIESEN, J. M. 1979. Definitions of ischaemia, infarction and necrosis. *Forensic Sci Int*, 13, 253-9.
- FICKENSCHER, K., AAB, A. & STUBER, W. 1991. A photometric assay for blood coagulation factor XIII. *Thromb Haemost*, 65, 535-40.
- FOWLER, W. E., HANTGAN, R. R., HERMANS, J. & ERICKSON, H. P. 1981. Structure of the fibrin protofibril. *Proc Natl Acad Sci U S A*, 78, 4872-6.
- FRASER, S. R., BOOTH, N. A. & MUTCH, N. J. 2011. The antifibrinolytic function of factor XIII is exclusively expressed through alpha(2)-antiplasmin cross-linking. *Blood*, 117, 6371-4.
- GAGE, B. F., WATERMAN, A. D., SHANNON, W., BOECHLER, M., RICH, M. W. & RADFORD, M. J. 2001. Validation of clinical classification schemes for predicting stroke: results from the National Registry of Atrial Fibrillation. *JAMA*, 285, 2864-70.
- GAILANI, D. & RENNE, T. 2007. Intrinsic pathway of coagulation and arterial thrombosis. *Arterioscler Thromb Vasc Biol*, 27, 2507-13.
- GERARDINO, L., PAPALEO, P., FLEX, A., GAETANI, E., FIORONI, G., POLA, P. & POLA, R. 2006. Coagulation factor XIII Val34Leu gene polymorphism and Alzheimer's disease. *Neurol Res*, 28, 807-9.
- GERHARDT, T. & LEY, K. 2015. Monocyte trafficking across the vessel wall. *Cardiovasc Res*, 107, 321-30.
- GHOSH, A., LI, W., FEBBRAIO, M., ESPINOLA, R. G., MCCRAE, K. R., COCKRELL, E. & SILVERSTEIN, R. L. 2008. Platelet CD36 mediates interactions with endothelial cell-derived microparticles and contributes to thrombosis in mice. *J Clin Invest*, 118, 1934-43.
- GREENBERG, C. S., ACHYUTHAN, K. E. & FENTON, J. W., 2ND 1987. Factor XIIIa formation promoted by complexing of alpha-thrombin, fibrin, and plasma factor XIII. *Blood*, 69, 867-71.
- GUIMARAES, A. H., DE BRUIJNE, E. L., LISMAN, T., DIPPEL, D. W., DECKERS, J. W., POLDERMANS, D., RIJKEN, D. C. & LEEBEEK, F. W. 2009. Hypofibrinolysis is a risk factor for arterial thrombosis at young age. *Br J Haematol*, 145, 115-20.
- GUPTA, S., BISWAS, A., AKHTER, M. S., KRETTLER, C., REINHART, C., DODT, J., REUTER, A., PHILIPPOU, H., IVASKEVICIUS, V. & OLDENBURG, J. 2016. Revisiting the mechanism of coagulation factor XIII activation and regulation from a structure/functional perspective. *Sci Rep*, 6, 30105.
- GUREWICH, V. 2016. Therapeutic Fibrinolysis: How Efficacy and Safety Can Be Improved. *J Am Coll Cardiol*, 68, 2099-2106.
- HANSSON, K. & STENFLO, J. 2005. Post-translational modifications in proteins involved in blood coagulation. *J Thromb Haemost*, 3, 2633-48.
- HARKER, L. A. 1998. Platelets in thrombotic disorders: quantitative and qualitative platelet disorders predisposing to arterial thrombosis. *Semin Hematol*, 35, 241-52.
- HAYWARD, C. P. M. 2018. How I investigate for bleeding disorders. *Int J Lab Hematol*, 40 Suppl 1, 6-14.
- HECHLER, B., MAGNENAT, S., ZIGHETTI, M. L., KASSACK, M. U., ULLMANN, H., CAZENAVE, J. P., EVANS, R., CATTANEO, M. & GACHET, C. 2005. Inhibition of platelet functions and thrombosis

- through selective or nonselective inhibition of the platelet P2 receptors with increasing doses of NF449 [4,4',4'',4'''-(carbonylbis(imino-5,1,3-benzenetriylbis-(carbonylimino)))tetrakis -benzene-1,3-disulfonic acid octasodium salt]. *J Pharmacol Exp Ther*, 314, 232-43.
- HEIJNEN, H. F., DEBILI, N., VAINCHENCKER, W., BRETON-GORIUS, J., GEUZE, H. J. & SIXMA, J. J. 1998. Multivesicular bodies are an intermediate stage in the formation of platelet alpha-granules. *Blood*, 91, 2313-25.
- HEIT, J. A. 2007. Thrombophilia: common questions on laboratory assessment and management. *Hematology Am Soc Hematol Educ Program*, 127-35.
- HELDEBRANT, C. M. & MANN, K. G. 1973. The activation of prothrombin. I. Isolation and preliminary characterization of intermediates. *J Biol Chem*, 248, 3642-52.
- HELMS, C. C., ARIENS, R. A., UITTE DE WILLIGE, S., STANDEVEN, K. F. & GUTHOLD, M. 2012. alpha-alpha Cross-links increase fibrin fiber elasticity and stiffness. *Biophys J*, 102, 168-75.
- HETHERSHAW, E. L., CILIA LA CORTE, A. L., DUVAL, C., ALI, M., GRANT, P. J., ARIENS, R. A. & PHILIPPOU, H. 2014. The effect of blood coagulation factor XIII on fibrin clot structure and fibrinolysis. *J Thromb Haemost*, 12, 197-205.
- HINCKER, A., FEIT, J., SLADEN, R. N. & WAGENER, G. 2014. Rotational thromboelastometry predicts thromboembolic complications after major non-cardiac surgery. *Crit Care*, 18, 549.
- HOAGLIN, D. C., IGLEWICZ, B. & TUKEY, J. W. 1986. Performance of Some Resistant Rules for Outlier Labeling. *Journal of the American Statistical Association*, 81, 991-999.
- HOFFMEISTER, K. M. 2011. The role of lectins and glycans in platelet clearance. *J Thromb Haemost*, 9 Suppl 1, 35-43.
- HOUSER, J. R., HUDSON, N. E., PING, L., O'BRIEN, E. T., 3RD, SUPERFINE, R., LORD, S. T. & FALVO, M. R. 2010. Evidence that alphaC region is origin of low modulus, high extensibility, and strain stiffening in fibrin fibers. *Biophys J*, 99, 3038-47.
- HUANG, R. S., MCDONALD, M. M., WETZEL, J. S., KAWANO-CASTILLO, J., PARKER, S., ARCHEVAL-LAO, J., CAI, C., RAHBAR, M. H., NGUYEN, A. N., BABA, S. J. & GROTTA, J. C. 2015. Clot Strength as Measured by Thrombelastography Correlates with Platelet Reactivity in Stroke Patients. *Ann Clin Lab Sci*, 45, 301-7.
- HUMPHRIES, S. E. 1993. The application of molecular biology techniques to the diagnosis of hyperlipidaemia and other risk factors for cardiovascular disease. *Clin Chim Acta*, 216, S5-18.
- ICHINOSE, A., MCMULLEN, B. A., FUJIKAWA, K. & DAVIE, E. W. 1986. Amino acid sequence of the b subunit of human factor XIII, a protein composed of ten repetitive segments. *Biochemistry*, 25, 4633-8.
- ICHINOSE, A., TAMAKI, T. & AOKI, N. 1983. Factor XIII-mediated cross-linking of NH2-terminal peptide of alpha 2-plasmin inhibitor to fibrin. *FEBS Lett*, 153, 369-71.
- INBAL, A. & MUSZBEK, L. 2003. Coagulation factor deficiencies and pregnancy loss. *Semin Thromb Hemost*, 29, 171-4.

- INOKUCHI, K., ASANO, T., OCHI, A., GOKAN, T., YOSHIKAWA, K., NAKAMURA, Y., OGAWA, K., CHIBA, Y., KAWASAKI, S., ONISHI, Y., MUNETSUGU, Y., ONUMA, Y., ONUKI, T., WATANABE, N., MINOURA, Y., KAWAMURA, M., ADACHI, T. & KOBAYASHI, Y. 2017. Gender Is a Significant Factor Affecting Blood Coagulation Systems. *The Showa University Journal of Medical Sciences*, 29, 151-162.
- JAIN, S. & ACHARYA, S. S. 2018. Management of rare coagulation disorders in 2018. *Transfus Apher Sci*, 57, 705-712.
- JAMBOR, C., REUL, V., SCHNIDER, T. W., DEGIACOMI, P., METZNER, H. & KORTE, W. C. 2009. In vitro inhibition of factor XIII retards clot formation, reduces clot firmness, and increases fibrinolytic effects in whole blood. *Anesth Analg*, 109, 1023-8.
- JANUS, T. J., LEWIS, S. D., LORAND, L. & SHAFER, J. A. 1983. Promotion of thrombin-catalyzed activation of factor XIII by fibrinogen. *Biochemistry*, 22, 6269-72.
- JESTY, J. & BELTRAMI, E. 2005. Positive feedbacks of coagulation: their role in threshold regulation. *Arterioscler Thromb Vasc Biol*, 25, 2463-9.
- JOHANNESSEN, K. A., NORDREHAUG, J. E., VON DER LIPPE, G. & VOLLSET, S. E. 1988. Risk factors for embolisation in patients with left ventricular thrombi and acute myocardial infarction. *Br Heart J*, 60, 104-10.
- KAIN, K., CARTER, A. M., BAMFORD, J. M., GRANT, P. J. & CATTO, A. J. 2003. Gender differences in coagulation and fibrinolysis in white subjects with acute ischemic stroke. *J Thromb Haemost*, 1, 390-2.
- KAMATH, S. & LIP, G. Y. 2003. Fibrinogen: biochemistry, epidemiology and determinants. *QJM*, 96, 711-29.
- KARIMI, M., BERECZKY, Z., COHAN, N. & MUSZBEK, L. 2009. Factor XIII Deficiency. *Semin Thromb Hemost*, 35, 426-38.
- KASAHARA, K., SOURI, M., KANEDA, M., MIKI, T., YAMAMOTO, N. & ICHINOSE, A. 2010. Impaired clot retraction in factor XIII A subunit-deficient mice. *Blood*, 115, 1277-9.
- KATONA, E., PENZES, K., CSAPO, A., FAZAKAS, F., UDVARDY, M. L., BAGOLY, Z., OROSZ, Z. Z. & MUSZBEK, L. 2014. Interaction of factor XIII subunits. *Blood*, 123, 1757-63.
- KATTULA, S., BYRNES, J. R., MARTIN, S. M., HOLLE, L. A., COOLEY, B. C., FLICK, M. J. & WOLBERG, A. S. 2018. Factor XIII in plasma, but not in platelets, mediates red blood cell retention in clots and venous thrombus size in mice. *Blood Adv*, 2, 25-35.
- KAWASHITA, E., KANNO, Y., ASAYAMA, H., OKADA, K., UESHIMA, S., MATSUO, O. & MATSUNO, H. 2013. Involvement of alpha2-antiplasmin in dendritic growth of hippocampal neurons. *J Neurochem*, 126, 58-69.
- KELLERMANN, K., MÜLLER, M., BLOBNER, M., KOCHS, E. F. & JUNGWIRTH, B. 2014. Influence of gender and sex hormones on blood coagulation and fibrinolysis after normothermic cardiopulmonary bypass in rats: 4AP1-8. *European Journal of Anaesthesiology (EJA)*, 31, 52-53.

- KIM, P. Y., TIEU, L. D., STAFFORD, A. R., FREDENBURGH, J. C. & WEITZ, J. I. 2012. A high affinity interaction of plasminogen with fibrin is not essential for efficient activation by tissue-type plasminogen activator. *J Biol Chem*, 287, 4652-61.
- KIMURA, S. & AOKI, N. 1986. Cross-linking site in fibrinogen for alpha 2-plasmin inhibitor. *J Biol Chem*, 261, 15591-5.
- KLINGEMANN, H. G., EGBRING, R., HOLST, F., GRAMSE, M. & HAVEMANN, K. 1982. Degradation of human plasma fibrin stabilizing factor XIII subunits by human granulocytic proteinases. *Thromb Res*, 28, 793-801.
- KOBAYASHI, M., TSUJITANI, S., KURISU, Y. & KAIBARA, N. 2004. Responses of cytokines and coagulation-fibrinolytic states to surgical stress following esophagectomy. *Hepatogastroenterology*, 51, 1376-8.
- KOMAROMI, I., BAGOLY, Z. & MUSZBEK, L. 2011. Factor XIII: novel structural and functional aspects. *J Thromb Haemost*, 9, 9-20.
- KORNBLITH, L. Z., HOWARD, B., KUNITAKE, R., REDICK, B., NELSON, M., COHEN, M. J. & CALLCUT, R. 2015. Obesity and clotting: Body mass index independently contributes to hypercoagulability after injury. *J Trauma Acute Care Surg*, 78, 30-6; discussion 37-8.
- KROLL, M. H., HARRIS, T. S., MOAKE, J. L., HANDIN, R. I. & SCHAFER, A. I. 1991. von Willebrand factor binding to platelet Gplb initiates signals for platelet activation. *J Clin Invest*, 88, 1568-73.
- KUCHER, N., SCHROEDER, V. & KOHLER, H. P. 2003. Role of blood coagulation factor XIII in patients with acute pulmonary embolism. Correlation of factor XIII antigen levels with pulmonary occlusion rate, fibrinogen, D-dimer, and clot firmness. *Thromb Haemost*, 90, 434-8.
- KUMAR, D. R., HANLIN, E., GLURICH, I., MAZZA, J. J. & YALE, S. H. 2010. Virchow's contribution to the understanding of thrombosis and cellular biology. *Clin Med Res*, 8, 168-72.
- KURNIAWAN, N. A., GRIMBERGEN, J., KOOPMAN, J. & KOENDERINK, G. H. 2014. Factor XIII stiffens fibrin clots by causing fiber compaction. *J Thromb Haemost*, 12, 1687-96.
- KURZ, K. D., MAIN, B. W. & SANDUSKY, G. E. 1990. Rat model of arterial thrombosis induced by ferric chloride. *Thromb Res*, 60, 269-80.
- LADENVALL, C., CSAJBOK, L., NYLEN, K., JOOD, K., NELLGARD, B. & JERN, C. 2009. Association between factor XIII single nucleotide polymorphisms and aneurysmal subarachnoid hemorrhage. *J Neurosurg*, 110, 475-81.
- LAUER, P., METZNER, H. J., ZETTLMEISSL, G., LI, M., SMITH, A. G., LATHE, R. & DICKNEITE, G. 2002. Targeted inactivation of the mouse locus encoding coagulation factor XIII-A: hemostatic abnormalities in mutant mice and characterization of the coagulation deficit. *Thromb Haemost*, 88, 967-74.
- LAVORINI, F., DI BELLO, V., DE RIMINI, M. L., LUCIGNANI, G., MARCONI, L., PALARETI, G., PESAVENTO, R., PRISCO, D., SANTINI, M., SVERZELLATI, N., PALLA, A. & PISTOLESI, M. 2013. Diagnosis and treatment of pulmonary embolism: a multidisciplinary approach. *Multidiscip Respir Med*, 8, 75.
- LEE, C. J. & ANSELL, J. E. 2011. Direct thrombin inhibitors. *Br J Clin Pharmacol*, 72, 581-92.

- LEE, K. N., LEE, C. S., TAE, W. C., JACKSON, K. W., CHRISTIANSEN, V. J. & MCKEE, P. A. 2000. Cross-linking of wild-type and mutant alpha 2-antiplasmins to fibrin by activated factor XIII and by a tissue transglutaminase. *J Biol Chem*, 275, 37382-9.
- LENTZ, B. R. 2003. Exposure of platelet membrane phosphatidylserine regulates blood coagulation. *Prog Lipid Res*, 42, 423-38.
- LEWIS, S. D., JANUS, T. J., LORAND, L. & SHAFER, J. A. 1985. Regulation of formation of factor XIIIa by its fibrin substrates. *Biochemistry*, 24, 6772-7.
- LEY, K. & HUO, Y. 2001. VCAM-1 is critical in atherosclerosis. *J Clin Invest*, 107, 1209-10.
- LEYS, D. 2001. Atherothrombosis: a major health burden. *Cerebrovasc Dis*, 11 Suppl 2, 1-4.
- LI, B., ZHANG, L., YIN, Y., PI, Y., YANG, Q., GAO, C., FANG, C., WANG, J. & LI, J. 2012. Lack of evidence for association between factor XIII-A Val34Leu polymorphism and ischemic stroke: a meta-analysis of 8,800 subjects. *Thromb Res*, 130, 654-60.
- LI, W., MCINTYRE, T. M. & SILVERSTEIN, R. L. 2013. Ferric chloride-induced murine carotid arterial injury: A model of redox pathology. *Redox Biol*, 1, 50-5.
- LI, W., NIEMAN, M. & SEN GUPTA, A. 2016a. Ferric Chloride-induced Murine Thrombosis Models. *J Vis Exp*.
- LI, W., SIGLEY, J., PIETERS, M., HELMS, C. C., NAGASWAMI, C., WEISEL, J. W. & GUTHOLD, M. 2016b. Fibrin Fiber Stiffness Is Strongly Affected by Fiber Diameter, but Not by Fibrinogen Glycation. *Biophys J*, 110, 1400-10.
- LIM, B. C., ARIENS, R. A., CARTER, A. M., WEISEL, J. W. & GRANT, P. J. 2003. Genetic regulation of fibrin structure and function: complex gene-environment interactions may modulate vascular risk. *Lancet*, 361, 1424-31.
- LITVINOV, R. I., GORKUN, O. V., GALANAKIS, D. K., YAKOVLEV, S., MEDVED, L., SHUMAN, H. & WEISEL, J. W. 2007. Polymerization of fibrin: Direct observation and quantification of individual B:b knob-hole interactions. *Blood*, 109, 130-8.
- LIU, W., JAWERTH, L. M., SPARKS, E. A., FALVO, M. R., HANTGAN, R. R., SUPERFINE, R., LORD, S. T. & GUTHOLD, M. 2006. Fibrin fibers have extraordinary extensibility and elasticity. *Science*, 313, 634.
- LORAND, J. B., PILKINGTON, T. R. & LORAND, L. 1966. Inhibitors of fibrin cross-linking: relevance for thrombolysis. *Nature*, 210, 1273-4.
- LORAND, L. 1986. Activation of blood coagulation factor XIII. *Ann N Y Acad Sci*, 485, 144-58.
- LORAND, L. 2000. Sol Sherry Lecture in Thrombosis : research on clot stabilization provides clues for improving thrombolytic therapies. *Arterioscler Thromb Vasc Biol*, 20, 2-9.
- LORAND, L. 2005. Factor XIII and the clotting of fibrinogen: from basic research to medicine. *J Thromb Haemost*, 3, 1337-48.
- LORAND, L., JEONG, J. M., RADEK, J. T. & WILSON, J. 1993. Human plasma factor XIII: subunit interactions and activation of zymogen. *Methods Enzymol*, 222, 22-35.

- LORAND, L. & KONISHI, K. 1964. Activation of the Fibrin Stabilizing Factor of Plasma by Thrombin. *Arch Biochem Biophys*, 105, 58-67.
- LYAKER, M. R., TULMAN, D. B., DIMITROVA, G. T., PIN, R. H. & PAPADIMOS, T. J. 2013. Arterial embolism. *Int J Crit Illn Inj Sci*, 3, 77-87.
- MACKMAN, N., TILLEY, R. E. & KEY, N. S. 2007. Role of the extrinsic pathway of blood coagulation in hemostasis and thrombosis. *Arterioscler Thromb Vasc Biol*, 27, 1687-93.
- MALINAUSKAS, R. A. 1997. Plasma hemoglobin measurement techniques for the in vitro evaluation of blood damage caused by medical devices. *Artif Organs*, 21, 1255-67.
- MALKHASSIAN, D. & SHARMA, S. 2019. Physiology, Factor XIII. *StatPearls*. Treasure Island (FL).
- MARSH LYLE, E., LEWIS, S. D., LEHMAN, E. D., GARDELL, S. J., MOTZEL, S. L. & LYNCH, J. J., JR. 1998. Assessment of thrombin inhibitor efficacy in a novel rabbit model of simultaneous arterial and venous thrombosis. *Thromb Haemost*, 79, 656-62.
- MARTINOD, K., DEMERS, M., FUCHS, T. A., WONG, S. L., BRILL, A., GALLANT, M., HU, J., WANG, Y. & WAGNER, D. D. 2013. Neutrophil histone modification by peptidylarginine deiminase 4 is critical for deep vein thrombosis in mice. *Proc Natl Acad Sci U S A*, 110, 8674-9.
- MARX, P. F., HAVIK, S. R., MARQUART, J. A., BOUMA, B. N. & MEIJERS, J. C. 2004. Generation and characterization of a highly stable form of activated thrombin-activable fibrinolysis inhibitor. *J Biol Chem*, 279, 6620-8.
- MASSBERG, S., GRAHL, L., VON BRUEHL, M. L., MANUKYAN, D., PFEILER, S., GOOSMANN, C., BRINKMANN, V., LORENZ, M., BIDZHEKOV, K., KHANDAGALE, A. B., KONRAD, I., KENNERKNECHT, E., REGES, K., HOLDENRIEDER, S., BRAUN, S., REINHARDT, C., SPANNAGL, M., PREISSNER, K. T. & ENGELMANN, B. 2010. Reciprocal coupling of coagulation and innate immunity via neutrophil serine proteases. *Nat Med*, 16, 887-96.
- MATSUKA, Y. V., MEDVED, L. V., MIGLIORINI, M. M. & INGHAM, K. C. 1996. Factor XIIIa-catalyzed cross-linking of recombinant alpha C fragments of human fibrinogen. *Biochemistry*, 35, 5810-6.
- MAUGERI, N., CAMPANA, L., GAVINA, M., COVINO, C., DE METRIO, M., PANCIROLI, C., MAIURI, L., MASERI, A., D'ANGELO, A., BIANCHI, M. E., ROVERE-QUERINI, P. & MANFREDI, A. A. 2014. Activated platelets present high mobility group box 1 to neutrophils, inducing autophagy and promoting the extrusion of neutrophil extracellular traps. *J Thromb Haemost*, 12, 2074-88.
- MAURICE, P., PIRES, V., AMANT, C., KAUSKOT, A., DA NASCIMENTO, S., SONNET, P., ROCHETTE, J., LEGRAND, C., FAUVEL-LAFEVE, F. & BONNEFOY, A. 2006. Antithrombotic effect of the type III collagen-related octapeptide (KOGEOGPK) in the mouse. *Vascul Pharmacol*, 44, 42-9.
- MEIER, H. L., HECK, L. W., SCHULMAN, E. S. & MACGLASHAN, D. W., JR. 1985. Purified human mast cells and basophils release human elastase and cathepsin G by an IgE-mediated mechanism. *Int Arch Allergy Appl Immunol*, 77, 179-83.

- MELTZER, M. E., DOGGEN, C. J., DE GROOT, P. G., ROSENDAAL, F. R. & LISMAN, T. 2010. Plasma levels of fibrinolytic proteins and the risk of myocardial infarction in men. *Blood*, 116, 529-36.
- MENOUD, P. A., SAPPINO, N., BOUDAL-KHOSHBEEN, M., VASSALLI, J. D. & SAPPINO, A. P. 1996. The kidney is a major site of alpha(2)-antiplasmin production. *J Clin Invest*, 97, 2478-84.
- MESSNER, B. & BERNHARD, D. 2014. Smoking and cardiovascular disease: mechanisms of endothelial dysfunction and early atherogenesis. *Arterioscler Thromb Vasc Biol*, 34, 509-15.
- MICHAEL PITTILO, R. 2000. Cigarette smoking, endothelial injury and cardiovascular disease. *Int J Exp Pathol*, 81, 219-30.
- MILJIC, P., HEYLEN, E., WILLEMSE, J., DJORDJEVIC, V., RADOJKOVIC, D., COLOVIC, M., ELEZOVIC, I. & HENDRIKS, D. 2010. Thrombin activatable fibrinolysis inhibitor (TAFI): a molecular link between coagulation and fibrinolysis. *Srp Arh Celok Lek*, 138 Suppl 1, 74-8.
- MITCHELL, J. L., LIONIENE, A. S., FRASER, S. R., WHYTE, C. S., BOOTH, N. A. & MUTCH, N. J. 2014. Functional factor XIII-A is exposed on the stimulated platelet surface. *Blood*, 124, 3982-90.
- MORENO, P. R., BERNARDI, V. H., LOPEZ-CUELLAR, J., MURCIA, A. M., PALACIOS, I. F., GOLD, H. K., MEHRAN, R., SHARMA, S. K., NEMERSON, Y., FUSTER, V. & FALLON, J. T. 1996. Macrophages, smooth muscle cells, and tissue factor in unstable angina. Implications for cell-mediated thrombogenicity in acute coronary syndromes. *Circulation*, 94, 3090-7.
- MOROI, M. & AOKI, N. 1976. Isolation and characterization of alpha2-plasmin inhibitor from human plasma. A novel proteinase inhibitor which inhibits activator-induced clot lysis. *J Biol Chem*, 251, 5956-65.
- MOSESSON, M. W. 2005. Fibrinogen and fibrin structure and functions. *J Thromb Haemost*, 3, 1894-904.
- MOSKAU, S., SMOLKA, K., SEMMLER, A., SCHWEICHEL, D., HARBRECHT, U., MULLER, J., POHL, C., KLOCKGETHER, T. & LINNEBANK, M. 2010. Common genetic coagulation variants are not associated with ischemic stroke in a case-control study. *Neurol Res*, 32, 519-22.
- MUNDI, S., MASSARO, M., SCODITTI, E., CARLUCCIO, M. A., VAN HINSBERGH, V. W. M., IRUELA-ARISPE, M. L. & DE CATERINA, R. 2018. Endothelial permeability, LDL deposition, and cardiovascular risk factors-a review. *Cardiovasc Res*, 114, 35-52.
- MURTHY, S. N. & LORAND, L. 1990. Cross-linked A alpha.gamma chain hybrids serve as unique markers for fibrinogen polymerized by tissue transglutaminase. *Proc Natl Acad Sci U S A*, 87, 9679-82.
- MURTHY, S. N., WILSON, J. H., LUKAS, T. J., VEKLICH, Y., WEISEL, J. W. & LORAND, L. 2000. Transglutaminase-catalyzed crosslinking of the Aalpha and gamma constituent chains in fibrinogen. *Proc Natl Acad Sci U S A*, 97, 44-8.
- MUSUKA, T. D., WILTON, S. B., TRABOULSI, M. & HILL, M. D. 2015. Diagnosis and management of acute ischemic stroke: speed is critical. *CMAJ*, 187, 887-93.
- MUSZBEK, L., ADANY, R., KAVAI, M., BODA, Z. & LOPACIU, S. 1988. Monocytes of patients congenitally deficient in plasma factor XIII lack

- factor XIII subunit a antigen and transglutaminase activity. *Thromb Haemost*, 59, 231-5.
- MUSZBEK, L., BERECZKY, Z., BAGOLY, Z., KOMAROMI, I. & KATONA, E. 2011. Factor XIII: a coagulation factor with multiple plasmatic and cellular functions. *Physiol Rev*, 91, 931-72.
- MUSZBEK, L., POLGAR, J. & BODA, Z. 1993. Platelet factor XIII becomes active without the release of activation peptide during platelet activation. *Thromb Haemost*, 69, 282-5.
- MUSZBEK, L., YEE, V. C. & HEVESSY, Z. 1999. Blood coagulation factor XIII: structure and function. *Thromb Res*, 94, 271-305.
- NAGY, J. A., KRADIN, R. L. & MCDONAGH, J. 1988. Biosynthesis of factor XIII A and B subunits. *Adv Exp Med Biol*, 231, 29-49.
- NARAYANAN, S. 1999. Multifunctional roles of thrombin. *Ann Clin Lab Sci*, 29, 275-80.
- NASKI, M. C., LORAND, L. & SHAFER, J. A. 1991. Characterization of the kinetic pathway for fibrin promotion of alpha-thrombin-catalyzed activation of plasma factor XIII. *Biochemistry*, 30, 934-41.
- NAUDIN, C., BURILLO, E., BLANKENBERG, S., BUTLER, L. & RENNE, T. 2017. Factor XII Contact Activation. *Semin Thromb Hemost*, 43, 814-826.
- NEEVES, K. B. 2015. Physicochemical artifacts in FeCl<sub>3</sub> thrombosis models. *Blood*, 126, 700-1.
- NIESWANDT, B. & WATSON, S. P. 2003. Platelet-collagen interaction: is GPVI the central receptor? *Blood*, 102, 449-61.
- NURMINSKAYA, M. & KAARTINEN, M. T. 2006. Transglutaminases in mineralized tissues. *Front Biosci*, 11, 1591-606.
- ORTEGA, M. A., ROMERO, B., ASUNSOLO, A., SOLA, M., ALAVREZ-ROCHA, M. J., SAINZ, F., ALAVREZ-MON, M., BUJAN, J. & GARCIA-HONDUVILLA, N. 2019. Patients with Incompetent Valves in Chronic Venous Insufficiency Show Increased Systematic Lipid Peroxidation and Cellular Oxidative Stress Markers. *Oxid Med Cell Longev*, 2019, 5164576.
- OTSUKA, F., YASUDA, S., NOGUCHI, T. & ISHIBASHI-UEDA, H. 2016. Pathology of coronary atherosclerosis and thrombosis. *Cardiovasc Diagn Ther*, 6, 396-408.
- OWENS, A. P., 3RD, LU, Y., WHINNA, H. C., GACHET, C., FAY, W. P. & MACKMAN, N. 2011. Towards a standardization of the murine ferric chloride-induced carotid arterial thrombosis model. *J Thromb Haemost*, 9, 1862-3.
- OWENS, A. P., 3RD & MACKMAN, N. 2010. Tissue factor and thrombosis: The clot starts here. *Thromb Haemost*, 104, 432-9.
- PAYNE, H. & BRILL, A. 2017. Stenosis of the Inferior Vena Cava: A Murine Model of Deep Vein Thrombosis. *J Vis Exp*.
- PHAM, C. T. 2006. Neutrophil serine proteases: specific regulators of inflammation. *Nat Rev Immunol*, 6, 541-50.
- PIECHOCKA, I. K., KURNIAWAN, N. A., GRIMBERGEN, J., KOOPMAN, J. & KOENDERINK, G. H. 2017. Recombinant fibrinogen reveals the differential roles of alpha- and gamma-chain cross-linking and molecular heterogeneity in fibrin clot strain-stiffening. *J Thromb Haemost*, 15, 938-949.

- PITKANEN, H. H., JOUPPILA, A., LEMPONEN, M., ILMAKUNNAS, M., AHONEN, J. & LASSILA, R. 2017. Factor XIII deficiency enhances thrombin generation due to impaired fibrin polymerization - An effect corrected by Factor XIII replacement. *Thromb Res*, 149, 56-61.
- PLUG, T. & MEIJERS, J. C. 2016. Structure-function relationships in thrombin-activatable fibrinolysis inhibitor. *J Thromb Haemost*, 14, 633-44.
- POLGAR, J., HIDASI, V. & MUSZBEK, L. 1990. Non-proteolytic activation of cellular protransglutaminase (placenta macrophage factor XIII). *Biochem J*, 267, 557-60.
- POURGHEYSARI, B., DREES, F. & HASHEMZADEH-CHALESHTORI, M. 2014. Factor XIII A-V34L and factor XIII B-H95R in venous thromboembolism in central Iran: protective and neutral. *Blood Coagul Fibrinolysis*, 25, 439-43.
- PREVITALI, E., BUCCIARELLI, P., PASSAMONTI, S. M. & MARTINELLI, I. 2011. Risk factors for venous and arterial thrombosis. *Blood Transfus*, 9, 120-38.
- PRISCO, D., FEDI, S., BRUNELLI, T., CELLAI, A. P., HAGI, M. I., GIANNI, R., SANTORO, E., CAPPELLETTI, C., PEPE, G., GENSINI, G. F. & ABBATE, R. 1996. Fibrinogen and factor VIIag in healthy adolescents: the Floren-teen (Florence teenager) Study. *Thromb Haemost*, 75, 778-81.
- PROTOPOPOVA, A. D., RAMIREZ, A., KLINOV, D. V., LITVINOV, R. I. & WEISEL, J. W. 2019. Factor XIII topology: organization of B subunits and changes with activation studied with single-molecule atomic force microscopy. *J Thromb Haemost*.
- PUDDU, P., PUDDU, G. M., ZACA, F. & MUSCARI, A. 2000. Endothelial dysfunction in hypertension. *Acta Cardiol*, 55, 221-32.
- RAO, L. V. & RAPAPORT, S. I. 1988. Activation of factor VII bound to tissue factor: a key early step in the tissue factor pathway of blood coagulation. *Proc Natl Acad Sci U S A*, 85, 6687-91.
- RENIER, N., ADAMS, E. L., KIRST, C., WU, Z., AZEVEDO, R., KOHL, J., AUTRY, A. E., KADIRI, L., UMADEVI VENKATARAJU, K., ZHOU, Y., WANG, V. X., TANG, C. Y., OLSEN, O., DULAC, C., OSTEN, P. & TESSIER-LAVIGNE, M. 2016. Mapping of Brain Activity by Automated Volume Analysis of Immediate Early Genes. *Cell*, 165, 1789-1802.
- RENIER, N., WU, Z., SIMON, D. J., YANG, J., ARIEL, P. & TESSIER-LAVIGNE, M. 2014. iDISCO: a simple, rapid method to immunolabel large tissue samples for volume imaging. *Cell*, 159, 896-910.
- RICHARDSON, D. S. & LICHTMAN, J. W. 2015. Clarifying Tissue Clearing. *Cell*, 162, 246-257.
- RIJKEN, D. C., ABDUL, S., MALFLIET, J. J., LEEBEEK, F. W. & UITTE DE WILLIGE, S. 2016. Compaction of fibrin clots reveals the antifibrinolytic effect of factor XIII. *J Thromb Haemost*, 14, 1453-61.
- RIJKEN, D. C. & LIJNEN, H. R. 2009. New insights into the molecular mechanisms of the fibrinolytic system. *J Thromb Haemost*, 7, 4-13.
- RIJKEN, D. C. & UITTE DE WILLIGE, S. 2017. Inhibition of Fibrinolysis by Coagulation Factor XIII. *Biomed Res Int*, 2017, 1209676.

- RITCHIE, H., LAWRIE, L. C., CROMBIE, P. W., MOSESSON, M. W. & BOOTH, N. A. 2000. Cross-linking of plasminogen activator inhibitor 2 and alpha 2-antiplasmin to fibrin(ogen). *J Biol Chem*, 275, 24915-20.
- ROBERTSON, J. O., LI, W., SILVERSTEIN, R. L., TOPOL, E. J. & SMITH, J. D. 2009. Deficiency of LRP8 in mice is associated with altered platelet function and prolonged time for in vivo thrombosis. *Thromb Res*, 123, 644-52.
- ROOTH, E., WALLEN, N. H., BLOMBACK, M. & HE, S. 2011. Decreased fibrin network permeability and impaired fibrinolysis in the acute and convalescent phase of ischemic stroke. *Thromb Res*, 127, 51-6.
- ROSENDAAL, F. R. 2005. Venous thrombosis: the role of genes, environment, and behavior. *Hematology Am Soc Hematol Educ Program*, 1-12.
- ROSENDAAL, F. R. 2016. Causes of venous thrombosis. *Thromb J*, 14, 24.
- RUBATTU, S., DI ANGELANTONIO, E., NITSCH, D., GIGANTE, B., ZANDA, B., STANZIONE, R., EVANGELISTA, A., PIRISI, A., ROSATI, G. & VOLPE, M. 2005. Polymorphisms in prothrombotic genes and their impact on ischemic stroke in a Sardinian population. *Thromb Haemost*, 93, 1095-100.
- RUDIJANTO, A. 2007. The role of vascular smooth muscle cells on the pathogenesis of atherosclerosis. *Acta Med Indones*, 39, 86-93.
- SAITO, M., ASAKURA, H., YOSHIDA, T., ITO, K., OKAFUJI, K., YOSHIDA, T. & MATSUDA, T. 1990. A familial factor XIII subunit B deficiency. *Br J Haematol*, 74, 290-4.
- SAKARIASSEN, K. S., ORNING, L. & TURITTO, V. T. 2015. The impact of blood shear rate on arterial thrombus formation. *Future Sci OA*, 1, FSO30.
- SAKATA, Y. & AOKI, N. 1980. Cross-linking of alpha 2-plasmin inhibitor to fibrin by fibrin-stabilizing factor. *J Clin Invest*, 65, 290-7.
- SALEH, M. & AMBROSE, J. A. 2018. Understanding myocardial infarction. *F1000Res*, 7.
- SCHERAGA, H. A. 1983. Interaction of thrombin and fibrinogen and the polymerization of fibrin monomer. *Ann N Y Acad Sci*, 408, 330-43.
- SCHMIDT, W., EGBRING, R. & HAVEMANN, K. 1975. Effect of elastase-like and chymotrypsin-like neutral proteases from human granulocytes on isolated clotting factors. *Thromb Res*, 6, 315-29.
- SCHOENWAEELDER, S. M. & JACKSON, S. P. 2015. Ferric chloride thrombosis model: unraveling the vascular effects of a highly corrosive oxidant. *Blood*, 126, 2652-3.
- SCHRODER, V. & KOHLER, H. P. 2000. Effect of factor XIII Val34Leu on alpha2-antiplasmin incorporation into fibrin. *Thromb Haemost*, 84, 1128-30.
- SCHROEDER, V., CHATTERJEE, T. & KOHLER, H. P. 2001. Influence of blood coagulation factor XIII and FXIII Val34Leu on plasma clot formation measured by thrombelastography. *Thromb Res*, 104, 467-74.
- SHAFEY, M., ANDERSON, J. L., SCARVELIS, D., DOUCETTE, S. P., GAGNON, F. & WELLS, P. S. 2007. Factor XIII Val34Leu variant and the risk of myocardial infarction: a meta-analysis. *Thromb Haemost*, 97, 635-41.

- SHANTSILA, E. & LIP, G. Y. 2009. The role of monocytes in thrombotic disorders. Insights from tissue factor, monocyte-platelet aggregates and novel mechanisms. *Thromb Haemost*, 102, 916-24.
- SHAYA, S. A., GANI, D. M., WEITZ, J. I., KIM, P. Y. & GROSS, P. L. 2019. Factor XIII Prevents Pulmonary Emboli in Mice by Stabilizing Deep Vein Thrombi. *Thromb Haemost*.
- SHEMIRANI, A. H., ANTALFI, B., PONGRACZ, E., MEZEI, Z. A., BERECZKY, Z. & CSIKI, Z. 2014. Factor XIII-A subunit Val34Leu polymorphism in fatal atherothrombotic ischemic stroke. *Blood Coagul Fibrinolysis*, 25, 364-8.
- SIEBENLIST, K. R., MEH, D. A. & MOSESSON, M. W. 1996. Plasma factor XIII binds specifically to fibrinogen molecules containing gamma chains. *Biochemistry*, 35, 10448-53.
- SIMCOX, L. E., ORMESHER, L., TOWER, C. & GREER, I. A. 2015. Pulmonary thrombo-embolism in pregnancy: diagnosis and management. *Breathe (Sheff)*, 11, 282-9.
- SIMON, D. I., EZRATTY, A. M., FRANCIS, S. A., RENNKE, H. & LOSCALZO, J. 1993. Fibrin(ogen) is internalized and degraded by activated human monocytoid cells via Mac-1 (CD11b/CD18): a nonplasmin fibrinolytic pathway. *Blood*, 82, 2414-22.
- SINGH, S., AKHTER, M. S., DODT, J., SHARMA, A., KANIYAPPAN, S., YADEGARI, H., IVASKEVICIUS, V., OLDENBURG, J. & BISWAS, A. 2019. Disruption of Structural Disulfides of Coagulation FXIII-B Subunit; Functional Implications for a Rare Bleeding Disorder. *Int J Mol Sci*, 20.
- SOBEL, J. H. & GAWINOWICZ, M. A. 1996. Identification of the alpha chain lysine donor sites involved in factor XIIIa fibrin cross-linking. *J Biol Chem*, 271, 19288-97.
- SOLOMON, C., RANUCCI, M., HOCHLEITNER, G., SCHOCHL, H. & SCHLIMP, C. J. 2015. Assessing the Methodology for Calculating Platelet Contribution to Clot Strength (Platelet Component) in Thromboelastometry and Thrombelastography. *Anesth Analg*, 121, 868-78.
- SOURI, M., KAETSU, H. & ICHINOSE, A. 2008a. Sushi domains in the B subunit of factor XIII responsible for oligomer assembly. *Biochemistry*, 47, 8656-64.
- SOURI, M., KOSEKI-KUNO, S., TAKEDA, N., DEGEN, J. L. & ICHINOSE, A. 2008b. Administration of factor XIII B subunit increased plasma factor XIII A subunit levels in factor XIII B subunit knock-out mice. *Int J Hematol*, 87, 60-8.
- SOURI, M., OSAKI, T. & ICHINOSE, A. 2015. The Non-catalytic B Subunit of Coagulation Factor XIII Accelerates Fibrin Cross-linking. *J Biol Chem*, 290, 12027-39.
- STANDEVEN, K. F., CARTER, A. M., GRANT, P. J., WEISEL, J. W., CHERNYSH, I., MASOVA, L., LORD, S. T. & ARIENS, R. A. 2007. Functional analysis of fibrin {gamma}-chain cross-linking by activated factor XIII: determination of a cross-linking pattern that maximizes clot stiffness. *Blood*, 110, 902-7.
- STEIN, P. D. & GOLDMAN, J. 2009. Obesity and thromboembolic disease. *Clin Chest Med*, 30, 489-93, viii.

- STEPIEN, E., PLICNER, D., KAPELAK, B., WYPASEK, E., SADOWSKI, J. & UNDAS, A. 2009. Factor XIII Val34Leu polymorphism as a modulator of fibrin clot permeability and resistance to lysis in patients with severe coronary artery disease. *Kardiol Pol*, 67, 947-55.
- STIELER, M., WEBER, J., HILS, M., KOLB, P., HEINE, A., BUCHOLD, C., PASTERNAK, R. & KLEBE, G. 2013. Structure of active coagulation factor XIII triggered by calcium binding: basis for the design of next-generation anticoagulants. *Angew Chem Int Ed Engl*, 52, 11930-4.
- STONE, J., HANGGE, P., ALBADAWI, H., WALLACE, A., SHAMOUN, F., KNUTTIEN, M. G., NAIDU, S. & OKLU, R. 2017. Deep vein thrombosis: pathogenesis, diagnosis, and medical management. *Cardiovasc Diagn Ther*, 7, S276-S284.
- SUCKER, C., FAROKHZAD, F., KURSCHAT, C., GRABENSEE, B., SCHARF, R. E., ZOTZ, R. B., MARUHN-DEBOWSKI, B. & HETZEL, G. R. 2009. The homozygous leu variant of the factor XIII Val34Leu polymorphism as a risk factor for the manifestation of thrombotic microangiopathies. *Clin Appl Thromb Hemost*, 15, 197-200.
- SWYSTUN, L. L. & LIAW, P. C. 2016. The role of leukocytes in thrombosis. *Blood*, 128, 753-62.
- TABAS, I. 2010. Macrophage death and defective inflammation resolution in atherosclerosis. *Nat Rev Immunol*, 10, 36-46.
- TAMAKI, T. & AOKI, N. 1981. Cross-linking of alpha 2-plasmin inhibitor and fibronectin to fibrin by fibrin-stabilizing factor. *Biochim Biophys Acta*, 661, 280-6.
- TAMAKI, T. & AOKI, N. 1982. Cross-linking of alpha 2-plasmin inhibitor to fibrin catalyzed by activated fibrin-stabilizing factor. *J Biol Chem*, 257, 14767-72.
- TARALLO, P., HENNY, J., GUEGUEN, R. & SIEST, G. 1992. Reference limits of plasma fibrinogen. *Eur J Clin Chem Clin Biochem*, 30, 745-51.
- TCHAIKOVSKI, S. N. & ROSING, J. 2010. Mechanisms of estrogen-induced venous thromboembolism. *Thromb Res*, 126, 5-11.
- THOMAS, A., BISWAS, A., DODT, J., PHILIPPOU, H., HETHERSHAW, E., ENSIKAT, H. J., IVASKEVICIUS, V. & OLDENBURG, J. 2016. Coagulation Factor XIII A Subunit Missense Mutations Affect Structure and Function at the Various Steps of Factor XIII Action. *Hum Mutat*, 37, 1030-41.
- THOMAS, R. H. 2001. Hypercoagulability syndromes. *Arch Intern Med*, 161, 2433-9.
- TRACY, P. B., EIDE, L. L. & MANN, K. G. 1985. Human prothrombinase complex assembly and function on isolated peripheral blood cell populations. *J Biol Chem*, 260, 2119-24.
- TSENG, M. T., DOZIER, A., HARIBABU, B. & GRAHAM, U. M. 2006. Transendothelial migration of ferric ion in FeCl<sub>3</sub> injured murine common carotid artery. *Thromb Res*, 118, 275-80.
- TURNER, B. T., JR., SABO, T. M., WILDING, D. & MAURER, M. C. 2004. Mapping of factor XIII solvent accessibility as a function of activation state using chemical modification methods. *Biochemistry*, 43, 9755-65.

- TUTWILER, V., LITVINOV, R. I., LOZHKIN, A. P., PESHKOVA, A. D., LEBEDEVA, T., ATAULLAKHANOV, F. I., SPILLER, K. L., CINES, D. B. & WEISEL, J. W. 2016. Kinetics and mechanics of clot contraction are governed by the molecular and cellular composition of the blood. *Blood*, 127, 149-59.
- ULRYCH, J., KVASNICKA, T., FRYBA, V., KOMARC, M., MALIKOVA, I., BURGET, F., BRZEZKOVA, R., KVASNICKA, J., JR., KRASKA, Z. & KVASNICKA, J. 2016. 28 day post-operative persisted hypercoagulability after surgery for benign diseases: a prospective cohort study. *BMC Surg*, 16, 16.
- UNDAS, A. 2017. Prothrombotic Fibrin Clot Phenotype in Patients with Deep Vein Thrombosis and Pulmonary Embolism: A New Risk Factor for Recurrence. *Biomed Res Int*, 2017, 8196256.
- UNDAS, A. & ARIENS, R. A. 2011. Fibrin clot structure and function: a role in the pathophysiology of arterial and venous thromboembolic diseases. *Arterioscler Thromb Vasc Biol*, 31, e88-99.
- UNDAS, A., NOWAKOWSKI, T., CIESLA-DUL, M. & SADOWSKI, J. 2011. Abnormal plasma fibrin clot characteristics are associated with worse clinical outcome in patients with peripheral arterial disease and thromboangiitis obliterans. *Atherosclerosis*, 215, 481-6.
- UNDAS, A., PLICNER, D., STEPIEN, E., DRWILA, R. & SADOWSKI, J. 2007. Altered fibrin clot structure in patients with advanced coronary artery disease: a role of C-reactive protein, lipoprotein(a) and homocysteine. *J Thromb Haemost*, 5, 1988-90.
- UNDAS, A., PODOLEC, P., ZAWILSKA, K., PIECULEWICZ, M., JEDLINSKI, I., STEPIEN, E., KONARSKA-KUSZEWSKA, E., WEGLARZ, P., DUSZYNSKA, M., HANSCHKE, E., PRZEWLOCKI, T. & TRACZ, W. 2009. Altered fibrin clot structure/function in patients with cryptogenic ischemic stroke. *Stroke*, 40, 1499-501.
- UNDAS, A., SZULDRZYNSKI, K., STEPIEN, E., ZALEWSKI, J., GODLEWSKI, J., TRACZ, W., PASOWICZ, M. & ZMUDKA, K. 2008. Reduced clot permeability and susceptibility to lysis in patients with acute coronary syndrome: effects of inflammation and oxidative stress. *Atherosclerosis*, 196, 551-7.
- VALNICKOVA, Z. & ENGHILD, J. J. 1998. Human procarboxypeptidase U, or thrombin-activable fibrinolysis inhibitor, is a substrate for transglutaminases. Evidence for transglutaminase-catalyzed cross-linking to fibrin. *J Biol Chem*, 273, 27220-4.
- VAN DER MEIJDEN, P. E., MUNNIX, I. C., AUGER, J. M., GOVERS-RIEMSLAG, J. W., COSEMANS, J. M., KUIJPERS, M. J., SPRONK, H. M., WATSON, S. P., RENNE, T. & HEEMSKERK, J. W. 2009. Dual role of collagen in factor XII-dependent thrombus formation. *Blood*, 114, 881-90.
- VAN KEMPEN, T. H. S., BOGAERDS, A. C. B., PETERS, G. W. M. & VAN DE VOSSE, F. N. 2014. A constitutive model for a maturing fibrin network. *Biophys J*, 107, 504-513.
- VERMA, A. K., GARG, A., XU, D., BRUNER, M., FAZEL-REZAI, R., BLABER, A. P. & TAVAKOLIAN, K. 2017. Skeletal Muscle Pump Drives Control of Cardiovascular and Postural Systems. *Sci Rep*, 7, 45301.

- VICKERS, J. D. 1999. Binding of polymerizing fibrin to integrin alpha(IIb)beta(3) on chymotrypsin-treated rabbit platelets decreases phosphatidylinositol 4,5-bisphosphate and increases cytoskeletal actin. *Platelets*, 10, 228-37.
- VILES-GONZALEZ, J. F., FUSTER, V. & BADIMON, J. J. 2004. Atherothrombosis: a widespread disease with unpredictable and life-threatening consequences. *Eur Heart J*, 25, 1197-207.
- VOKO, Z., BERECZKY, Z., KATONA, E., ADANY, R. & MUSZBEK, L. 2007. Factor XIII Val34Leu variant protects against coronary artery disease. A meta-analysis. *Thromb Haemost*, 97, 458-63.
- VON BRUHL, M. L., STARK, K., STEINHART, A., CHANDRARATNE, S., KONRAD, I., LORENZ, M., KHANDOGA, A., TIRNICERIU, A., COLETTI, R., KOLLNBERGER, M., BYRNE, R. A., LAITINEN, I., WALCH, A., BRILL, A., PFEILER, S., MANUKYAN, D., BRAUN, S., LANGE, P., RIEGGER, J., WARE, J., ECKART, A., HAIDARI, S., RUDELIUS, M., SCHULZ, C., ECHTLER, K., BRINKMANN, V., SCHWAIGER, M., PREISSNER, K. T., WAGNER, D. D., MACKMAN, N., ENGELMANN, B. & MASSBERG, S. 2012. Monocytes, neutrophils, and platelets cooperate to initiate and propagate venous thrombosis in mice in vivo. *J Exp Med*, 209, 819-35.
- WANG, D., WANG, Z., ZHANG, L. & WANG, Y. 2017. Roles of Cells from the Arterial Vessel Wall in Atherosclerosis. *Mediators Inflamm*, 2017, 8135934.
- WANG, X., SMITH, P. L., HSU, M. Y., OGLETREE, M. L. & SCHUMACHER, W. A. 2006. Murine model of ferric chloride-induced vena cava thrombosis: evidence for effect of potato carboxypeptidase inhibitor. *J Thromb Haemost*, 4, 403-10.
- WANG, Z., LEISNER, T. M. & PARISE, L. V. 2003. Platelet alpha2beta1 integrin activation: contribution of ligand internalization and the alpha2-cytoplasmic domain. *Blood*, 102, 1307-15.
- WARTIOVAARA, U., MIKKOLA, H., SZOKE, G., HARAMURA, G., KARPATI, L., BALOGH, I., LASSILA, R., MUSZBEK, L. & PALOTIE, A. 2000. Effect of Val34Leu polymorphism on the activation of the coagulation factor XIII-A. *Thromb Haemost*, 84, 595-600.
- WEI, L. K., GRIFFITHS, L. R., KOOL, C. W. & IRENE, L. 2019. Meta-Analysis of Factor V, Factor VII, Factor XII, and Factor XIII-A Gene Polymorphisms and Ischemic Stroke. *Medicina (Kaunas)*, 55.
- WEISBERG, L. J., SHIU, D. T., CONKLING, P. R. & SHUMAN, M. A. 1987. Identification of normal human peripheral blood monocytes and liver as sites of synthesis of coagulation factor XIII a-chain. *Blood*, 70, 579-82.
- WEISEL, J. W. & LITVINOV, R. I. 2013. Mechanisms of fibrin polymerization and clinical implications. *Blood*, 121, 1712-9.
- WELLS, P. S., ANDERSON, J. L., SCARVELIS, D. K., DOUCETTE, S. P. & GAGNON, F. 2006. Factor XIII Val34Leu variant is protective against venous thromboembolism: a HuGE review and meta-analysis. *Am J Epidemiol*, 164, 101-9.
- WHINNA, H. C. 2008. Overview of murine thrombosis models. *Thromb Res*, 122 Suppl 1, S64-9.

- WIMAN, B. & COLLEN, D. 1977. Purification and characterization of human antiplasmin, the fast-acting plasmin inhibitor in plasma. *Eur J Biochem*, 78, 19-26.
- WIMAN, B., LIJNEN, H. R. & COLLEN, D. 1979. On the specific interaction between the lysine-binding sites in plasmin and complementary sites in alpha2-antiplasmin and in fibrinogen. *Biochim Biophys Acta*, 579, 142-54.
- WOLPL, A., LATTKE, H., BOARD, P. G., ARNOLD, R., SCHMEISER, T., KUBANEK, B., ROBIN-WINN, M., PICHELMAYR, R. & GOLDMANN, S. F. 1987. Coagulation factor XIII A and B subunits in bone marrow and liver transplantation. *Transplantation*, 43, 151-3.
- WOOLLARD, K. J., STURGEON, S., CHIN-DUSTING, J. P., SALEM, H. H. & JACKSON, S. P. 2009. Erythrocyte hemolysis and hemoglobin oxidation promote ferric chloride-induced vascular injury. *J Biol Chem*, 284, 13110-8.
- WU, Y. 2015. Contact pathway of coagulation and inflammation. *Thromb J*, 13, 17.
- XING, X., BAFFIC, J. & SPARROW, C. P. 1998. LDL oxidation by activated monocytes: characterization of the oxidized LDL and requirement for transition metal ions. *J Lipid Res*, 39, 2201-8.
- XU, J., ZHANG, X., PELAYO, R., MONESTIER, M., AMMOLLO, C. T., SEMERARO, F., TAYLOR, F. B., ESMON, N. L., LUPU, F. & ESMON, C. T. 2009. Extracellular histones are major mediators of death in sepsis. *Nat Med*, 15, 1318-21.
- YEE, V. C., PEDERSEN, L. C., LE TRONG, I., BISHOP, P. D., STENKAMP, R. E. & TELLER, D. C. 1994. Three-dimensional structure of a transglutaminase: human blood coagulation factor XIII. *Proc Natl Acad Sci U S A*, 91, 7296-300.
- ZHANG, Y., LI, L., ZHAO, Y., HAN, H., HU, Y., LIANG, D., YU, B. & KOU, J. 2017. The Myosin II Inhibitor, Blebbistatin, Ameliorates FeCl<sub>3</sub>-induced Arterial Thrombosis via the GSK3beta-NF-kappaB Pathway. *Int J Biol Sci*, 13, 630-639.
- ZHAO, L., MORSER, J., BAJZAR, L., NESHEIM, M. & NAGASHIMA, M. 1998. Identification and characterization of two thrombin-activatable fibrinolysis inhibitor isoforms. *Thromb Haemost*, 80, 949-55.

## **Chapter 8 Appendices**

## 8.1 Appendix 1

**Clustal Omega web tool alignment of a portion CMV-SPORT6 vector containing WT mFXIII-A sequence with a PCR amplification product.**

CMV-SPORT6 pCR2.1 - WT	cttttgaggaagtacccagaggcacacagagagactaccagagcacctctcaggagcac -----
CMV-SPORT6 pCR2.1 - WT	aagcaggatccagtaaaagctgagaATGtccagatactccagcaagcacctttggggggaggg -----ATGTCAGATACTCCAGCAAGCACCTTTGGGGGAGG *****
CMV-SPORT6 pCR2.1 - WT	CGAGCAGTCCCGCCAATAACTCCAATGCTGCAGAAGTGGACCTCCCAACTGAGGAGCTA CGAGCAGTCCCGCCAATAACTCCAATGCTGCAGAAGTGGACCTCCCAACTGAGGAGCTA *****
CMV-SPORT6 pCR2.1 - WT	CAAGGCCTGGTGCCAAGGGGTGTCAACCTGAAAGATTACCTGAATGTCACAGCTGTTTCAC CAAGGCCTGGTGCCAAGGGGTGTCAACCTGAAAGATTACCTGAATGTCACAGCTGTTTCAC *****
CMV-SPORT6 pCR2.1 - WT	CTGTTC AAGGAGAGATGGGACAGTAACAAGATTGATCACCACACAGACAAATATGACAAC CTGTTC AAGGAGAGATGGGACAGTAACAAGATTGATCACCACACAGACAAATATGACAAC *****
CMV-SPORT6 pCR2.1 - WT	AATAAGTTGATTGTCCGCAGAGGGCAGACCTTCTACATCCAGATTGACTTCAACCGTCCC AATAAGTTGATTGTCCGCAGAGGGCAGACCTTCTACATCCAGATTGACTTCAACCGTCCC *****
CMV-SPORT6 pCR2.1 - WT	TATGACCCCAGGAAGGATCTCTTCAGAGTGGAAATATGTCATTGGTCGCTACCCCTCAGGAG TATGACCCCAGGAAGGATCTCTTCAGAGTGGAAATATGTCATTGGTCGCTACCCCTCAGGAG *****
CMV-SPORT6 pCR2.1 - WT	AACAAGGGCACCTACATCCCTGTGCCTGTAGTGAAAGAGCTGCAAAGCGGAAAGTGGGGA AACAAGGGCACCTACATCCCTGTGCCTGTAGTGAAAGAGCTGCAAAGCGGAAAGTGGGGA *****
CMV-SPORT6 pCR2.1 - WT	GCCAAGGTTATCATGAATGAGGACCGGTCCGGTGCAGCTTCCGTTTCAGTCTTCTCCGGAA GCCAAGGTTATCATGAATGAGGACCGGTCCGGTGCAGCTTCCGTTTCAGTCTTCTCCGGAA *****
CMV-SPORT6 pCR2.1 - WT	TGCATTGTGGGAAATTCCGCATGTATGTTGCAGTCTGGACTCCCTATGGCATCCTGCGT TGCATTGTGGGAAATTCCGCATGTATGTTGCAGTCTGGACTCCCTATGGCATCCTGCGT *****
CMV-SPORT6 pCR2.1 - WT	ACTCGAAGAGACCCAGAAACAGACACATATATTTCTTCAACCCCTTGGTGTGAAGAGGAC ACTCGAAGAGACCCAGAAACAGACACATATATTTCTTCAACCCCTTGGTGTGAAGAGGAC *****
CMV-SPORT6 pCR2.1 - WT	GCTGTGTATCTGGATGATGAGAAGGAAAGAGAAGAGTACGTCTGAATGACATTGGAGTG GCTGTGTATCTGGATGATGAGAAGGAAAGAGAAGAGTACGTCTGAATGACATTGGAGTG *****
CMV-SPORT6 pCR2.1 - WT	ATATTTTATGGGACTTCAAAGACATCAAGAGCAGAAGCTGGAGCTATGGCCAGTTCGAA ATATTTTATGGGACTTCAAAGACATCAAGAGCAGAAGCTGGAGCTATGGCCAGTTCGAA *****
CMV-SPORT6 pCR2.1 - WT	GACGGCATCCTGGATACTTGCTTGTATGTGATGGACAAAGCTGAGATGGACCTTCTTGCC GACGGCATCCTGGATACTTGCTTGTATGTGATGGACAAAGCTGAGATGGACCTTCTTGCC *****
CMV-SPORT6 pCR2.1 - WT	AGAGGCAACCCCATCAAAGTCAGCCGAGTTGGATCAGCAATGGTGAATGCCAAGGATGAT AGAGGCAACCCCATCAAAGTCAGCCGAGTTGGATCAGCAATGGTGAATGCCAAGGATGAT *****
CMV-SPORT6 pCR2.1 - WT	GAAGGTGTTCTTGGTGGATCATGGGACAATGTCTATGCCTACGGCATCCCTCCATCAGCC GAAGGTGTTCTTGGTGGATCATGGGACAATGTCTATGCCTACGGCATCCCTCCATCAGCC *****
CMV-SPORT6 pCR2.1 - WT	TGGACAGGAAGTGTGACATTCTACTAGAATACAGAAGCTCGGAAACACCAGTCCGATAT TGGACAGGAAGTGTGACATTCTACTAGAATACAGAAGCTCGGAAACACCAGTCCGATAT

```

*****
CMV-SPORT6      GGCCAGTGTGGGTTTTTGTCTGGTGTCTTTAACACATTTTAAAGATGCCTTGGAAATCCCT
pCR2.1 - WT     GGCCAGTGTGGGTTTTTGTCTGGTGTCTTTAACACATTTTAAAGATGCCTTGGAAATCCCT
*****

CMV-SPORT6      GCACGAGTCATTACCAATTACTTCTCGGCCACGACAATGATGCCAATCTGCAAAATGGAC
pCR2.1 - WT     GCACGAGTCATTACCAATTACTTCTCGGCCACGACAATGATGCCAATCTGCAAAATGGAC
*****

CMV-SPORT6      ATCTTCTTGAAGAAGATGGGAATGTGAGCTCCAAACTCACCAAGGATTCGGTGTGGAAAC
pCR2.1 - WT     ATCTTCTTGAAGAAGATGGGAATGTGAGCTCCAAACTCACCAAGGATTCGGTGTGGAAAC
*****

CMV-SPORT6      TACCACTGCTGGAACGAAGCGTGGATGACAAGGCTGATCTTCTGTGGATTGGAGGC
pCR2.1 - WT     TACCACTGCTGGAACGAAGCGTGGATGACAAGGCTGATCTTCTGTGGATTGGAGGC
*****

CMV-SPORT6      TGGCAAGCTGTGGACAGCACACCCAGGAAAACAGTATGGCATGTACCGCTGTGGCCCT
pCR2.1 - WT     TGGCAAGCTGTGGACAGCACACCCAGGAAAACAGTATGGCATGTACCGCTGTGGCCCT
*****

CMV-SPORT6      GCCTCTGTCCAAGCCGTTAAGCATGGCCATGTCTGCTTCCAGTTTGTATGCCCGTTTGT
pCR2.1 - WT     GCCTCTGTCCAAGCCGTTAAGCATGGCCATGTCTGCTTCCAGTTTGTATGCCCGTTTGT
*****

CMV-SPORT6      TTTGCAGAGGTCAACAGTGATCTTGTTTACATCACAGCTAAGCAAGATGGCACTCACGTG
pCR2.1 - WT     TTTGCAGAGGTCAACAGTGATCTTGTTTACATCACAGCTAAGCAAGATGGCACTCACGTG
*****

CMV-SPORT6      GTGGAAGCCGTGGATGCCACCCATATCGGGAAGCTAATTGTGACCAAGCAAATGGAGGA
pCR2.1 - WT     GTGGAAGCCGTGGATGCCACCCATATCGGGAAGCTAATTGTGACCAAGCAAATGGAGGA
*****

CMV-SPORT6      GATGGCATGCAGGATATCACGGATACTTACAAATTTCAAGAAGGCCAAGAAGAAGAGAGA
pCR2.1 - WT     GATGGCATGCAGGATATCACGGATACTTACAAATTTCAAGAAGGCCAAGAAGAAGAGAGA
*****

CMV-SPORT6      CTAGCCCTTGAAACTGCTCTGATGTATGGAGCCAAGAAGACCCCTCAACACTGAAGGTGT
pCR2.1 - WT     CTAGCCCTTGAAACTGCTCTGATGTATGGAGCCAAGAAGACCCCTCAACACTGAAGGTGT
*****

CMV-SPORT6      GTCAAATCAAGGTCTGATGTGACCATGAACTTTGATGTGAAAATGCTGTGCTGGGAAAG
pCR2.1 - WT     GTCAAATCAAGGTCTGATGTGACCATGAACTTTGATGTGAAAATGCTGTGCTGGGAAAG
*****

CMV-SPORT6      GACTTCAAAGTACTATCACCTTCCAGAACAATAGCTCCAATCTGTACACCATCCTGGCC
pCR2.1 - WT     GACTTCAAAGTACTATCACCTTCCAGAACAATAGCTCCAATCTGTACACCATCCTGGCC
*****

CMV-SPORT6      TATCTTTCTGGCAACATCACCTTCTACACTGGGGTATCCAAGAAAGAGTTCAAGAAGGAG
pCR2.1 - WT     TATCTTTCTGGCAACATCACCTTCTACACTGGGGTATCCAAGAAAGAGTTCAAGAAGGAG
*****

CMV-SPORT6      TCCTTTGAAGAGACGCTGGATCCCTTTTCTTCCAAGAAAAGGAGGTGCTGGTTCAGAGCG
pCR2.1 - WT     TCCTTTGAAGAGACGCTGGATCCCTTTTCTTCCAAGAAAAGGAGGTGCTGGTTCAGAGCG
*****

CMV-SPORT6      GGCGAGTACATGAGCCACCTTCTAGAACAGGGCTTCTTGCCTTCTTCTGTCACGGCACGC
pCR2.1 - WT     GGCGAGTACATGAGCCACCTTCTAGAACAGGGCTTCTTGCCTTCTTCTGTCACGGCACGC
*****

CMV-SPORT6      ATCAACGAGTCCAGGGATGTCTTGGCCAAACAAAAGTCCATAATACTGACTATCCCCAAG
pCR2.1 - WT     ATCAACGAGTCCAGGGATGTCTTGGCCAAACAAAAGTCCATAATACTGACTATCCCCAAG
*****

CMV-SPORT6      ATCACCATCAAGGTCCGAGGTGCTGCCATGGTTGGCTCTGATATGGTTGTGACTGTTGAG
pCR2.1 - WT     ATCACCATCAAGGTCCGAGGTGCTGCCATGGTTGGCTCTGATATGGTTGTGACTGTTGAG
*****

CMV-SPORT6      TTCACTAATCCTTTAAAAGAAACACTACAAAATGTCTGGATTCAATTTGGATGGTCTTGG
pCR2.1 - WT     TTCACTAATCCTTTAAAAGAAACACTACAAAATGTCTGGATTCAATTTGGATGGTCTTGG
*****

CMV-SPORT6      GTGATGAGACCCAAGAGAAAGGTGTTCCGTGAAATCCGGCCCAACACCACGGTGCAGTGG
pCR2.1 - WT     GTGATGAGACCCAAGAGAAAGGTGTTCCGTGAAATCCGGCCCAACACCACGGTGCAGTGG
*****

```

```

*****
CMV-SPORT6      GAAGAAGTCTGTCGGCCTTGGGTCTCTGGCCATCGGAAGCTGATTGCCAGCATGACCAGT
pCR2.1 - WT     GAAGAAGTCTGTCGGCCTTGGGTCTCTGGCCATCGGAAGCTGATTGCCAGCATGACCAGT
*****

CMV-SPORT6      GACTCCCTGAGACATGTGTATGGAGAGCTGGATCTTCAGATTCAAAGACGACCTACTATG
pCR2.1 - WT     GACTCCCTGAGACATGTGTATGGAGAGCTGGATCTTCAGATTCAAAGACGACCTACTATG
*****

CMV-SPORT6      TAAATCCCAGAAGGCTCAAGTGGGCTGGGGCACATGGCCTCTTGCAGTCTTGGCTATGG
pCR2.1 - WT     TAA-----
***

CMV-SPORT6      agattctaatgcaaaacatagctagctcttgctttaattgggtgtgaagactgagaccg
pCR2.1 - WT     -----

```

## 8.2 Appendix 2

***Clustal Omega web tool alignment of WT mFXIII-A insert in pLIVE vector with a pLIVE+mFXIII-A DNA template.***

```

pLIVE+mFXIII-A  aaaattttcatgatgttttcttttttgctaaaactaagaattattcttttacatttcag
mFXIII-A       -----

pLIVE+mFXIII-A  tttttctgctagcaggatccagtaaagctgagaATGTCAGATACTCCAGCAAGCACCTTT
mFXIII-A       -----ATGTCAGATACTCCAGCAAGCACCTTT
*****

pLIVE+mFXIII-A  GGGGGGAGGCGAGCAGTCCC GCCAATAACTCCAATGCTGCAGAAGTGGACCTCCCAACT
mFXIII-A       GGGGGGAGGCGAGCAGTCCC GCCAATAACTCCAATGCTGCAGAAGTGGACCTCCCAACT
*****

pLIVE+mFXIII-A  GAGGAGCTACAAGGCCTGGTGCCAAGGGGTGTCAACCTGAAAGATTACCTGAATGTCACA
mFXIII-A       GAGGAGCTACAAGGCCTGGTGCCAAGGGGTGTCAACCTGAAAGATTACCTGAATGTCACA
*****

pLIVE+mFXIII-A  GCTGTTACCTGTTCAAGGAGAGATGGGACAGTAACAAGATTGATCACCACACAGACAAA
mFXIII-A       GCTGTTACCTGTTCAAGGAGAGATGGGACAGTAACAAGATTGATCACCACACAGACAAA
*****

pLIVE+mFXIII-A  TATGACAACAATAAGTTGATGTCCGCAGAGGGCAGACCTTCTACATCCAGATTGACTTC
mFXIII-A       TATGACAACAATAAGTTGATGTCCGCAGAGGGCAGACCTTCTACATCCAGATTGACTTC
*****

pLIVE+mFXIII-A  AACCGTCCCTATGACCCAGGAAGGATCTTTCAGAGTGAATATGTCATTGGTCGCTAC
mFXIII-A       AACCGTCCCTATGACCCAGGAAGGATCTTTCAGAGTGAATATGTCATTGGTCGCTAC
*****

pLIVE+mFXIII-A  CCTCAGGAGAACAAGGGCACCTACATCCCTGTGCCTGTAGTGAAGAGCTGCAAAGCGGA
mFXIII-A       CCTCAGGAGAACAAGGGCACCTACATCCCTGTGCCTGTAGTGAAGAGCTGCAAAGCGGA
*****

pLIVE+mFXIII-A  AAGTGGGGAGCCCAAGGTTATCATGAATGAGGACCGGTCGGTGCAGCTTCCGTTCACTCT
mFXIII-A       AAGTGGGGAGCCCAAGGTTATCATGAATGAGGACCGGTCGGTGCAGCTTCCGTTCACTCT
*****

pLIVE+mFXIII-A  TCTCCGGAATGCATTGTGGGGAAATTCGCATGTATGTTGCAGTCTGGACTCCCTATGGC
mFXIII-A       TCTCCGGAATGCATTGTGGGGAAATTCGCATGTATGTTGCAGTCTGGACTCCCTATGGC
*****

pLIVE+mFXIII-A  ATCCTGCGTACTCGAAGAGACCCAGAAACAGACACATATATTTCTCTCAACCCCTGGTGT
mFXIII-A       ATCCTGCGTACTCGAAGAGACCCAGAAACAGACACATATATTTCTCTCAACCCCTGGTGT
*****

pLIVE+mFXIII-A  GAAGAGGACGCTGTGTATCTGGATGATGAGAAGGAAAGAGAAGAGTACGCTCCTGAATGAC

```

mFXIII-A	GAAGAGGACGCTGTGTATCTGGATGATGAGAAGGAAAGAGAAGAGTACGTCCTGAATGAC *****
pLIVE+mFXIII-A mFXIII-A	ATTGGAGTGATATTTTATGGGGACTTCAAAGACATCAAGAGCAGAAGCTGGAGCTATGGC ATTGGAGTGATATTTTATGGGGACTTCAAAGACATCAAGAGCAGAAGCTGGAGCTATGGC *****
pLIVE+mFXIII-A mFXIII-A	CAGTTCGAAGACGGCATCCTGGATACTTGCTTGTATGTGATGGACAAAGCTGAGATGGAC CAGTTCGAAGACGGCATCCTGGATACTTGCTTGTATGTGATGGACAAAGCTGAGATGGAC *****
pLIVE+mFXIII-A mFXIII-A	CTTCTGGCAGAGGCAACCCCATCAAAGTCAGCCGAGTTGGATCAGCAATGGTGAATGCC CTTCTGGCAGAGGCAACCCCATCAAAGTCAGCCGAGTTGGATCAGCAATGGTGAATGCC *****
pLIVE+mFXIII-A mFXIII-A	AAGGATGATGAAGGTGTTCTTGTGGATCATGGGACAATGTCTATGCCTACGGCATCCCT AAGGATGATGAAGGTGTTCTTGTGGATCATGGGACAATGTCTATGCCTACGGCATCCCT *****
pLIVE+mFXIII-A mFXIII-A	CCATCAGCCTGGACAGGAAGTGTGACATTTACTAGAATACAGAAGCTCGGAAACACCA CCATCAGCCTGGACAGGAAGTGTGACATTTACTAGAATACAGAAGCTCGGAAACACCA *****
pLIVE+mFXIII-A mFXIII-A	GTCCGATATGGCCAGTGTGGGTTTTTGCTGGTGTCTTTAACACATTTTAAAGATGCCTT GTCCGATATGGCCAGTGTGGGTTTTTGCTGGTGTCTTTAACACATTTTAAAGATGCCTT *****
pLIVE+mFXIII-A mFXIII-A	GGAATCCCTGCACGAGTCATTACCAATTACTTCTCGGCCACGACAATGATGCCAATCTG GGAATCCCTGCACGAGTCATTACCAATTACTTCTCGGCCACGACAATGATGCCAATCTG *****
pLIVE+mFXIII-A mFXIII-A	CAAATGGACATCTTCTGGAAGAAGATGGGAATGTGAGCTCCAAACTCACCAAGGATTGC CAAATGGACATCTTCTGGAAGAAGATGGGAATGTGAGCTCCAAACTCACCAAGGATTGC *****
pLIVE+mFXIII-A mFXIII-A	GTGTGGAAC TACCACTGCTGGAACGAAGCGTGGATGACAAGGCCTGATCTTCCTGTTGGA GTGTGGAAC TACCACTGCTGGAACGAAGCGTGGATGACAAGGCCTGATCTTCCTGTTGGA *****
pLIVE+mFXIII-A mFXIII-A	TTTGGAGGCTGGCAAGCTGTGGACAGCACACCCAGGAAAACAGTGATGGCATGTACCGC TTTGGAGGCTGGCAAGCTGTGGACAGCACACCCAGGAAAACAGTGATGGCATGTACCGC *****
pLIVE+mFXIII-A mFXIII-A	TGTGGCCCTGCCTCTGTCCAAGCCGTTAAGCATGGCCATGTCTGCTTCCAGTTTGATGCC TGTGGCCCTGCCTCTGTCCAAGCCGTTAAGCATGGCCATGTCTGCTTCCAGTTTGATGCC *****
pLIVE+mFXIII-A mFXIII-A	CCGTTTGT TTTTGCAGAGGTCAACAGTGATCTTGT TTTACATCAGCTAAGCAAGATGGC CCGTTTGT TTTTGCAGAGGTCAACAGTGATCTTGT TTTACATCAGCTAAGCAAGATGGC *****
pLIVE+mFXIII-A mFXIII-A	ACTCACGTGGTGAAGCCGTGGATGCCACCCATATCGGGAAGCTAATGTGACCAAGCAA ACTCACGTGGTGAAGCCGTGGATGCCACCCATATCGGGAAGCTAATGTGACCAAGCAA *****
pLIVE+mFXIII-A mFXIII-A	ATTGGAGGAGATGGCATGCAGGATATCACGGATACTTACAAATTTCAAGAAGGCCAAGAA ATTGGAGGAGATGGCATGCAGGATATCACGGATACTTACAAATTTCAAGAAGGCCAAGAA *****
pLIVE+mFXIII-A mFXIII-A	GAAGAGAGACTAGCCCTTGAAACTGCTCTGATGTATGGAGCCAGAAGACCCCTCAACACT GAAGAGAGACTAGCCCTTGAAACTGCTCTGATGTATGGAGCCAGAAGACCCCTCAACACT *****
pLIVE+mFXIII-A mFXIII-A	GAAGGTGTTGTCAAATCAAGGTCTGATGTGACCATGAACTTTGATGTGAAAATGCTGTG GAAGGTGTTGTCAAATCAAGGTCTGATGTGACCATGAACTTTGATGTGAAAATGCTGTG *****
pLIVE+mFXIII-A mFXIII-A	CTGGGAAAGGACTTCAAAGTGACTATCACCTTCCAGAACAATAGCTCCAATCTGTACACC CTGGGAAAGGACTTCAAAGTGACTATCACCTTCCAGAACAATAGCTCCAATCTGTACACC *****
pLIVE+mFXIII-A mFXIII-A	ATCCTGGCCTATCTTCTGGCAACATCACCTTCTACACTGGGGTATCCAAGAAAGAGTTC ATCCTGGCCTATCTTCTGGCAACATCACCTTCTACACTGGGGTATCCAAGAAAGAGTTC *****
pLIVE+mFXIII-A	AAGAAGGAGTCTTTGAAGAGACGCTGGATCCCTTTCTCCAGAAAAGGAGGTGCTG

mFXIII-A	AAGAAGGAGTCCTTTGAAGAGACGCTGGATCCCTTTTCCTCCAAGAAAAGGAGGTGCTG *****
pLIVE+mFXIII-A mFXIII-A	GTCAGAGCGGGCGAGTACATGAGCCACCTTCTAGAACAGGGCTTCTTGCACTTCTTCGTC GTCAGAGCGGGCGAGTACATGAGCCACCTTCTAGAACAGGGCTTCTTGCACTTCTTCGTC *****
pLIVE+mFXIII-A mFXIII-A	ACGGCACGCATCAACGAGTCCAGGGATGTCCTGGCCAAACAAAAGTCCATAATACTGACT ACGGCACGCATCAACGAGTCCAGGGATGTCCTGGCCAAACAAAAGTCCATAATACTGACT *****
pLIVE+mFXIII-A mFXIII-A	ATCCCAAGATCACCATCAAGGTCCGAGGTGCTGCCATGGTTGGCTCTGATATGGTTGTG ATCCCAAGATCACCATCAAGGTCCGAGGTGCTGCCATGGTTGGCTCTGATATGGTTGTG *****
pLIVE+mFXIII-A mFXIII-A	ACTGTTGAGTTCACATAATCCTTTAAAAGAAACACTACAAAATGCTGGATTCAATTTGGAT ACTGTTGAGTTCACATAATCCTTTAAAAGAAACACTACAAAATGCTGGATTCAATTTGGAT *****
pLIVE+mFXIII-A mFXIII-A	GGTCCTGGAGTGATGAGACCAAGAGAAAGGTGTTCCGTGAAATCCGGCCCAACACCACG GGTCCTGGAGTGATGAGACCAAGAGAAAGGTGTTCCGTGAAATCCGGCCCAACACCACG *****
pLIVE+mFXIII-A mFXIII-A	GTGCAGTGGGAAGAAGTCTGTCTGGCCTTGGGTCTCTGGCCATCGGAAGCTGATTGCCAGC GTGCAGTGGGAAGAAGTCTGTCTGGCCTTGGGTCTCTGGCCATCGGAAGCTGATTGCCAGC *****
pLIVE+mFXIII-A mFXIII-A	ATGACCAGTGACTCCCTGAGACATGTGTATGGAGAGCTGGATCTCAGATTCAAAGACGA ATGACCAGTGACTCCCTGAGACATGTGTATGGAGAGCTGGATCTCAGATTCAAAGACGA *****
pLIVE+mFXIII-A mFXIII-A	CCTACTATGTAAattcccagaaggctcgagtaacatcacatttaaagcatctcaggtaa CCTACTATGTAA----- *****
pLIVE+mFXIII-A mFXIII-A	ctatattttgaattttttaaaaagtaactgtaatagtattattataaaatagcaaagatt -----

### 8.3 Appendix 3

**Clustal Omega alignment of a portion of pLIVE vector containing WT (34Leu) and 34Val mFXIII-A sequences. mFXIII-A L34V mutagenesis from WT FXIII-A in pLIVE vector with L34V point mutation highlighted. Underlined is the location of mFXIII-A amino acid codon number 34.**

pLIVE-WT pLIVE-L34V	aaaattttcatgatggttttcttttttctgctaaaactaaagaattattcttttacatttcag -----
pLIVE-WT pLIVE-L34V	tttttctgctagcaggatccagtaaaagctgagaATGTCAGATACTCCAGCAAGCACCTTT -----ATGTCAGATACTCCAGCAAGCACCTTT *****
pLIVE-WT pLIVE-L34V	GGGGGAGGCGAGCAGTCCCGCCCAATAACTCCAATGCTGCAGAAGTGGACCTCCCAACT GGGGGAGGCGAGCAGTCCCGCCCAATAACTCCAATGCTGCAGAAGTGGACCTCCCAACT *****
pLIVE-WT pLIVE-L34V	GAGGAGCTACAAGGC <u>CT</u> GGTGCCAAGGGGTGTCACCTGAAAGATTACCTGAATGTCACA GAGGAGCTACAAGGC <u>CT</u> GGTGCCAAGGGGTGTCACCTGAAAGATTACCTGAATGTCACA *****
pLIVE-WT pLIVE-L34V	GCTGTTACCTGTTCAAGGAGAGATGGGACAGTAACAAGATTGATCACCACACAGACAAA GCTGTTACCTGTTCAAGGAGAGATGGGACAGTAACAAGATTGATCACCACACAGACAAA *****

pLIVE-WT pLIVE-L34V	TATGACAACAATAAGTTGATTGTCCGCAGAGGGCAGACCTTCTACATCCAGATTGACTTC TATGACAACAATAAGTTGATTGTCCGCAGAGGGCAGACCTTCTACATCCAGATTGACTTC *****
pLIVE-WT pLIVE-L34V	AACCGTCCCTATGACCCAGGAAGGATCTCTCAGAGTGGAATATGTCATTGGTCGTAC AACCGTCCCTATGACCCAGGAAGGATCTCTCAGAGTGGAATATGTCATTGGTCGTAC *****
pLIVE-WT pLIVE-L34V	CCTCAGGAGAACAAGGGCACCTACATCCCTGTGCCTGTAGTGAAAGAGCTGCAAAGCGGA CCTCAGGAGAACAAGGGCACCTACATCCCTGTGCCTGTAGTGAAAGAGCTGCAAAGCGGA *****
pLIVE-WT pLIVE-L34V	AAGTGGGGAGCCAAGGTTATCATGAATGAGGACCGGTGCGGACTTTCGGTTCAGTCT AAGTGGGGAGCCAAGGTTATCATGAATGAGGACCGGTGCGGACTTTCGGTTCAGTCT *****
pLIVE-WT pLIVE-L34V	TCTCCGGAATGCATTGTGGGAAATTCGCATGTATGTTGCAGTCTGGACTCCCTATGGC TCTCCGGAATGCATTGTGGGAAATTCGCATGTATGTTGCAGTCTGGACTCCCTATGGC *****
pLIVE-WT pLIVE-L34V	ATCCTGCGTACTCGAAGAGACCCAGAAACAGACACATATATCTCTTCAACCCTTGGTGT ATCCTGCGTACTCGAAGAGACCCAGAAACAGACACATATATCTCTTCAACCCTTGGTGT *****
pLIVE-WT pLIVE-L34V	GAAGAGGACGCTGTGTATCTGGATGATGAGAAGGAAAGAGAAGAGTACGTCCTGAATGAC GAAGAGGACGCTGTGTATCTGGATGATGAGAAGGAAAGAGAAGAGTACGTCCTGAATGAC *****
pLIVE-WT pLIVE-L34V	ATTGGAGTGATATTTTATGGGGACTTCAAGACATCAAGAGCAGAAGCTGGAGCTATGGC ATTGGAGTGATATTTTATGGGGACTTCAAGACATCAAGAGCAGAAGCTGGAGCTATGGC *****
pLIVE-WT pLIVE-L34V	CAGTTCGAAGACGGCATCCTGGATACTTGCTTGTATGTGATGGACAAAGCTGAGATGGAC CAGTTCGAAGACGGCATCCTGGATACTTGCTTGTATGTGATGGACAAAGCTGAGATGGAC *****
pLIVE-WT pLIVE-L34V	CTTCTGGCAGAGGCAACCCCATCAAAGTCAGCCGAGTTGGATCAGCAATGGTGAATGCC CTTCTGGCAGAGGCAACCCCATCAAAGTCAGCCGAGTTGGATCAGCAATGGTGAATGCC *****
pLIVE-WT pLIVE-L34V	AAGGATGATGAAGGTGTTCTTGTGGATCATGGGACAATGTCTATGCCTACGGCATCCCT AAGGATGATGAAGGTGTTCTTGTGGATCATGGGACAATGTCTATGCCTACGGCATCCCT *****
pLIVE-WT pLIVE-L34V	CCATCAGCCTGGACAGGAAGTGTGACATTTCTACTAGAATACAGAAGCTCGGAAACACCA CCATCAGCCTGGACAGGAAGTGTGACATTTCTACTAGAATACAGAAGCTCGGAAACACCA *****
pLIVE-WT pLIVE-L34V	GTCCGATATGGCCAGTGTGGGTTTTTGTGGTGTCTTTAACACATTTTTAAGATGCCTT GTCCGATATGGCCAGTGTGGGTTTTTGTGGTGTCTTTAACACATTTTTAAGATGCCTT *****
pLIVE-WT pLIVE-L34V	GGAATCCCTGCACGAGTCATTACCAATTACTTCTCGGCCACGACAATGATGCCAATCTG GGAATCCCTGCACGAGTCATTACCAATTACTTCTCGGCCACGACAATGATGCCAATCTG *****
pLIVE-WT pLIVE-L34V	CAAATGGACATCTTCCTGGAAGAAGATGGGAATGTGAGCTCCAAACTCACCAAGGATTCG CAAATGGACATCTTCCTGGAAGAAGATGGGAATGTGAGCTCCAAACTCACCAAGGATTCG *****
pLIVE-WT pLIVE-L34V	GTGTGGAACCTACCACTGCTGGAACGAAGCGTGGATGACAAGGCCCTGATCTTCTGTTGGA GTGTGGAACCTACCACTGCTGGAACGAAGCGTGGATGACAAGGCCCTGATCTTCTGTTGGA *****
pLIVE-WT pLIVE-L34V	TTTGGAGGCTGGCAAGCTGTGGACAGCACACCCAGGAAAACAGTGATGGCATGTACCGC TTTGGAGGCTGGCAAGCTGTGGACAGCACACCCAGGAAAACAGTGATGGCATGTACCGC *****
pLIVE-WT pLIVE-L34V	TGTGGCCCTGCCTCTGTCCAAGCCGTTAAGCATGGCCATGTCTGCTTCCAGTTTGTATGCC TGTGGCCCTGCCTCTGTCCAAGCCGTTAAGCATGGCCATGTCTGCTTCCAGTTTGTATGCC *****
pLIVE-WT pLIVE-L34V	CCGTTTGTTTTTGCAGAGGTCAACAGTGATCTTGTTTACATCACAGCTAAGCAAGATGGC CCGTTTGTTTTTGCAGAGGTCAACAGTGATCTTGTTTACATCACAGCTAAGCAAGATGGC *****

pLIVE-WT pLIVE-L34V	ACTCACGTGGTGAAGCCGTGGATGCCACCCATATCGGGAAGCTAATTGTGACCAAGCAA ACTCACGTGGTGAAGCCGTGGATGCCACCCATATCGGGAAGCTAATTGTGACCAAGCAA *****
pLIVE-WT pLIVE-L34V	ATTGGAGGAGATGGCATGCAGGATATCACGGATACTTACAAATTTCAAGAAGGCCAAGAA ATTGGAGGAGATGGCATGCAGGATATCACGGATACTTACAAATTTCAAGAAGGCCAAGAA *****
pLIVE-WT pLIVE-L34V	GAAGAGAGACTAGCCCTTGAAACTGCTCTGATGTATGGAGCCAAGAAGACCCCTCAACACT GAAGAGAGACTAGCCCTTGAAACTGCTCTGATGTATGGAGCCAAGAAGACCCCTCAACACT *****
pLIVE-WT pLIVE-L34V	GAAGGTGTTGTCAAATCAAGGTCTGATGTGACCATGAACTTTGATGTGGAAAATGCTGTG GAAGGTGTTGTCAAATCAAGGTCTGATGTGACCATGAACTTTGATGTGGAAAATGCTGTG *****
pLIVE-WT pLIVE-L34V	CTGGAAAGGACTTCAAAGTGACTATCACCTTCCAGAACAAATAGCTCCAATCTGTACACC CTGGAAAGGACTTCAAAGTGACTATCACCTTCCAGAACAAATAGCTCCAATCTGTACACC *****
pLIVE-WT pLIVE-L34V	ATCCTGGCCTATCTTTCTGGCAACATCACCTTCTACACTGGGGTATCCAAGAAAGAGTTC ATCCTGGCCTATCTTTCTGGCAACATCACCTTCTACACTGGGGTATCCAAGAAAGAGTTC *****
pLIVE-WT pLIVE-L34V	AAGAAGGAGTCCTTTGAAGAGACGCTGGATCCCTTTTCTCCAAGAAAAGGAGGTGCTG AAGAAGGAGTCCTTTGAAGAGACGCTGGATCCCTTTTCTCCAAGAAAAGGAGGTGCTG *****
pLIVE-WT pLIVE-L34V	GTCAGAGCGGGCAGTACATGAGCCACCTTCTAGAACAGGGCTTCTTGCACTTCTTCGTC GTCAGAGCGGGCAGTACATGAGCCACCTTCTAGAACAGGGCTTCTTGCACTTCTTCGTC *****
pLIVE-WT pLIVE-L34V	ACGGCACGCATCAACGAGTCCAGGGATGTCCTGGCCAAACAAAAGTCCATAATACTGACT ACGGCACGCATCAACGAGTCCAGGGATGTCCTGGCCAAACAAAAGTCCATAATACTGACT *****
pLIVE-WT pLIVE-L34V	ATCCCCAAGATCACCATCAAGGTCCGAGGTGCTGCCATGGTTGGCTCTGATATGGTTGTG ATCCCCAAGATCACCATCAAGGTCCGAGGTGCTGCCATGGTTGGCTCTGATATGGTTGTG *****
pLIVE-WT pLIVE-L34V	ACTGTTGAGTTCACATAATCCTTTAAAAGAAACACTACAAAATGTCTGGATTCAATTTGGAT ACTGTTGAGTTCACATAATCCTTTAAAAGAAACACTACAAAATGTCTGGATTCAATTTGGAT *****
pLIVE-WT pLIVE-L34V	GGTCCTGGAGTGATGAGACCCAAGAGAAAGGTGTTCCGTGAAATCCGGCCCAACACCACG GGTCCTGGAGTGATGAGACCCAAGAGAAAGGTGTTCCGTGAAATCCGGCCCAACACCACG *****
pLIVE-WT pLIVE-L34V	GTGCAGTGGGAAGAAGTCTGTGCGCCTTGGGTCTCTGGCCATCGGAAGCTGATTGCCAGC GTGCAGTGGGAAGAAGTCTGTGCGCCTTGGGTCTCTGGCCATCGGAAGCTGATTGCCAGC *****
pLIVE-WT pLIVE-L34V	ATGACCAGTGACTCCCTGAGACATGTGTATGGAGAGCTGGATCTTCAAGACGGA ATGACCAGTGACTCCCTGAGACATGTGTATGGAGAGCTGGATCTTCAAGACGGA *****
pLIVE-WT pLIVE-L34V	CCTACTATGTAAattcccagaaggctcgagtaaacatcacatttaaaagcatctcaggtaa CCTACTATGTAA----- *****
pLIVE-WT pLIVE-L34V	ctatatatttgaatttttaaaaagtaactgtaaatagttattattaaaatagcaagatt -----

## 8.4 Appendix 4

### **Clustal Omega web tool alignment of inserted WT and L34V mFXIII-A sequences into pGEX-6P-1 vector.**

*Included pGEX-6P-1 sequence alongside WT mFXIII-A sequence is shown for vector demonstration purposes. L34V point mutation is highlighted, while underlined is the location of mFXIII-A amino acid codon number 34.*

pGEX6P1-WT pGEX6P1-L34V	atcctccaaaatcggatctggaagtctgttccaggggcccctgggatccccggaattcA -----A *
pGEX6P1-WT pGEX6P1-L34V	TGTCAGATACTCCAGCAAGCACCTTTGGGGGGAGGCGAGCAGTCCC GCCAATAACTCCA TGTCAGATACTCCAGCAAGCACCTTTGGGGGGAGGCGAGCAGTCCC GCCAATAACTCCA *****
pGEX6P1-WT pGEX6P1-L34V	ATGCTGCAGAAGTGGACCTCCCAACTGAGGAGCTACAAGGC <u>CTGGT</u> GCCAAGGGGTGTCA ATGCTGCAGAAGTGGACCTCCCAACTGAGGAGCTACAAGGC <u>CTGGT</u> GCCAAGGGGTGTCA *****
pGEX6P1-WT pGEX6P1-L34V	ACCTGAAAGATTACCTGAATGTCACAGCTGTTACCTGTTCAAGGAGAGATGGGACAGTA ACCTGAAAGATTACCTGAATGTCACAGCTGTTACCTGTTCAAGGAGAGATGGGACAGTA *****
pGEX6P1-WT pGEX6P1-L34V	ACAAGATTGATCACCACACAGACAAATATGACAACAATAAGTTGATTGTCCGCAGAGGGC ACAAGATTGATCACCACACAGACAAATATGACAACAATAAGTTGATTGTCCGCAGAGGGC *****
pGEX6P1-WT pGEX6P1-L34V	AGACCTTCTACATCCAGATTGACTTCAACCGTCCCTATGACCCAGGAAGGATCTCTTCA AGACCTTCTACATCCAGATTGACTTCAACCGTCCCTATGACCCAGGAAGGATCTCTTCA *****
pGEX6P1-WT pGEX6P1-L34V	GAGTGGAAATATGTCATTGGTCGCTACCCTCAGGAGAACAAGGGCACCTACATCCCTGTGC GAGTGGAAATATGTCATTGGTCGCTACCCTCAGGAGAACAAGGGCACCTACATCCCTGTGC *****
pGEX6P1-WT pGEX6P1-L34V	CTGTAGTCAAAGAGCTGCAAAGCGGAAAGTGGGGAGCCAAGGTTATCATGAATGAGGACC CTGTAGTCAAAGAGCTGCAAAGCGGAAAGTGGGGAGCCAAGGTTATCATGAATGAGGACC *****
pGEX6P1-WT pGEX6P1-L34V	GGTCGGTGCGACTTCCGTTCACTCTTCCGGAATGCATTGTGGGGAAATCCGCATGT GGTCGGTGCGACTTCCGTTCACTCTTCCGGAATGCATTGTGGGGAAATCCGCATGT *****
pGEX6P1-WT pGEX6P1-L34V	ATGTTGCAGTCTGGACTCCCTATGGCATCCTGCGTACTCGAAGAGACCCAGAAACAGACA ATGTTGCAGTCTGGACTCCCTATGGCATCCTGCGTACTCGAAGAGACCCAGAAACAGACA *****
pGEX6P1-WT pGEX6P1-L34V	CATATATTCTCTTCAACCCCTGGTGTGAAGAGGACGCTGTGTATCTGGATGATGAGAAGG CATATATTCTCTTCAACCCCTGGTGTGAAGAGGACGCTGTGTATCTGGATGATGAGAAGG *****
pGEX6P1-WT pGEX6P1-L34V	AAAGAGAAGAGTACGTCTGAATGACATTGGAGTGATATTTTATGGGGACTTCAAAGACA AAAGAGAAGAGTACGTCTGAATGACATTGGAGTGATATTTTATGGGGACTTCAAAGACA *****
pGEX6P1-WT pGEX6P1-L34V	TCAAGAGCAGAAGCTGGAGCTATGGCCAGTTCGAAGACGGCATCCTGGATACTTGCTTGT TCAAGAGCAGAAGCTGGAGCTATGGCCAGTTCGAAGACGGCATCCTGGATACTTGCTTGT *****
pGEX6P1-WT pGEX6P1-L34V	ATGTGATGGACAAAGCTGAGATGGACCTTCTGGCAGAGGCAACCCCATCAAAGTCAGCC ATGTGATGGACAAAGCTGAGATGGACCTTCTGGCAGAGGCAACCCCATCAAAGTCAGCC *****
pGEX6P1-WT pGEX6P1-L34V	GAGTTGGATCAGCAATGGTGAATGCCAAGGATGATGAAGGTGTTCTTGTGGATCATGGG GAGTTGGATCAGCAATGGTGAATGCCAAGGATGATGAAGGTGTTCTTGTGGATCATGGG *****

pGEX6P1-WT pGEX6P1-L34V	ACAATGTCTATGCCTACGGCATCCCTCCATCAGCCTGGACAGGAAGTGTGACATTCTAC ACAATGTCTATGCCTACGGCATCCCTCCATCAGCCTGGACAGGAAGTGTGACATTCTAC *****
pGEX6P1-WT pGEX6P1-L34V	TAGAATACAGAAGCTCGGAAACACCAGTCCGATATGGCCAGTGTGGGTTTTGTGGTGGT TAGAATACAGAAGCTCGGAAACACCAGTCCGATATGGCCAGTGTGGGTTTTGTGGTGGT *****
pGEX6P1-WT pGEX6P1-L34V	TCTTTAACACATTTTTAAGATGCCTTGGAAATCCCTGCACGAGTCATTACCAATTACTTCT TCTTTAACACATTTTTAAGATGCCTTGGAAATCCCTGCACGAGTCATTACCAATTACTTCT *****
pGEX6P1-WT pGEX6P1-L34V	CGGCCACGACAATGATGCCAATCTGCAAATGGACATCTTCCTGGAAGAAGATGGGAATG CGGCCACGACAATGATGCCAATCTGCAAATGGACATCTTCCTGGAAGAAGATGGGAATG *****
pGEX6P1-WT pGEX6P1-L34V	TGAGCTCCAAACTCACCAAGGATTCGGTGTGGAATACCCTGCTGGAACGAAGCGTGGGA TGAGCTCCAAACTCACCAAGGATTCGGTGTGGAATACCCTGCTGGAACGAAGCGTGGGA *****
pGEX6P1-WT pGEX6P1-L34V	TGACAAGGCCTGATCTTCCTGTTGGATTGGAGGCTGGCAAGCTGTGGACAGCACACCCC TGACAAGGCCTGATCTTCCTGTTGGATTGGAGGCTGGCAAGCTGTGGACAGCACACCCC *****
pGEX6P1-WT pGEX6P1-L34V	AGGAAAACAGTGATGGCATGTACCGCTGTGGCCCTGCCTCTGTCCAAGCCGTTAAGCATG AGGAAAACAGTGATGGCATGTACCGCTGTGGCCCTGCCTCTGTCCAAGCCGTTAAGCATG *****
pGEX6P1-WT pGEX6P1-L34V	GCCATGCTGCTTCCAGTTTGATGCCCGTTTGTTTTTGCAGAGGTCAACAGTGATCTTG GCCATGCTGCTTCCAGTTTGATGCCCGTTTGTTTTTGCAGAGGTCAACAGTGATCTTG *****
pGEX6P1-WT pGEX6P1-L34V	TTTACATCACAGCTAAGCAAGATGGCACTCACGTGGTGAAGCCGTGGATGCCACCCATA TTTACATCACAGCTAAGCAAGATGGCACTCACGTGGTGAAGCCGTGGATGCCACCCATA *****
pGEX6P1-WT pGEX6P1-L34V	TCGGGAAGCTAATTGTGACCAAGCAAATTGGAGGAGATGGCATGCAGGATATCACGGATA TCGGGAAGCTAATTGTGACCAAGCAAATTGGAGGAGATGGCATGCAGGATATCACGGATA *****
pGEX6P1-WT pGEX6P1-L34V	CTTACAAATTTCAAGAAGGCCAAGAAGAAGAGAGACTAGCCCTTGAAACTGCTCTGATGT CTTACAAATTTCAAGAAGGCCAAGAAGAAGAGAGACTAGCCCTTGAAACTGCTCTGATGT *****
pGEX6P1-WT pGEX6P1-L34V	ATGGAGCCAAGAAGACCCCTCAACACTGAAGGTGTTGTCAAATCAAGGTCTGATGTGACCA ATGGAGCCAAGAAGACCCCTCAACACTGAAGGTGTTGTCAAATCAAGGTCTGATGTGACCA *****
pGEX6P1-WT pGEX6P1-L34V	TGAACTTTGATGTGAAAAATGCTGTGCTGGGAAAGGACTTCAAAGTACTATCACCTTCC TGAACTTTGATGTGAAAAATGCTGTGCTGGGAAAGGACTTCAAAGTACTATCACCTTCC *****
pGEX6P1-WT pGEX6P1-L34V	AGAACAATAGCTCCAATCTGTACACCATCCTGGCCTATCTTTCTGGCAACATCACCTTCT AGAACAATAGCTCCAATCTGTACACCATCCTGGCCTATCTTTCTGGCAACATCACCTTCT *****
pGEX6P1-WT pGEX6P1-L34V	ACACTGGGGTATCCAAGAAAGAGTTCAAGAAGGAGTCCTTTGAAGAGACGCTGGATCCCT ACACTGGGGTATCCAAGAAAGAGTTCAAGAAGGAGTCCTTTGAAGAGACGCTGGATCCCT *****
pGEX6P1-WT pGEX6P1-L34V	TTTCTCCAAGAAAAGGAGGTGCTGGTCAGAGCGGGCGAGTACATGAGCCACCTTCTAG TTTCTCCAAGAAAAGGAGGTGCTGGTCAGAGCGGGCGAGTACATGAGCCACCTTCTAG *****
pGEX6P1-WT pGEX6P1-L34V	AACAGGGCTTCTTGCACTTCTTCGTACGGCACGCATCAACGAGTCCAGGGATGCTCTGG AACAGGGCTTCTTGCACTTCTTCGTACGGCACGCATCAACGAGTCCAGGGATGCTCTGG *****
pGEX6P1-WT pGEX6P1-L34V	CCAAACAAAAGTCCATAAATACTGACTATCCCCAAGATCACCATCAAGTCCGAGGTGCTG CCAAACAAAAGTCCATAAATACTGACTATCCCCAAGATCACCATCAAGTCCGAGGTGCTG *****
pGEX6P1-WT pGEX6P1-L34V	CCATGGTTGGCTCTGATATGGTTGTGACTGTTGAGTTCATAATCCTTTAAAGAAACAC CCATGGTTGGCTCTGATATGGTTGTGACTGTTGAGTTCATAATCCTTTAAAGAAACAC *****

pGEX6P1-WT	TACAAAATGTCTGGATTCAATTTGGATGGTCCTGGAGTGATGAGACCCAAGAGAAAGGTGT
pGEX6P1-L34V	TACAAAATGTCTGGATTCAATTTGGATGGTCCTGGAGTGATGAGACCCAAGAGAAAGGTGT *****
pGEX6P1-WT	TCCGTGAAATCCGGCCCAACACCACGGTGCAGTGGGAAGAAGTCTGTCCGCCTTGGGTCT
pGEX6P1-L34V	TCCGTGAAATCCGGCCCAACACCACGGTGCAGTGGGAAGAAGTCTGTCCGCCTTGGGTCT *****
pGEX6P1-WT	CTGGCCATCGGAAGCTGATTGCCAGCATGACCAGTGACTCCCTGAGACATGTGTATGGAG
pGEX6P1-L34V	CTGGCCATCGGAAGCTGATTGCCAGCATGACCAGTGACTCCCTGAGACATGTGTATGGAG *****
pGEX6P1-WT	AGCTGGATCTTCAGATTCAAAGACGACCTACTATGTAAattccagaaggctcgagcggc
pGEX6P1-L34V	AGCTGGATCTTCAGATTCAAAGACGACCTACTATGTAA----- *****
pGEX6P1-WT	cgcacgtgactgactgacgatctgcctcgcgcgtttcggatgacggtgaaaacctct
pGEX6P1-L34V	-----